In compliance with the
Canadian Privacy Legislation
some supporting forms
may have been removed from
this dissertation.

While these forms may be included
in the document page count,
their removal does not represent
any loss of content from the dissertation.

University of Alberta

Cyclic Behaviour of Unstiffened Steel Plate Shear Walls

By: ©

Mohammad R. Behbahanifard

A thesis submitted to the Faculty of Graduate Studies and Research in partial fulfilment of the requirement for the degree of Doctor of Philosophy

in

Structural Engineering

Department of Civil & Environmental Engineering

Edmonton, Alberta

Fall 2003

National Library
of Canada

Acquisitions and
Bibliographic Services

395 Wellington Street
Ottawa ON K1A 0N4
Canada

Bibliothèque nationale
du Canada

Acquisisitons et
services bibliographiques

395, rue Wellington
Ottawa ON K1A 0N4
Canada

Your file Votre référence
ISBN: 0-612-87936-4
Our file Notre référence
ISBN: 0-612-87936-4

The author has granted a non-exclusive licence allowing the National Library of Canada to reproduce, loan, distribute or sell copies of this thesis in microform, paper or electronic formats.

The author retains ownership of the copyright in this thesis. Neither the thesis nor substantial extracts from it may be printed or otherwise reproduced without the author's permission.

L'auteur a accordé une licence non exclusive permettant à la Bibliothèque nationale du Canada de reproduire, prêter, distribuer ou vendre des copies de cette thèse sous la forme de microfiche/film, de reproduction sur papier ou sur format électronique.

L'auteur conserve la propriété du droit d'auteur qui protège cette thèse. Ni la thèse ni des extraits substantiels de celle-ci ne doivent être imprimés ou aturement reproduits sans son autorisation.

Canada

University of Alberta

Library Release Form

Name of Author: Mohammad R. Behbahanifard

Title of Thesis: Cyclic Behaviour of Unstiffened Steel Plate Shear Walls

Degree: Doctor of Philosophy

Year this Degree granted: 2003

Permission is hereby granted to the University of Alberta Library to reproduce single copies of this thesis and to lend or sell such copies for private, scholarly or scientific research purposes only.

The author reserves all other publication and other rights in association with the copyright in the thesis, and except as herein provided, neither the thesis or any substantial portion thereof may be printed or otherwise reproduced in any form whatever without the author's prior written permission.

August 12, 2003

University of Alberta

Faculty of Graduate Studies and Research

The undersigned certify that they have read, and recommended to the Faculty of Graduate Studies and Research for acceptance, a thesis entitled Cyclic Behaviour of Unstiffened Steel Plate Shear Walls by Mohammad Reza Behbahanifard in partial fulfilment of the requirement for the degree of Doctor of Philosophy in Structural Engineering.

Dr. Gilbert Grondin (Supervisor)

Dr. Alaa Elwi (Co-Supervisor)

Dr. Geoffrey L. Kulak

Dr. Robert G. Driver

Dr. Chongqing Ru

Dr. Carlos Ventura (External Examiner)

Date: July 29, 2003

With the Grace of the Almighty Allah

Dedicated with love to:

my wife, Mahnaz

my parents, and

my daughter, Maryam

ABSTRACT

Unstiffened steel plate shear walls (SPSWs) are effective and economical lateral load resisting system, especially in regions of severe earthquakes. The system consists of columns intersected at the floor levels by beams and steel infill plates connected to its boundary members over the full height of the frame bay. Despite the recent research progress on this system and the attention from the structural engineering community, to date, relatively few structures that use this system have been constructed in North America. The lack of a reliable and effective analytical tool is likely one of the barriers for wide application of this system. Until now, the finite element analysis of SPSWs has been implemented with only limited success.

A large-scale three-storey SPSW was tested under a combination of constant gravity load and cyclic lateral loads in a quasi-static condition in order to increase the database of test results and monitor closely the behaviour of the boundary members. Twenty-four cycles of loading were applied to the test specimen, of which 14 cycles were in the inelastic range. Characteristic pinching of hysteresis loops was observed in the inelastic range. The specimen showed high initial stiffness, excellent ductility and energy absorption capacity, and stable hysteresis loops. Although one of the beam-to-column moment connections ruptured during the test, this rupture did not detrimentally affect the strength and behaviour of the specimen.

A finite element model based on nonlinear dynamic explicit formulation was developed. A kinematic hardening material model subroutine was implemented to simulate the Bauschinger effect and a special loading frame was developed to implement

a displacement control analysis. The effectiveness and validity of the model was demonstrated by comparing its monotonic and cyclic predictions with the results of tests conducted on a four storey and the three storey SPSW tested in this research.

A set of ten scale independent non-dimensional parameters that affect the behaviour of a SPSW panel under shear and gravity load was identified. Effect of some of the main parameters on the stiffness and capacity of SPSWs were investigated. It was concluded that column flexibility parameter has a significant effect on the behaviour of SPSWs. A method for considering the effect of overturning moment was proposed.

ACKNOWLEDGMENTS

This research project was conducted with the financial assistance from the Steel Structures Education Foundation and the Natural Sciences and Engineering Research Council of Canada (NSERC). Personal financial support in the form of scholarship was provided from the Ministry of Culture and Higher Education of Iran. These supports are acknowledged with thanks.

The experimental phase of this research was conducted at the Centre for Engineering Research (C-FER Technologies). Cooperation of the staff in this centre contributed to the successful completion of the test and is gratefully appreciated.

I would like to sincerely thank my supervisors Dr. Gilbert Grondin, Dr. Alaa Elwi, and Dr. Geoffrey L. Kulak for their guidance, valuable comments, and support in all aspects of the work. I would not have been able to accomplish as much without their assistance.

Many people have contributed to the success of this research. Dr. D. J. L. Kennedy helped establishing the initial direction of the research and provided valuable comments on various aspects of the testing program. Dr. R. G. Driver provided the necessary details of the previous four-storey steel plate shear wall test and provided assistance on various stages of the project. Larry Burden and Richard Helfrich from I. F. Morrison Structural Engineering Laboratory provided technical assistance in all aspects of the testing program. Thanks are also extended to the fellow graduate students Ahmed Memon (construction), Kam Deng (testing), Dr. Heng Aik Khoo and Dr. Sreekanta Das for various discussions on numerical stage of the research.

Last, but certainly not the least, I would like to thank my family. My wife, Mahnaz, has always been the greatest motivation; and her patience, moral support, and encouragement were the main source of inspiration in successful completion of this work.

TABLE OF CONTENTS

1 INTRODUCTION 1
   1.1 General 1
   1.2 Scope and objectives 3
   1.3 Outline of the thesis 4

2 LITERATURE REVIEW 7
   2.1 Introduction 7
   2.2 Takahashi, Y., Takemoto, Y., Takeda, T., and Takagi, M. (1973) 8
   2.3 Mimura and Akiyana (1977) 9
   2.4 Thorburn, L.J., Kulak, G.L., and Montgomery, C.J. (1983) 10
   2.5 Timler and Kulak (1983) 11
   2.6 Tromposch and Kulak (1987) 12
   2.7 Sabouri-Ghomi and Roberts (1991, 1992) 13
   2.8 Caccese, V., Elgaaly, M. and Chen, R. (1993) 14
   2.9 Xue and Lu (1994) 15
   2.10 Driver, R.G., Kulak, G.L., Kennedy, D.J.L., and Elwi, A.E. (1997, 1998) .. 18
   2.11 Elgaaly and Liu (1997) 19
   2.12 Kulak, G.L., Kennedy, D.J.L., Driver, R.G., and Medhekar, M. (1999) 20
   2.13 Rezai (1999) 21
   2. 14 Lubell, A.S., Prion, H.G.L., Ventura, C.E., and Rezai, M. (2000) 22
   2.15 Astaneh-Asl and Zhao (2002) 25
   2.16 Summary 26

3 STEEL PLATE SHEAR WALL TEST 32
   3.1 Introduction 32
   3.2 Description of the test specimen 32
   3.3 Preliminary numerical analysis of test specimen 34
   3.4 Test set up 35
   3.5 Instrumentation and data acquisition 38
   3.6 Loading protocol 40

4 DISCUSSION OF TEST RESULTS 54
   4.1 Introduction 54
   4.2 Gravity load application 54
   4.3 Specimen behaviour during the test 54
      4.3.1 Cycles before significant yielding 54
      4.3.2 Cycles after significant yielding 55
   4.4 Hysteresis behaviour 59
   4.5 Discussion of test results 60
   4.6 Inclination of the tension field 64

5 FINITE ELEMENT MODEL 81
- 5.1 Introduction 81
- 5.2 Convergence problem in implicit finite element method 82
  - 5.2.1 Solution strategies in a static implicit method 82
  - 5.2.2 Convergence problem 84
- 5.3 Explicit finite element method 84
  - 5.3.1 Formulation of the dynamic explicit finite element method 85
  - 5.3.2 Computational procedures in a dynamic explicit method 86
  - 5.3.3 Stability limit of a dynamic explicit method 88
  - 5.3.4 Simulation of a quasi-static analysis with the dynamic explicit method 89
  - 5.3.5 Methods to accelerate a quasi-static analysis 90
  - 5.3.6 Evaluation of a quasi-static solution 91
    - 5.3.6.1 Energy balance 91
    - 5.3.6.2 Strategies for evaluating a quasi-static solution 92
- 5.4 Description of the finite element model 93
  - 5.4.1 Element selection 93
  - 5.4.2 Geometry and initial imperfections 95
  - 5.4.3 Boundary conditions and loading of finite element model 96
  - 5.4.4 Residual stresses and history of plastic deformation from previous test 97
  - 5.4.5 Material properties 97
- 5.5 Kinematic hardening model 100
- 5.6 Displacement control analysis 101

6 VALIDATION OF THE FINITE ELEMENT MODEL 116
- 6.1 Introduction 116
- 6.2 Finite element analysis of the three-storey steel plate shear wall 116
  - 6.2.1 Pushover analysis 116
  - 6.2.2 Cyclic analysis 120
  - 6.2.3 Energy dissipation 123
- 6.3 Finite element analysis of the four-storey steel plate shear wall tested by Driver *et al.* (1997) 124
  - 6.3.1 Pushover analysis 125
  - 6.3.2 Cyclic analysis 126
  - 6.3.3 Energy dissipation 127

7 EVALUATION OF STRAIN DATA 152
- 7.1 Introduction 152
- 7.2 Strain measurements in the flanges 152
- 7.3 Strain measurements in the web 153
- 7.4 Comparison of finite element analysis with test results 154
  - 7.4.1 Strain distribution in boundary members 154
  - 7.4.2 Bending moment and axial force diagrams in the boundary members 155
- 7.5 Summary 159

8 PARAMETRIC STUDY 174
8.1 Introduction 174
8.2 System selected for investigation 174
8.2.1 Model parameters 175
8.2.2 Simplification of parametric study- Dimensional analysis 176
8.2.3 Application of dimensional analysis to the selected model 177
8.2.4 Suitability of non-dimensional parameters 182
8.3 Effect of the β -parameters on the behaviour steel plate shear wall panels 183
8.3.1 Effect of aspect ratio (β_1) 183
8.3.2 Effect of axial stiffness ratio (β_2) 184
8.3.3 Effect of column flexibility parameter (β_3) 185
8.3.4 Effect of the imperfection index (β_9) 186
8.4 Inclusion of overturning moment in the one-storey model 187
8.5 Effect of gravity load and overturning moment 190

9 SUMMARY, CONCLUSIONS, AND RECOMMENDATIONS 210
9.1 Summary 210
9.2 Conclusions and recommendations 212
9.3 Recommendations for future research 213

LIST OF REFERENCES 216

APPENDIX A 221

APPENDIX B 223

LIST OF TABLES

3.1 Material properties used for analysis of the three-storey steel plate shear wall (taken from Driver *et al.*, 1997) 43
3.2 Loading protocol for quasi-static cyclic test of three-storey steel plate shear wall 44

4.1 Measured tension field inclination (First panel – Pushing) 66
4.2 Measured tension field inclination (First panel – Pulling) 66
4.3 Measured tension field inclination (Second panel – Pushing) 67
4.4 Measured tension field inclination (Second panel – Pulling) 67

5.1 Measured initial imperfections in the infill plate of panel 1 104

8.1 Parameters for investigation of potential scale effects 193
8.2 Cross-sectional dimensions of columns in the trial cases 193
8.3 β-parameters for trial cases (A, C, and E) 193
8.4 Primary parameters for investigation of the effect of β_1 194
8.5 Cross-sectional dimensions of columns used to study the effect of β_1 194
8.6 β-parameters in the study of the effect of β_1 (β_1=0.7, 1.0, 1.5, and 2.0) 194
8.7 Primary parameters for investigation of β_2 195
8.8 Cross-sectional dimensions of columns used to study the effect of β_2 195
8.9 β-parameters in the study of the effect of β_2 (β_2=0.31, 0.44, and 0.62) 195
8.10 Primary parameters for investigation of β_3 196
8.11 Cross-sectional dimensions of columns used to study the effect of β_3 196
8.12 β-parameters in the study of the effect of β_3 (β_3=1.5, 2.5, and 3.5) 196

LIST OF FIGURES

2.1 Hysteresis behaviour of steel plate shear walls (Takahashi *et al.*, 1973) 28
2.2 Strip model proposed by Thorburn and Kulak (1983) 28
2.3 Schematic of specimen tested by Tromposch and Kulak (1987) 29
2.4 Hysteresis behaviour of specimen tested by Tromposch and Kulak (1987) 29
2.5 Four-storey steel plate shear wall tested by Driver *et al.* (1997) 30
2.6 Steel plate shear wall system studied by Astaneh-Asl and Zhao (2002) 31
2.7 Specimens tested by Astaneh-Asl and Zhao (2002) 31

3.1 Schematic of three-storey steel plate shear wall 45
3.2 Three-storey steel plate shear wall specimen 46
3.3 Fish plate detail used for connection of infill plate to the frame 47
3.4 Preliminary finite element analysis of test specimen 48
3.5 Three-storey steel plate shear wall test set up 49
3.6 Overview of test set up 50
3.7 Detail of connection of hydraulic jacks to the test specimen 51
3.8 Schematic of in-plane bracing at the base of specimen 52
3.9 Instrumentation used to measure strains and displacements 53

4.1 Initial yield lines along the west edge of panel 2 (cycle 7) 68
4.2 Yield line pattern in the web of the beam at level 1 (south face at west end – cycle 10) 68
4.3 Extent of yielding at north face of second panel (cycle 14) 69
4.4 Initiation of flange local buckling – beam at level 1, east end (cycle 20) 69
4.5 Fracture of beam–to–column connection (cycle 21) 70
4.6 Local buckling of west column in panel 1 (end of test) 71
4.7 Tear at the bottom east corner of first panel (end of test) 71
4.8 Specimen at the end of the test 72
4.9 Location of tears in the test specimen at the end of the test (north side) 73
4.10 Base shear versus first storey drift 74
4.11 Second storey shear versus second storey drift 74
4.12 Third storey shear versus third storey drift 75
4.13 Base shear versus top storey displacement 75
4.14 Typical hysteresis curve, 2nd panel, cycle 18 76
4.15 Response of four-storey steel plate shear wall specimen (cycles 29 and 30) 77
4.16 Cumulative energy absorbed by each panel through the test 78
4.17 Tension field orientation in panels 1 and 2 79
4.18 Average inclination of the tension field in the first and second panels 80

5.1 Illustration of Newton-Raphson iterative method 105
5.2 Illustration of modified Newton-Raphson iterative method 105
5.3 Modified Riks solution strategy 106
5.4 Summary of explicit dynamic algorithm 107
5.5 Example of smooth step amplitude function with two data points 108
5.6 Energy history for quasi-static tensile test 108

5.7 Default local axis and integration points for shell element S4R 109
5.8 Hourglass mode: (a) shape; (b) common source of hourglass mode; (c) method of improvement 110
5.9 Imperfection shape used in finite element model (magnification factor = 5.0) . 111
5.10 Boundary and loading conditions for the finite element model 112
5.11 Cyclic response of a cantilever beam loaded at the free end 113
5.12 Loading frame for displacement control of the three-storey steel plate shear wall specimen 114
5.13 Loading frame for displacement control of the four-storey steel plate shear wall specimen 115

6.1 First vibration mode of the three-storey steel plate shear wall 128
6.2 Velocity history for node B7 in the pushover analysis of the three-storey steel plate shear wall 129
6.3 Energy history of the pushover analysis of the three-storey steel plate shear wall 129
6.4 History of kinetic energy of the pushover analysis of the three-storey steel plate shear wall 130
6.5 Top storey velocity history during a pushover analysis of the three-storey steel plate shear wall for two different time periods 130
6.6 Monotonic finite element analysis compared with the envelope of the test cyclic response — Panel 1 131
6.7 Monotonic finite element analysis compared with the envelope of the test cyclic response — Panel 2 131
6.8 Monotonic finite element analysis compared with the envelope of the test cyclic response — Panel 3 132
6.9 Monotonic finite element analysis compared with the envelope of the test cyclic response — Top displacement 132
6.10 Vector plot of maximum in-plane principal stress at ultimate load —Mid surface of shell elements 133
6. 11 History of horizontal velocity applied to node B7 on loading frame 134
6.12 History of horizontal displacement at node B7 on loading frame 134
6.13 History of first storey drift 135
6.14 Energy history in cyclic analysis of the three-storey steel plate shear wall 135
6.15 Comparison of finite element hysteresis analysis with test results—Panel 1 136
6.16 Comparison of finite element hysteresis analysis with test results—Panel 2 136
6.17 Comparison of finite element hysteresis analysis with test results—Panel 3 137
6.18 Comparison of finite element hysteresis analysis with test results— Top displacement 137
6.19 Deformed shape of steel plate shear wall loaded in positive 1-direction — Tension field fully developed 138
6.20 Deformed shape of steel plate shear wall loaded in negative 1-direction — Early stage of tension field redevelopment 139
6.21 Deformed shape of steel plate shear wall loaded in negative 1-direction — Tension field fully redeveloped 139
6.22 Energy dissipation as a [illegible] of drift level—Panel 1 140

6.23 Energy dissipation as a function of drift level—Panel 2 140
6.24 Energy dissipation as a function of drift level—Panel 3 141
6.25 Energy dissipation as a function of displacement at the top 141
6.26 Monotonic finite element analysis compared with the envelope of the test cyclic response — Panel 1 142
6.27 Monotonic finite element analysis compared with the envelope of the test cyclic response — Panel 2 142
6.28 Monotonic finite element analysis compared with the envelope of the test cyclic response — Panel 3 143
6.29 Monotonic finite element analysis compared with the envelope of the test cyclic response — Panel 4 143
6.30 Monotonic finite element analysis compared with the envelope of the test cyclic response — Top displacement 144
6.31 Vector plot of maximum in-plane principal stress at ultimate load —Mid-surface of shell elements 145
6.32 Comparison of finite element hysteresis analysis with test results—Panel 1 146
6.33 Comparison of finite element hysteresis analysis with test results—Panel 2 146
6.34 Comparison of finite element hysteresis analysis with test results—Panel 3 147
6.35 Comparison of finite element hysteresis analysis with test results—Panel 4 147
6.36 Comparison of finite element hysteresis analysis with test results —Displacement at the top 148
6.37 Energy dissipation as a function of drift level—Panel 1 149
6.38 Energy dissipation as a function of drift level—Panel 2 149
6.39 Energy dissipation as a function of drift level—Panel 3 150
6.40 Energy dissipation as a function of drift level—Panel 4 150
6.41 Energy dissipation as a function of displacement at the top 151

7.1 Strain versus base shear at points c and d of section 8 161
7.2 Strain distribution at section 13 in west column 162
7.3 Strain distribution at section 20 in beam at level 2 162
7.4 Strain distribution at section 10 in west column 163
7.5 Strain distribution at section 11 in west column 163
7.6 Strain distribution at section 12 in west column 164
7.7 Strain distribution at section 13 in west column 164
7.8 Strain distribution at section 7 in west column 165
7.9 Strain distribution at section 8 in west column 165
7.10 Strain distribution at section 9 in west column 166
7.11 Strain distribution at section 17 in the beam at level 2 167
7.12 Strain distribution at section 18 in the beam at level 2 167
7.13 Strain distribution at section 19 in the beam at level 2 168
7.14 Strain distribution at section 20 in the beam at level 2 168
7.15 Effect of residual stresses on the moment versus curvature response for a W118×60 169
7.16 Error introduced when residual stresses are ignored in moment calculation 169
7.17 Axial force diagram of the west column in the first storey 170
7.18 Bending moment diagram of the west column in the first storey 170

7.19 Axial force diagram of the west column in the second storey ... 171
7.20 Bending moment diagram of the west column in the second storey ... 171
7.21 Axial force diagram of the east column in the second storey ... 172
7.22 Bending moment diagram of the east column in the second storey ... 172
7.23 Axial force diagram in the beam at level 2 ... 173
7.24 Bending moment diagram in the beam at level 2 ... 173

8.1 Selected model for parametric study of a panel ... 197
8.2 Base shear versus drift for three models with similar β -parameters ... 198
8.3 Normalized responses for three different models with similar β -parameters ... 198
8.4 Effect of aspect ratio parameter, β_1, on behaviour of steel plate shear wall ... 199
8.5 Column local buckling and deformation of model with $\beta_1 = 0.7$ ... 199
8.6 Normalized response for different aspect ratios (if column local buckling prevented) ... 200
8.7 Effect of β_2 on steel plate shear wall response ... 200
8.8 Effect of β_3 on the normalized response of steel plate shear wall ... 201
8.9 Effect of imperfection magnitude on the behaviour of a steel plate shear wall panel ... 201
8.10 Free body diagram of panel j from a multi-storey steel plate shear wall ... 202
8.11 Panel *j* of a steel plate shear wall in deformed configuration ... 203
8.12 Base shear versus first storey drift obtained from the analysis of whole model and single storey model ... 204
8.13 Rotation of the first floor obtained from the analysis of a single storey model of the first panel ... 204
8.14 Panel shear versus storey drift obtained from single storey model of the second panel with fixed boundary condition ... 205
8.15 Panel shear versus storey drift obtained from the analysis of whole model and single storey model of the second panel ... 205
8.16 Rotation of the second floor ... 206
8.17 Third storey shear versus third storey drift obtained from the analysis of whole model and single storey model of the third panel ... 206
8.18 Elastic stiffness of the panel versus β_4 at different β_{11} parameters ... 207
8.19 Effect of β_4 and β_{11} on shear wall panel capacity ... 207
8.20 Effect of β_4 and β_{11} on reduction of shear wall panel capacity ... 208
8.21 Normalized response of the first panel of an eight-storey shear wall at various β_4 parameter ... 208
8.22 Normalized response at β_4 equal to 0.5 and various β_{11} parameter ... 209

LIST OF SYMBOLS

$A_1,...A_n$	set of n variables defining the behaviour of a physical problem
A_b	cross-sectional area of beam
A_c	cross-sectional area of column
b_f	width of flange in a W-section
$\underline{B}$	strain operator matrix
C_d	dilatational wave speed of a material
d	web depth in a W-section
E	modulus of elasticity
E_{FD}	frictional energy (energy dissipated by frictional forces in a contact problem)
E_I	internal energy (both elastic strain energy and plastic work)
E_{KE}	kinetic energy
E_{tr}	transverse shear strain energy
E_{TOTAL}	total energy in a system
E_V	energy absorbed by viscous dissipation
E_W	work done by external forces
f	mass scaling factor
f^B	body force per unit volume
f^S	surface traction force per unit area
$\underline{f}_t(U^*)$	vector of residual unbalanced forces evaluated at nodes at time t as a function of approximate displacement field
F	typical horizontal force applied at each floor in a multi-storey shear wall
F_i	horizontal force applied to i^{th} floor
$\underline{F}_t$	vector of internal nodal force at time t
G	elastic shear modulus
G_{13}, G_{23}	elastic shear modulus in plane (1-3) and (2-3), respectively

h	height of shear wall panel
H_i	distance of i^{th} floor to the base of the shear wall
I_c	moment of inertia of column
K^{tr}_{13}, K^{tr}_{23}	transverse shear stiffness in plane (1-3) and (2-3), respectively
L	length dimension
L	width of the infill plate
L'	width of the panel (centre-to-centre of column axis)
L_e	smallest characteristic length of an element
$\mathbf{M}$	bending moment
M	mass dimension
$\underline{M}$	consistent mass matrix
$(M_{ov})_j$	overturning moment at top of panel *j*
n	total number of storeys
n	number of variables included in a dimensional matrix
$\mathbf{N}$	axial force
$\underline{N}$	matrix of shape functions
$\underline{P}$	applied concentrated force vector at nodes
$\mathrm{Q_y}$	shear force at point of significant yielding
r	rank of dimensional matrix
R	force modification factor
$\underline{R}_t$	vector of external nodal loads at time t
$S(t)$	state variables at time t
t_p	infill plate thickness
t	time
t_f	flange thickness in a W-section
t_w	web thickness in a W-section
T	time dimension
u_j	total drift of panel *j*

u_x, u_y, u_z	translational degree of freedom in global coordinate system
$(u_j)_{fix}$	drift of panel *j* assuming a fixed boundary condition at the lower floor beam
$\ddot{u}$	acceleration field
U_i	horizontal displacement of i^{th} floor relative to the base of the shear wall
U^*	approximate of real displacement field
$\underline{U}$	nodal displacement vector
$\underline{\dot{U}}$	nodal velocity vector
$\underline{\ddot{U}}$	nodal acceleration vector
V	shear force in one storey model
V_j	shear force in panel *j*
V_y	shear force that yield the whole cross section of the shear panel
w_i	gravity load applied to i^{th} floor
W	gravity load in one storey model
W_j	total gravity load applied to panel *j* from panels above
W_y	axial force that yield the whole cross section of the shear wall panel, including the columns
α	angle of inclination of tension field from the vertical
α_{ave}	average inclination of buckles from vertical measured during the test
β_1	L / h (aspect ratio)
β_2	$\frac{t_p L}{2A_c}$ (ratio of axial stiffness of infill plate to that of columns)
β_3	$0.7\sqrt[4]{\frac{h^4 t_p}{2LI_c}}$ (column flexibility parameter)
β_4	W / W_y (ratio of gravity load to axial yield load or normalized gravity load)
β_5	δ / h (drift index)

β_6	V / V_y (ratio of shear load to the shear yield capacity or normalized base shear)
β_7	$\frac{\sigma_{yc}}{E} = \varepsilon_{yc}$ (column yield strain in single storey model)
β_8	$\frac{\sigma_{ypl}}{E} = \varepsilon_{ypl}$ (infill plate yield strain)
β_9	$\frac{\Delta_{imp}}{\sqrt{Lh}}$ (imperfection ratio)
β_{10}	$\frac{(A_c)^2}{I_c}$ (local buckling index)
β_{11}	$\frac{M_{ov}}{VL'}$ (normalized overturning moment)
δ	panel drift
δe	virtual strain field
δu	virtual displacement field
δ_y	deflection at point of significant yielding
$\delta \underline{U}$	virtual displacement vector
Δ_{imp}	maximum out-of-plane imperfection in infill plate
Δt	time increment
Δt_{stable}	stable time increment
$\Delta \varepsilon$	strain increment
$\Delta \underline{\varepsilon}$	strain increment vector in local directions $\langle \Delta\varepsilon_{11}, \Delta\varepsilon_{22}, \Delta\varepsilon_{33}, \Delta\varepsilon_{12}, \Delta\varepsilon_{23}, \Delta\varepsilon_{31} \rangle$
$\Delta \varepsilon_{el}$	elastic part of strain increment
$\Delta \varepsilon_{pl}$	plastic part of strain increment
$\varepsilon_{\ln}^{pl}$	plastic component of logarithmic strain
ε_{yc}	yield strain of column material in single storey model
ε_{ypl}	yield strain of infill plate material
ε_{nom}	nominal strain (engineering strain)

$\omega_{\max}$	highest frequency of a structural system
ν	Poisson's ratio
$\theta_x, \theta_y, \theta_z$	rotational degree of freedom in global coordinate system
$\theta_{j/j-1}$	rotation of the floor beam at level j to the floor beam at level (j-1)in radian
θ_{j-1}	total rotation of the floor beam at level (j-1) in radian
ρ	material density
σ	Cauchy stress
$\underline{\sigma}$	stress vector in local coordinate system $\langle \sigma_{11}, \sigma_{22}, \sigma_{33}, \sigma_{12}, \sigma_{23}, \sigma_{31} \rangle$
σ_{nom}	engineering stress (force per initial unit area)
σ_r	residual stress
σ_{true}	true stress (force per actual unit area)
σ_{yc}	static yield stress of the column material in single storey model
σ_{ypl}	static yield stress of the infill plate
Φ	curvature
ω_h	column flexibility (equivalent to β_3 parameter)
ξ	fraction of critical damping

1 INTRODUCTION

1.1 General

Experimental and numerical studies conducted in the past three decades have demonstrated that a steel plate shear wall is an effective and economical lateral load resisting system against both wind and earthquake forces. The system consists of infill steel plates connected to boundary beams and columns over the full height of the framed bay. The infill plates can be stiffened or unstiffened and the beam-to-column connections can be rigid or shear connections. A properly designed steel plate shear wall has superior ductility, high initial stiffness, stable hysteresis loops, inherent redundancy, and good energy absorption capacity. These characteristics make the system attractive in high-risk seismic regions. The system has been used for new buildings as well as for upgrading existing steel or reinforced concrete buildings. An example of such applications is the Olive View Hospital, which performed extremely well during the 1994 Northridge earthquake (Celebi, 1997).

Use of steel plate shear wall systems has been shown to be more cost effective than the other lateral load resisting systems (Timler and Ventura, 1999). Steel plate shear walls are much lighter than the commonly used reinforced concrete shear walls, which reduce both the gravity loads and seismic forces. This aspect significantly reduces the foundation costs and makes the system attractive for application in rehabilitation projects.

The design philosophy of existing steel plate shear wall systems is to prevent shear buckling of infill plate by using either a thick plate or heavily stiffened plate. This reduces the economic attractiveness of the system. However, Wagner (1931) showed that shear buckling of a thin plate that is adequately supported along its edges does not constitute failure. At the point of buckling the load carrying mechanism of the plate changes from in-plane shear to an inclined tension field to resist the panel shear. This concept has been used for many years in shear design of plate girders (Basler, 1961), but it was first applied to design of steel plate shear walls in the early 1980's through a series of analytical (Thorburn *et al.*, 1983) and experimental (Timler and Kulak, 1983;

Tromposch and Kulak, 1987) research. A steel plate shear wall is analogous to a vertical cantilevered plate girder, with the columns acting as the flanges and the floor beams as transverse stiffeners. For a thin panel, the shear buckling strength is low and, as a result, the tension field action is the main mechanism for carrying the applied shear forces. In order for the tension field to fully develop, the boundary members should have sufficient bending stiffness.

Clause 27.8 of the latest version of the Canadian standard on Limit States Design of Steel Structures (CSA-S16-01) provides guidelines for the analysis and design of thin unstiffened steel plate shear walls. The analytical model proposed in Clause 27.8 is based on the model developed by Thorburn *et al.* (1983). Although the model predicts the capacity of the system reasonably well, it fails to predict the stiffness of the system accurately in some cases (Rezai, 1999). Accurate prediction of stiffness is of paramount importance in drift calculations of high-rise buildings. To provide improved design guidelines more research is needed in areas that are still unknown. For example, it is necessary to quantify the effects of infill panel aspect ratio and the stiffness ratios of the infill plate to beams and columns stiffnesses. Because of the expense involved in an experimental program to investigate these parameters, an analytical tool that can accurately predict the monotonic and cyclic behaviour of thin unstiffened steel plate shear walls is needed. This model can be used for a comprehensive parametric study of this system.

The research described herein consists of two phases. The first phase describes a quasi-static cyclic test on a large-scale three-storey unstiffened steel plate shear wall. In the second phase, a finite element model for monotonic and cyclic analysis of this system is presented and validated. Using the analytical model, the non-dimensional parameters describing the behaviour of a panel of this system with rigid floor beams are identified. The cumulative effects of several panels can be used to deduce the behaviour of multiple storey shear wall systems.

1.2 Scope and objectives

In the experimental part of this study, a large-scale test on a three-storey steel plate shear wall specimen was conducted under lateral quasi-static cyclic loading in the presence of gravity loads. The specimen formed the upper part of a four-storey steel plate shear wall, which had been tested earlier by Driver *et al.* (1997). Standard fabrication techniques were used in fabrication of the specimen and the loading history was based on established guidelines for simulating earthquake loading (Applied Technology Council, 1992). In the second phase of this study, a nonlinear finite element model was developed in order to accurately simulate the monotonic and cyclic behaviours of thin unstiffened steel plate shear walls. The model was validated using the results of both the three and four storey shear wall tests. The numerical model was then used for a parametric study of this system.

The primary objective of the experimental phase was to increase the database of test results on large-scale multi-storey unstiffened steel plate shear walls under extreme cyclic loading, such as would be expected in a severe earthquake. Since the test specimen had gone through a history of plastic deformation from previous testing by Driver *et al.* (1997), evaluating the effect of the previous test on the overall performance of the specimen was one of the objectives. Stiffness, ductility, energy absorption capacity, and strength degradation were all assessed.

Another objective of the test was to monitor closely the behaviour of boundary members and to assess how the storey shear forces are shared between the infill panel and the moment-resisting frame. This was achieved by evaluation of the strains at various sections in the beams and columns. In addition, the influence of moment resisting beam–to–column connections in enhancing the pinching behaviour of hysteresis loops was an important aspect of the test.

A third objective of the test was to monitor the formation of buckles in the infill plates and to measure the angle of inclination of the tension field in the first and second panels of the specimen in each cycle. Investigation of the stability of the hysteresis loops under cyclic loading and the redundancy and ability of the system to redistribute the load was the fourth objective of this experimental program.

A final objective of the experimental program was to study the failure mode of the test specimen and identify the primary energy-absorbing element in the system (infill plate or frame) in resisting the applied shear load

The finite element analysis of unstiffened steel plate shear walls has been implemented to date with only limited success. Because of local instabilities and snap-through buckling of infill plates, commonly used solution techniques fail to converge to the solution path as the tension field develops in the plate. Lack of convergence is a major problem in finite element analysis of these systems especially when geometric nonlinearities are included in the model (Driver *et al.*, 1997 and Rezai, 1999). The primary objective of the analytical phase was therefore to develop a suitable finite element model that includes geometric and material nonlinearity in order to capture the behaviour of this system both under monotonic and cyclic loading.

The final objective of this research was to identify the non-dimensional geometric and material parameters that describe the behaviour of a typical thin steel plate shear wall panel subjected to shear and gravity load. The effect of these parameters can then be systematically investigated.

1.3 Outline of the thesis

Chapter 2 provides a chronological review of earlier research on steel plate shear walls. The review includes a summary of both the experimental and analytical investigations available.

An overview of the experimental programme is presented in Chapter 3. The objectives of the experiment, description of the specimen details and fabrication procedures, test set-up, instrumentation and data acquisition, as well as the loading protocol are discussed in detail in this chapter. A brief summary of the preliminary finite element analysis of the test specimen is also presented.

Chapter 4 presents the results of the test on a three-storey steel plate shear wall. The observations during the test, the test results, presented in the form of hysteresis loops, and the overall performance of the specimen are discussed.

Chapter 5 describes the finite element model that was developed to predict the behaviour of thin unstiffened steel plate shear walls. The convergence problems in the analysis of these systems with a static implicit method are described. As an alternative, the nonlinear dynamic explicit finite element method is proposed. The formulation of the method and strategies for simulating a quasi-static response are discussed in detail. A method for controlling the displacement during cyclic analysis of multi-storey shear walls is presented.

In Chapter 6, the proposed finite element model is used to predict the behaviour of the three-storey steel plate shear wall. Pushover analysis, cyclic behaviour, energy dissipation, and inclination of the tension field are obtained and compared with the test results. The finite element method is also used for the four-storey steel plate shear wall tested by Driver *et al.* (1997) and the predictions are compared with the test results. This provides a validation for the proposed finite element model and analysis technique.

The strain data are evaluated in Chapter 7. The distribution of axial force and bending moment along the boundary members are obtained from the strains measured during the test and compared with the predictions from the pushover finite element analysis.

The non-dimensional parameters that affect the behaviour of a panel of steel plate shear wall with rigid floor beams are identified in Chapter 8. The influence of some of the primary non-dimensional parameters on the stiffness and capacity of the selected model are investigated through a parametric study.

Summary, conclusions, and recommendations for future research are presented in Chapter 9.

2 LITERATURE REVIEW

2.1 Introduction

Research on steel plate shear walls was initiated in the early 1970's. Experimental and analytical studies that have been conducted so far have all demonstrated that a properly designed steel plate shear wall can be the most effective and economical lateral load resisting system, especially for application in severe earthquake regions. Steel plate shear walls have been used in several buildings, mainly in Japan and in the United States (Thorburn *et al.*, 1983; Fujitani *et al.*, 1996; Celebi, 1997; Astaneh-Asl, 2001). Early designs of steel plate shear walls were based on the concept of preventing shear buckling of infill plate under the design loads, thus neglecting any post-buckling strength. In order to meet this design requirement, Japanese designs have relied on heavily stiffened thin plates whereas designers in the United States have used unstiffened or moderately stiffened thick plates.

For many years, it has been known that buckling does not represent the limit of useful behaviour of a shear panel. When shear panels are designed properly, the load-resisting mechanism changes from in-plane shear to an inclined tension field after buckling. Wagner (1931) showed that thin aluminium shear panels used in aircrafts and supported by stiff boundary members develop a diagonal tension field after buckling. Wagner developed the "pure" tension field theory whereby the shear capacity of a thin plate supported by relatively stiff boundary members depends primarily on tension field action. Kuhn *et al.* (1952) studied intermediate cases between pure diagonal tension field action and pure shear and proposed the "incomplete" diagonal tension theory. This theory is based on the assumption that the panel shear capacity results from both pure shear and diagonal tension field. Following the works of Wagner and Kuhn, Basler (1961) developed an incomplete diagonal tension field model to predict the shear capacity of plate girders. Basler's work has been widely accepted and has formed the basis for the design of steel plate girders in many modern design standards (CSA, 2001; AISC, 1999).

Utilization of the post-buckling strength of a panel in shear was first applied to steel plate shear wall through a series of analytical and experimental work at the University of Alberta in the early 1980's (Thorburn *et al.*, 1983; Timler and Kulak, 1983; Tromposch and Kulak, 1987). In recent years, however, this concept has gained wide attention from researchers in Canada, the United States and England (in US Caccese *et al., 1993;* Elgaaly *et al.*, 1993; Xue and Lu, 1994a, 1994b; Elgaaly and Liu, 1997; Astaneh-Asl and Zhao, 2002; and in the UK Roberts and Sabouri-Ghomi, 1991; Sabouri-Ghomi and Roberts, 1991 and 1992). In addition to analytical investigations a number of static, quasi-static and shake table tests have been performed on large and small-scale models of this system (Timler and Kulak, 1983; Tromposch and Kulak, 1987; Elgaaly *et al.* 1993; Driver *et al.* 1997; Lubell, 1997; Rezai, 1999; Astaneh-Asl and Zhao, 2002). A brief review of studies conducted on steel plate shear walls around the world is presented in the following. A similar historical review can be found in Driver *et al.* (1997) that also included related topics such as strengthening of reinforced concrete frames with steel infill plates, concrete encased steel plate shear walls, and the use of steel plate panels as hysteretic dampers.

2.2 Takahashi, Y., Takemoto, Y., Takeda, T., and Takagi, M. (1973)

Japan appears to be the first country to have extensively designed, tested, and constructed buildings using steel plate shear walls. Takahashi *et al.* (1973) conducted a series of 12 single panel tests and two single bay, two-storey full-scale stiffened steel plate shear walls with and without reinforced openings. The single panel specimens were fabricated with and without stiffeners in a pin jointed frame. The series of tests on single panels indicated that panels stiffened to prevent buckling of the infill plate showed excellent behaviour under cyclic loading with hardly any pinching. In contrast, the unstiffened panel showed significant pinching of the hysteresis loops (see Figure 2.1). The full-scale two-storey test specimens, designed to behave plastically, also showed good behaviour under cyclic loading. Takahashi *et al.* (1973) developed guidelines for the design of stiffened steel plate shear walls to prevent elastic buckling and a finite element model for the in-plane inelastic behaviour of stiffened steel plate shear walls (the out–of–plane buckling of the infill plate was not considered in their finite element analysis). The finite element model was able to trace accurately the envelope of the hysteresis loops.

Based on their test results, Takahashi *et al.* (1973) recommended that stiffened steel plate shear panels be designed so that the panel does not buckle elastically and if inelastic buckling occurs, it should be limited to local buckling between the stiffeners. They also concluded that the classical shear theory, wherein the horizontal shear is transferred by beam action alone, can be used to calculate the stiffness and yield strength of the stiffened shear panels.

2.3 Mimura and Akiyana (1977)

Mimura and Akiyana (1977) developed a general method for predicting the monotonic and cyclic behaviour of unstiffened steel plate shear panels through a series of experimental and analytical studies. The monotonic behaviour of a shear wall panel was obtained by superimposing the behaviour of the infill plate and the frame separately. Classical plate theory was used to predict the infill plate buckling capacity and a diagonal tension field action was assumed in the post-buckling range. The contribution of the moment resisting frame was obtained from an elastic–plastic frame analysis.

Mimura and Akiyana (1997) proposed a model to predict the cyclic behaviour based on their monotonic behaviour model and a number of simplifying assumptions. The main assumption was that after plastic deformation of the panel in one direction the amount of deformation required to develop the tension field in the opposite direction is one half of the permanent plastic deformation during the previous loading cycle. This statement is based on the assumptions of inelastic Poisson's ratio of 0.5 and an angle of inclination of the tension field of 45°. The stiffness of the frame during the redevelopment of the tension field was neglected

Mimura and Akiyana (1977) conducted a series of tests to validate their proposed model. The tests were conducted on small-scale simply supported stiffened plate girders subjected to a single cyclic point load at mid-span. The test results were in good agreement with their proposed model except in the redevelopment phase of the tension field where stiffness of the frame was neglected.

2.4 Thorburn, L.J., Kulak, G.L., and Montgomery, C.J. (1983)

Thorburn *et al.* (1983) developed a simple analytical model to study the shear behaviour of thin unstiffened steel plate shear walls. The model was based on the pure diagonal tension field introduced originally by Wagner (1931). The shear strength of the panel prior to buckling was neglected, leaving only the tension field action as the load carrying mechanism. In this model, referred to as the strip model, the action of the tension field was modelled by a series of pin-ended inclined tension-only members. These strips were oriented parallel to the direction of the tension field. Each strip was assigned an area equal to the width of the strip times the plate thickness. The strip model for a typical interior panel is shown in Figure 2.2. In this model the interior beams are assumed to be infinitely rigid in bending. The angle of inclination of the tension field was obtained using the principle of least work and considering only the energy of the tension field and axial energy in the beams and columns. The proposed equation for angle of inclination of the tension field by Thorburn *et al.* (1983) takes the following form:

$$\tan\alpha = \sqrt[4]{\frac{1+\dfrac{Lt_p}{2A_c}}{1+\dfrac{ht_p}{A_b}}} \qquad 2.1$$

where, α is the angle of inclination of tension field (see Figure 2.2), t_p is the infill plate thickness, L is the width, h is the height of the panel, and A_b and A_c are the cross-sectional area of the beam and an individual column, respectively.

By using a plane frame program and the strip representation of the infill plate a steel plate shear wall system can be analysed. The beams and columns are assigned their actual stiffness. The researchers also studied the use of a single equivalent diagonal brace suitable for preliminary analysis of multi-storey shear walls. The area of the brace is obtained in such a way that the stiffness of the panel is equivalent to that derived from the strip model.

2.5 Timler and Kulak (1983)

In order to verify the strip model proposed by Thorburn *et al.* (1983), Timler and Kulak (1983) conducted a large-scale, single-storey steel plate shear wall test. The major areas of interest were the study of the tension field development in the infill plate, the out–of–plane behaviour of the plate under service load reversals (quasi-wind cyclic loading), and the ultimate load behaviour of the system. The test specimen consisted of a pair of single-storey, one-bay, shear wall with pinned joints at the four extreme corners.

Timler and Kulak (1983) modified the angle of inclination of tension field proposed by Thorburn *et al.* (1983). The method and the basic model used by Timler and Kulak was the same as used by Thorburn *et al.* except that the bending strain energy of the columns was added to the energy calculation. The revised equation for the angle of inclination of the tension field takes the following form:

$$\alpha = \tan^{-1}\sqrt[4]{\frac{1+\dfrac{t_pL}{2A_c}}{1+t_ph\left(\dfrac{1}{A_b}+\dfrac{h^3}{360I_cL}\right)}} \qquad (2.2)$$

where, I_c is the moment of inertia of the boundary column and the other variables were defined in Equation 2.1. Although the formulation of Equation 2.2 involved a number of simplifying assumptions, Timler and Kulak (1983) showed a reasonable agreement between the predicted value of the angle of inclination of the tension field and the angle measured during the test. The measured value for α, as obtained from the strain gauge reading, was between 47° and 53° in the lower portion of the panel as compared to the predicted value of 51°.

A comparison between the test results and the predicted behaviour using the strip model of Thorburn *et al.* with the angle of the tension field given by Equation 2.2 showed good agreement. The measured axial strains in the columns were also in good agreement with the predicted values, but the bending strains were overpredicted by the analysis.

The strip model proposed by Thorburn *et al.* (1983) and the modified equation for the angle of inclination of tension field proposed by Timler and Kulak (1983) have been adopted by the Canadian Standard CSA–S16–01 as a simple approach for the analysis of unstiffened steel plate shear walls.

2.6 Tromposch and Kulak (1987)

Tromposch and Kulak (1987) conducted a large-scale test similar to the one conducted by Timler and Kulak (1983). The test specimen, shown in Figure 2.3, was different from Timler's specimen in two respects: it used typical bolted shear beam–to–column connections and gravity loads were applied to the columns. Cyclic loading was applied to the test specimen, with gradually increasing displacements in a quasi-static condition, up to the limit of the loading device at 67% of the ultimate load. The test was followed by monotonic loading up to the ultimate capacity of the specimen. As shown in Figure 2.4, the specimen showed very ductile and stable behaviour, but the hysteresis loops were severely pinched due to use of very thin plate and flexible boundary frame. By using the strip model developed by Thorburn *et al.* (1983), the researchers conducted a pushover analysis of the specimen. Good agreement was found between the analysis and the envelope of the hysteresis loops obtained in the test.

Tromposch and Kulak (1987) proposed a model for predicting the hysteresis behaviour of unstiffened steel plate shear walls. Similar to the model proposed by Mimura and Akiyana (1977), the hysteresis loops were generated using a monotonic load versus deflection curve (obtained from a strip analysis) and assumptions about the hysteresis behaviour of the shear panel. The model incorporated the effect of frame stiffness and the effect of low panel buckling strength.

Tromposch and Kulak (1987) demonstrated that the proposed model was able to predict reasonably well the experimentally observed hysteresis behaviour of their test specimen. A parametric study showed the significance of connection type on the stiffness and energy absorption capacity of steel plate shear walls. Changing simple beam–to–column connections to rigid beam–to–column connections can increase significantly the energy absorption capacity of the system.

2.7 Sabouri-Ghomi and Roberts (1991, 1992)

Sabouri-Ghomi and Roberts (1991) proposed a method for nonlinear dynamic analysis of thin steel plate shear walls whereby the system was idealized as a vertical cantilever plate girder. The governing differential equation of motion for a continuous cantilever beam was discretized to a multi-storey shear wall in which the associated storey masses and the dynamic forces were concentrated at each floor. Initially, the governing equations were formulated assuming only shear deformation and later, a more general formulation that included both bending and shear deformations was presented (Sabouri-Ghomi and Roberts, 1992). The governing differential equations were solved using a finite difference time stepping technique.

Material nonlinearity was incorporated in the analysis by using an approximate elastic–plastic hysteresis model for each panel of the shear wall. The hysteresis model took into account the shear buckling and yielding of the web plate as well as the boundary members. The hysteresis behaviour of the web plate was obtained from a series of quasi-static tests on small-scale single panel unstiffened plates with stiff, pin-ended boundary frames (Roberts and Sabouri-Ghomi, 1991). An elastic–perfectly plastic material model was assumed for the boundary frame alone, assuming plastic hinges at the top and bottom of the columns. The hysteresis curve for the entire shear wall panel was defined by superposition of hysteresis curves for the web plate and the boundary columns. The theoretical model was in reasonable agreement with the test results.

Sabouri-Ghomi and Roberts evaluated their analytical model by analysing a five-storey single bay steel plate shear wall subjected to three different periodic loadings.

The loads were selected in such a way as to examine the elastic, elastic–plastic, and resonance response of the model. The results were interpreted only by engineering judgment. The analytical technique developed by the researchers has not been validated with any experimental test results.

2.8 Caccese, V., Elgaaly, M. and Chen, R. (1993)

To assess the effectiveness of using the thin-plate shear wall system in seismic zones Caccese *et al.* (1993) conducted quasi-static cyclic tests on six quarter-scale, single-bay three-storey unstiffened steel plate shear walls. Beam–to–column connection type (simple and rigid) and panel width–to–thickness ratio were the parameters that were investigated. The experimental program included cyclic and monotonic tests. The specimens were loaded with a single horizontal load at the top of the shear walls. The load history, similar to that proposed in ATC-24 (Applied Technology Council, 1992), consisted of displacement peaks that were increased in eight increments up to 2% drift measured at the top of the shear walls.

The test results demonstrated that addition of an unstiffened thin steel plate to a steel frame results in a system with a substantial increase in stiffness, capacity, and energy absorption. The researchers concluded that the beam–to–column connection type has a minor effect in the behaviour of a steel plate shear wall system. This conclusion was discussed by Kulak *et al.* (1994) who pointed out that because of different plate thickness and material properties among the test specimens, plus a failed weld in one of the tests, made a direct comparison of the test results impossible. Their assessment of the effect of connection type was therefore rejected. Caccese *et al.* also concluded that when a slender plate is used as an infill, inelastic behaviour is initiated by yielding of the plate and the strength of the system is governed by the formation of plastic hinges in the columns. When the infill plate thickness is increased the failure mode is governed by column instability and only a negligible increase in system capacity is achieved.

Following their experimental study, Elgaaly *et al.* (1993) carried out numerical investigations of the test specimens under monotonic loading. Two numerical models were considered. First, a nonlinear finite element model, including material and geometric nonlinearity, was used. The infill plates were modelled with shell elements and beam elements were used to model the boundary members. The finite element model greatly overestimated both the stiffness and the capacity of the test specimens.

In the second study, the simple model developed by Thorburn *et al.* (1983) was used. In this model the infill plates were replaced by a perpendicular grid of tension members oriented in the direction of the principal tensile and compressive stresses. By using an elastic–perfectly plastic material model for the strips, only the initial slope of the response and the capacity of the specimens were predicted accurately. Based on the observed test behaviour, a bilinear elastic–plastic stress versus strain curve was proposed for the infill plate and the parameters of the model obtained empirically, which resulted in a better fit of the test results. The parameters used in the model were a linear function of the ratio between the buckling and the yield strength of the infill plate. An empirical model was also developed for predicting the hysteretic behaviour of the specimens. This model predicted the behaviour of the test specimens reasonably well. The researchers indicated that their empirical formula was valid within a specific range of the parameters and should not be applied outside that range without further test results (the ratio of the buckling to yield strength of the infill plates used in their experimental program varied between 0.0098 and 0.123). Although the influence of the number of truss elements used in the strip model was found to be important for an accurate calculation of internal forces in the boundary members, the variation of the angle of inclination of tension field was found to have only a small effect on the predicted capacity of the steel plate shear wall.

2.9 Xue and Lu (1994)

Xue and Lu (1994a) conducted a numerical investigation of the effect of different arrangements for connecting the infill plate to the boundary members and the effect of beam–to–column connection type on the behaviour of unstiffened steel plate shear walls. A three-bay, 12-storey frame with moment resisting beam–to–column connections in the two exterior bays and with steel infill plate in the middle bay was used for their investigation. The system was designed to resist the earthquake loads specified in the

Uniform Building Code (UBC, 1988). Based on two different beam–to–column connection types (rigid for all connections, **F**, or shear type at intermediate bay and rigid for the exterior bays, **P**) and two different arrangements for connecting the infill plate to the boundary members in a panel (connecting to both girders and columns, **GC**, or connecting only to the girders, **G**), a total of four frame–wall combinations were considered, namely, **F-GC, F-G, P-GC,** and **P-G**. Lower bound and upper bound solutions were also produced for comparison with the numerical analysis results. The upper bound solution consisted of a frame with all moment-resisting connections, infill plates connected along all four edges, and infill plates assumed not to buckle under load. The lower bound was a frame with simple beam–to–column connections in the interior bay, and no infill plate.

The primary parameter investigated in this study was the lateral stiffness of the system, since drift control is often a major design consideration. A total of six frame–wall structures were modelled using the finite element method. Elastic beam elements were used to model the frame members and 4-node shell elements with large deformation capability were used for the infill plates. The initial imperfections introduced in the panels consisted of the superposition of several shear buckling modes of the infill plates. A bi-linear stress versus strain curve with kinematic hardening model was used for the infill plates. Vertical distribution of the lateral loads at each floor was based on UBC (1988). The lateral loads were applied monotonically at each floor and no gravity loads were applied.

The base shear versus top storey displacement obtained from the analysis demonstrated that the infill plates increased significantly the stiffness of the system, but the type of beam–to–column connection in the infilled bay had a negligible effect on lateral stiffness. The stiffness of the systems with infill plates connected to both girders and columns (**GC**) were as high as the stiffness predicted using the upper bound solution and were only slightly higher than the stiffness of the systems with infill plates connected to girders only (**G**). A number of factors led to the conclusion that the **P-G** system (simple beam–to–column connections in the infilled bay and infill plates connected to the girders only) has the best performance.

Xue and Lu (1994b) also conducted a parametric study to investigate the load versus deformation characteristics of the frame–wall system consisting of a panel of steel plate shear wall with simple beam–to–column connections and infill plate connected to beams only. Rigid boundary members were used in the analysis. The width–to–thickness ratio of the infill plate and the panel aspect ratio (width/height) were investigated by finite element analysis of 20 different cases. The researchers found that the width–to–thickness ratio has no significant effect on the response of the system while the aspect ratio of the panel had a significant effect on the panel behaviour. The load at significant yield increased significantly as the aspect ratio increased while the post-buckling stiffness remained almost the same. From the results of their parametric study, Xue and Lu proposed a simplified empirical equation to predict the yield strength, yield displacement, and the post-yield stiffness of the system.

Xue and Lu (1994b) also conducted a cyclic analysis on a single panel of a twelve-storey three-bay structure described by Xue and Lu (1994a). Although the researchers used a simple panel with infill plate connected to girders only and neglected the deformation of the boundary members, they reported numerical difficulties in the analysis due to snap-through behaviour of the infill plate in the intermediate deformation range. Six cycles of gradually increasing displacements were applied up to a storey drift of 1.68%. The panel demonstrated significant energy dissipation capacity even with some pinching. The pinching became relatively less severe as the shear deformation increased.

The merit of the approach proposed by these researchers, compared to the traditional approach for a frame–wall system, should be further investigated. A comparative study should highlight the differences of the two systems in terms of cyclic behaviour and failure mode in severe earthquake simulations. No experiment is available to confirm the cyclic behaviour of the proposed system.

2.10 Driver, R.G., Kulak, G.L., Kennedy, D.J.L., and Elwi, A.E. (1997, 1998)

Driver *et al.* (1997, 1998a) conducted a quasi-static cyclic test on a half-scale four-storey unstiffened steel plate shear wall. The main objective of the test was to evaluate the overall in-plane performance of the shear wall under extreme cyclic loading. The specimen, shown in Figure 2.5, had rigid beam–to–column connections and the infill plates were welded to the boundary members through fish plates.

Gravity loads were applied at the top of the columns and were kept constant during the test. Equal horizontal loads were applied cyclically at each floor under quasi-static condition. The load and deflection sequences were selected based on recommendations by Applied Technology Council (1992). The storey shear versus storey deformation of the first panel was used to control the test.

A total of 30 load cycles were applied to the specimen and 20 of those cycles were in the inelastic range. The shear wall specimen was found to be initially stiff, very ductile, and it exhibited hysteresis behaviour with significant energy absorption. In the final cycle the panel had reached a deformation of nine times the yield deformation. The post-ultimate degradation was slow and controlled. The moment resisting boundary frame used in the test specimen improved the behaviour and prevented the severe pinching of the hysteresis loops that was seen in the shear walls with shear type beam–to–column connections (Tromposch and Kulak, 1987).

Driver *et al.* (1997, 1998b) developed a finite element model for the analysis of their test specimen. Beams and columns were modeled with beam elements and the infill plate was modelled with shell elements. Initial imperfections based on the first buckling mode of the plate were incorporated in the model and residual stresses were included in the boundary members. A bilinear stress versus strain curve, along with a kinematic hardening model, was used for the material modelling. Because of convergence problems, geometric nonlinearity could not be included up to the ultimate load. The model was loaded both monotonically and cyclically. The analysis conducted with monotonic loading gave a good prediction of the capacity but overestimated the stiffness of the specimen. The analysis under cyclic loading was not able to capture the important feature of the system, namely, the pinching of the hysteresis loops due to buckling and redevelopment of the tension field. The researchers recommended that more research be conducted to improve the finite element model.

Driver *et al.* (1997) also analysed their test specimen using the strip model proposed by Thorburn *et al.* (1987). The infill plate in each panel was replaced by 10 pin-ended diagonal tension strips. The angle of inclination of the tension field was obtained from equation (2.2). Using a plane frame analysis program capable of only elastic analysis, an incremental analysis was conducted up to the ultimate strength. As yielding of the strips was detected in the elastic analysis, the yielded strips were removed. The strip model gave a good prediction of the ultimate strength, but it underestimated the initial stiffness of the specimen.

2.11 Elgaaly and Liu (1997)

Earlier research by Elgaaly *et al.* (1993) showed that the strain distribution in the infill plate along a diagonal tension strip is not uniform (higher near the boundary members). As a result, yielding of the tension strips starts at the boundaries and then gradually extends towards the centre of the strips. Based on the model originally developed by Thorburn *et al.* (1983), Elgaaly and Liu (1997) introduced the concept of strip–gusset elements in order to simulate the non-uniform distribution of strain along the length of the tension strips. In this concept the strips are connected through square gusset plates at both ends to the boundary members. The dimensions of the gussets are determined by equating the buckling shear stress of the equivalent square plate to the shear yield stress of the plate material. The gusset area represents the shear zone near the boundary members that yield in shear before buckling.

To simplify the analysis, the strip–gusset elements were replaced by equivalent truss elements at an inclination of 45°. The researchers assumed that the stress versus strain relationship for the equivalent truss element is elastic, elasto–plastic, and perfectly plastic (i.e., a tri-linear behaviour). The initial yielding and the post-initial yielding modulus of the model were obtained from the strip–gusset element The equivalent truss element was developed for both welded and bolted connections of infill plate to the boundary members.

The numerical model was implemented on some of the specimens tested by Elgaaly *et al.* (1993). The numerical model was able to simulate the test results accurately. Comparing the bolted shear wall with welded shear walls, the researchers stated that, because of slippage and local deformation at the connections, a bolted shear wall can have a lower stiffness and initial yielding but the ultimate capacity is comparable provided that no premature failure of the columns or connections occurs.

2.12 Kulak, G.L., Kennedy, D.J.L., Driver, R.G., and Medhekar, M. (1999)

Kulak *et al.* (1999) conducted a numerical study of an eight-storey steel plate shear wall building to investigate the seismic performance of the system. The shear wall had a width of 8 m and storey height of 4.5 m in the first panel and 3.6 m in the remaining stories. The design base shear and the vertical distribution of lateral forces on the shear wall were obtained from the National Building Code of Canada (NBCC, 1995). The preliminary design of the shear wall was carried out by single strut idealization of the system as proposed by Thorburn *et al.* (1983). This gave a panel thickness ranging from 3.33 mm for the bottom panel to 0.66 mm for the top panel. In the order to make the plate thickness more realistic, a thickness of 4.8 mm was used for all panels. A detailed design was then carried out by using a linear static analysis program and the tension-only strip model proposed by Thorburn *et al.* (1983). The strength design satisfied both wind and seismic drift limits set by NBCC (1995). A response spectrum analysis was then carried out to estimate the effect of higher modes on the vertical distribution of lateral forces.

A pushover analysis of the system, conducted using the commercial software DRAIN-2DX, demonstrated that the structure could resist up to two times the NBCC prescribed base shear. This over-strength was largely due to using infill plate thickness of 4.8 mm, which was significantly greater than required. Although most of the plastic deformations occurred in a column at the third storey, a ductility ratio, δ / δ_y, greater than 10 was still obtained for this storey with the structure still carrying more than the NBCC shear for that panel. Therefore, the system showed significant robustness in the storey that was deforming.

The researchers also conducted a nonlinear dynamic time history analysis of the tension-compression model by applying 20 scaled earthquake records to the structure. The maximum interstorey drift ratio in any storey for the suite of 20 earthquakes considered did not exceed 0.009 (compared to a limit of 0.02 specified by NBCC). This small interstorey drift provides protection to the structural and non-structural elements of the building. The maximum calculated storey shear varied from 2.07 to 2.97 times the prescribed NBCC (1995) values. In the most severe earthquake a maximum ductility demand of $1.9\delta_y$ was calculated, which was only one-fifth of the ductility obtained from the pushover analysis. This demonstrated that a large reserve of energy dissipation exists in the system. Although significant yielding occurred in one of the columns in storeys 1 and 3, the yielding did not progress to create a soft storey since the lateral deformation of the storey as well as strains were stabilized by the elastic tension field.

2.13 Rezai (1999)

Rezai (1999) conducted the first shaking table test, using a 25% scale model of a 4-storey unstiffened steel plate shear wall. The main objective of the shaking table test was to obtain more information regarding seismic performance of the system. A similar specimen was also tested under quasi-static loading by Lubell (1997). The test specimen consisted of a four-storey one-bay steel plate shear wall with typical storey height of 900 mm and centre-to-centre column spacing of 920 mm. The beams in the lower three stories were made from S75×8 sections and a stiff S200×34 beam was used at the top storey. The columns were made of B100×9 sections over the full height of the test specimens. The column sizes differed slightly from quasi-static test specimen (a B100×9 section was used instead of a S75×8 section for the quasi-static test specimen) to increase the out–of–plane buckling strength of the columns and to accommodate the installation of lateral braces. Full moment connections were provided at all joints. An infill plate thickness of 1.5 mm was used for all panels. The infill plates were welded to the boundary frame using fish plate connections similar to those used in the Driver *et al.* (1998) investigation. Stacks of steel plates were mounted to the test specimen at each storey level to provide a 1700 kg dead load at each storey. The specimen was braced in the out–of–plane direction. The fundamental frequency of the shake table specimen with surrounding support frame was obtained as 6.1 Hz in the longitudinal direction.

Four different types of earthquake time histories at various intensities were selected as an input to the shake table test. The limited capacity of the shake table prevented attainment of the significant inelastic response in the specimen. The maximum computed tensile principal strain in the infill plate was 65% of the yield strain. Compressive principal strains were about one-third of the tensile principal strains at the centre of infill plates. The specimen deformed mainly in the first mode and the contribution of the higher mode was very small. The interstorey drift observed in the specimen during the tests demonstrated the domination of the flexural mode at the top panels. The researchers found that the first natural frequency of the specimen decreased as the intensity of the shaking increased. By comparing the measured displacements during the test with the maximum interstorey drift limitation prescribed in the National Building Code of Canada (NBCC, 1995), the researchers concluded that the design of test specimen would be governed by the drift limitation and not by strength, which is an undesirable situation. Based on this test, the researchers emphasized the importance of accurately estimating the stiffness of steel plate shear wall systems and the need for a reliable analytical tool.

2. 14 Lubell, A.S., Prion, H.G.L., Ventura, C.E., and Rezai, M. (2000)

Lubell *et al.* (2000) conducted a series of experimental and numerical investigations on quarter-scale models of unstiffened steel plate shear walls. The experimental programme consisted of two single-storey (SPSW1 and SPSW2) and one four-storey specimen (SPSW4) under cyclic quasi-static loading. The single storey specimens represented the bottom storey panel of the four-storey specimen. Column-to-column spacing and beam-to-beam dimensions were 900 mm, resulting in an aspect ratio of 1 for all the panels. All material was hot-rolled. Beam and columns were

S75×8 sections and the infill plate thickness was 1.5 mm. In specimen SPSW2 an additional S75×8 top beam was welded along adjoining flange tips to better anchor the tension field at the top of the panel whereas in SPSW4 specimen a S200×34 beam was used at the top. Rigid beam–to–column connections were provided for all joints. Specimen SPSW1 was fabricated with no special precaution to eliminate frame and plate distortion due to welding and, as a result, initial out–of–plane deformations up to 26 mm (15 times the plate thickness) were measured in the infill plate.

All the specimens were tested under quasi-static cyclic conditions. The load history followed the procedures recommended in Applied Technology Council (1992) guidelines. The single storey specimens were loaded with a horizontal cyclic load at the top of the panel. Specimen SPSW4 was loaded with equal horizontal cyclic loads at each floor level and a constant gravity load of 13.5 kN used at each floor. Gravity loads were applied using by steel masses attached to the test specimen.

Well defined elastic–plastic load deformation envelopes, high initial stiffness, good displacement ductility, and stable S-shape hysteresis behaviour were observed in the experiments. Specimen SPSW2 showed significant improvement in stiffness and capacity relative to SPSW1, mainly due to the stiffer storey beam and, to some extent, the reduction in the out–of–plane imperfections in the infill plate. The sequence of yielding in the single-panel specimens was yielding of the infill plate followed by yielding of boundary frames whereas in specimen SPSW4 the columns yielded before significant yielding in the infill plates. The less desirable behaviour observed in SPSW4 was attributed to influence of overturning moments and the small aspect ratio of the panels, which resulted in a state of global instability and termination of the test at a ductility ratio of $1.5\delta_y$.

The researchers noticed significant " pull-in" of the columns in all specimens. The inward deformation of the columns reduces the magnitude of the tension field stress near the mid-height of the storey and increases the stress near the horizontal beams at the top and bottom of the panel. In specimen SPSW2, inward column deformation resulted in the formation of plastic hinges at the top and bottom of the columns, with the specimen taking on an "hourglass" shape at the end of test. The "pull-in" effect, which was observed in these series of tests, was discussed by Montgomery and Medhekar (2001). The discussers believed that the specimens tested by Lubell *et al.* (2000) had inadequate column stiffness and unusual geometric characteristics.

Lubell *et al.* (2000) also conducted a series of numerical studies to assess the ability of the current simplified analysis technique presented in the Canadian steel design standard, CAN/CSA-S16.1-94, to accurately simulate the behaviour of their test specimens. The simplified model is basically the model proposed by Thorburn *et al.* (1983). The investigated numerical models were developed using the recommendations in the design standard and were analysed using nonlinear frame analysis software. Rigid beams were used to simulate rigid floor action.

The capacity of all the test specimens was predicted reasonably well by the numerical models. However, the elastic stiffness was significantly overpredicted for SPSW1 and SPSW4 specimens. The researchers argued that the presence of flexural modes caused by the specimen height and the small panel aspect ratio influenced significantly the behaviour of the system. An increased overturning moment in the multi-storey specimen resulted in high axial and flexural force effects in the columns and, therefore, altered the inelastic deformation characteristics of the system by changing the yielding sequence in the shear wall (columns yielding prior to the infill plate). The researchers stated that as the height of the steel plate shear wall is increased while keeping the other parameters constant, the flexural action caused by the overturning moment will dominate at the upper stories where the story shear is low. This leads to a condition that is not consistent with the panel shear mechanism assumed by Thorburn *et al.* (1983). As a result of this investigation the researchers recommended that design standards should require steel plate shear walls to be analysed as a whole since the analysis of single panel behaviour is significantly different from the multiple panel behaviour.

The researchers concluded that the current design guidelines contained in the CSA–S16–01 (CSA, 2001) may not be directly applicable to some steel plate shear walls. Although the recommended procedure in the standard shows a good correlation with the specimen post-yield strength, it may significantly overestimate the elastic stiffness under certain conditions. They also stated that current design standard provisions do not adequately address design issues related to multi-storey shear walls, including the effect of large overturning moments, influence of aspect ratio, and the potential for undesirable yielding sequences of the shear wall components.

2.15 Astaneh-Asl and Zhao (2002)

Astaneh-Asl and Zhao (2002) conducted two half-scale tests to investigate the cyclic behaviour of a steel plate shear wall system developed by Skilling Ward Magnusson Barkshire of Seattle. The system, which is shown in Figure 2.6, is a dual system where a coupled unstiffened steel plate shear wall is the primary lateral load resisting system with a ductile moment frame being used as a back up system. Large steel tubes filled with high strength concrete are used for the exterior columns whereas rolled wide flange sections are used for the interior beams and columns. The exterior columns carry a major portion of the gravity loads and contribute significantly to the storey shear resistance.

Astaneh-Asl and Zhao tested two specimens. The specimens, shown in Figure 2.7, were half-scale and representative of a two-storey (specimen 1) and a three-storey (specimen 2) portion of this system. Specimen 1 had an aspect ratio (width–to–height ratio) of 0.67 while the aspect ratio of the panels in the second specimen was 1.0. More details about the specimens can be found elsewhere (Astaneh-Asl and Zhao, 2002). To simulate the boundary condition existing at mid length of a coupling beam, the test specimens were supported on sliding load cells. The specimens were subjected to fully reversed cyclic displacements by applying a single horizontal load at the top level, which increased in a controlled manner in each cycle. Both specimens showed a very ductile behaviour and resisted a large number of inelastic cycles.

Specimen 1 resisted a total of 79 cycles, of which 39 cycles were in the inelastic range. Up to an inter-storey drift of 0.7% the behaviour was elastic. At an inter-storey drift of 2.2% local buckling occurred in the interior columns. At an inter-storey drift of 3.3% and base shear of about 4000 kN, the upper floor-coupling beam fractured at the face of the column. The fracture, which was a result of low cycle fatigue, resulted in a loss of 40% of the load and the test was terminated at this point.

Specimen 2 resisted 29 cycles of loading, of which 15 cycles were in the inelastic range. As for specimen 1, specimen 2 showed an elastic behaviour up to an inter-storey drift of about 0.7%. At an inter-storey drift of 2.2%, when the specimen had reached a base shear of 5451 kN, the upper floor-coupling beam fractured at the face of the column due to low cycle fatigue. At this point the load dropped by about 25% and the test was terminated.

Both test specimens demonstrated large ductility. Yielding of the infill plates, beams, and interior columns was found to be the main contributing factor to energy dissipation. In both specimens the coupling beams developed plastic hinges at the face of the columns and fracture occurred only after a large number of inelastic cycles. The concrete filled steel tube column behaved elastically during both tests. The performance of bolted splices was very good and, although they were slipping during the later cycles of the test, they did not fracture. The beam-to-tubular column connections also performed in a ductile manner.

2.16 Summary

Research on unstiffened steel plate shear walls has demonstrated the effectiveness of the system as a lateral load resisting system. The distinct advantages of the system are enhanced stiffness, strength and ductility, stable hysteretic characteristics and a large capacity for plastic energy absorption. The system is also believed to be more economical than an equivalent reinforced concrete shear wall (Timler and Ventura, 1999).

Despite the recent research progress on steel plate shear walls and attention from structural engineering community, to date, relatively few of these structures have been constructed in North America. The lack of codified design guidelines is likely one of the main barriers for wide application of this system. In 1994, the Canadian standard for structural steel design, CAN/CSA-S16.1-94, included a non-mandatory appendix "Design requirements for steel plate shear wall" and in the latest edition of this standard, CSA-S16-01, the appendix was moved to the body of the standard, thus making it a mandatory part of the standard. The guidance provided in the standard is based on the unstiffened thin-panel concept and the proposed analysis method is the strip model developed by Thorburn *et al.* (1983). As reported by Rezai (1999) and Lubell *et al.* (2000), the strip model cannot be considered a reliable analytical tool for all steel plate shear wall configurations. Considering the expense in conducting large-scale tests the need for a reliable analytical model that simulates accurately the monotonic and cyclic behaviour of this system is necessary. Despite many attempts to develop analytical tools for steel plate shear walls, to date no comprehensive finite element model that simulates accurately the monotonic and cyclic behaviour of thin unstiffened steel plate shear walls has been developed.

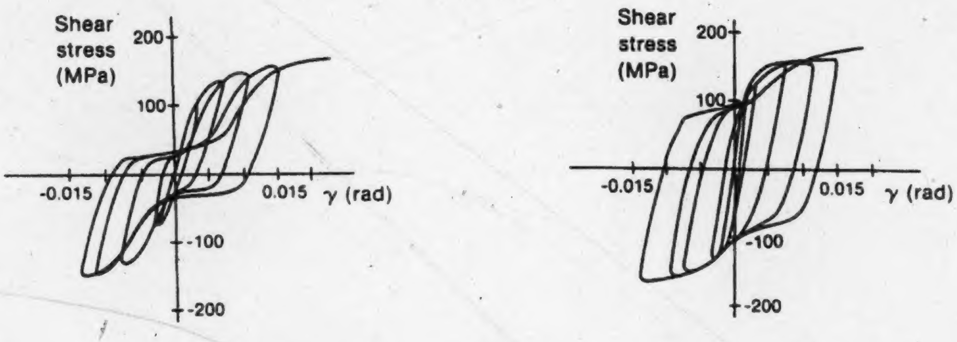

(a) Unstiffened

(b) Heavily stiffened

Figure 2.1: Hysteresis behaviour of steel plate shear walls (Takahashi *et al.*, 1973)

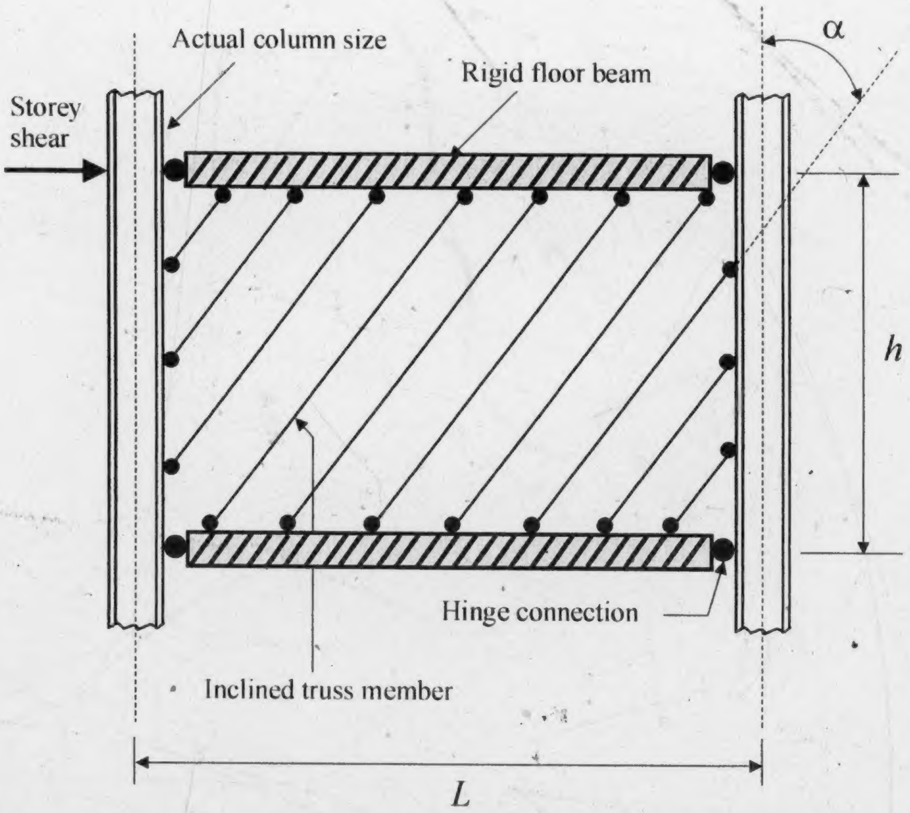
Actual column size
α
Rigid floor beam
Storey shear
h
Hinge connection
Inclined truss member
L

Figure 2.2: Strip model proposed by Thorburn and Kulak (1983)

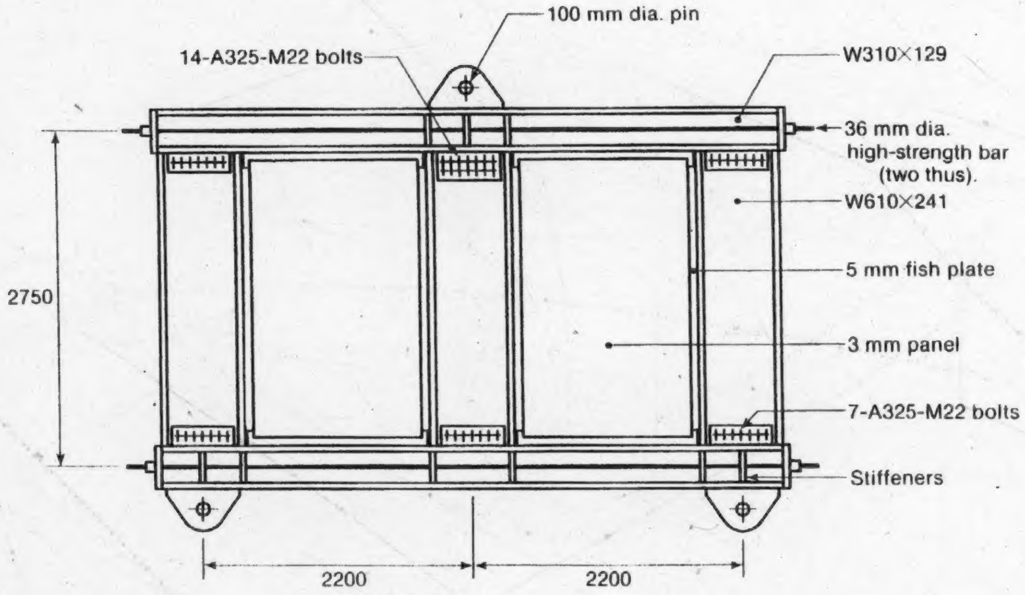
100 mm dia. pin
14-A325-M22 bolts
W310×129
36 mm dia. high-strength bar (two thus).
W610×241
5 mm fish plate
2750
3 mm panel
7-A325-M22 bolts
Stiffeners
2200
2200

Figure 2.3: Schematic of specimen tested by Tromposch and Kulak (1987)

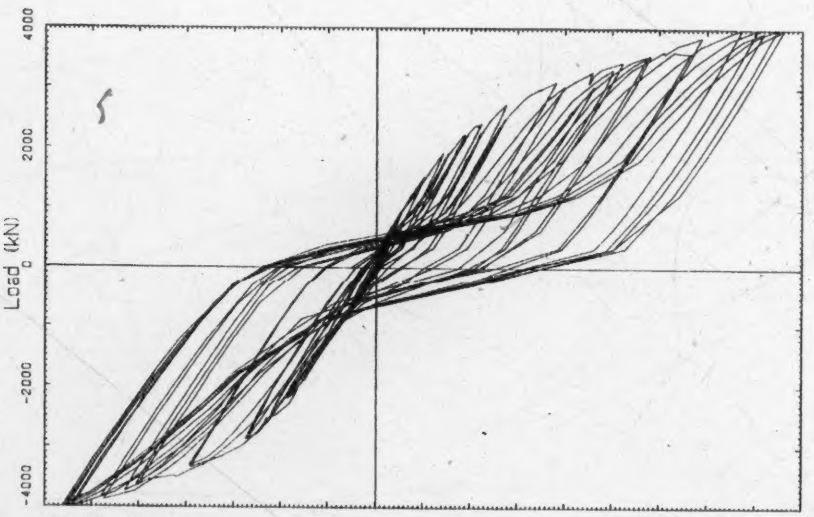

Figure 2.4: Hysteresis behaviour of specimen tested by Tromposch and Kulak (1987)

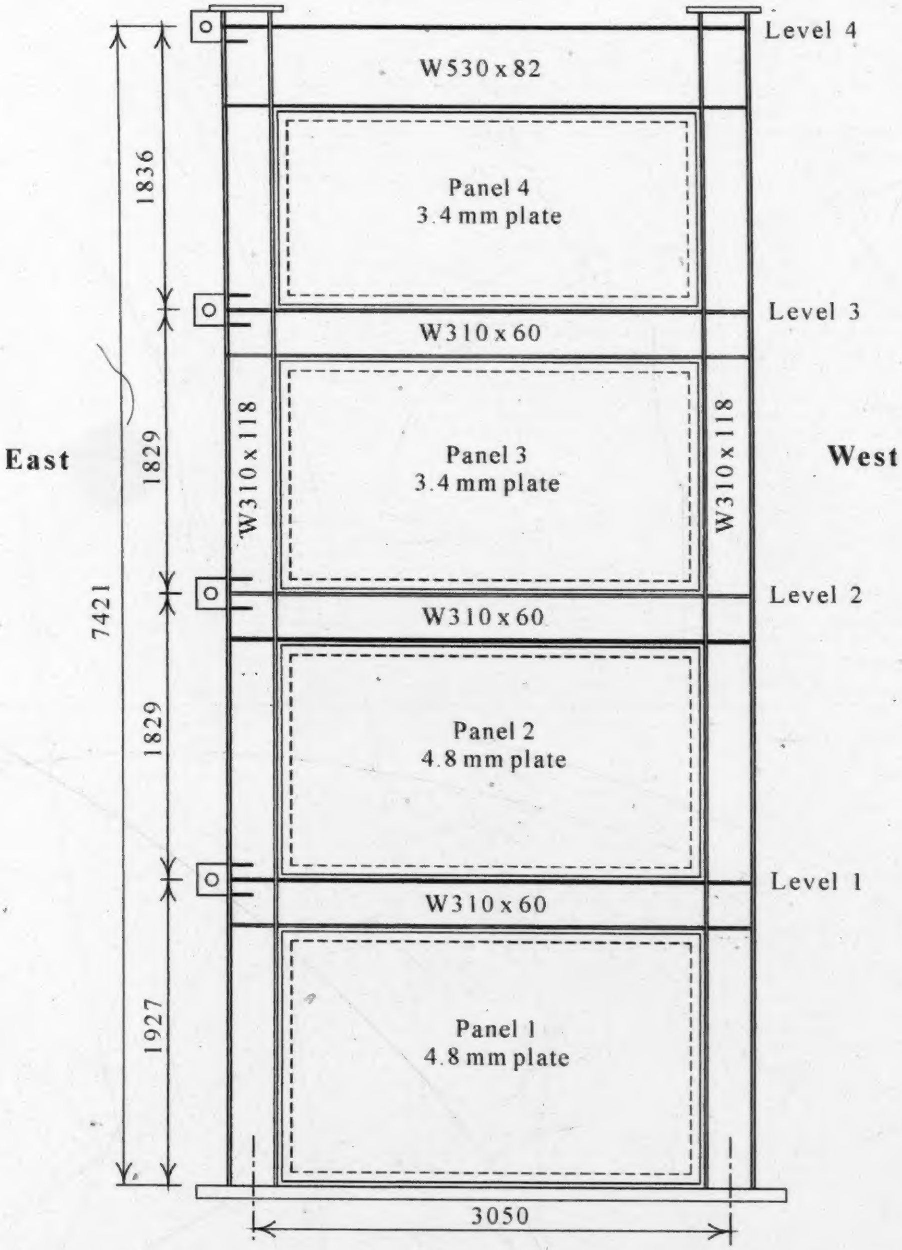
Level 4
W530 x 82
Panel 4
3.4 mm plate
Level 3
W310 x 60
Panel 3
3.4 mm plate
East
West
W310 x 118
W310 x 118
Level 2
W310 x 60
Panel 2
4.8 mm plate
Level 1
W310 x 60
Panel 1
4.8 mm plate
1836
1829
1829
1927
7421
3050

Figure 2.5: Four-storey steel plate shear wall tested by Driver *et al.* (1997)

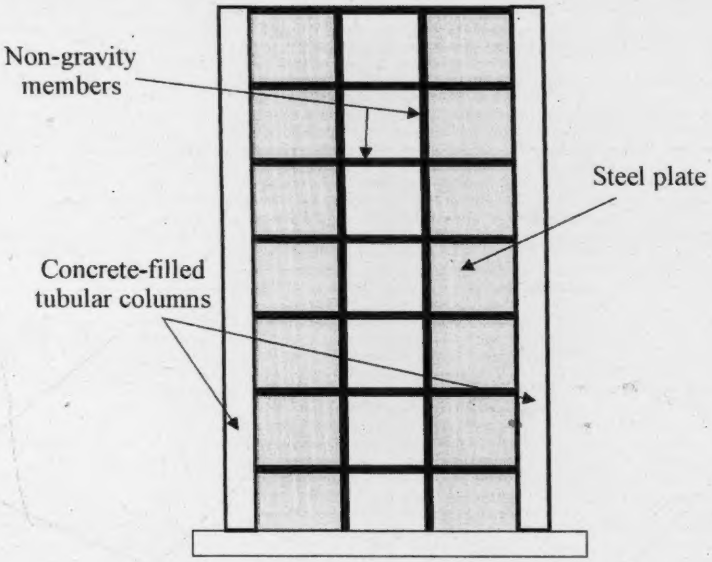
Non-gravity members
Steel plate
Concrete-filled tubular columns

Figure 2.6: Steel plate shear wall system studied by Astaneh-Asl and Zhao (2002)

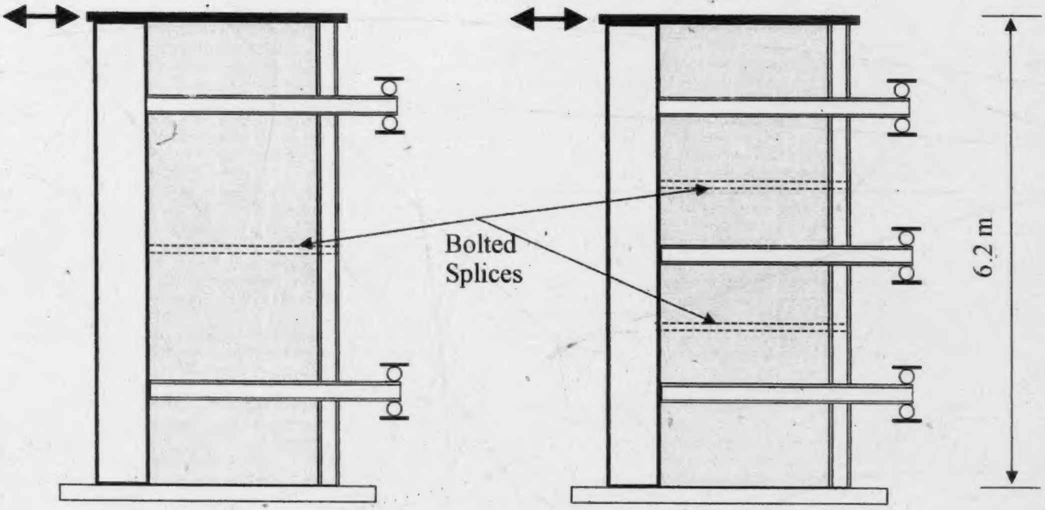
Bolted Splices
6.2 m

Specimen 1

Specimen 2

Figure 2.7: Specimens tested by Astaneh-Asl and Zhao (2002)

3 STEEL PLATE SHEAR WALL TEST

3.1 Introduction

A test on a large-scale three-storey unstiffened steel plate shear wall was conducted at the Centre for Engineering Research (C-FER) during the summer 2000. C-FER's laboratory facility is equipped with a 500 mm thick reinforced concrete reaction wall, supported by concrete buttresses. The strong wall was used to apply the horizontal loads on the steel plate shear wall specimen, which was anchored at its base to a prestressed concrete strong floor. A specially built reaction frame was used to apply gravity loads.

The test specimen consisted of the upper three storeys of the four-storey steel plate shear wall tested by Driver *et al.* (1997). Details of this test were presented in section 2.10. Most of the damage in the specimen tested by Driver was concentrated in the bottom storey and, although the infill plate in the second storey buckled and deformed plastically during the test, no significant permanent damage was noticeable in the top three storeys. For this reason, the first storey, including the beam at level 1, was removed and the remaining part was welded to a 90 mm thick base plate to provide a three-storey unstiffened steel plate shear wall specimen.

The shear wall, shown in Figure 3.1, had moment resisting beam–to–column connections with column-to-column spacing of 3050 mm and floor-to-floor spacing of 1830 mm. The infill plate thickness of panel 1, the bottom panel, was 4.8 mm and the other two panels had 3.4 mm thick infill plates. The main objectives of the testing program were to increase the database of large scale steel plate shear wall tests and to monitor closely the behaviour of the boundary members in the system. The following sections describe how the test program was conducted to meet these objectives.

3.2 Description of the test specimen

A schematic and photograph of the test specimen are shown in Figures 3.1 and 3.2, respectively. The columns consist of W310×118 sections spaced at 3050 mm, centre-to-centre and the beams are W310×60 sections at levels 1 and 2 and W530×82 at the top. The overall height of the shear wall, excluding the height of the pedestals at the top of the test specimen, is 5497 mm, with a typical storey height of 1830 mm. These dimensions are representative of a shear wall at approximately 50% scale for an office building.

Since the test specimen consisted of the top three storeys from the Driver *et al.* four-storey steel plate shear wall specimen, the lower storey, which suffered severe damage during the test, was removed by flame cutting along the top flange of the first beam, thus leaving the fish plate welded to the infill plate. The bottom edge of the three-storey test specimen was cut straight and ground in preparation for welding. The columns were connected to a 3800×800×90 mm steel base plate using full penetration groove welds for the flanges and fillet welds for the web. The fish plate for the lower storey was also welded to the base plate using fillet welds.

As reported by Driver *et al.* (1997), the grade of steel for panel 1 was G40.21-300W (CSA, 1992) and the plate thickness selected was the thinnest plate readily available in this grade (4.8 mm). In order to obtain the thinner plates used in the second and third storeys, grade A569 (ASTM, 1991) steel was used for the second storey and grade J403 GR1010 (SAE, 1994) was used for the top storey. The mean static yield strengths for the first, second, and third storey infill plates were 341 MPa, 257 MPa, and 262 MPa, respectively. The infill plates exhibited the classical stress versus strain curve of hot-rolled structural steel, that is, a well-defined yield plateau followed by strain hardening. All the beams and the columns meet the requirements of class 1 (plastic design) sections. Rigid beam–to–column connections were provided by using complete penetration groove welds for the flanges and two fillet welds for the web. Column web stiffeners were also added along the beam flanges. Weld access holes and backing bars with run-off tabs were used to ensure complete penetration and continuity of the weld across the full width of both flanges. The backing bars were left in place after fabrication, which was common industry practice at the time the specimen was fabricated. The beam–

to–column welds were deposited using a 1.6 mm flux cored wire E4802 T-9-CH. No pre- or post-heat was applied in the welding process.

The infill plates were connected to the boundary members by using a fish plate connection as shown in Figure 3.3. Continuous fish plates, 6 mm thick and 100 mm wide were fillet-welded to the boundary beams and columns. The fish plates were connected at the corners using strap plates. The infill plates were positioned against one side of the fish plates (in the plane of the beam and column webs) with a lap of approximately 40 mm all around and then welded with continuous fillet welds on both sides. This detail provides a simple means of compensating for normal dimensional tolerances in the plane of the shear wall. The fillet welds between the infill plates and fish plates were designed to develop the full capacity of the infill plate.

3.3 Preliminary numerical analysis of test specimen

In order to estimate the shear capacity and the behaviour of the wall prior to the test, a preliminary finite element analysis was carried out using the commercial general-purpose finite element software ABAQUS (Hibbitt *et al.*, 1998) The measured dimensions reported by Driver *et al.* (1997) were used in the finite element model of the specimen. All the components of the steel plate shear wall test specimen, including the beams and the columns, were modelled using four-node shell elements (element S4R in ABAQUS). All the nodes along the lower edge of the model were fixed to simulate attachment of the test specimen to the rigid base plate. The model was braced in the out–of–plane direction at beam–to–column joints as these locations were braced against out–of–plane displacement during the test. Residual stresses were not considered in the model. Since the specimen was expected to undergo large displacements and strains, both material nonlinearity and geometric nonlinearity were considered in the analysis.

Virgin material properties measured by Driver *et al.* (1997) for the four-storey shear wall were used for the preliminary finite element analysis of the test specimen, as it was not possible to measure the material properties from the three-storey specimen. A brief summary of the material properties reported by Driver *et al.* (1997) is provided in

Table 3.1. The possible impact of using these material properties on the predicted behaviour of the three-storey steel plate shear wall specimen is discussed in chapter 6. The material behaviour for both infill plates and boundary members were assumed to be initially isotropic with an elastic–plastic strain-hardening material model. Von Mises yield criterion was used as the yield surface.

Initial imperfections were considered in the finite element model. The infill plates were assumed to have an initial imperfection pattern corresponding to the buckling mode of the shear wall loaded in the same way as the test specimen. The maximum amplitude was set to 10 mm. Further refinement of the initial imperfection pattern is considered in section 5.4.2.

Because the computational demands on this system are high, due to shear buckling and localized instabilities in the infill plate, monotonic loading was used to estimate the envelope of load versus deflection response. The results of this analysis were needed for the design of the test set up. The details of the solution strategy and difficulties with convergence encountered during the analysis are discussed in detail in chapter 5. Base shear versus total displacement of the specimen at each beam level are presented in Figure 3.4. Based on the preliminary analysis, the required capacity for horizontal jacks and reaction wall and the range of motion required for the jacks and instrumentations at each level were obtained. Using 250 mm stroke jacks (125 mm limit stroke for a fully reversed loading condition) at the first and second floors and a 380 mm stroke jack at the top floor, the capacity of the specimen was estimated at 3300 kN. This was governed by the limit of jack stroke at level 2 (see Figure 3.4). At the ultimate capacity the displacement of the first and top levels, relative to the base of the specimen, was estimated at 80 mm and 165 mm, respectively.

3.4 Test set up

The test set up for the shear wall is shown in Figures 3.5 and 3.6. A 90 mm thick concrete pad (with minimum reinforcement) was placed between the base plate of the shear wall and the strong floor in order to move the specimen up to the proper elevation, suitable for installation of the horizontal jacks and connecting them to the strong wall. Fourteen 50.8 mm diameter high strength steel anchor rods were used to anchor the base plate of the shear wall to the strong floor. In order to provide more friction between the specimen and the strong floor and to reduce vertical deformations of the anchor rods under forces produced by the expected large overturning moment, all the anchor rods were pre-tensioned to 70% of their expected tensile strength.

The magnitude of the horizontal forces at different floor levels depends typically on building geometry, mass distribution and the particular earthquake event considered. Assuming simple geometry and uniform mass distribution, equal horizontal loads were applied at each floor level using 890 kN double-acting hydraulic jacks. Since the capacity of the test specimen was estimated at about 3300 kN, based on the preliminary pushover analysis of the test specimen, the hydraulic jacks at each floor should have a minimum capacity of 1100 kN. This load level exceeded the capacity of the hydraulic jacks available for this test and it was therefore necessary to pair two hydraulic jacks at each level. The detail of the connection of the hydraulic jacks at each level is shown in Figure 3.7. All six jacks were connected to a common manifold and manual valves were placed between each jack and the manifold to facilitate the application of equal forces at each floor level. The loads were applied at the level of the beam top flange to simulate the location of the inertial forces induced by floor masses. The laboratory reaction wall resisted the horizontal actuator forces.

Gravity loads of a magnitude representing reasonable unfactored values for a typical building were applied at the top of the columns. The loads were applied through a distributing beam at the top of the specimen and four calibrated tension rods connected to four 645 kN hydraulic jacks at the base (see Figure 3.5). The tension rods were connected at the top to the distributing beam outriggers (see Figure 3.5b), two at the north face and two at the south face of the shear wall. The vertical hydraulic jacks were hydraulically independent so that they could be controlled separately. This was necessary to keep the distributing beam outriggers in a horizontal position to provide full contact between the distributing beam and the top of the columns during the test. The position of the distributing beam was monitored during the test by an electronic rotation meter (clinometer), which was mounted on the distributing beam web.

To keep the axis of the tension rods vertical in a plane parallel to the specimen, all four vertical hydraulic jacks were connected separately to gravity load simulators, shown in Figure 3.5. A gravity load simulator is a pin-jointed mechanism that keeps the orientation of the tension rods close to vertical during the in-plane displacement of the shear wall. The working capacity of each gravity load simulator available for this test was 420 kN. As a result, four gravity load simulators were used to apply 540 kN vertical loads to each of the two columns of the test specimen in a symmetric configuration. The gravity load applied to each column was kept constant at 540 kN throughout the test, except during the first three lateral load cycles during which the load was 400 kN.

Out–of–plane bracing was provided at the ends of each beam (six locations) as well as at each end of the distributing beam. An articulated bracing, which is based on the principle of the Watt mechanism, was used. Since the bracing was articulated, it did not offer any significant restraint in the direction of the applied loads and did not require manual adjustment. One such brace is shown in Figure 3.5b. This system consists of three rigid links connected by ball-and-socket joints. The brace point on the specimen was connected to the mid-point of the centre link and the two other links were connected, through a ball-and-socket attachment bracket, to an independent reaction frame erected around the test specimen (see Figure 3.6). The brace points at the lower two beams were located on the columns 100 mm below the beam bottom flange in order to prevent any contact between the centre link and the horizontal connection tabs during the test. At the top level, the bracing point was on the top flange of the beam.

Since the friction between the specimen and the concrete floor was not sufficient to prevent in-plane slippage of the shear wall during the test (as reported by Driver *et al.* (1997), a heavy in-plane bracing member was designed and welded to the specimen at the base plate and connected to the strong wall by two 50 mm high strength tension rods. A schematic of this bracing is shown in Figure 3.8

3.5 Instrumentation and data acquisition

All the kinematic parameters that seemed to be important either in interpreting the results or in controlling the test were measured. The following forces and displacements were monitored and recorded during the test: horizontal load and in-plane displacement at each floor level and at the base plate; gravity loads in the columns; out–of–plane displacement of the wall at the joints to ensure that the frame remained in the plane of the applied loads throughout the test; strains at 20 cross-sections in the columns and in the beams; and the orientation of the tension field in panels 1 and 2. The location of the instrumentation used to measure strains and displacements is shown in Figure 3.9.

Horizontal loads at each floor level were measured with custom–built load cells, manufactured at the University of Alberta. The load cells, shown in Figure 3.7, were placed between the double clevis, connecting the two jacks, and the horizontal connection tabs at each level. To provide extra measurement for horizontal loads, two pressure transducers were used to measure the oil pressure in the horizontal jacks. There was an excellent agreement between the horizontal load cells and the measurement by pressure transducers. The difference between the two measurements was always less than 1%.

Commercial, flat load cells of 890 kN capacity, shown in Figure 3.5a, were used to measure the vertical loads on the top of each column. Four strain gauges were mounted to each tension rod in a Wheatstone bridge circuit and calibrated so that they acted as additional load cells. This provided a redundant set of measurements for gravity loads. There was an excellent agreement between the two measurements and the difference remained below 2% throughout the test.

In-plane displacements were measured at each of the three levels of the shear wall using three long–range cable transducers. Out–of–plane displacements at all beam–to–column connections were measured using six linearly variable displacement transformers (LVDTs) to assess the effectiveness of the lateral bracing during the test. Measurements were also taken to monitor any movements of the base plates. Two LVDTs were used to measure the in-plane slippage of the base plate. Any out–of–plane movement of the base plate, resulting from rigid body translation and rotation of the base plate about a vertical axis, was captured with two mechanical dial gauges that monitored the transverse displacement at the north east and north west corners of the base plate. In order to assess the anchorage of the base plate to the strong floor, four LVDTs and two dial gauges were installed on the base plate to measure any vertical displacement. The LVDTs were installed on the north and the south sides of both columns and the dial gauges were placed at intermediate locations between the anchor bolts. Figure 3.9 shows the location of all translational measurement devices.

Three clinometers were used to measure the rotation of the shear wall at the points of attachment of the hydraulic jacks to the test specimen (see Figure 3.9). In addition, one clinometer was installed on the web of the distributing beam to monitor the condition of the distributing beam. This rotation was controlled during the test by adjusting the gravity loads in the jacks on the north and south sides of the wall to make the distributing beam outriggers horizontal at the desired gravity load.

To study the behaviour of beams and columns, especially of the boundary members around the second panel and the columns at the first level, a total of 91 strain gauges were mounted at twenty different sections as shown in Figure 3.9. Most of the strain gauges were placed on the boundary members of the second panel for two reasons. First, the second panel was an intermediate panel and, therefore, its behaviour is more representative of the behaviour of most panels in a multi-storey frame. Second, the preliminary finite element analysis of the test specimen indicated that the second panel might be more critical than the first panel. To avoid localized effects from the beam–to–column connections, the strain gauges were placed at least 300 mm (almost the depth of beam or column) away from the connections. In order to obtain an estimate of the average strain in the flange at any cross-section, two strain gauges were positioned longitudinally on each flange at each cross-section. In addition, strain gauges were mounted at mid-depth at some cross-sections in order to evaluate the distribution of axial strain across the depth. The measured strains were used to evaluate the bending moments and axial forces at instrumented cross-sections. All the strain gauges were single grid electrical resistance gauges with a gauge length of 5 mm.

A data acquisition system with 130 channels was used to read the input from the electronic devices during the test. The data was processed using the commercial software Lab View® to plot the load versus deflection curves for all panels and to monitor the parameters that were important to control the test. The dial gauges used to monitor the base plate movements were recorded manually and were closely monitored throughout the test to ensure that no undesirable displacements were imposed on the test specimen.

3.6 Loading protocol

The test was conducted under fully reversed cyclic loading based on the recommendations outlined in ATC-24 (Applied Technology Council, 1992). The document provides guidance on loading history and the presentation of the results for slow cyclic loading tests. Based on ATC-24 a "deformation control parameter"(taken here as some parameter related to interstorey drift) should be selected for controlling the test in the inelastic range. In multi-storey buildings, usually the majority of deformation and energy absorption takes place in the bottom storeys. The deformation control parameter selected for this test was the interstorey drift in the second panel. The selection of this parameter for controlling the test in the inelastic phase was based on the preliminary pushover analysis of the test specimen, which indicated that buckling and yielding of the second panel would initiate slightly before the first panel due to the smaller thickness and lower yield strength of the panel in the second storey. During the test signs of yielding were indeed detected in the second panel earlier than in the first panel. Lateral loads were applied to the test specimen very slowly in order to simulate a quasi-static condition. In each plastic cycle and before recording the data, the target displacement at both excursions were maintained for a while to allow yielding and plastic deformation take place in the specimen. In average about one cycle per day were applied to the test specimen.

Before application of the lateral loads, a gravity load of 400 kN was applied at the top of each column. This load was maintained constant for the first three cycles while the lateral loads were applied to the test specimen. After the third loading cycle, the gravity load in the columns was increased to 540 kN and kept constant for the remainder of the test. The application of the gravity loads did not cause any visible signs of distress anywhere in the test specimen.

The point of significant yielding (δ_y, Q_y), which is the essential parameter for controlling the test in the inelastic range, was first estimated from the preliminary finite element analysis. It was estimated that the shear wall would undergo significant yielding (detected from plots of load versus displacements) at a base shear, Q_y, of 2650 kN. During the test, significant yielding was observed first in the second panel in load cycle 10 at a base shear Q_y=2300 kN. The drift at significant yielding, δ_y, was determined to be 9.5 mm when the test specimen was pushed in the west direction and 7.0 mm when pulled in the east direction. Since the drift in panel 2 at significant yielding was not the same in both directions, the smaller of the two values was used for controlling the test (*i.e.*, δ_y = 7.0 mm). The reason for the lack of symmetrical behaviour observed in the test specimen will be discussed in Chapter 4.

Prior to the point of significant yielding, the test was conducted under load control condition. Single loading cycles, resulting in a base shear of ±200 kN, ±400 kN, ±600 kN and three blocks of cycles with ±1000 kN and ±2020 kN were applied to investigate the elastic and early inelastic behaviour, which constituted cycles 1 to 9. After cycles 10,11, and 12 with a second storey drift of 9.5 mm in the west direction and 7.0 mm in the east direction, the drift of the second storey was increased by δ_y = 7.0 mm in each subsequent deformation step. Based on the ATC-24 guideline, three cycles were applied at each deformation step up to a deformation of $3\delta_y$ (cycles 16-18). Two cycles were applied at each deformation step thereafter.

In cycle 21, when the specimen was being loaded in the east direction, an unexpected fracture occurred at the east beam–to–column connection at the first level at a base shear of 3400 kN. This fracture resulted in only a slight reduction of base shear, mainly because the test was being conducted under displacement control. After completing that cycle, which reached a target drift of $\pm 5\delta_y$, the connection was repaired and the remaining cycles were conducted to the full stroke of the hydraulic jacks to obtain the capacity and investigate the behaviour of the specimen beyond the peak load. The test was ended after cycle 24. Although the specimen had not yet failed at this time, severe local buckling deformations in the beam at level 1 and in the columns at the base, and the rapid growth of plate tears in panel 1, indicated potential rapid deterioration of the test specimen.

Table 3.2 shows the loading protocol used to conduct the test. Cycles designated as + or – refer to loading in the west and in the east directions (away from or towards the reaction wall), respectively.

Table 3.1: Material properties used for analysis of the three-storey steel plate shear wall (taken from Driver *et al.*, 1997)

	Elastic Modulus (MPa)	Static Yield (MPa)	Static Ultimate (MPa)	Yield Strain %	Hardening Strain %	Ultimate Strain %	Rupture Strain %
W310×118	203 000	313	482	0.169	1.41	15.5	26.3
W310×60	203 900	332	478	0.191	1.76	16.8	26.2
W530×82	206 100	349	493	0.204	1.85	15.5	28.2
Panel 1	208 800	341	456	0.175	2.62	20.1	34.2
Panel 2	210 900	257	344	0.134	2.44	20.0	42.5
Panel 3	203 100	262	375	0.145	1.53	17.7	34.1

Table 3.2:Loading protocol for quasi-static cyclic test of three-storey steel plate shear wall

Cycle No.	Behaviour	Push (Load applied in west direction)		Pull (Load applied in east direction)	
		Base Shear (kN)	2nd Panel drift (mm)	Base Shear (kN)	2nd Panel drift (mm)
1	Elastic	+200	0.75	-200	-0.2
2	Elastic	+400	1.6	-400	-.75
3	Elastic	+600	2.0	-600	-1.8
4	Elastic	+1000	3.7	-1000	-2.8
5	Elastic	+1000	3.7	-1000	-2.9
6	Elastic	+1000	3.6	-1000	-2.8
7	Elastic	+2025	7.3	-2025	-6
8	Elastic	+2025	7.9	-2025	-5.7
9	Elastic	+2025	8.0	-2025	5.7
10[a]	Plastic	+2290	+9.5	-2300	-7.0
11	Plastic	+2282	+9.5	-2280	-7.0
12	Plastic	+2265	+9.5	-2295	-7.0
13	Plastic	+2679	+14	-2876	-14
14	Plastic	+2696	+14	-2860	-14
15	Plastic	+2710	+14	-2848	-14
16	Plastic	+2963	+21	-3174	-21
17	Plastic	+2970	+21	-3182	-21
18	Plastic	+2961	+21	-3123	-21
19	Plastic	+3174	+28	-3419	-28
20	Plastic	+3208	+28	-3430	-28
21	Plastic	+3313	+35	-3423	-35
22[b]	Plastic	+3339	+55	-3343	-32.8
23[c]	Plastic	+3163	+53.8	-3272	-31.6
24	Plastic	+2848	+55	—	—

[a] Significant yielding observed in second panel.

[b] Push and pull to the maximum stroke of hydraulic jacks. The specimen reached its maximum base shear of 3500 kN in the east and west directions at a second storey drift of +50.8 mm in the west direction and a second storey drift of – 31.4 mm in the east direction.

[c] Pushed and pulled to the maximum stroke of the hydraulic jack at level 2.

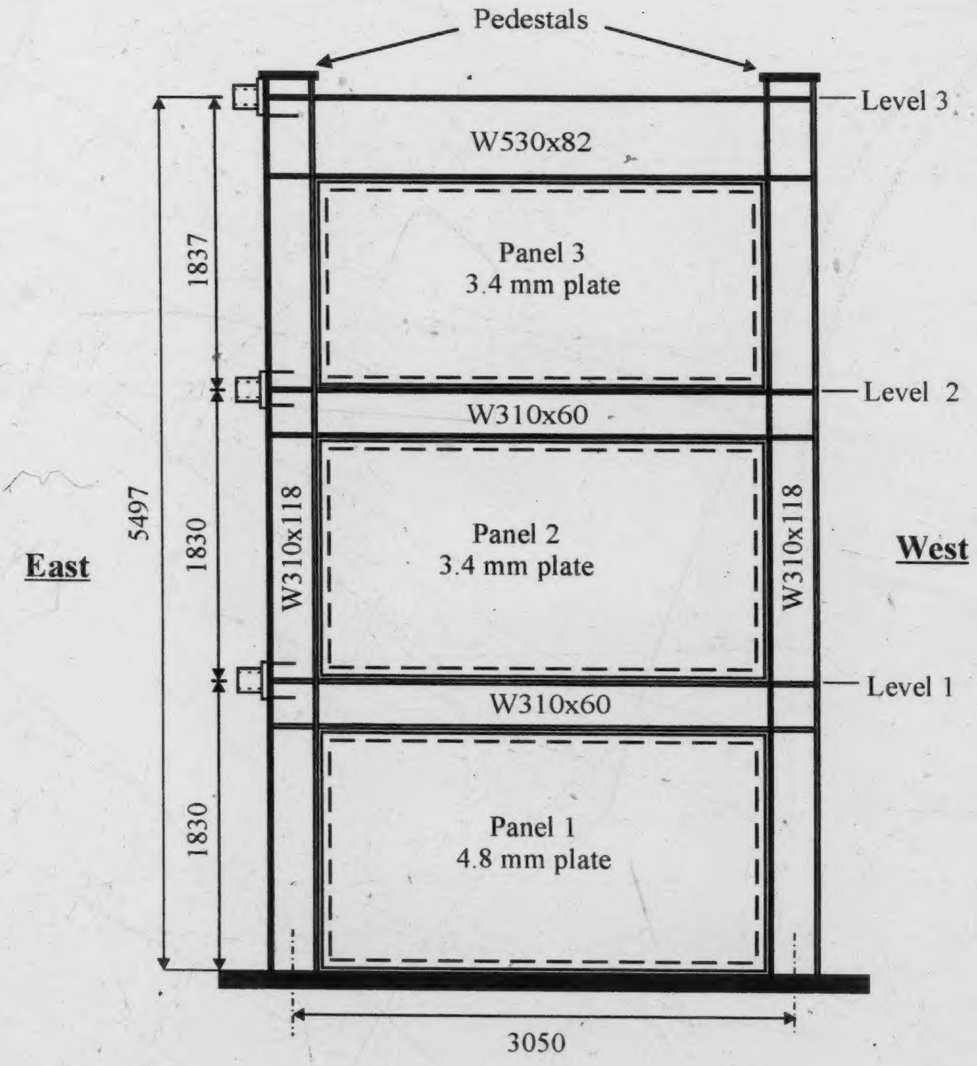
Pedestals
Level 3
W530x82
1837
Panel 3
3.4 mm plate
Level 2
W310x60
5497
1830
East
W310x118
Panel 2
3.4 mm plate
W310x118
West
Level 1
W310x60
1830
Panel 1
4.8 mm plate
3050

Figure 3.1: Schematic of three-storey steel plate shear wall

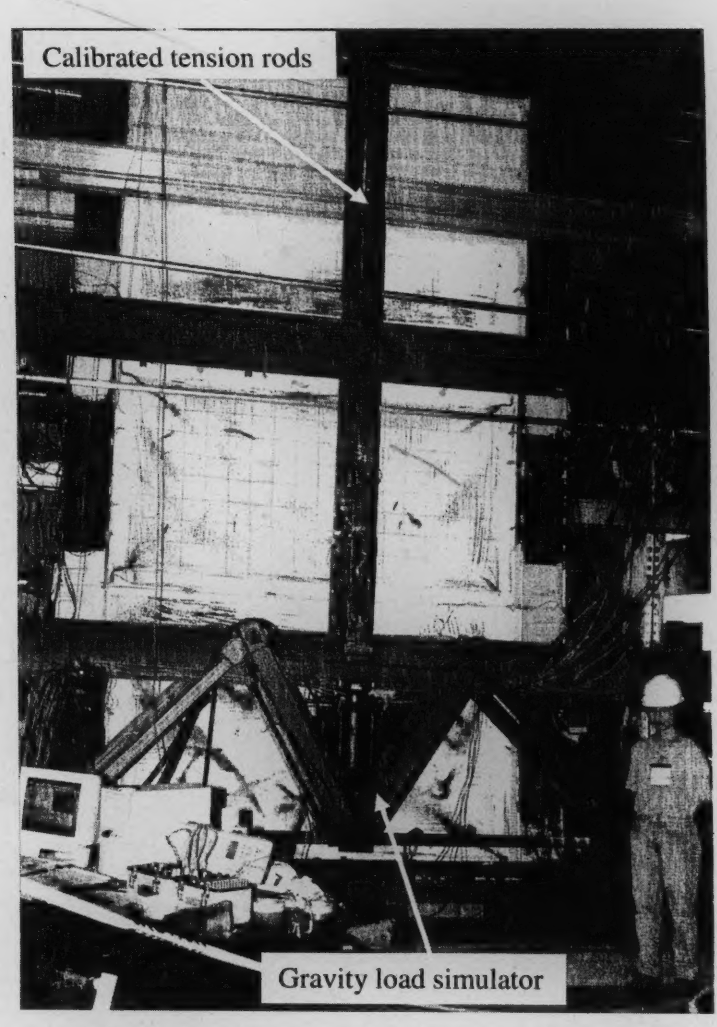
Calibrated tension rods
Gravity load simulator

Figure 3.2: Three-storey steel plate shear wall specimen

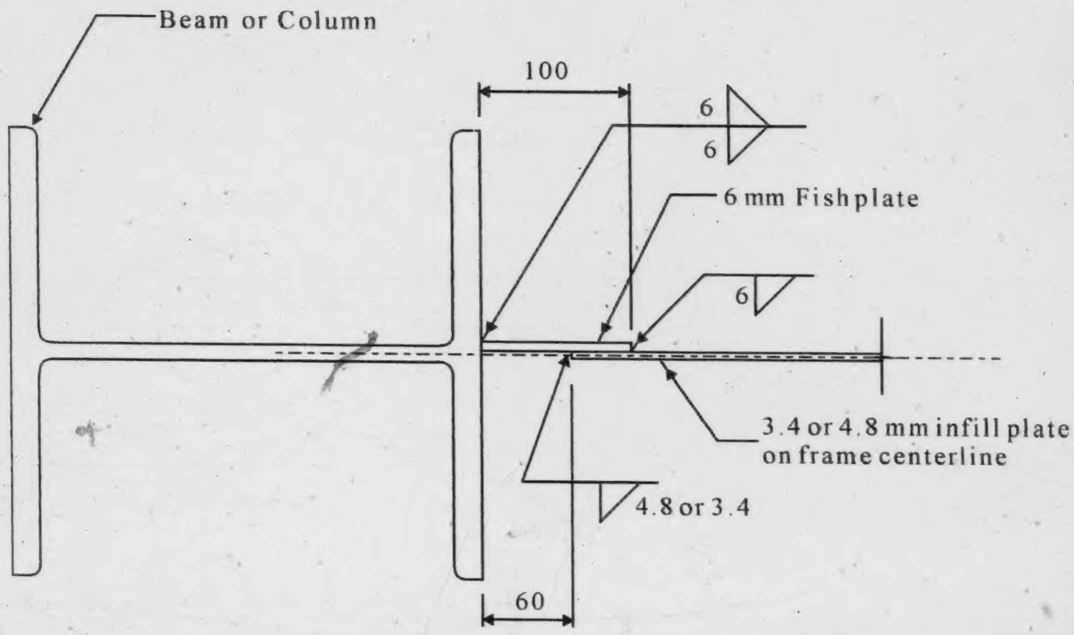
Beam or Column
100
6
6
6 mm Fishplate
6
3.4 or 4.8 mm infill plate on frame centerline
4.8 or 3.4
60

Figure 3.3: Fish plate detail used for connection of infill plate to the frame

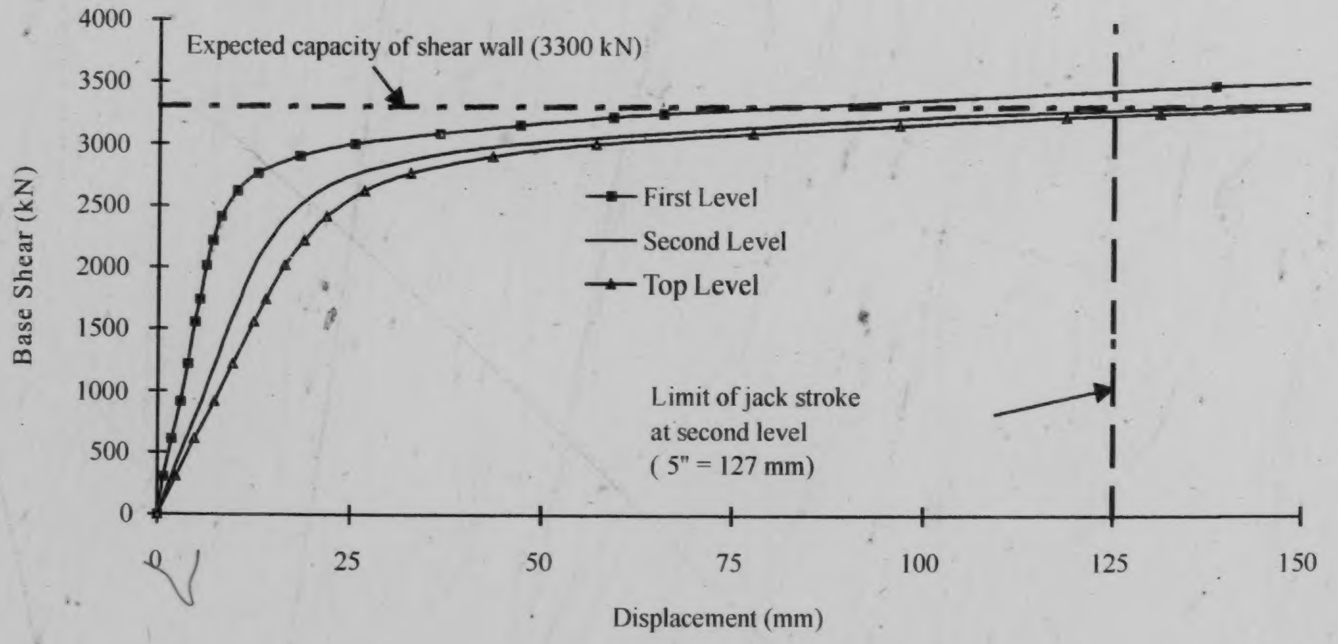

Figure 3.4: Preliminary finite element analysis of test specimen

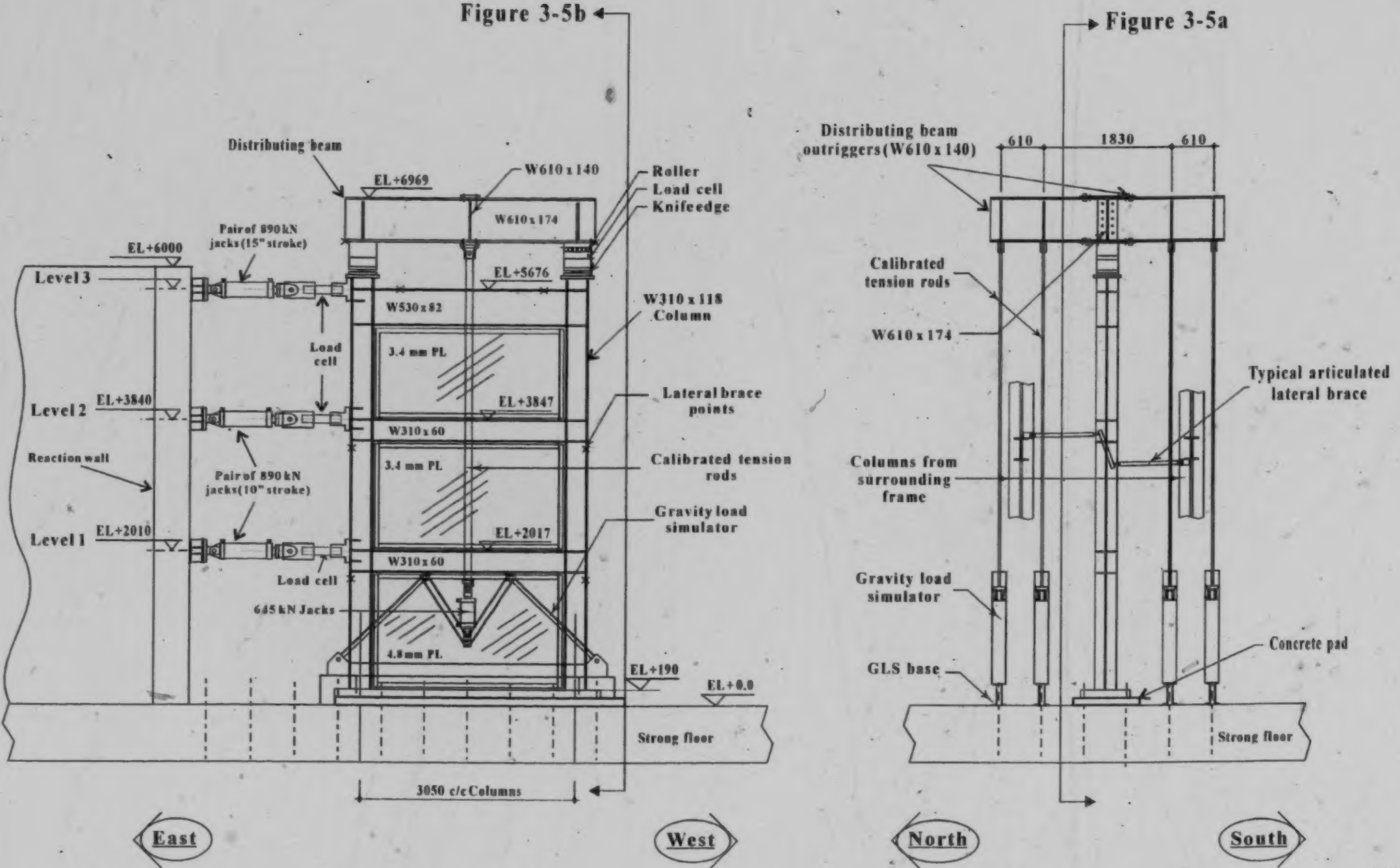
Figure 3-5b
Figure 3-5a
Distributing beam
EL+6969
W610 x 140
W610 x 174
Roller
Load cell
Knifeedge
EL+6000
Level 3
Pair of 890 kN jacks(15" stroke)
EL+5676
W530 x 82
W310 x 118 Column
Load cell
3.4 mm PL
Level 2
EL+3840
EL+3847
Lateral brace points
W310 x 60
Reaction wall
Pair of 890 kN jacks(10" stroke)
3.4 mm PL
Calibrated tension rods
Gravity load simulator
Level 1
EL+2010
EL+2017
W310 x 60
Load cell
645 kN Jacks
4.8 mm PL
EL+190
EL+0.0
Strong floor
3050 c/c Columns
East
West
Distributing beam outriggers(W610 x 140)
610
1830
610
Calibrated tension rods
W610 x 174
Typical articulated lateral brace
Columns from surrounding frame
Gravity load simulator
Concrete pad
GLS base
Strong floor
North
South

(a) North elevation

(b) West elevation

Figure 3.5: Three-storey steel plate shear wall test set up

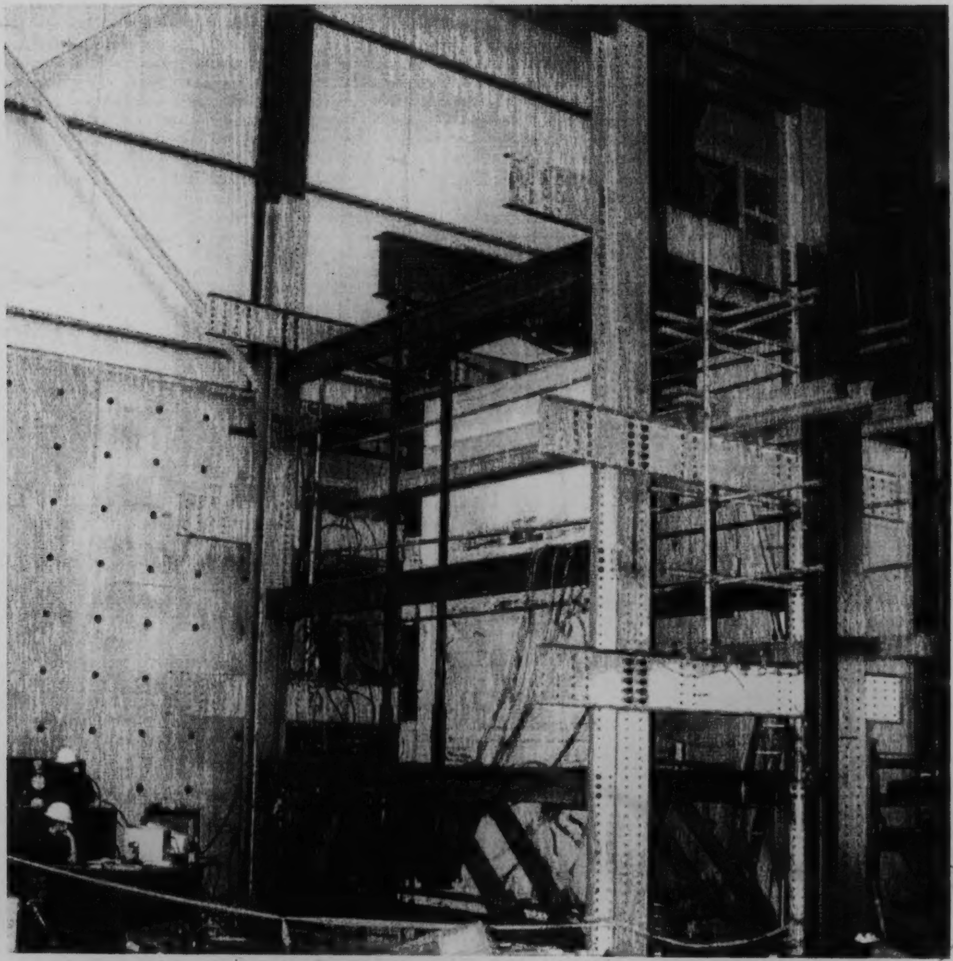

Figure 3.6:Overview of test set up

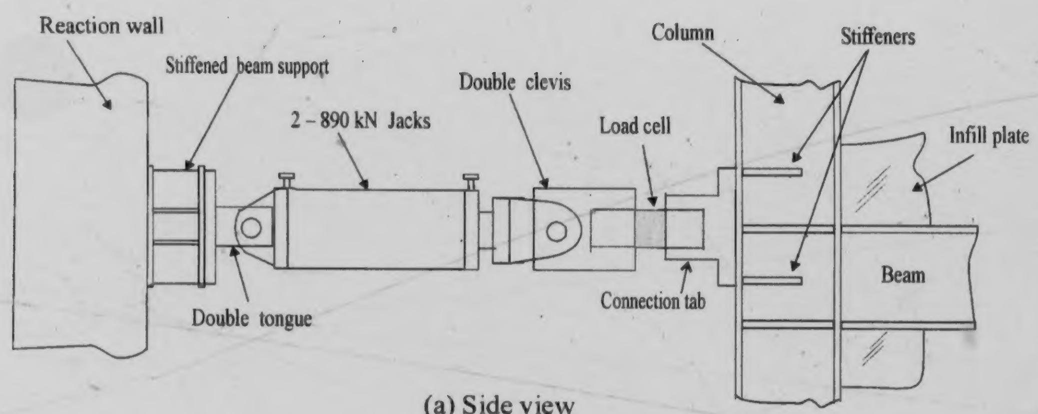
Reaction wall
Stiffened beam support
2 – 890 kN Jacks
Double clevis
Column
Stiffeners
Load cell
Infill plate
Beam
Double tongue
Connection tab

(a) Side view

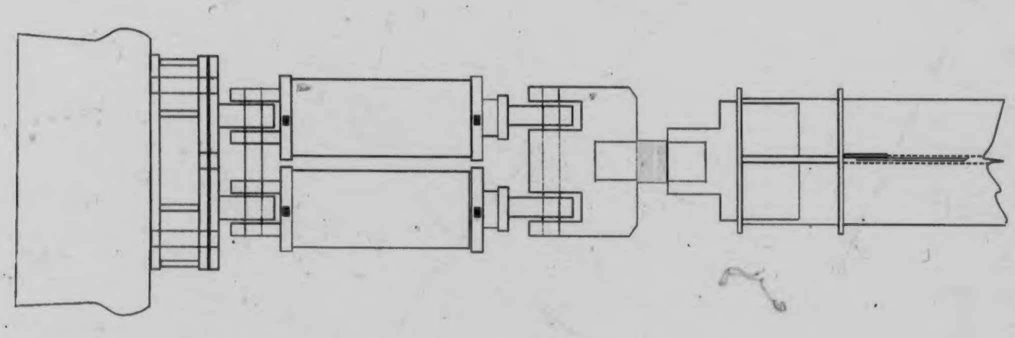

(b) Top view

Figure 3.7: Detail of connection of hydraulic jacks to the test specimen

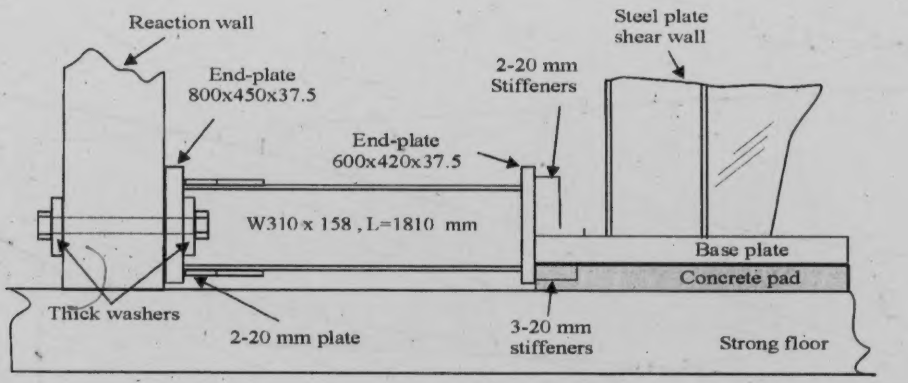
Reaction wall
Steel plate shear wall
End-plate 800x450x37.5
2-20 mm Stiffeners
End-plate 600x420x37.5
W310 x 158 , L=1810 mm
Base plate
Concrete pad
Thick washers
2-20 mm plate
3-20 mm stiffeners
Strong floor

(a) Side view

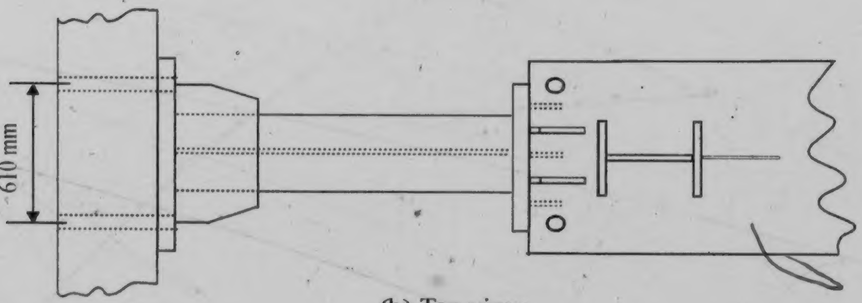

(b) Top view

Figure 3.8: Schematic of in-plane bracing at the base of specimen

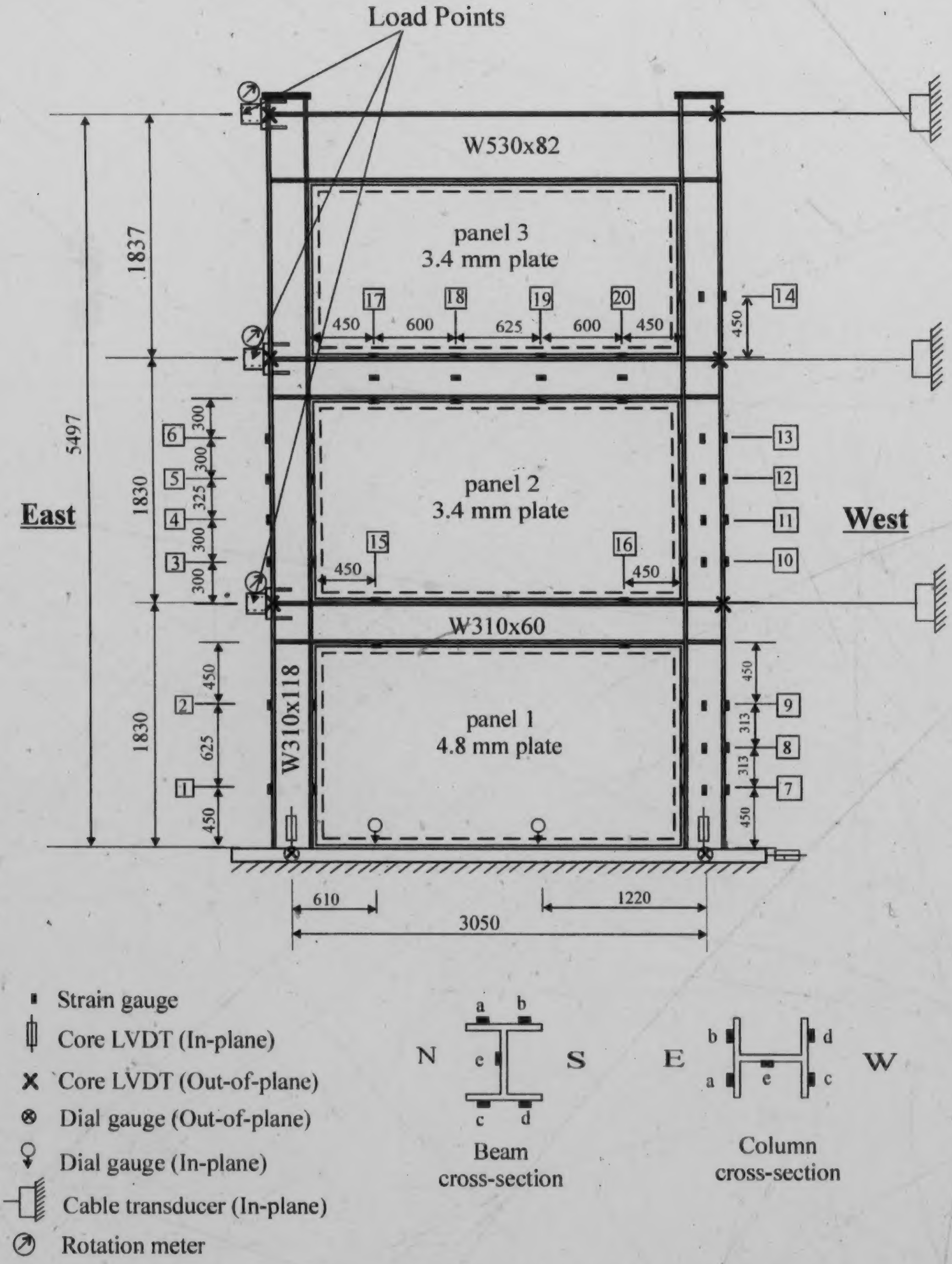
Load Points
W530x82
panel 3
3.4 mm plate
17
18
19
20
450
600
625
600
450
14
450
1837
5497
East
West
6
5
4
3
300
300
325
300
300
1830
panel 2
3.4 mm plate
15
16
450
450
13
12
11
10
W310x60
W310x118
2
1
450
625
450
1830
panel 1
4.8 mm plate
9
8
7
450
313
313
450
610
1220
3050
Strain gauge
Core LVDT (In-plane)
Core LVDT (Out-of-plane)
Dial gauge (Out-of-plane)
Dial gauge (In-plane)
Cable transducer (In-plane)
Rotation meter
N
a
b
c
e
d
S
Beam
cross-section
E
b
d
a
e
c
W
Column
cross-section

Figure 3.9: Instrumentation used to measure strains and displacements

4 DISCUSSION OF TEST RESULTS

4.1 Introduction

The three-storey steel plate shear wall test specimen performed very well during the test. The specimen reached an ultimate load of 3500 kN and a displacement ductility of $7.9\delta_y$. The maximum load predicted by the preliminary finite element model was slightly lower than the maximum load achieved in the test but the stiffness of the specimen was the same as predicted by the finite element model. Although one of the beam–to–column connections fractured during the test, this fracture had no significant impact on the load carrying capacity of the system. The large ductility, the system redundancy, and the high energy absorption capability of steel plate shear walls once again demonstrated the ability of the system to resist extreme cyclic loading representative of severe earthquakes.

This chapter presents a discussion of the general behaviour of the steel plate shear wall specimen observed during testing. A discussion of the data obtained from the strain gauges mounted on the beams and columns is postponed until chapter 7.

4.2. Gravity load application

Gravity loads were applied at the top of each column through a distributing beam installed on the top of the shear wall. For the first three loading cycles only 75% of the target gravity load, i.e. 400 kN, was applied to each column in order to check the functionality of gravity load simulators. For the remaining cycles of the test, the full gravity load of 540 kN was applied to each column. During the application of gravity load no yielding or significant deformation was observed in any part of the test specimen.

4.3 Specimen behaviour during the test

4.3.1 Cycles before significant yielding

The response of the shear wall during the first nine cycles was virtually linear despite some localized yielding detected in the infill plate. The first yield line was detected in the bottom west corner of panel 2 during cycle 7 at a base shear of 1800 kN (51% of the test specimen capacity) when the specimen was pulled in the east direction (see Figure 4.1). The yield lines were vertical lines adjacent to the fish plate, indicating high horizontal tensile stresses in that area due to development of diagonal tension field. In addition, local yielding was observed at the base of the east column and some localized yielding was observed at the bottom west corner of panel 1 during cycles 7, 8 and 9. None of these signs of local yielding had any noticeable effect on the global load versus deflection response of the shear wall and the behaviour remained linear elastic.

4.3.2 Cycles after significant yielding

The first cycle following significant yielding was cycle 10. In this cycle the base shear reached 2290 kN as the lateral loads were applied in the west direction, corresponding to a drift of 9.5 mm in panel 2. A base shear of 2300 kN was reached in the opposite direction, corresponding to drift of 7 mm in panel 2. Yield lines developed around the fish plate to infill plate connections at both top corners and the bottom east corner of the first panel. New yield lines formed in the second storey infill plate and in the web of the beam at level 1 (see Figure 4.2). Buckling of panels 1 and 2 was accompanied by several loud reports as the plate buckles popped through and reoriented themselves upon reversal of the loading direction. These loud reports were heard in all subsequent cycles. The average orientation of the buckles (measured relative to the vertical) that formed during this series of cycles was found to be about 47.4° in panel 1 and 46.8° in panel 2 (with a standard deviation of 3° in panel 1 and 1.2° in panel 2). The angle of the buckles, measured at their crest, corresponds to the orientation of the tension field. This angle changed slightly during the later cycles as will be discussed in section 4.5. Cycles 11 and 12 were applied in the same manner as cycle 10.

The next block of three cycles was carried out at a second storey drift equal to twice the storey drift at significant yielding ($\delta = 2\ \delta_y = 14$ mm). During the first cycle of this block (i.e. cycle 13) the yield lines extended over the full surface of panel 2 and the beam web at level 1. Figure 4.3 shows the extent of yielding in panel 2 in the following cycle (cycle 14). More yield lines developed in the infill plate at the first level during cycle 13, mainly around the fish plate at the corners and in the top half region of the infill plate. In this cycle, the first signs of yielding in panel 3 were detected along the bottom fish plate and in the bottom corners of the infill plate at the top level. In addition, yield lines were observed in the web of the beam at level 2 at both ends. The applied base shears in the east and west directions were about 2860 kN and 2700 kN, respectively, during this deformation step ($\delta = 2\delta_y$).

The first sign of yielding in the web and the flanges of the columns in the first storey, immediately below the beam at level 1, was observed during cycle 16 ($\delta = 3\ \delta_y$). The yielding at the base of both columns was pronounced and yielding extended further in the beam web at level 2 and in infill panel 3. The base shear in this block of cycles varied from 2963 kN in the west direction to 3182 kN in the east direction.

Starting from cycle 19, the first cycle at the second storey drift of 4 $\delta_y = 28$ mm, each displacement block consisted of two cycles only. In cycle 20, flange local buckling was detected at both ends of the beam at the first level near the beam–to–column connection (see Figure 4.4). Local buckling in the west flange of the east column was also observed at a distance of 300 mm below the beam at level 1. Cycle 20 was the second cycle in this block of two cycles with the base shear varying from 3200 kN in the west direction to 3420 kN in the east direction.

A 15 mm tear at the bottom east corner of the infill plate of panel 1 was observed in cycle 21 ($\delta = 5\ \delta_y$). The tear was initiated by low cycle fatigue resulting from the cyclic kinking of the infill plate at the corner of the panel as the infill plate buckled cyclically with load reversals. Four tears were also observed at the top west and bottom east corners of panel 2 around the strap plate and one tear was observed at the top east corner. The tears in panel 2 initiated in the fish plates or in the strap plates. At this time, the local buckles at both ends of the beam at level 1 and in the west column had grown significantly. As the load was reversed in cycle 21, local buckling was observed at the base of the east column. The load reversal caused the existing tears to open more. At a base shear of 3400 kN, applied in the east direction, sudden rupture of the beam top flange of level 1 at the east beam–to–column connection occurred. The fracture of the beam–to–column connection, shown in Figure 4.5, seems to have initiated at the beam flange–to–web junction and propagated outward towards the flange tips. Because the fracture was later repaired, it was not possible to examine the fracture surface to determine the exact origin of the flange rupture. The fracture also extended in the web at a distance of about 45 mm. Because the test was conducted under displacement control, fracture of the flange caused a reduction of base shear of 200 kN. The shear wall was still able to carry more loads and, despite the beam failure, cycle 21 was completed under a base shear of 3420 kN.

Rupture of the beam flange also triggered the formation of a large crack in the infill plate of panel 2. It was suspected that the rupture of the beam–to–column connection and the large tear at the corner of panel 2 might affect the behaviour of the shear wall. Since one objective of the test was to evaluate the maximum capacity of the wall and investigate the behaviour of infill plates under extreme loading conditions, the beam–to–column connection was repaired after completing cycle 21. The connection repair consisted of gouging the crack in the flange, web, fish plate and infill plate, re-welding the crack and adding welded moment plates to the joint at the top flange. The moment plates, consisting of two plates half the width of the beam flange, were placed on both sides of the infill plate and were fillet welded to the beam and column flanges The repair thus prevented further local buckling distortion of the beam flange at the face of the column.

Testing of the specimen resumed after repair of the connection. In cycle 22, the wall was loaded until the limit of the stroke of the hydraulic jacks in both directions was reached in order to determine the capacity of the shear wall. The shear wall reached its base shear capacity in both directions, namely, 3530 kN in the west direction and 3500 kN in the east direction. In both directions the load started on a descending branch before the stroke capacity of the actuators was reached. The maximum storey drift in panel 2 during cycle 22 was 55 mm ($\delta = 7.9\delta_y$) in the west direction and 33 mm

($\delta = 4.7\delta_y$) in the east direction. The stroke limit in the hydraulic jacks at level 2 was reached sooner in the east direction because of the unsymmetrical drift observed in panel 1. The local buckling distortion of the west column flange, shown in Figure 4.6, was severe, both at level 1 and at the base. The magnitude of the distortion when the column was in compression due to the overturning moment reached a magnitude of 70 mm. During this cycle, new tears were detected in panel 1.

Cycle 22 was repeated to investigate how the specimen would behave after the load carrying capacity in the previous cycle had started to decrease. During cycle 23 the shear wall reached a base shear of 3160 kN in the west direction and 3270 kN in the east direction. This represents a decrease in capacity of 10% in the west direction and 6% in the east direction. It should be noted that in this cycle the wall did not reach its peak capacity in the east direction because of the stroke limitation of the hydraulic jack at the second level. The reduction of 6% is therefore an overestimate of the reduction in capacity in the east direction. It is believed that the observed degradation of the shear wall capacity was caused by an increase in the number of tears, growth of the existing tears, and local buckling of the boundary members.

The size of the tear in the bottom east corner of panel 1, which was 15 mm in cycle 21, reached 300 mm in cycle 22 and 540 mm in cycle 23. The tear, shown in Figure 4.7, was oriented perpendicular to the tension field, thus reducing anchorage of the tension field at the corner of the infill plate.

The test was completed with one half cycle applied in the west direction. Once again, the storey drift in panel 2 was brought to 55 mm in the west direction. The maximum base shear reached in this half cycle was 2850 kN, which represents a 10% reduction from the previous cycle. The test was terminated at this point. The shear wall specimen at the end of the test is shown in Figure 4.8 and the location of observed tearing is depicted in Figure 4.9. It can be seen that, despite the fact that panel 1 sustained the most damage, panel 2 also sustained severe plastic deformations, indicating the ability of both panels to absorb significant amount of energy. Panel 3 shows signs of extensive yielding, although the damage in that panel is much less severe than in the other two panels.

4.4 Hysteresis behaviour

The load versus deformation behaviour of panel 2 was used to control the test based on ATC-24 (Applied Technology Council, 1992). The base shear versus storey drift for panels 1, 2, and 3 are presented in figures 4.10, 4.11, and 4.12, respectively. The base shear is plotted in Figure 4.13 as a function of the displacement measured at the top of the test specimen. All the curves exhibit the same characteristics as those observed in the previous tests (Driver *et al.*, 1997; Tromposch *et al.*, 1987). In cycles 1 to 9 the specimen behaviour was elastic and exhibited high initial stiffness (to be discussed in next section). This high initial stiffness is a necessary requirement for an ideal lateral load resisting system in order to minimise drift under wind and service loads.

Well defined hysteresis curves began to develop at cycle 10, where unloading and reloading in opposite directions developed a consistent and typical pinched hysteresis curve. Pinching of hysteresis curves is reflected by a substantial drop of the stiffness due to the release of the tension field developed in the previous load excursion. The slope of the unloading curve represents the elastic stiffness of the specimen. As can be seen, there is a slight reduction of stiffness after each loading cycle. This is attributed to the plastic deformations taking place in the infill plate at each cycle. The infill plate effectively becomes larger than the space delineated by the beams and columns, resulting in a "bulged out" panel once the load is removed. As a result, the test on the original four-storey shear affected the stiffness of the three-storey shear wall specimen. This stiffness reduction due to previous loading history should be taken into consideration for a more accurate analysis of the present specimen.

The behaviour of the steel plate shear wall in the plastic range can be better understood by studying closely a typical hysteresis curve. Once the specimen was loaded in the inelastic range, unloading and reloading in the opposite direction produced typical pinching of the hysteresis curve. Figure 4.14 shows a typical hysteresis loop taken from the response of the second panel at cycle 18. Point d shows the peak displacement in this cycle while loading the shear wall in the west direction. When unloading the specimen from point d, the response follows path de, which is linear and has a similar stiffness to the elastic stiffness of the panel during loading (with the increasing peak deflection in each cycle, the slope of the unloading portion decreases slightly). When loading starts in the opposite direction, the specimen shows a substantial drop in the stiffness, as indicated by the slope of segment ef. This reduction in stiffness is due to the absence of tension field action. In this region of the shear versus drift curve, the frame is the main lateral load resisting system. The stiffness of segment ef is obtained as 47 kN/mm, which is slightly higher than the initial stiffness of the frame alone (32 kN/mm) but is much lower than the initial stiffness of the steel plate shear wall in the second panel (220 kN/mm), which indicates that in segment ef the infill plate is not very effective. After sufficient panel deformation, the tension field redevelops at point f. Redevelopment of the tension field increases the stiffness of the shear wall. As the load approaches the ultimate load, various portions of the shear wall, mainly the infill plate, yields. This results in a gradual stiffness reduction starting at point g. Segment habcd of the hysteresis loop represents unloading and reloading in the opposite direction, thus repeating the same behaviour completes the hysteresis loop.

In each block of cycles, as the deflection magnitude increased to a new level, the maximum load in the shear wall increased gradually. The primary difference in the hysteresis curves is the stiffness of the panel during redevelopment of the tension field and the deflection required for the redevelopment of the tension field. The response of the control panel was kept symmetrical up to cycle 22. In the last three cycles the test specimen was loaded to the stroke limit of the jacks in both directions, and this resulted in an unsymmetrical loading of the wall. This can be observed in figures 4.10 to 4.13.

4.5 Discussion of test results

A total of 24 load cycles were applied to the test specimen. Fourteen of these cycles caused significant yielding in the wall. Including the 20 inelastic load cycles that were applied in the previous test on the four-storey specimen tested by Driver *et al.*

(1997), the bottom storey of the test specimen underwent 34 inelastic load cycles. This is clearly more severe than the number of inelastic cycles that a structure would be subjected to during an earthquake (Derecho *et al.*, 1980). The two tests conducted on the top three storeys of the Driver *et al.* specimen have demonstrated the high shear capacity, the very high ductility, and the potential for high energy dissipation capacity of steel plate shear walls. The shear wall reached its maximum capacity at a base shear of 3500 kN and a drift of 50 mm in the second storey, which represents seven times the drift at first significant yield (i.e., $7\,\delta_y$).

In the elastic range (cycles 1 to 9), the shear wall was very stiff. The initial stiffness of panel 1, taken as the slope of the base shear versus storey drift, was 320 kN/mm. This is greater than the initial stiffness displayed by the corresponding panel in the four-storey specimen (the second storey in the four-storey specimen), which was 242 kN/mm (see Figure 4.15a). The difference in stiffness between the panel in the three-storey specimen and the corresponding panel in the four-storey specimen is mainly attributable to the change in boundary condition at the base of the panel and the reduced gravity load used for the three-storey steel plate shear wall. A similar stiffening phenomenon was also observed in panel 2, showing a stiffness of about 190 kN/mm in the pre-yield cycles, compared to 159 kN/mm (see Figure 4.15b) that would have been predicted based on the four-storey shear wall test.

The effectiveness of the infill plate can be demonstrated by comparing the stiffness of the steel plate shear wall system with that of the frame alone. The initial stiffness of the steel plate shear wall specimen is obtained as 320 kN/mm in the first panel and 190 kN/mm in the second panel. A comparison of these stiffness with the corresponding stiffness for the frame alone (61 kN/mm in the first storey and 32 kN/mm in the second storey) indicates that infill plates significantly increase the stiffness of the frame. This increase is 425% for the first panel and 494% for the second panel.

An interesting aspect of this system, which was clearly demonstrated in this test, is its redundancy. Despite the fact that a beam–to–column connection fractured during the test, this did not seem to affect the ability of the frame to carry the shear force. The connection fracture resulted in a small drop of shear force (5.9%) in the test specimen but the full load was quickly recovered, as demonstrated in figures 4.10 and 4.11.

The behaviour of the test specimen was not symmetric during the test, especially in the first panel. The reason for this unsymmetrical behaviour becomes apparent when the response of the four-storey shear wall from which the present test specimen was obtained is examined. During the four-storey shear wall test, the specimen failed by rupture of the column base during the second half of cycle 30 at a base shear of 1640 kN. At the time of rupture of the column base the loads were applied in the east direction (corresponding to the west direction in the present test since the specimen was turned 180^{o} for testing of the top three storeys) and the tension field in the second panel (first panel in the present test) had developed in the east direction. After failure and subsequent unloading, a pattern of residual buckles, consistent with the orientation of the tension field in that direction, remained in the second panel. Consequently, when the three-storey shear wall was loaded in the west direction, the tension field was already active. In the opposite direction, the specimen showed more flexibility because the tension field had to develop.

The test on the original four-storey steel plate shear wall not only affected the symmetry of the three-storey shear wall test results, but it also affected the stiffness of the specimen. Figure 4.15(a), which shows the response of the second storey of the four-storey specimen, indicates that the test would have ended at point B when the load was removed after failure at point A. As the test specimen was reloaded in the three-storey steel plate shear wall test, the stiffness in one direction is significantly different from the stiffness in the other direction (54 kN/mm when loading towards point C versus 162 kN/mm when re-loading towards point A). It was also observed during the four-storey steel plate shear wall test that the stiffness of the wall decreased with the number of cycles. In cycles 29 and 30 of the four-storey test the stiffness had dropped to almost 54 kN/mm even after development of the tension field, compared to the initial stiffness of 242 kN/mm. Panel 1 from the three-storey test specimen had significant buckles present before the start of the test. It is expected that its stiffness would be reduced as a result of these buckles. Figure 4.15(b) indicates that a similar effect would be expected from the infill plate in the second storey of the three-storey specimen. This change in stiffness, the significant change in the boundary condition at panel 1 when the four-storey specimen was cut to a three-storey specimen, combined with the effect of the different gravity loads in the two test specimens, makes a direct comparison between the three-storey specimen and the four-storey specimen difficult.

The area enclosed by a hysteresis curve is a measure of the energy dissipated by the system through a load cycle. The hysteresis curves generated by a steel plate shear wall, especially at the lower panels, are fairly wide, indicating good energy absorption of the system. In order to assess the performance of the test specimen quantitatively, the energy dissipated by the test specimen was calculated for each of the three storeys. Figure 4.16 shows a summary of the cumulative energy absorbed by each panel throughout the test. As expected, because the behaviour in the first ten cycles was essentially elastic, little energy was absorbed in the early stages of the test. Figure 4.16 also confirms that panel 3 did not contribute very much to the total energy absorption. Although in the early stages of inelastic behaviour panel 2 contributed to the total energy dissipation as much as panel 1, its relative contribution decreased near the end of the test when severe plastic deformations and tearing were observed in panel 1. The contribution of panel 2, nevertheless, remained significant. At the end of the test, panel 1 had absorbed 1740 kJ, panel 2 had absorbed 790 kJ, and the top panel had absorbed 130 kJ. Therefore, panel 1 contributed 65% of the total energy dissipation and panel 2 contributed 30%.

The ability to develop tension field action and to dissipate a significant amount of energy in more than one storey would be an important aspect of the design of steel plate shear walls in multi-storey buildings. Consideration of this aspect in the design of steel plate shear walls results in a more economical system in resisting lateral loads, especially in region with severe earthquakes.

4.6 Inclination of the tension field

The angle of the tension field in the first and second panels was measured during the test. As a result of shear buckling of infill plate, a number of relatively large waves, at least two in each panel, were formed. The inclination of the tension field can be assumed to be represented by the orientation of the buckle waves. Therefore, the angle of the tension field was obtained by measuring the angle of the crest of the buckle waves (relative to the vertical). Because of unsymmetrical behaviour in the response of the shear wall, the inclination of the tension field was measured as the load was applied in each directions and the average was taken to obtain the tension field orientation.

Figure 4.17 shows a schematic of the buckles as seen on the north face of the first and second panels as the shear wall was loaded in the east and west directions. Tables 4.1 to 4.4 present the measured orientation of the tension field at various load cycles. The measurements were taken from cycle 10 when significant yielding was first observed in the load versus deflection response of the shear wall. Figure 4.18 shows the variation of this angle at different loading cycles for both panels. As it can be seen, there is a fluctuation of a few degrees in the inclination of tension field between cycles 10 and 16. However, after cycle 16 the orientation of the tension field remained approximately at 51 degrees in the first panel and 45 degrees in the second panel. Equation 2.2 (Timler and Kulak, 1983) predicts a tension field inclination of 41.2° for the first panel and 42.4° for the second panel.

Equation 2.2, which is the form used in the Canadian Standard CSA–S16–01, is based on a number of simplifying assumptions, mainly elastic behaviour of the infill plate and the boundary members. However, the measurements were obtained when the test specimen was in the plastic range. Therefore, the measured value at cycle 10, which represents the beginning of general yielding, is a more appropriate value to compare with the theoretical formula. The angle of inclination of the tension field in cycle 10 was 47.6° in panel 1 (compared to a predicted value of 41.2°) and 46.7° in the second panel (compared to a predicted value of 42.4°). Another simplifying assumption made in the derivation of equation 2.2 was a simple beam–to–column connection for the steel plate shear wall panel whereas in this specimen rigid connections were used. Considering the simplifying assumptions made in the derivation of equation 2.2, the equation presented in CSA–S16–01 gives a reasonable prediction of the orientation of the tension field.

Table 4.1: Measured tension field inclination (First panel – Pushing)

Cycle No.	**Base Shear** kN	α_2 Degree	α_3 Degree	α_4 Degree	$\alpha_{ave.}$ Degree
10	2290	46	50	43	46.3
11	2282	45	49	44	46.0
12	2265	46	50	47	47.7
13	2679	46	53	46	48.3
14	2697	46	54	47	49.0
15	2710	47	55	47	49.7
16	2964	47	55	47	49.7
17	2970	48	56	45	49.7
18	2961	48	56	44	49.3
19	3174	49	56	44	49.7
20	3208	48	55	45	49.3
21	3313	48	55	45	49.3

Table 4.2: Measured tension field inclination (First panel – Pulling)

Cycle No.	**Base Shear** kN	α_2 Degree	α_3 Degree	$\alpha_{ave.}$ Degree
10	-2301	50	48	49.0
11	-2280	49	48	48.5
12	-2294	50	51	50.5
13	-2876	51	52	51.5
14	-2861	49	50	49.5
15	-2849	50	53	51.5
16	-3174	52	53	52.5
17	-3182	50	55	52.5
18	-3123	50	56	53.0
19	-3419	50	56	53.0
20	-3430	50	56	53.0
21	-3424	50	56	53.0

Table 4.3: Measured tension field inclination (Second panel – Pushing)

Cycle No.	**Base Shear** kN	α_2 Degree	α_3 Degree	α_4 Degree	$\alpha_{ave.}$ Degree
10	2290	49	47	47	47.7
11	2282	47	46	45	46.0
12	2265	46	47	45	46.0
13	2679	48	48	47	47.7
14	2697	48	48	47	47.7
15	2710	48	46	46	46.7
16	2964	48	48	43	46.3
17	2970	50	49	42	47.0
18	2961	49	49	42	46.7
19	3174	49	49	42	46.7
20	3208	48	48	42	46.0
21	3313	47	48	42	45.7

Table 4.4: Measured tension field inclination (Second panel – Pulling)

Cycle No.	**Base Shear** kN	α_1 Degree	α_2 Degree	α_3 Degree	α_4 Degree	$\alpha_{ave.}$ Degree
10	-2301	46	46	46	—	46.0
11	-2280	48	47	45	—	46.7
12	-2294	48	47	46	—	47.0
13	-2876	47	46	46	—	46.3
14	-2861	46	46	46	—	46.0
15	-2849	44	44	44	—	44.0
16	-3174	45	43	43	—	43.7
17	-3182	45	45	45	43	44.5
18	-3123	44	44	45	44	44.3
19	-3419	44	44	42	42	43.0
20	-3430	44	44	42	42	43.0
21	-3424	45	45	43	42	43.8

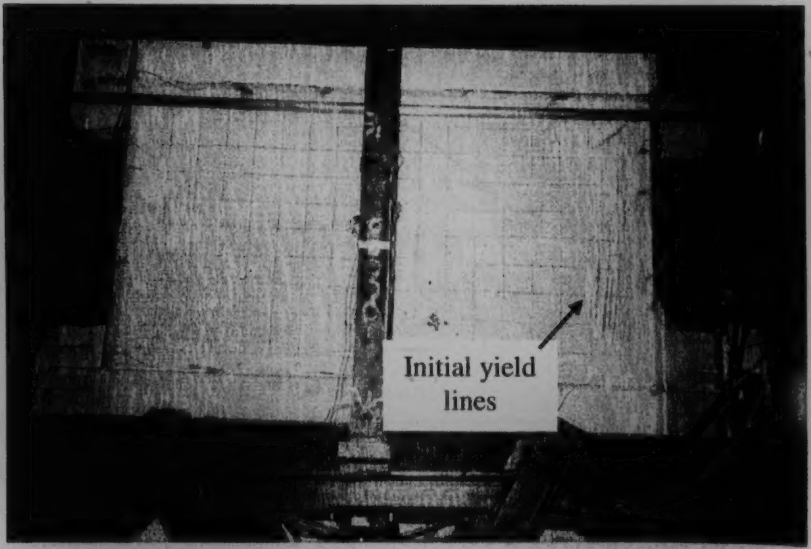
Initial yield
lines

Figure 4.1: Initial yield lines along the west edge of panel 2 (cycle 7)

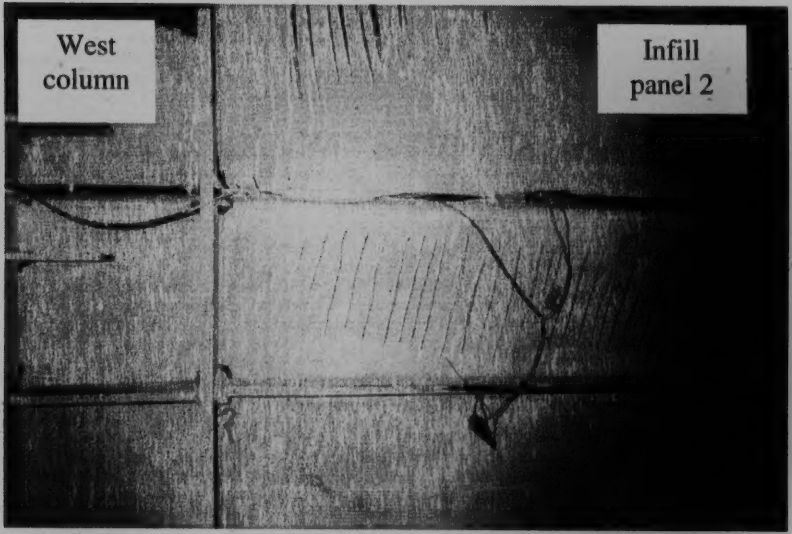
West
column
Infill
panel 2

Figure 4.2: Yield line pattern in the web of the beam at level 1
(south face at west end – cycle 10)

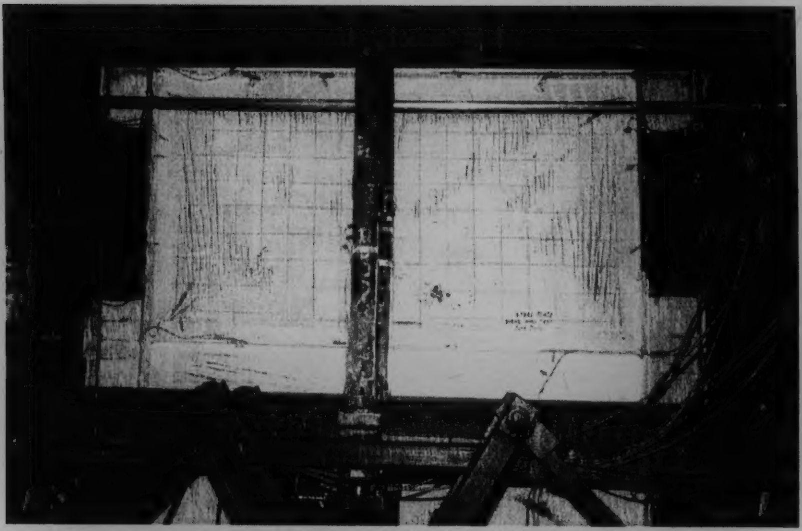

Figure 4.3: Extent of yielding at north face of second panel (cycle 14)

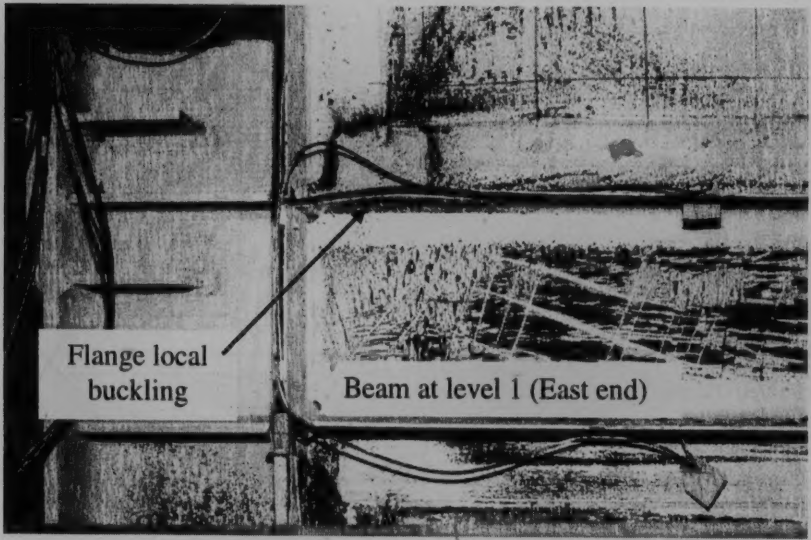
Flange local buckling
Beam at level 1 (East end)

Figure 4.4: Initiation of flange local buckling – beam at level 1, east end (cycle 20)

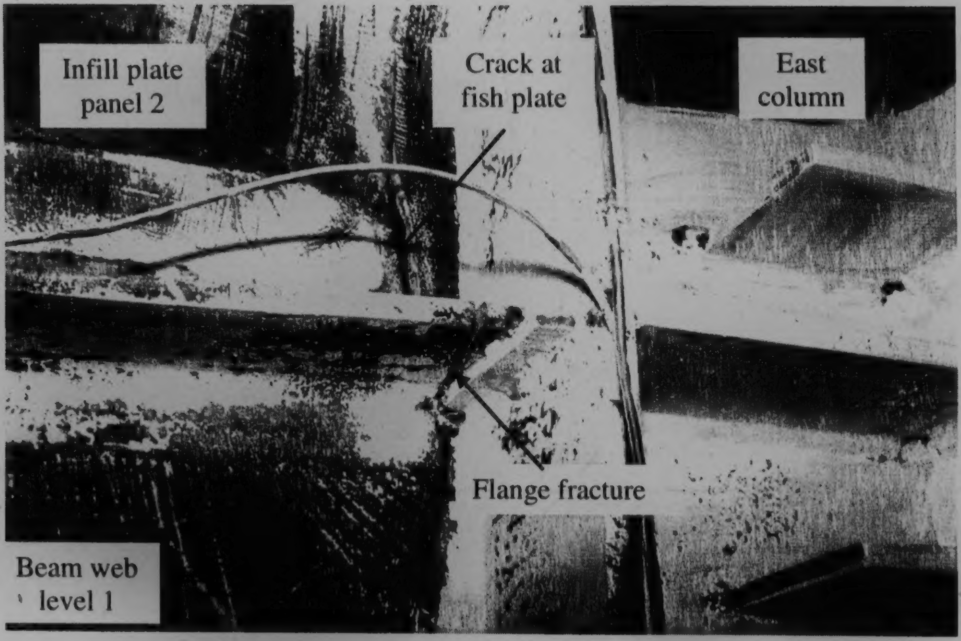
Infill plate panel 2
Crack at fish plate
East column
Flange fracture
Beam web level 1

Figure 4.5: Fracture of beam–to–column connection (cycle 21)

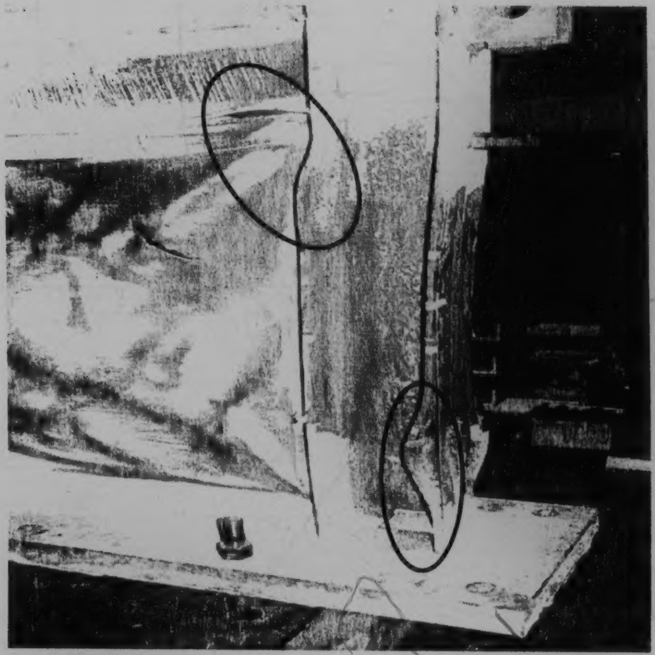

Figure 4.6: Local buckling of west column in panel 1 (end of test)

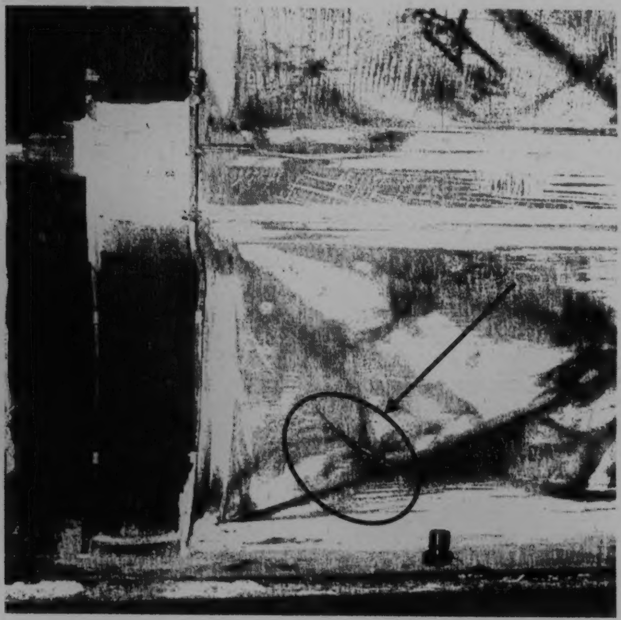

Figure 4.7:Tear at the bottom east corner of first panel (end of test)

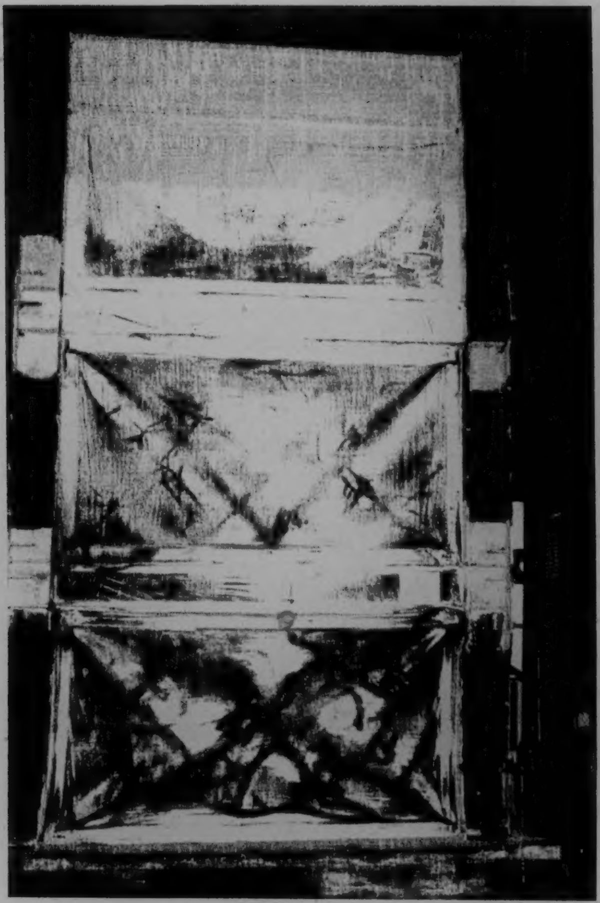

Figure 4.8: Specimen at the end of the test

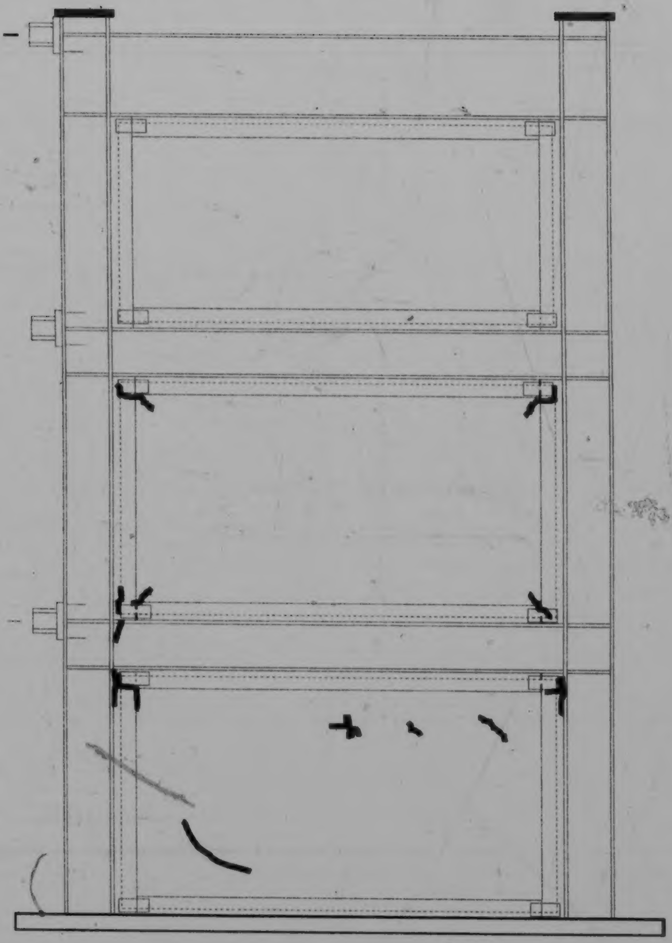

Figure 4.9: Location of tears in the test specimen at the end of the test (north side)

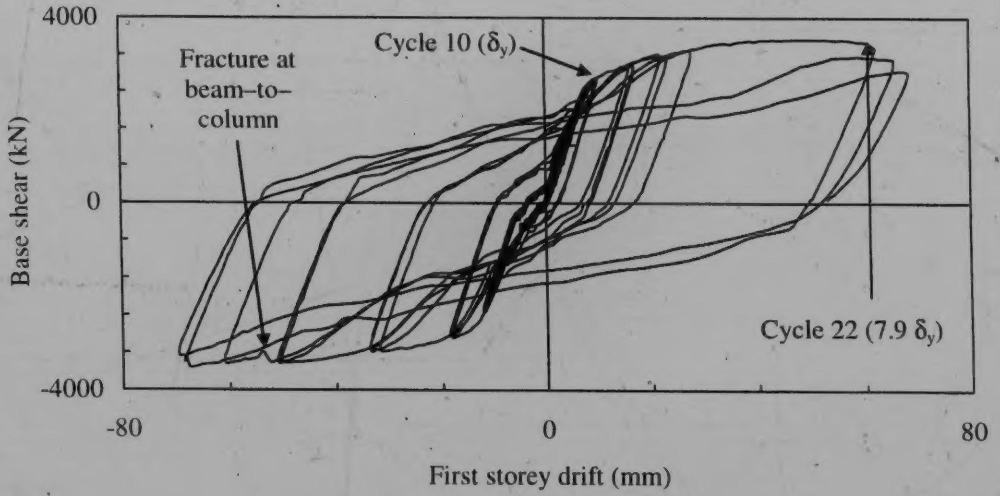

Figure 4.10: Base shear versus first storey drift

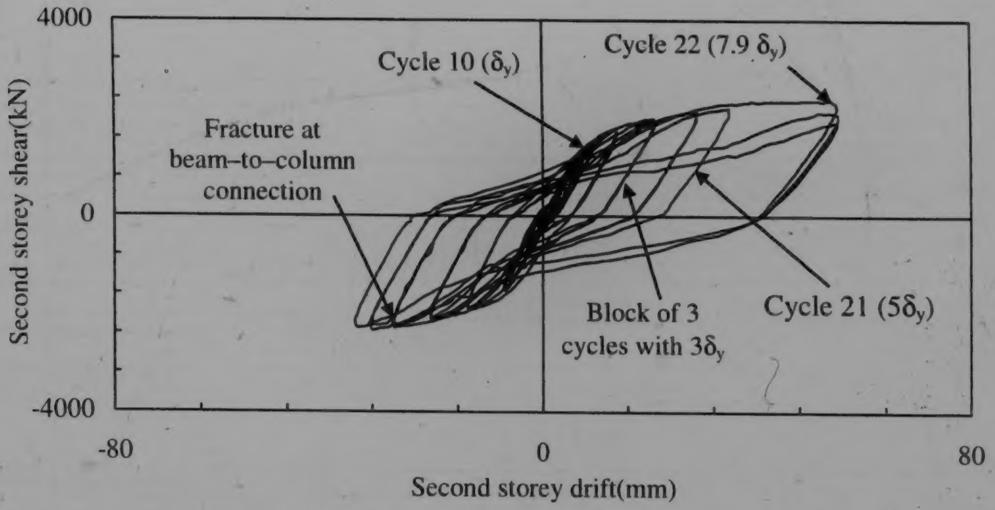

Figure 4.11: Second storey shear versus second storey drift

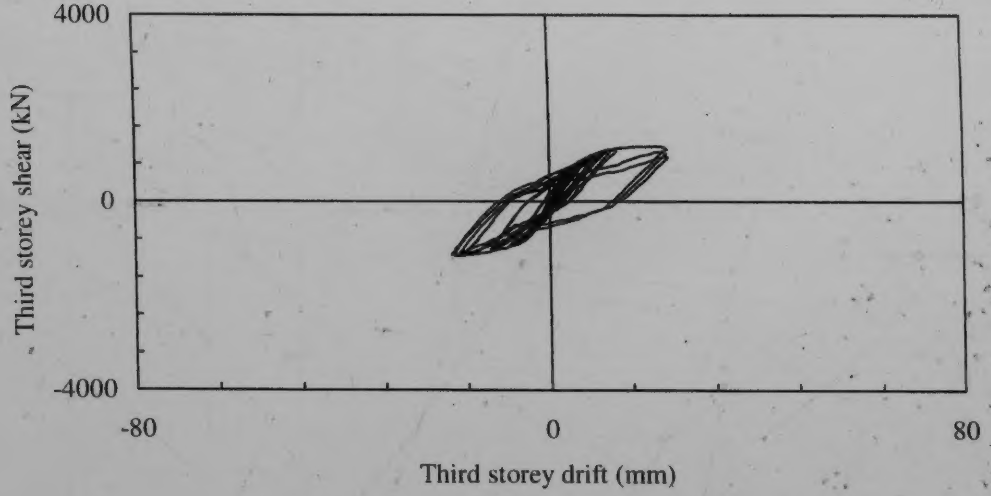

Figure 4.12: Third storey shear versus third storey drift

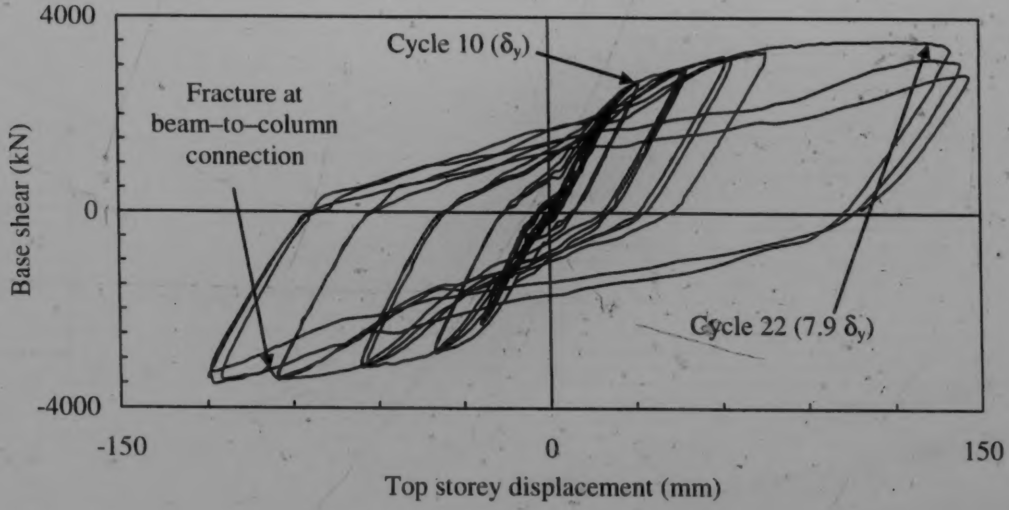

Figure 4.13: Base shear versus top storey displacement

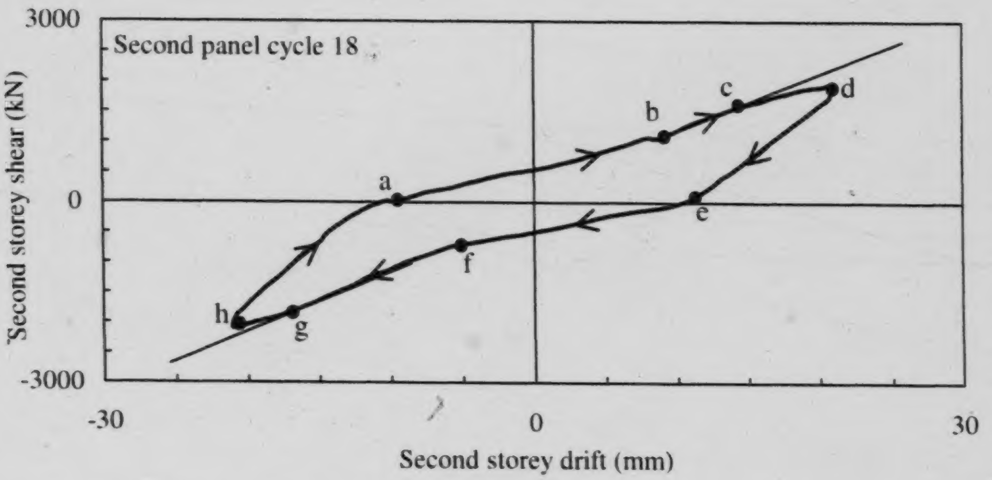

Figure 4.14: Typical hysteresis curve, 2nd panel, cycle 18

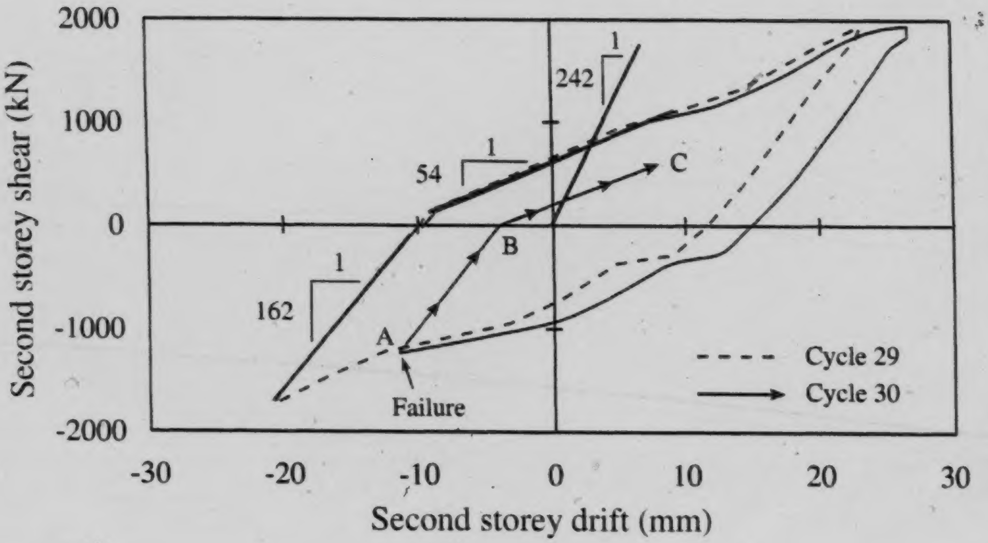

(a) Second panel

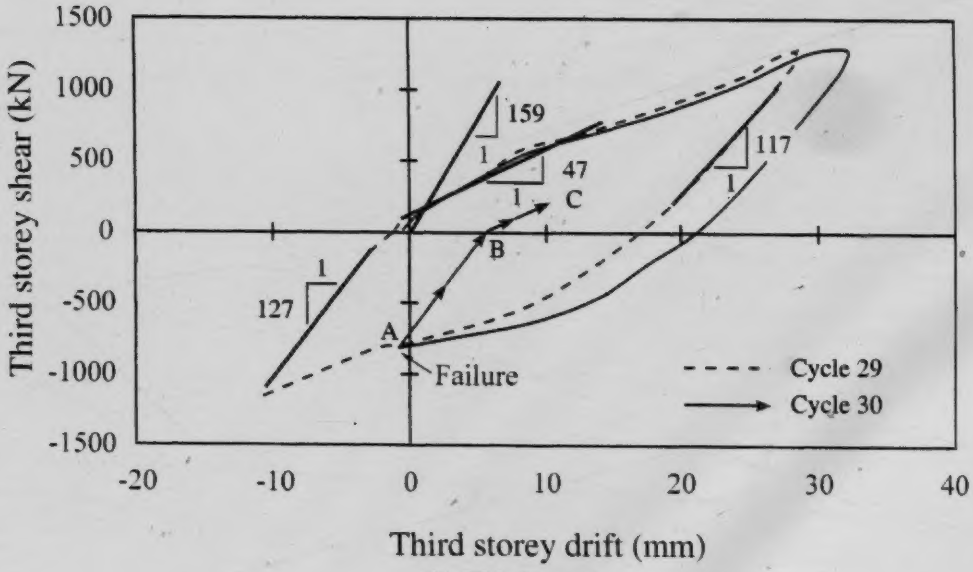

(b) Third panel

Figure 4.15: Response of four-storey steel plate shear wall specimen (cycles 29 and 30)

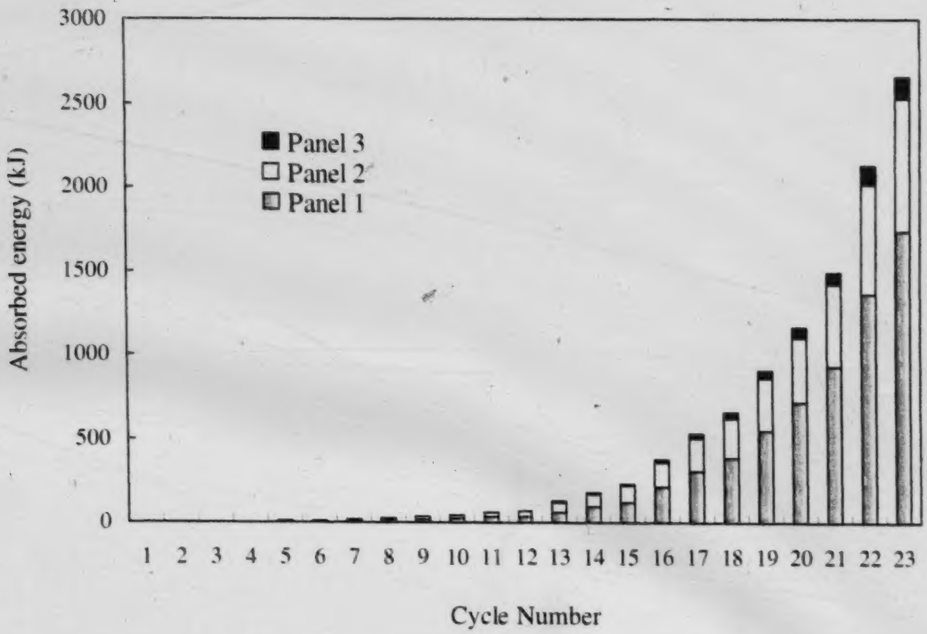

Figure 4.16: Cumulative energy absorbed by each panel through the test

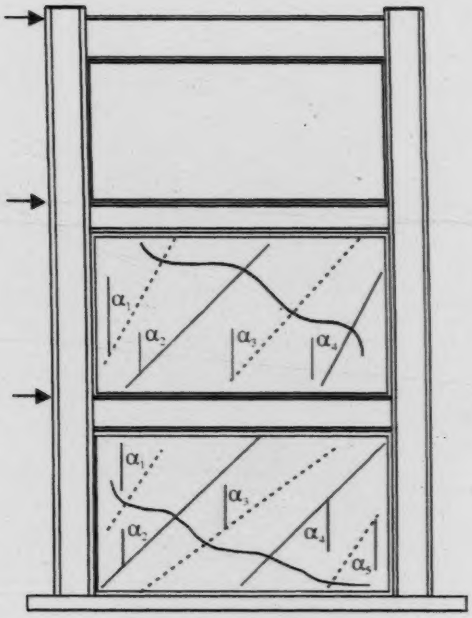
α1
α2
α3
α4
α1
α2
α3
α4
α5

(a) Pushing

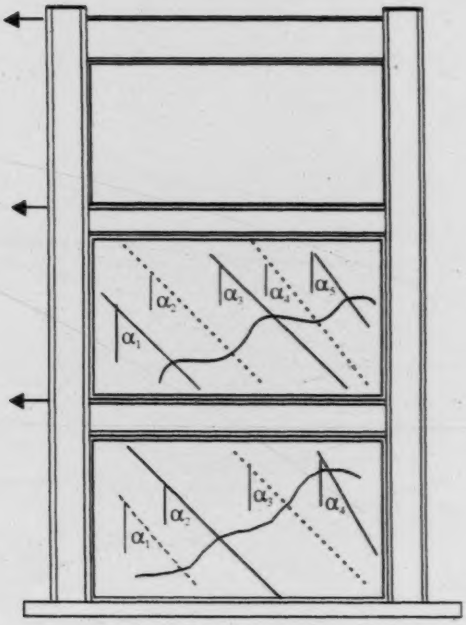
α2
α3
α4
α5
α1
α2
α3
α4
α1

(b) Pulling

Figure 4.17: Tension field orientation in panels 1 and 2

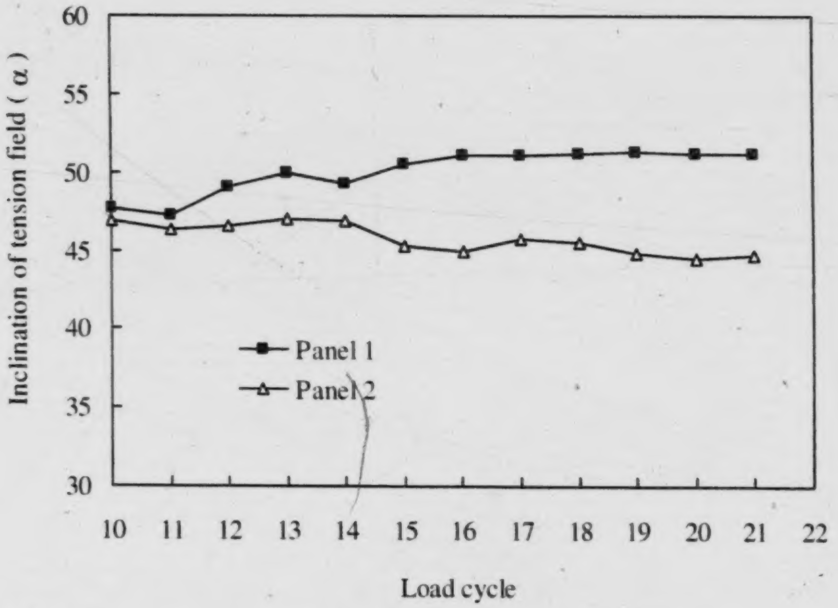

Figure 4.18 Average inclination of the tension field in the first and second panels

5 FINITE ELEMENT MODEL

5.1 Introduction

The large scale test of a three storey unstiffened steel plate shear wall presented in chapters 3 and 4, along with the test results by other researchers (see Chapter 2), are significant contributions towards understanding of the cyclic behaviour of this system. However, the specific dimensions and parameters investigated in the laboratory tests do not cover the full range of cases that might be encountered in practice. It is therefore necessary to develop analytical tools to investigate the behaviour of steel plate shear walls with different geometry and loading conditions, thus avoiding the large expense of performing additional tests. The main objective of this chapter is to develop a reliable finite element model that can simulate the behaviour of steel plate shear walls under cyclic loading. The numerical model will be validated using the available test data. The model can then be refined so that other shear wall configurations can be analysed reliably.

In a limit states design context both strength and serviceability must be considered. This means that the numerical model of a steel plate shear wall should be able to simulate accurately both the stiffness and the capacity. A numerical model of the three-storey steel plate shear wall described in Chapter 3 was developed using the commercial general-purpose nonlinear finite element program ABAQUS (Hibbitt *et al.*, 2001). This software is well suited for the solution of highly nonlinear engineering problems. It contains an extensive library of elements that can model virtually all geometric boundary conditions.

ABAQUS consists of two main analysis modules: ABAQUS/Standard and ABAQUS/Explicit. In ABAQUS/Standard, an implicit method is used for analysis of systems under quasi-static and dynamic loads. In implicit method, equilibrium is achieved through an iterative procedure, from which the deformed configuration of the structure is obtained. ABAQUS/Explicit uses a nonlinear explicit dynamic formulation and can be used for analysis of systems under both dynamic and quasi-static conditions.

In dynamic explicit method the unbalanced forces between the internal and external forces at the beginning of the increment is considered as a driving force acting on a mass, from which the deformed state after a very small time increment using the central difference method, thus no iteration is involved in this technique.

Because large-scale tests on steel plate shear walls have been conducted under quasi-static conditions the steel plate shear wall was initially analysed with the static implicit method implemented in ABAQUS/Standard. Development of the tension field and shear buckling of infill plate as the load increases creates local instabilities in the infill plates. These local instabilities make it very difficult to trace the solution up to the limit point due to convergence problems in the solution process with an implicit method. For this reason, and since in an explicit formulation the solution is obtained without any iteration, the explicit version of ABAQUS was used for analysis of steel plate shear walls.

A brief discussion of the static implicit method and the convergence problems associated with this method of analysis of steel plate shear walls is presented in section 5.2. The explicit finite element method and the issues related to quasi-static simulation of steel plate shear walls with this method are explained in detail in section 5.3 to provide the necessary background to the remaining portion of the this Chapter, which discusses the issues related to the finite element modelling of steel plate shear walls investigated in this research.

5.2 Convergence problem in implicit finite element method

5.2.1 Solution strategies in a static implicit method

When the response of a system is nonlinear, the solution should be obtained incrementally. In general, the equation of equilibrium at the end of a load increment, at time $t + \Delta t$, can be written as:

$$\underline{R}_{t+\Delta t} - \underline{F}_{t+\Delta t} = 0 \qquad 5.1$$

where $\underline{R}_{t+\Delta t}$ is the vector of externally applied loads and the vector $\underline{F}_{t+\Delta t}$ represents the internal nodal point forces that are equivalent to the element stresses. Since $\underline{F}_{t+\Delta t}$ depends on the history of the nodal point displacements, it is necessary to adopt an iterative process to solve equation (5.1) for the exact configuration of the system or to obtain a reasonable solution and accept some error in the equilibrium. The equilibrium equation can be written as:

$$\underline{R}_{t+\Delta t}(U^{*}) - \underline{F}_{t+\Delta t}(U^{*}) = \underline{f}_{t+\Delta t}(U^{*}) \tag{5.2}$$

where U^{*} is an approximation of the real solution and $\underline{f}_{t+\Delta t}(U^{*})$ is a vector of residual unbalanced forces at time $t + \Delta t$, which drives the iterative process.

The basic approach used in ABAQUS/Standard to solve the above nonlinear equation is a load-control Newton-Raphson iterative method. The solution procedure is shown in Figure 5.1 (Bathe, 1996). The solution seeks equilibrium through a horizontal path at a constant load vector of $\underline{R}_{t+\Delta t}$. In this method the stiffness matrix ideally is updated at the end of every iteration. Since the major computational cost per iteration in Newton-Raphson iterations lies in the calculation and decomposition of the tangent stiffness matrix, a modification to the method is often made by using the stiffness matrix developed at the beginning of a time step for all iterations within the time step. The solution path followed in a modified Newton-Raphson iterative method is illustrated in Figure 5.2. However, both methods fail to converge in the neighbourhood of unstable responses, including local instabilities.

In a steel plate shear wall the local instability occurs as the tension field in the infill plate re-orients itself during loading and unloading paths. This makes it very difficult to obtain a complete solution up to the ultimate capacity using a load control strategy. The situation is aggravated when modelling cyclic loading of the steel plate shear wall and the solution quickly becomes intractable.

To allow tracking of system response past limiting points the so-called "arc length control" was introduced. The technique was first developed by Riks (1979) and was later modified by (Ramm, 1981). In the Riks solution algorithm both the load level and displacements are treated as unknowns. The basic algorithm remains the Newton-Raphson iteration method, but the search for equilibrium is based on an iterative path perpendicular to a tangent plane taken in the equilibrium surface at the previously converged point (see Figure 5.3). In this method the perpendicular solution path is easily controlled to intersect the equilibrium surface and converges well past limiting points. The strategy, however, still shows convergence problems at local instabilities that arise during the loading and unloading processes.

5.2.2 Convergence problem

In the analysis of a steel plate shear wall, because of the sudden out–of–plane deformation of the infill plates due to tension field development, convergence is a serious problem. The preliminary pushover analysis of the three-storey steel plate shear wall, obtained before conducting the experiment, was very time consuming. To overcome the convergence problem many different approaches were tried, including application of lateral and gravity loads in various steps and sequences, use of different imperfection shapes and sizes, use of different initial increment sizes, relaxation of the convergence criteria, etc. In most of the cases during the iteration, the size of the increments had to be reduced to a value less than 10^{-5} in order to obtain convergence. This increment size is suitable for an explicit scheme but not for a multiple iteration implicit method. Because of the poor performance of the implicit finite element method, the explicit dynamic method was adopted as a tool for the analysis of steel plate shear wall systems.

5.3 Explicit finite element method

The explicit dynamic procedure can be used as an effective tool for solving a wide variety of nonlinear solids and structural mechanics problems. Originally it was developed to analyse high-speed dynamic events that are extremely expensive to analyse using implicit methods (Benson, 1992). With proper control of the kinetic energy, the explicit approach can be used for quasi-static problems that include complex contact problems, complex post-buckling behaviour, highly nonlinear processes and material degradation and failure. All are problems that experience severe convergence difficulties in implicit analysis methods.

5.3.1 Formulation of the dynamic explicit finite element method

The governing equilibrium equations of a body in a dynamic state can be obtained using the principle of virtual work. This principle states that for a body under static or dynamic equilibrium and for any compatible, small virtual displacements that satisfy the boundary conditions, the total internal virtual work is equal to the total external virtual work:

$$\int_V \delta u f^B dV + \int_S \delta u f^S dS + \delta \underline{U}^T \underline{P} = \int_V (\delta e \sigma + \rho \delta u \ddot{u}) dV \tag{5.3}$$

where f^B is the body force per unit volume, f^S is the traction force per unit area, $\underline{P}$ is applied concentrated force vector at nodes, σ is Cauchy stress, ρ is the material density, $\ddot{u}$ is the acceleration field, δu is a virtual displacement field applied to the system at the state of dynamic equilibrium, $\delta \underline{U}$ is the vector of virtual displacement evaluated at nodes, and δe is the virtual strain field. The superscript T indicates the transpose of the associated vector. By introducing a shape function matrix, $\underline{N}$, the displacement, acceleration, and virtual displacement field can be related to the nodal displacements and accelerations as:

$$u = \underline{N}^T \underline{U}; \qquad \ddot{u} = \underline{N}^T \underline{\ddot{U}}; \qquad \delta u = \underline{N}^T \delta \underline{U} \tag{5.4}$$

Where $\underline{U}$ and $\underline{\ddot{U}}$ are nodal displacement and nodal acceleration vector, respectively. Combining equations (5.3) and (5.4), the following dynamic force balance, in matrix form, can be obtained:

$$\underline{M}\underline{U} = \underline{R} - \underline{F} \tag{5.5}$$

in which

$$\underline{M} = \int_V \rho \underline{N}^T \underline{N} dV \tag{5.6}$$

$$\underline{F} = \int_V \underline{B}^T \sigma dV \tag{5.7}$$

$$\underline{R} = \int_V \underline{N}^T f^B dV + \int_V \underline{N}^T f^S dV + \underline{P} \tag{5.8}$$

The matrix $\underline{B}$ in equation (5.7) is the strain operator matrix, $\underline{M}$ is the consistent mass matrix, $\underline{F}$ is a vector containing the internal forces evaluated at the nodes, and $\underline{R}$ is a concentrated external force vector evaluated at the nodes. If, instead of using a consistent mass matrix, a lumped or diagonal mass matrix is used, equation (5.5) can be decoupled and the dynamic balance equation can be written separately for each node. This is an important step in the dynamic explicit formulation since by doing so the time integration procedure can be carried out quite effectively explicitly.

5.3.2 Computational procedures in a dynamic explicit method

ABAQUS/Explicit uses the central difference method, which is the most commonly used time integration procedure. The equilibrium of the system is considered at time t in order to calculate the kinematic conditions at time $t + \Delta t$ (the next increment).

Neglecting the effect of viscous damping and using a diagonal mass matrix, the dynamic equilibrium equations are written at node level, as discussed above. The dynamic equilibrium equation at time t states that the inertial force, $\underline{M}\underline{\ddot{U}}_t$, equals the total nodal forces (the difference between the externally applied force, $\underline{R}_t$, and the internal element force, $\underline{F}_t$ evaluated at the nodes) which is the same as equation (5.5) but at time t and for individual nodes.

Since the explicit method uses a diagonal mass matrix, solving for the acceleration is trivial because no simultaneous equations need to be solved:

$$\ddot{\underline{U}}_t = (\underline{M})^{-1}.(\underline{R}_t - \underline{F}_t) \tag{5.9}$$

As a result, the acceleration of any node is determined completely by its nodal mass and the net force acting on the node, making the nodal calculation very inexpensive. Using central difference method the accelerations are integrated through time to obtain the change in velocity, assuming a constant acceleration. The change in velocity is added to the velocity from the middle of the previous increment to determine the velocities at the middle of present increment:

$$\dot{\underline{U}}_{(t+\frac{\Delta t}{2})} = \dot{\underline{U}}_{(t-\frac{\Delta t}{2})} + (\frac{\Delta t_{(t+\Delta t)} + \Delta t_t}{2}).\ddot{\underline{U}}_t \tag{5.10}$$

The velocities are then integrated through time and added to the displacements at the beginning of the increment to determine the displacements at the end of the increment as follows:

$$\underline{U}_{(t+\Delta t)} = \underline{U}_t + \Delta t_{(t+\Delta t)}.\dot{\underline{U}}_{(t+\frac{\Delta t}{2})} \tag{5.11}$$

Therefore, by satisfying dynamic equilibrium at the beginning of the increment, the velocities and the displacements are obtained at the middle and end of the increment, respectively. A summary of the computational procedure for the dynamic explicit procedure is depicted in Figure 5.4.

5.3.3 Stability limit of a dynamic explicit method

With the explicit method the state of the model is advanced through an increment of time, Δt, based on the state of the model at time t. Since the central difference method, which is a conditionally stable algorithm (Bathe, 1996), is used as time integrator, the amount of time that the state can be advanced, keeping the error bounded, should be less than a stability limit. The stability limit is defined in terms of the highest frequency of the system, $\omega_{\max}$. Without damping the stability limit is defined as:

$$\Delta t_{stable} = \frac{2}{\omega_{\max}} \tag{5.12}$$

and if damping is present in the model, the stable time increment is defined as:

$$\Delta t_{stable} = \frac{2}{\omega_{\max}}(\sqrt{1+\xi^2} - \xi) \tag{5.13}$$

where ξ is the fraction of critical damping in the mode with the highest frequency. In ABAQUS/Explicit, a small amount of damping in the form of bulk viscosity is always added to the model to control the high frequency oscillations. As can be seen from equation (5.13), damping reduces the stable time increment and requires more CPU time for the analysis.

Since obtaining the actual highest frequency in a model is not computationally feasible, especially in large models, a simple estimate, that is feasible and conservative, is used by ABAQUS/Explicit. In this method the highest frequency is estimated from the individual elements in the model. The highest frequency, based on element–by–element method is higher than the highest frequency of the global model (Hibbitt, *et al.*, 2001b). Therefore, a stable time increment based on element–by–element calculation is smaller than the global value and is a more conservative estimate. The highest frequency of an element is associated with the dilatational mode, and the critical time increment is given by:

$$\Delta t_{stable} = \frac{L_e}{C_d} \tag{5.14}$$

where, L_e is the smallest characteristic length of the element and C_d is the dilatational wave speed of the material defined as:

$$C_d = \sqrt{\frac{E}{\rho}} \tag{5.15}$$

where, E is the modulus of elasticity and ρ is the density of the material. Examination of these equations reveals that a conservative value for critical time increment is the time that a dilatational wave passes across the smallest characteristic element length.

Two main parameters can change the critical time increment and, as a result, can change the required computational time for an explicit analysis. These are material properties and size of the finite element mesh. The dilatational wave speed depends on both stiffness and density of the material. The stiffer the material the higher the wave speed, resulting in a smaller stable time increment. On the other hand, a higher material density results in a reduction of the wave speed and an increase in the critical time increment. For a specific material the wave speed is constant in the linear portion of the analysis since the modulus of elasticity is constant and, therefore, the critical time depends only on the smallest element size in the finite element mesh. In the nonlinear range, however, the modulus of elasticity decreases, which reduces the wave speed and increases the critical time increment. Since the critical time increment is approximately proportional to the shortest element dimension, it is recommended that the element size be kept as large as possible as long as the accuracy of analysis is acceptable.

5.3.4 Simulation of a quasi-static analysis with the dynamic explicit method

Almost all of the tests on unstiffened steel plate shear walls available in the literature, including the test reported herein, have been conducted in a quasi-static manner. However, the explicit finite element method is based on a dynamic formulation in which the inertial forces resulting from the acceleration and mass of the system play an important role. As a result, applying the explicit dynamic procedure to a quasi-static problem requires some special considerations. The main goal is to simulate the analysis in the shortest period of time in which the inertial forces remain insignificant. The speed of an analysis often can be increased substantially without significantly reducing the accuracy of quasi-static solutions. However, if the speed of an analysis increases to a point where the inertial forces dominate, the solution tends to localize and the results will be quite different from the quasi-static solution.

For accuracy and efficiency of a quasi-static analysis, loads should be applied as smoothly as possible such that the accelerations change only a small amount from one increment to the next increment. If the acceleration is smooth, it results in a smooth velocity and displacement. ABAQUS/Explicit has a simple built-in type of amplitude, called SMOOTH STEP, which automatically creates the smoothest possible loading amplitude between two points. Using this option, each of the data pairs will be connected with curves whose first and second derivatives are smooth and whose slopes are zero at each data point (see Figure 5.5). Using this type of loading amplitude, a quasi-static analysis can be performed in the shortest possible time.

In a quasi-static analysis the slowest mode of the structure dominates the response. As a result, by calculating the frequency and period of the slowest mode of the system, a lower bound time period for doing a quasi-static simulation can be obtained. In most structural problems a loading duration corresponding to 10 times the period of the slowest mode is recommended in order to make sure that a solution is quasi-static.

5.3.5 Methods to accelerate a quasi-static analysis

The analysis time can be optimized by artificially increasing the speed of the simulation, increasing the loading rate, and then checking for acceptance of the static solution (to be discussed later). Another option to optimize the analysis is to increase the critical time increment by artificially increasing the density of the whole or part of the model. This method is called "Mass Scaling" (Hibbitt, et al., 2001a). Mass scaling is a technique that enables the analysis to be performed economically without artificially increasing the loading rate. This method is suitable in simulations involving a rate dependent material or a rate dependent damping. In these simulations increasing the load rate is not an option since material strain rate increases by the same rate as the load rate. Since the properties of the material changes with the strain rate, artificially increasing the load rate artificially changes the solution and is not acceptable.

According to equations (5.14) and (5.15), an artificial increase of the material density ρ, by a factor of f^2 decreases the dilatational wave speed by a factor f and increases the stable time increment by a factor f. This increases the global stability limit and, as a result, fewer increments are required to perform the same analysis for the same time period, resulting in less computing time. Scaling the mass, however, has exactly the same influence on inertial effects as artificially increasing the load rate. Excessive mass scaling, just like excessive loading rate, can lead to a wrong solution. As the mass scaling increases, the solution time decreases and at the same time the quality of the solution decreases because of increase in inertial forces. Methods of evaluating the quality of the solution in order to determine the acceptable loading rate scale factor or acceptable mass scaling factor are discussed in the following.

5.3.6 Evaluation of a quasi-static solution

5.3.6.1 Energy balance

The most general tool for evaluating whether or not a response is quasi-static is to monitor the different energies in the model during the simulation. The energy balance equation can be defined as:

$$E_I + E_V + E_{FD} + E_{KE} - E_W = E_{TOTAL} = 0.0 \tag{5.16}$$

where,

E_I : internal energy (both elastic strain energy and plastic work),

E_V : energy absorbed by viscous dissipation.

E_{FD} : frictional energy (energy dissipated by frictional forces in a contact problem).

E_{KE} : kinetic energy.

E_W : work done by external forces.

E_{TOTAL} : total energy in the system.

For example, the energy balance for a uniaxial tensile test is shown in Figure 5.6. As can be seen in a tension test, the work done by external forces is almost equal to the internal energy in the bar. Viscous dissipated energy is usually small unless viscous materials, dashpots, or material damping is used. Since velocities of the material are small in a quasi-static simulation, the kinetic energy should be negligible. As a general rule, the kinetic energy of the deforming material should not exceed a small fraction (typically 5% to 10%) of its internal energy during most of the simulation (Hibbitt *et al.*, 2001a).

5.3.6.2 Strategies for evaluating a quasi-static solution

The first check that must be performed after completion of an analysis is the assessment of the suitability of the quasi-static simulation. The first step in the verification process is to compare the ratio of the kinetic energy history, E_{KE}, to the internal energy history, E_I, and see if this ratio is small throughout the analysis. As mentioned above, this ratio should be less than 5% to 10 %. If the ratio is less than the proposed value, the next step is to evaluate the two energies separately to see if they are reasonable.

Generally, a smooth loading history should produce smooth results. If the loading is smooth but the energy results during the analysis are oscillatory or noisy, the quality of the simulation may not be adequate. Since the energy ratio is incapable of showing such behaviour, the kinetic energy history itself should be studied to determine if it is smooth or noisy. If the kinetic energy does not show quasi-static behaviour, it can be useful to look at the velocity history of some of the critical nodes to see which part of the model is acquiring velocity and causing the high kinetic energy. For the analysis of steel plate shear walls, in addition to evaluating energy of the system, the velocity history of the top floor is also obtained to evaluate the quality of the response. These issues will be discussed in Chapter 6.

5.4 Description of the finite element model

5.4.1 Element selection

A steel plate shear wall system typically consists of beams and columns with thin steel plate infills in the openings delineated by the columns and beams. In order to capture local buckling of beam and column flanges, the infill plate and the boundary members were discretized with shell elements. Most of the continuum and plate elements in ABAQUS/Explicit are based on an updated Lagrangian formulation (Bathe, 1996). This means that at the beginning of each increment the nodal coordinates are updated to reflect current positions in space and all the shape functions and derivatives are re-evaluated using these updated nodal coordinates. This formulation is useful since the deformation magnitude and strains in the infill plates after many cycles are so large that the shape of the shear wall, especially in the first panel, is changed considerably.

The S4R shell element was selected from the ABAQUS/Explicit library of elements to model the shear wall. This element is a general-purpose 4-node doubly curved shell element with reduced integration. The element accounts for finite (large) membrane strains and arbitrary large rotations. Each node has six degrees of freedom, namely, three translations (u_x, u_y, u_z) and three rotations ($\theta_x, \theta_y, \theta_z$) defined in a global coordinate system. The default local directions (see Figure 5.7) are used on the surface of the shell to define anisotropic material properties and to report stress and strain components. These local directions rotate with the average rotation of the surface. The positive normal on a shell is given by the right-hand rule going around the nodes of the element in the order that they are defined in the element data line. The "top" surface of a shell element is the surface in the positive normal direction and the "bottom" surface is in the negative normal direction.

The S4R shell element can be used to model the behaviour of both thin and thick shells. This element is sufficient for shell problems that are adequately described by either the classical (Kirchhoff) theory or the shear flexible (Mindlin) theory.

The S4R shell element is based on an isoparametric formulation, meaning that the same shape functions are used for interpolation of the displacement field as well as the geometry of the element. This element uses one integration point on its mid-surface to form the element internal force vector. Reduced integration elements give more accurate results and significantly reduce running time if the elements are not distorted. However, since S4R is a linear reduced element it may suffer from hourglassing under certain loading conditions. This may impact both the load application and required mesh size for the steel plate shear wall model. Hourglassing is a pattern of zero energy non-physical deformations (Belytschko *et al.*, 1984b). ABAQUS/Explicit uses a small artificial stiffness associated with rotation about the normal to the shell surface to prevent hourglass modes. The default hourglass stiffness values are small such that the artificial energy content is negligible. During the analysis described in this work, the default value was sufficient to prevent the hourglass mode.

There are number of ways to diagnose hourglassing in an analysis. Examining the deformed shape, hourglassing appears as a pattern of alternating trapezoid deformations (see Figure 5.8). If the artificial energy is excessive, it means that too much strain energy may be going into controlling this mode. The most useful approach is to compare the artificial energy to the internal energy. This ratio should be less than 5% to 10% during most of the analysis. For modeling beams and columns it is recommended that at least four elements in the depth of a web or the width of a flange be used in order to prevent hourglassing (Hibbitt *et al.*, 2001a). To discourage hourglass modes, all the concentrated loads and boundary conditions are distributed on a number of nodes (see Figure 5.8). The size of the mesh used in modeling the steel plate shear wall was fine enough so that no sign of hour glassing was observed during the simulation, either in the deformed shape or the history of artificial energy.

The default number of integration points through the thickness of this element is five (Figure 5.7), which is usually sufficient for simulating the elasto–plastic response of a shell structure under monotonic loading. The pushover analysis of the three-storey steel plate shear wall was conducted with 5 and 9 integration points and no significant difference was observed between the two analyses. Although the pushover analysis indicated that five integration points through the thickness is sufficient, for more complex analysis involving strain reversal (cyclic loading) and high localized curvatures more integration points may be required. Therefore, for the cyclic analysis of steel plate shear walls, nine integration points were used, which should be sufficient for the thin shell elements of the steel plate shear wall model.

5.4.2 Geometry and initial imperfections

Before conducting the shear wall test described in Chapter 3, the specimen was measured to determine the as-built dimensions required for the finite element analysis. The imperfections can be categorised as camber and sweep of beams and columns and out–of–flatness of the plate. The camber and sweep of the beams and columns and the column out–of–plumb were considered small and were neglected in the formulation of the finite element model.

The fish plate connection tabs were not considered in the finite element analysis. The assumption that neglecting the fish plate will not affect the overall behaviour of steel plate shear wall was shown to be adequate by Driver *et al.* (1997).

The behaviour of thin plates subjected to in-plane membrane stresses is affected by initial out–of–plane deformations. The stiffness of a perfectly flat plate is very high under in-plane-shear forces, but slight initial imperfections will substantially reduce the in-plane shear stiffness of the plate. Therefore, initial imperfections of the infill plates, were considered in the finite element model. Out–of–plane displacements of only the first panel were measured before the test. The previous four-storey steel plate shear wall test (Driver *et al.*, 1997) had introduced a pattern of residual buckles in the infill plate at the first level. The maximum value of the out–of–plane initial imperfection was measured to be 39 mm in the first panel. Table 5.1 shows the coordinates and values of the measured out–of–plane imperfections. This pattern was considered as an initial imperfection pattern for the present study. The measured out–of–plane displacement pattern was then mapped onto the finite element mesh in order to get a finite element mesh that accurately modelled the tested steel plate shear wall. For the second and third panels, the infill plate was taken to have an initial imperfection pattern corresponding to the buckling mode of the shear wall loaded in the same way as in the test. The peak amplitude for the second and third panel out–of–plane displacement was set 10 mm. The initial imperfection pattern used in the finite element model is depicted in Figure 5.9.

5.4.3 Boundary conditions and loading of finite element model

In order to provide the rigid boundary at the base of the shear wall that the 90 mm steel base plate anchored to the laboratory strong floor provided to the test specimen, all the nodes at the base of the steel plate shear wall model were fully fixed.

In order to simulate the out-of-plane bracing provided in the physical test, the out-of-plane displacements at both ends of the beam at the locations shown in Figure 5.10 were restrained. In order to prevent local distortions at the brace points, a number of nodes were restrained at each brace point.

In the physical test the horizontal loads at each floor level and also the gravity loads at the top of each column were applied through thick bearing plates welded to the test specimen. To simulate the effect of bearing plates in the finite element model a rigid body surface was defined by connecting the nodes under the bearing plates to a reference node with rigid links at each loading points and at the top of the columns where the gravity loads were applied (see Figure 5.10). Loads were delivered to the reference nodes through a loading frame described in section 5.6.

5.4.4 Residual stresses and history of plastic deformation from previous test

Residual stresses are present in all fabricated steel structures and are the result of differential plastic deformations. They are frequently the result of welding, but are also the result of differential cooling during the manufacture of hot rolled structural shapes, rolling of shapes and plates, force fitting or grinding. In steel plate shear walls residual stresses are present in the beams and columns as a result of the manufacturing process of the rolled shapes, welding of beams to columns and welding of the infill plates to the boundary members through fish plates. The test specimen had additional local residual stresses resulting from welding of attachments and stiffeners to transfer the loads to the test specimen. The resulting pattern of residual stresses is complex and since no measurements were taken, these residual stresses were not considered in the finite element model. The initial residual stresses will be dissipated and new patterns of residual stresses will arise as the steel plate shear wall deforms plastically. In a cyclic finite element analysis that considers material yielding, the cyclic plastic deformations will capture these new residual stresses. It is therefore believed that the initial residual stresses would only play a role in the initial elastic load cycles.

The previous test conducted by Driver *et al.* (1997) resulted in some plastic deformations, mainly in the first panel of the present specimen. These plastic deformations changed the material properties of the specimen and they should be considered in the analysis. Due to its complexity, the history of plastic deformations is neglected in the analysis of the three-storey steel plate shear wall.

5.4.5 Material properties

The constitutive relationship in the analysis is based on stress versus strain responses obtained from tension coupon tests of different parts of the steel plate shear wall. Although Driver *et al.* (1997) reported material properties for the four-storey steel plate shear wall from which the test specimen in this study was obtained, these material properties are not directly applicable to the three-storey specimen. The material properties reported by Driver *et al.* (1997) do not reflect any of the changes that took place as a result of the plastic deformations during four-storey shear wall test. It was not possible to conduct material tests for the three-storey specimen. As a consequence, the results of the tension tests from Driver *et al.* (1997) were used. The steel used in all parts of the shear wall exhibited the classical stress versus strain behaviour of hot rolled ductile steel with a well defined yield plateau. A simple rate independent constitutive behaviour that is identical in tension and compression is used. The elasto–plastic kinematic hardening material modelling, discussed later, requires a bilinear representation of stress versus strain curve. The bilinear stress versus strain curve is obtained by extending a line from the origin to the mean value of static yield point (the slope is equal to the mean modulus of elasticity) and then to the mean static ultimate stress and corresponding strain.

The material properties obtained from a tension coupon test are nominal values, i.e., engineering stress and engineering strain, which are defined in terms of an initial gauge length and initial cross sectional area of the coupon. The finite element analysis uses true stress (Cauchy stress) and logarithmic strain as stress and strain measures regardless of the type of analysis. To obtain the true stress (σ_{true}) and logarithmic plastic strain ($\varepsilon_{\ln}^{pl}$) the following transformations are applied to the tension coupon data (Lubliner, 1990):

$$\sigma_{true} = \sigma_{nom}(1 + \varepsilon_{nom}) \tag{5.17}$$

and

$$\varepsilon_{\ln}^{pl} = \ln(1 + \varepsilon_{nom}) - \frac{\sigma_{true}}{E} \tag{5.18}$$

Where, E is the modulus of elasticity σ_{nom} is the nominal (engineering) stress and ε_{nom} is the nominal (engineering) strain obtained from material tests.

The material models in ABAQUS/Explicit are based on "incremental" theories in which the mechanical strain increment, $\Delta\varepsilon$, is decomposed into an elastic part, $\Delta\varepsilon_{el}$, and a plastic part, $\Delta\varepsilon_{pl}$. An incremental plasticity model usually is formulated in terms of a yield surface, flow rule, and a hardening model. The von Mises yield surface is used in ABAQUS/Explicit to specify the state of multi-axial stress corresponding to start of plastic flow. This yield surface assumes that yielding of metals is independent of the hydrostatic stress and has the form of a cylinder that is centred on the hydrostatic axis in a three-dimensional principal stress space.

The associated flow rule is used to obtain the plastic strain increment. Based on this flow rule, as the material yields the inelastic deformation rate (plastic strain increment vector) is normal to the yield surface. Thus, the plastic deformation is volume invariant. This assumption is generally acceptable for most metals.

A hardening rule specifies the evolution of the yield surface during plastic flow. In ABAQUS/Explicit (Hibbitt *et al.*, 2001a) three types of work hardening models are provided for metals: a perfectly plastic model, an isotropic hardening model, and the Johnston-Cook hardening model. In the perfectly plastic model the yield stress does not change with plastic strain and, as a result, no hardening or softening occurs in the material. This model was tried for the pushover analysis as well as for cyclic analysis of the three-storey steel plate shear wall, but was not successful in predicting the post-yielding behaviour of the specimen. In the isotropic hardening model the size of the yield surface changes (increases or decreases) uniformly in all directions as plastic straining occurs. The isotropic hardening model in ABAQUS/Explicit is nonlinear and a full range of effective plastic stress versus effective plastic strain can be defined. The Johnston-Cook hardening model is a particular type of isotropic model. In this model the yield stress is defined as an analytical function of effective plastic strain, strain rate, and temperature. This hardening rule is suitable for modelling monotonic high rate deformations of most metals.

The isotropic hardening model was used only for the pushover analysis of the shear wall. However, cyclic loading of the test specimen implies many strain and stress reversals occur during the process. The Bauschinger effect becomes important and should be considered in the model. The kinematic hardening flow rule is intended to simulate the behaviour of metals subjected to cyclic loading and is typically applied to studies of low cycle fatigue. In this model the basic concept is that the yield surface translates in stress space without any rotation or changes in size. This means that yielding in one direction reduces the yield stress in the opposite direction, thus simulating the Bauschinger effect and anisotropy by work hardening.

Although ABAQUS/Explicit is intended for dynamic, hence cyclic, analysis, it does not have a kinematic hardening model. However, it allows the user to implement a material model through a user subroutine. In this respect a kinematic material model suitable for analysis of a shell element was prepared and used successfully for cyclic simulation of steel plate shear walls. Some specific issues that were encountered in this model are discussed below.

5.5 Kinematic hardening model

The stress tensor, $\underline{\sigma}$, for the case of a 3-D shell element is defined at an integration point in the local element axis coordinates as:

$$\underline{\sigma} = \langle \sigma_{11}, \sigma_{22}, \sigma_{33}, \sigma_{12}, \sigma_{23}, \sigma_{31} \rangle \tag{5.19}$$

in which 1, 2, and 3 refer to the element coordinate axes with direction 3 normal to the surface of the element. The stress σ_{33}, which is the through thickness stress, is normally neglected in shell elements.

Transverse shear stresses, σ_{23} and σ_{31}, are not calculated from the constitutive behaviour at points through the shell section. These stresses are obtained in ABAQUS from the transverse shear stiffness of the section. In general, the transverse shear stiffness is calculated by matching the shear response of the case of a shell element bending about one axis using a parabolic distribution of transverse shear stress (Hibbitt *et al.*, 2001b). This approach usually produces a reasonable estimate of shear flexibility of shells. In ABAQUS/Explicit, when using a user subroutine for material modeling the transverse shear stiffness values should be given as an input to the model. The equations used for calculating the transverse shear stiffness are presented in Appendix A.

From the above discussion, the constitutive model is based on the membrane stresses σ_{11}, σ_{22}, and σ_{12} as well as the strain increments $\Delta\varepsilon_{11}$, $\Delta\varepsilon_{22}$, $\Delta\varepsilon_{12}$, and $\Delta\varepsilon_{33}$. The subroutine also defines part of the internal energy due to membrane deformations and returns it to the main program in each increment. The required options in the input file and the subroutine are presented in Appendix B.

The kinematic hardening subroutine was verified by simulating the cyclic behaviour of a cantilever beam loaded with a concentrated force at the free end. All the details are depicted in Figure 5.11. The web and the flanges of the beam were discretized with shell elements (element S4R). Comparison of the cyclic behaviour of the beam obtained with ABAQUS/Explicit and ABAQUS/Standard, shown in Figure 5.11(d), indicates that ABAQUS/Explicit with the new material model subroutine gives the same result as ABAQUS/Standard and the Bauschinger effect is clearly simulated by the model. This indicates that the kinematic hardening model is valid and can be used for cyclic analysis of steel plate shear walls.

5.6 Displacement control analysis

Displacement control is preferred as a solution strategy over a load control scheme in this project. As discussed in Chapter 6, the finite element model was used to carry out a pushover analysis as well as a cyclic analysis of the three and four-storey steel plate shear walls. In a pushover analysis the objective is to obtain the stiffness and the capacity of the shear wall. In order to obtain the capacity properly, the solution strategy should be able to trace the response near the limit point and be able to pass the limit point. Because of the load response is flat near the limit point, a very small increment of load results in a large displacement. In addition, applying a load in a load control scheme that is larger than the capacity of the shear wall will result in an unstable dynamic solution. The response of a system after the limit point is important, but a load control scheme cannot pass the limit point and trace the descending branch. Therefore, in a pushover analysis a displacement control method in which the load level can be adjusted based on the displacement level is more useful.

The need for a displacement control strategy is more vital in a cyclic analysis. As explained in Chapter 3, a typical loading procedure for a cyclic test of a structure is to select a deformation control parameter such as the inter-storey drift, and control the magnitude of this parameter during the test. In the elastic range the load control strategy is adequate to determine the point of significant yielding of the deformation control parameter, δ_y. In the plastic range the cyclic behaviour should be obtained by successively increasing the deformation control parameter as a multiple of the yield deformation parameter.

In ABAQUS/Explicit the available control option is to apply a history of displacement, velocity and/or acceleration to one or more nodes separately. These nodes are treated as boundary nodes and the required force at each node to reach a specific displacement (velocity and/or acceleration) is obtained from equilibrium.

During cyclic loading of the three-storey steel plate shear wall, the gravity loads are constant and the cyclic loads are equal horizontal loads applied at each level. In order to implement a displacement control type analysis, the distributing beam system shown in Figure 5.12 was used as a loading frame. The loading frame consists of a system of rigid beam elements that are connected to the shear wall at beam levels in order to transfer horizontal forces only. The geometry and the connections are defined in such a way that any loads applied at node B7 on loading frame will be transferred equally to each level of the shear wall. For stability, out–of–plane displacement and rotation along the axis of the loading frame element are prevented. Since the selected system is statically determinate, it will not impose any constraint to the shear wall. Therefore, a system of equal horizontal loads can be applied to the shear wall only by controlling the displacement, velocity, or acceleration of node B7, as shown in Figure 5.12.

By changing the geometry of the loading frame, any proportion of loads can be applied to the shear wall and the response can be traced in the post limit state and unloading regions without any difficulty as well. However, with this system only the kinematics of node B7 on the loading frame can be controlled directly, so that, for a parameter other than this node, the control is indirect. For example, to run a cyclic simulation in which the control parameter is first storey drift of the shear wall, a pushover analysis is required to obtain an approximate relationship between node B7 and the first storey drift. This relationship allows a reasonable displacement history at node B7 to yield an approximate drift history for the first panel.

The loading frame developed for implementing a displacement control analysis of the four-storey steel plate shear wall with equal horizontal loads is shown in Figure 5.13. As can be seen the load or displacement should be applied at node B14.

Table 5.1: Measured initial imperfections in the infill plate of panel 1

Point	X(mm)	Y(mm)	Z(mm)
1	623	1212.5	-16
2	923	1212.5	-9
3	1223	1212.5	4
4	1523	1212.5	11
5	1823	1212.5	12
6	2123	1212.5	7
7	2423	1212.5	-3
8	2723	1212.5	-13
9	623	912.5	-7
10	923	912.5	-27
11	1223	912.5	-16
12	1523	912.5	11
13	1823	912.5	28
14	2123	912.5	21
15	2423	912.5	11
16	2723	912.5	7
17	623	612.5	4
18	923	612.5	-5
19	1223	612.5	-31
20	1523	612.5	-19
21	1823	612.5	15
22	2123	612.5	39
23	2423	612.5	27
24	2723	612.5	10
25	623	312.5	-2
26	923	312.5	4
27	1223	312.5	-12
28	1523	312.5	-24
29	1823	312.5	-4
30	2123	312.5	23
31	2423	312.5	27
32	2723	312.5	-3

Maximum out–of–plane displacement

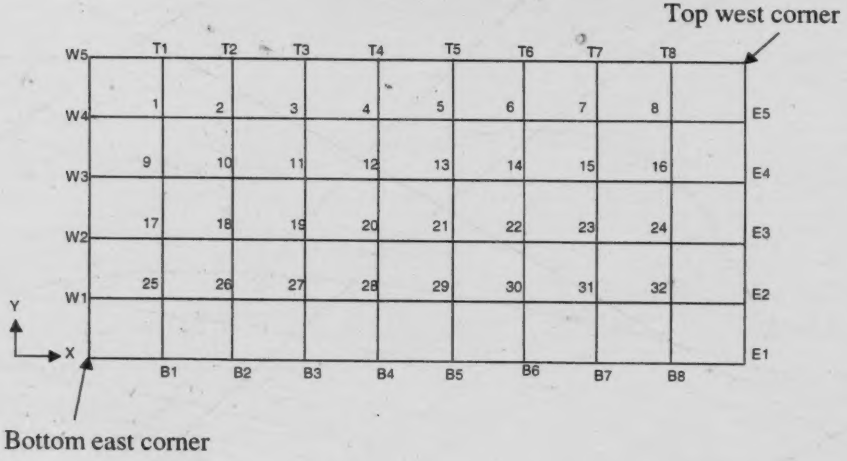
Top west corner
W5
W4
W3
W2
W1
T1
T2
T3
T4
T5
T6
T7
T8
E5
E4
E3
E2
E1
B1
B2
B3
B4
B5
B6
B7
B8
1
2
3
4
5
6
7
8
9
10
11
12
13
14
15
16
17
18
19
20
21
22
23
24
25
26
27
28
29
30
31
32
Y
X
Bottom east corner

Location of initial imperfection measurements

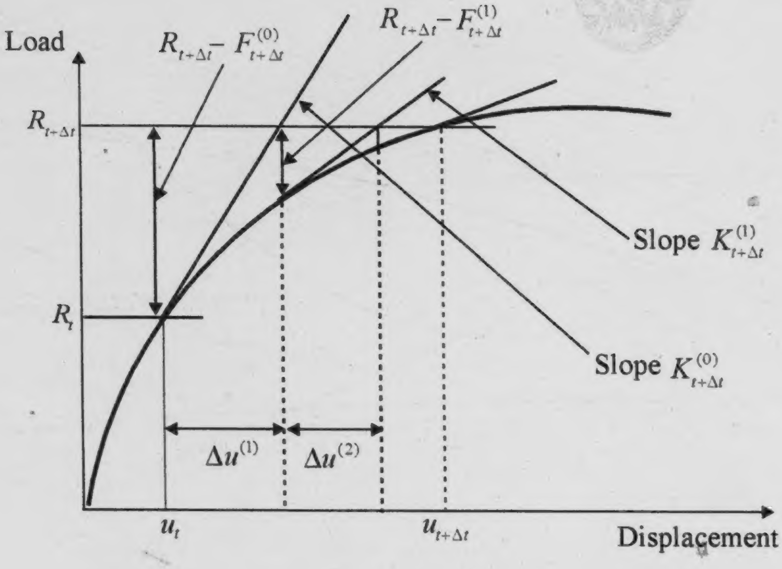
Load
$R_{t+\Delta t} - F^{(0)}_{t+\Delta t}$
$R_{t+\Delta t} - F^{(1)}_{t+\Delta t}$
$R_{t+\Delta t}$
R_t
Slope $K^{(1)}_{t+\Delta t}$
Slope $K^{(0)}_{t+\Delta t}$
$\Delta u^{(1)}$
$\Delta u^{(2)}$
u_t
$u_{t+\Delta t}$
Displacement

Figure 5.1: Illustration of Newton-Raphson iterative method

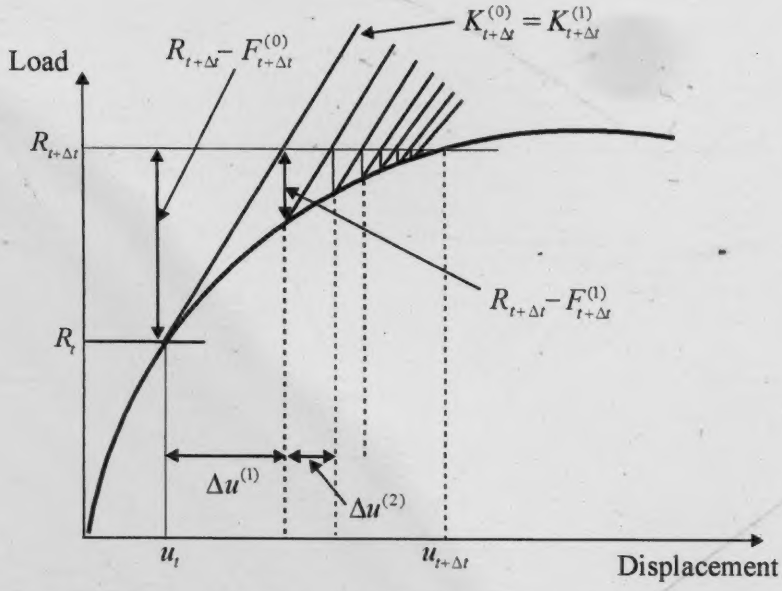
Load
$K^{(0)}_{t+\Delta t} = K^{(1)}_{t+\Delta t}$
$R_{t+\Delta t} - F^{(0)}_{t+\Delta t}$
$R_{t+\Delta t}$
$R_{t+\Delta t} - F^{(1)}_{t+\Delta t}$
R_t
$\Delta u^{(1)}$
$\Delta u^{(2)}$
u_t
$u_{t+\Delta t}$
Displacement

Figure 5.2 Illustration of modified Newton-Raphson iterative method

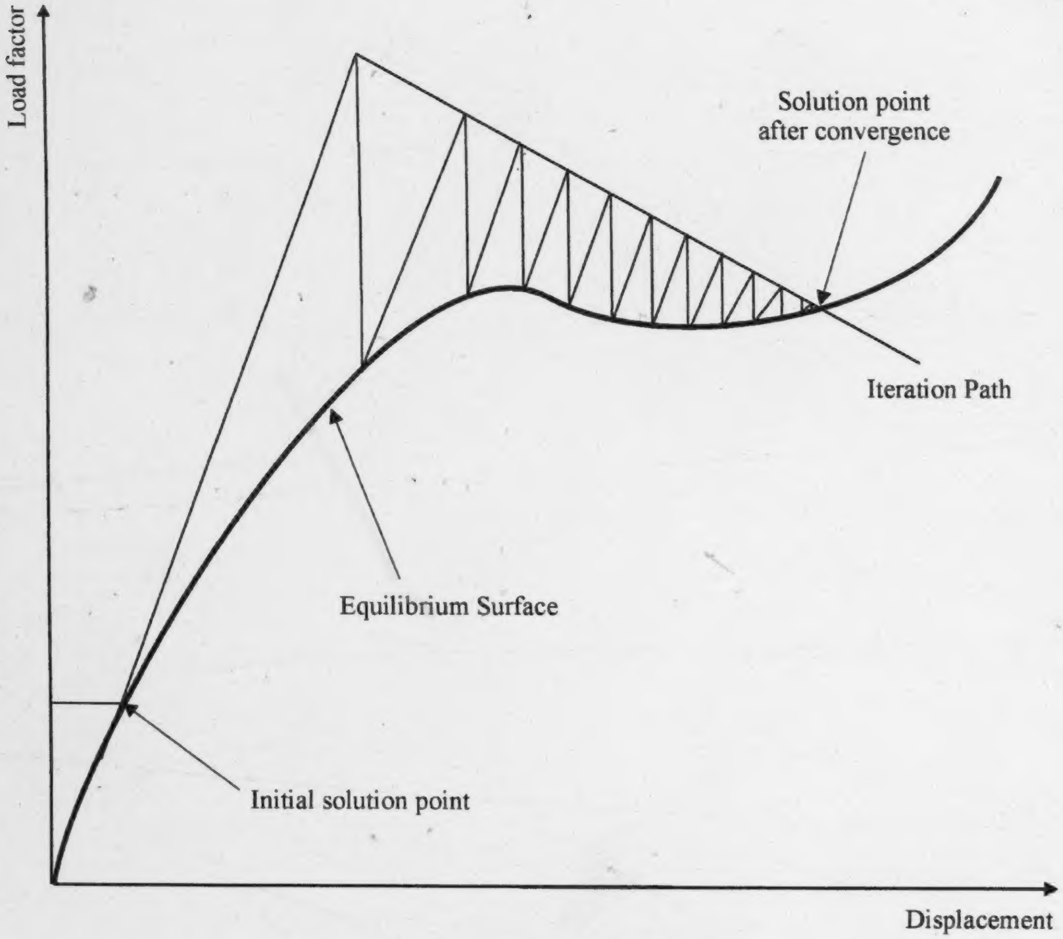
Load factor
Solution point
after convergence
Iteration Path
Equilibrium Surface
Initial solution point
Displacement

Figure 5.3: Modified Riks solution strategy

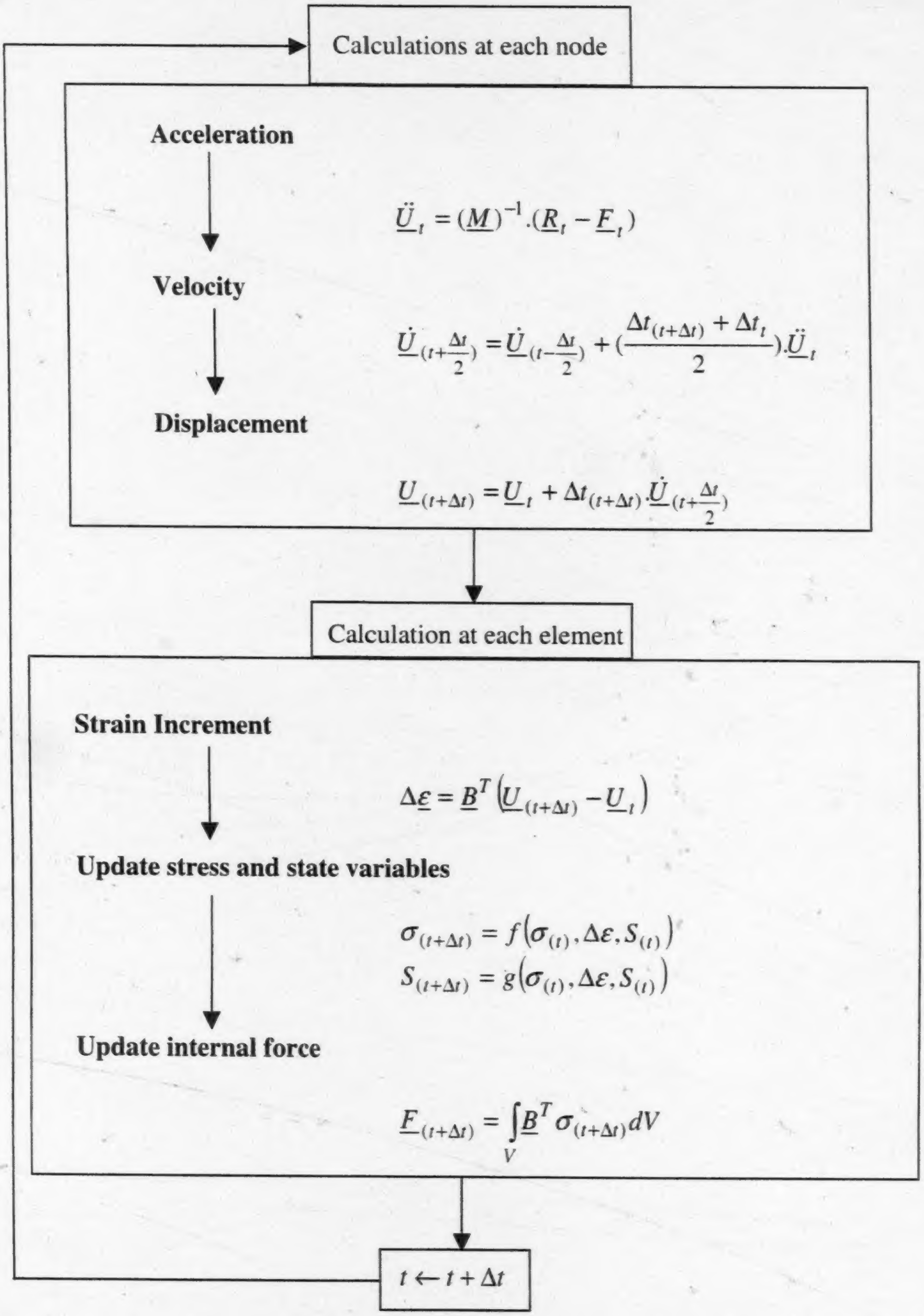
Calculations at each node
Acceleration
$\ddot{\underline{U}}_t = (\underline{M})^{-1}.(\underline{R}_t - \underline{F}_t)$
Velocity
$\dot{\underline{U}}_{(t+\frac{\Delta t}{2})} = \dot{\underline{U}}_{(t-\frac{\Delta t}{2})} + (\frac{\Delta t_{(t+\Delta t)} + \Delta t_t}{2}).\ddot{\underline{U}}_t$
Displacement
$\underline{U}_{(t+\Delta t)} = \underline{U}_t + \Delta t_{(t+\Delta t)}.\dot{\underline{U}}_{(t+\frac{\Delta t}{2})}$
Calculation at each element
Strain Increment
$\Delta\underline{\varepsilon} = \underline{B}^T\left(\underline{U}_{(t+\Delta t)} - \underline{U}_t\right)$
Update stress and state variables
$\sigma_{(t+\Delta t)} = f\left(\sigma_{(t)}, \Delta\varepsilon, S_{(t)}\right)$
$S_{(t+\Delta t)} = g\left(\sigma_{(t)}, \Delta\varepsilon, S_{(t)}\right)$
Update internal force
$\underline{F}_{(t+\Delta t)} = \int_V \underline{B}^T \sigma_{(t+\Delta t)} dV$
$t \leftarrow t + \Delta t$

Figure 5.4: Summary of explicit dynamic algorithm

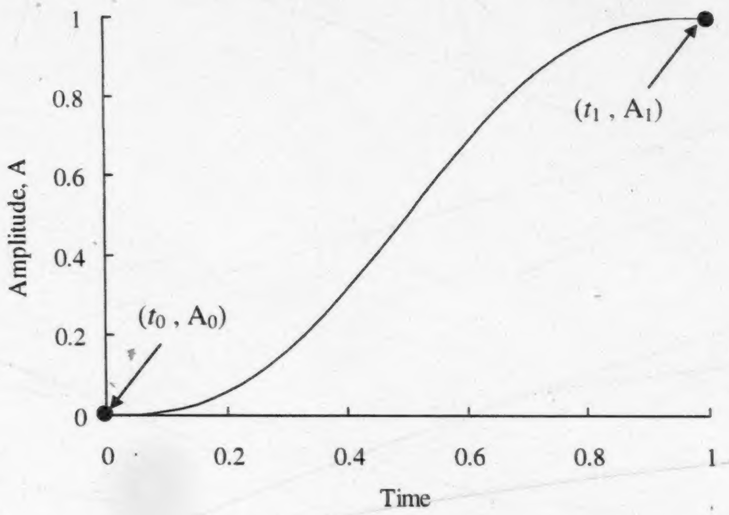

Figure 5.5: Example of smooth step amplitude function with two data points ($t_0 = 0.0$, $A_0 = 0.0$) and ($t_1 = 1.0, A_1 = 1.0$)

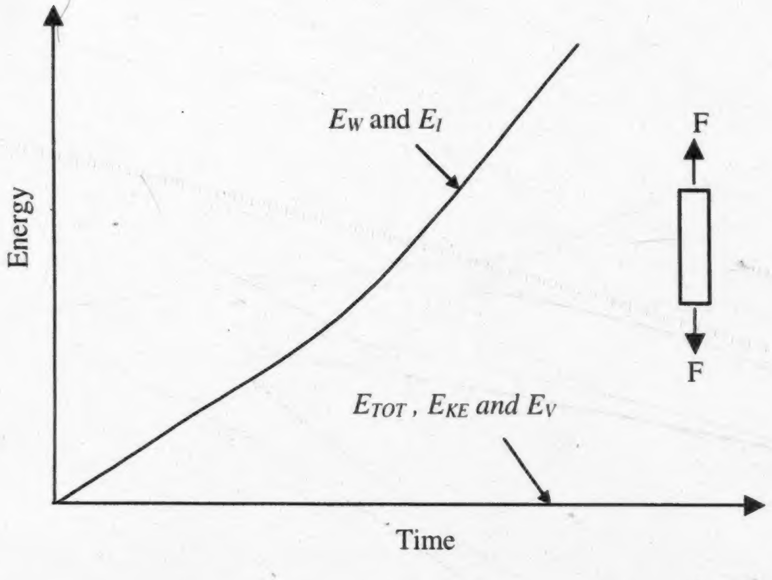

Figure 5.6: Energy history for quasi-static tensile test

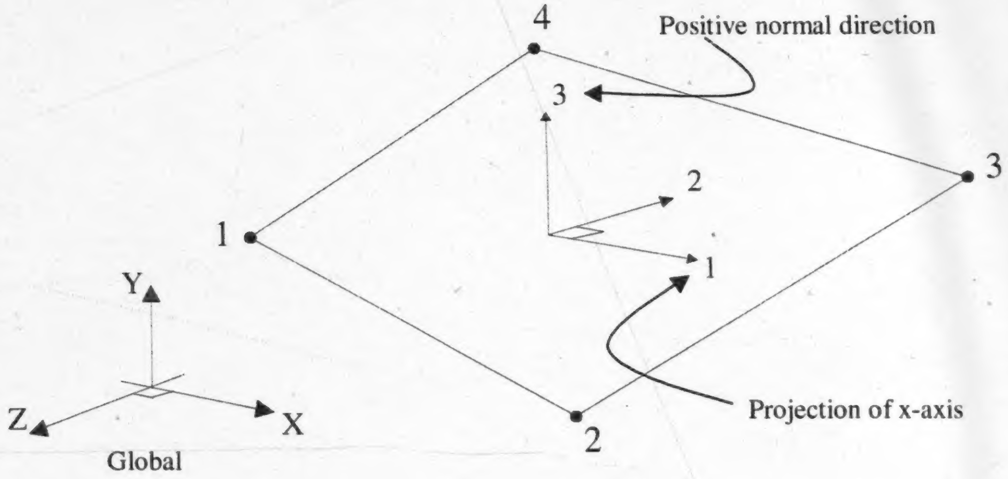
4
Positive normal direction
3
3
2
1
1
Y
Z
X
Global
2
Projection of x-axis

Default local axis direction for shell element

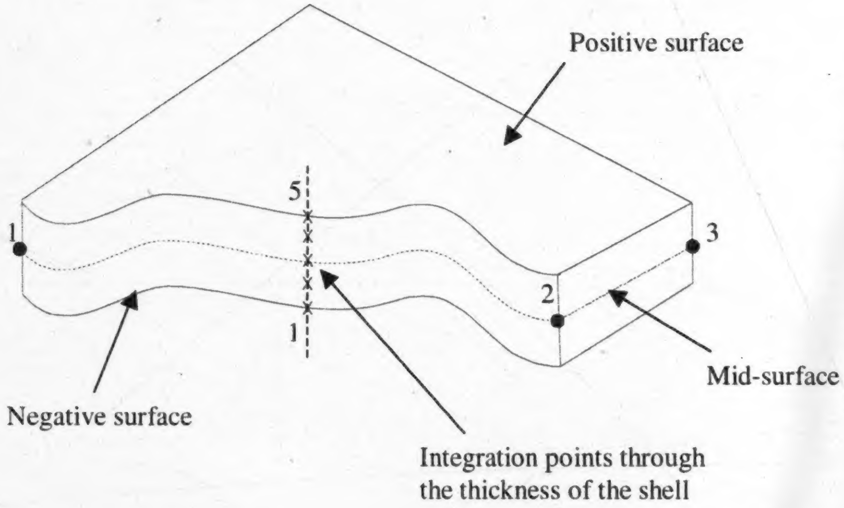
Positive surface
5
1
3
2
1
Mid-surface
Negative surface
Integration points through the thickness of the shell

Integration points through the thickness of shell element

Figure 5.7: Default local axis and integration points for shell element S4R

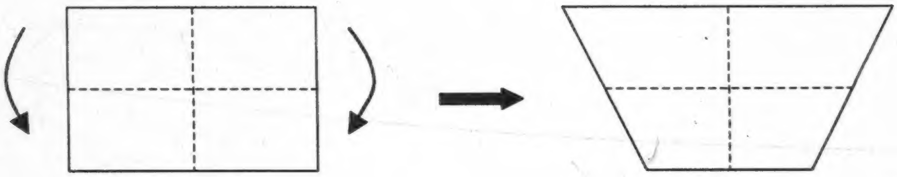

(a) Deformation of a first-order element with reduced integration subjected to bending

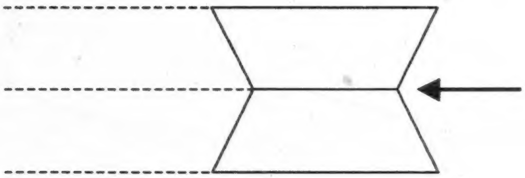

Concentrated force or boundary condition at a single node

(b) Concentrated force or boundary condition creating hourglass deformation

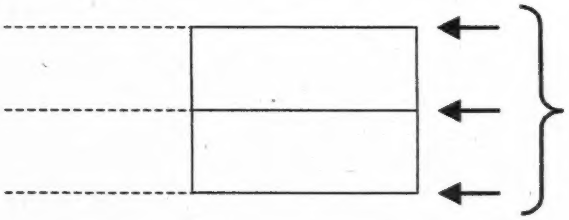

Force or constraint distributed over more nodes

(c) Improved deformation pattern with distributed force or constraint

Figure 5.8: Hourglass mode: (a) shape; (b) common source of hourglass mode; (c) method of improvement

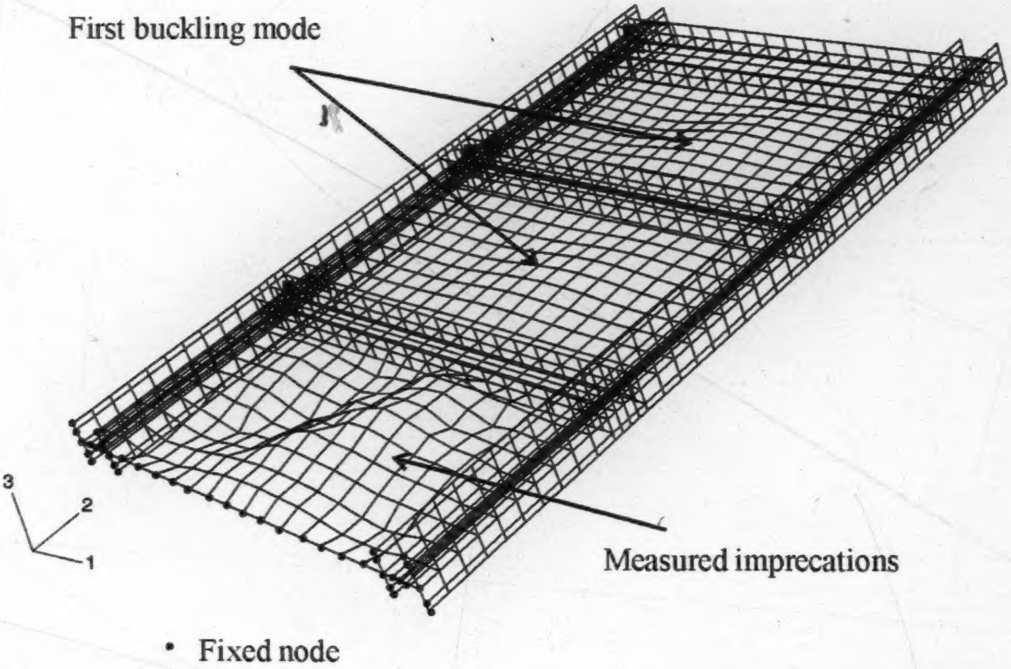
First buckling mode
3
2
1
Measured imprecations
• Fixed node

Figure 5.9: Imperfection shape used in finite element model (magnification factor = 5.0)

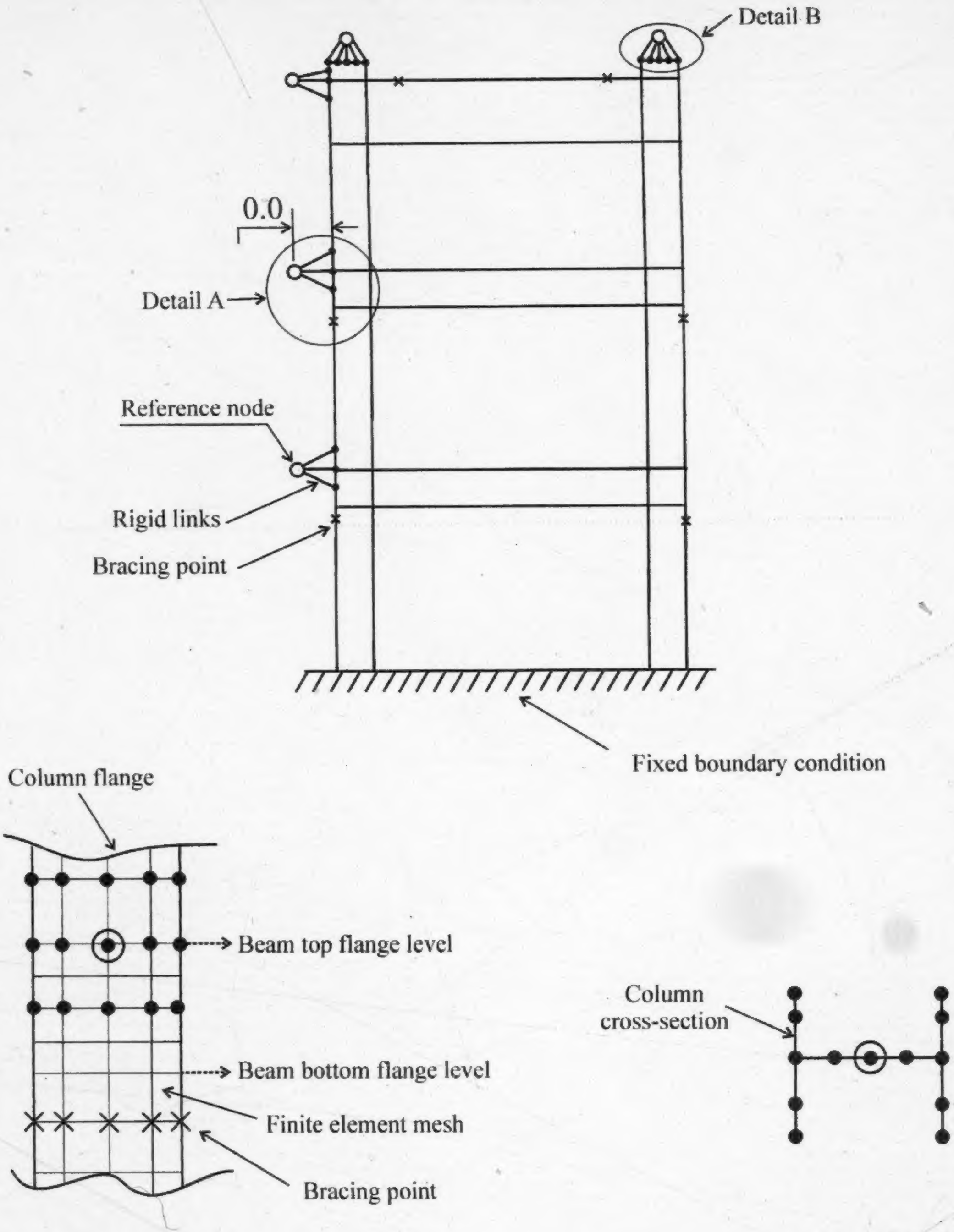
Detail B
0.0
Detail A
Reference node
Rigid links
Bracing point
Fixed boundary condition
Column flange
Beam top flange level
Beam bottom flange level
Finite element mesh
Bracing point
Column
cross-section

Side view of detail A

Top view of detail B

Figure 5.10: Boundary and loading conditions for the finite element model

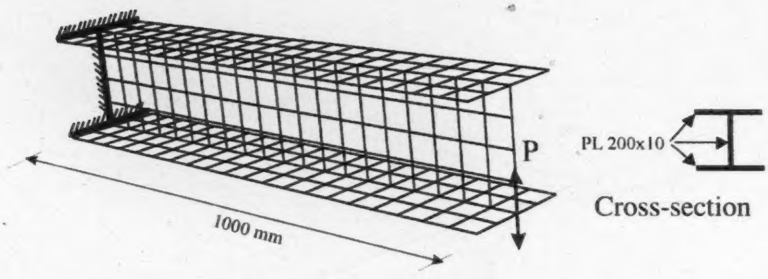
P
PL 200x10
Cross-section
1000 mm

(a) Finite element mesh with load and boundary condition

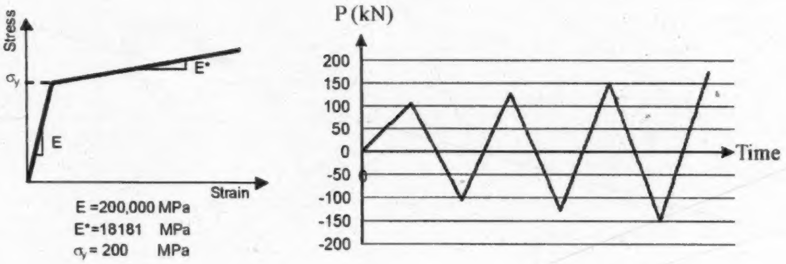

(b) Material model

(c) Applied load history

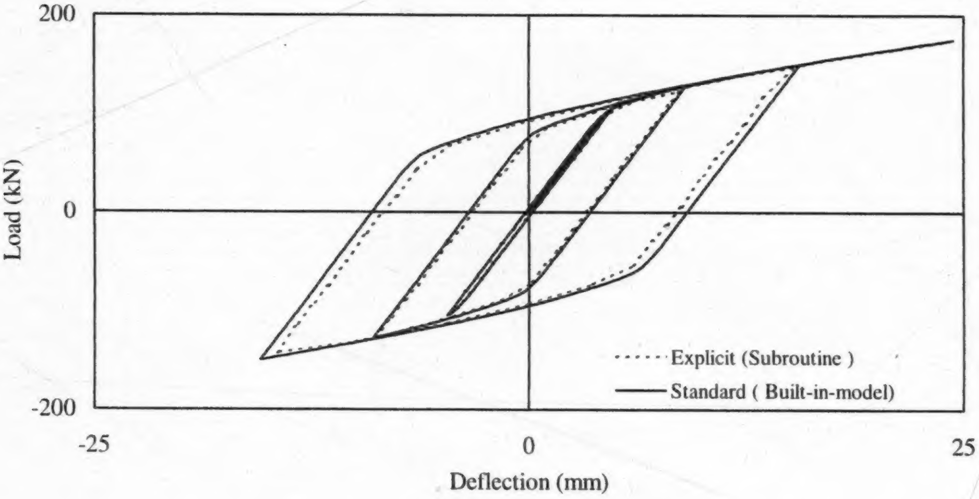

(d) Load versus deflection response

Figure 5.11: Cyclic response of a cantilever beam loaded at the free end

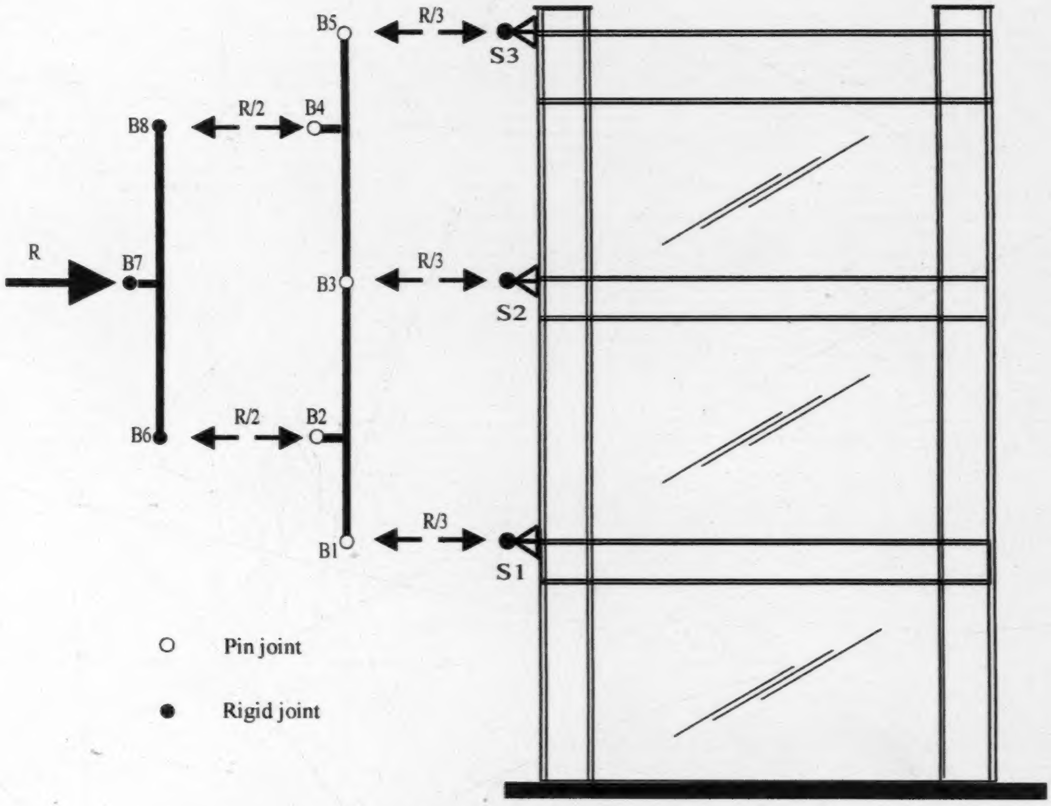
B5
R/3
S3
B8
R/2
B4
R
B7
B3
R/3
S2
B6
R/2
B2
B1
R/3
S1
○ Pin joint
● Rigid joint

Figure 5.12: Loading frame for displacement control of the three-storey steel plate shear wall specimen

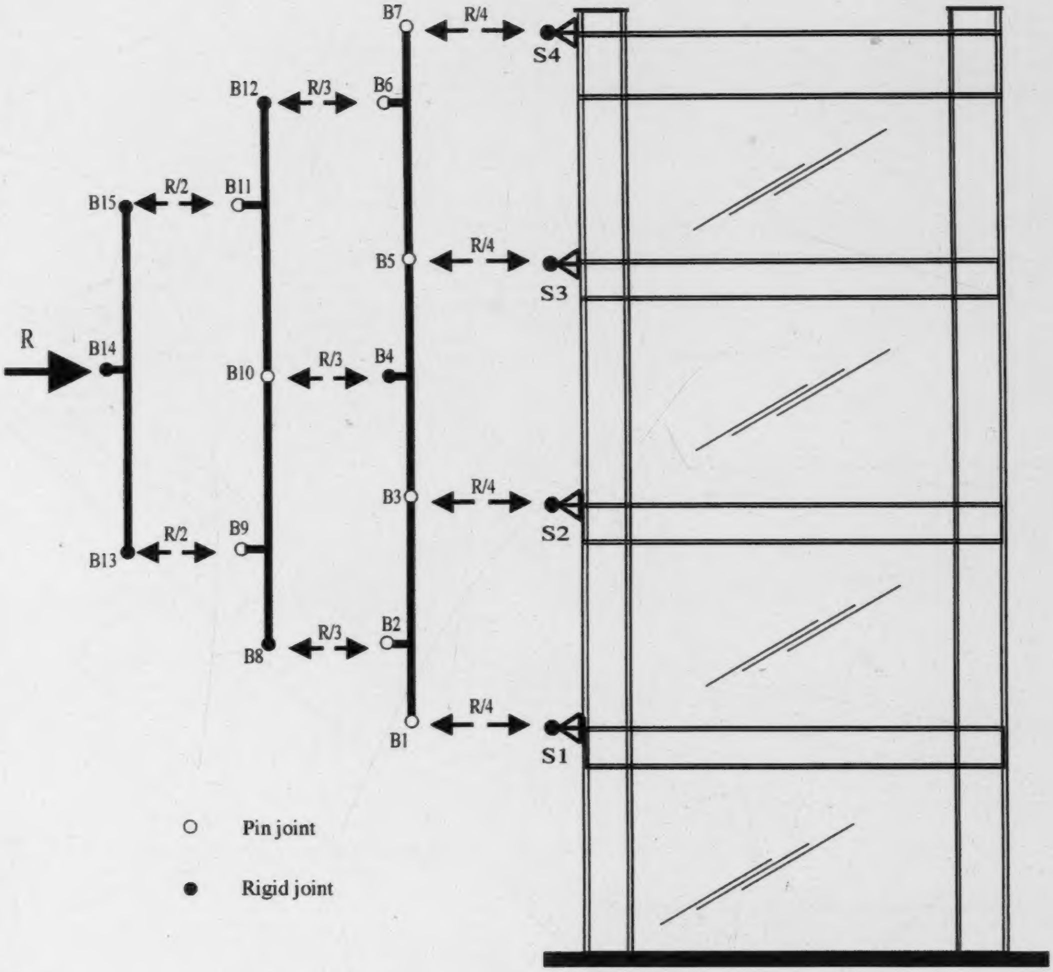
B7
R/4
S4
B12
R/3
B6
B15
R/2
B11
B5
R/4
S3
R
B14
B10
R/3
B4
B3
R/4
S2
B13
R/2
B9
B8
R/3
B2
B1
R/4
S1
○ Pin joint
● Rigid joint

Figure 5.13: Loading frame for displacement control of the four-storey steel plate shear wall specimen

6 VALIDATION OF THE FINITE ELEMENT MODEL

6.1 Introduction

The finite element model developed for analysis of unstiffened steel plate shear walls was presented in Chapter 5. The model is based on a nonlinear dynamic formulation and an explicit strategy is used to obtain the state of the model at each increment without any iteration.

In this chapter the model is used to simulate the behaviour of the three-storey steel plate shear wall described in chapters 3 and 4. The pushover analysis results and the cyclic behaviour are used as a basis of comparison with the test results. The finite element model is then applied to the four-storey steel plate shear wall tested by Driver *et al.* (1997) and the results of the analysis are compared with the test results.

The characteristics of the steel plate shear wall behaviour that were used to compare the result of the pushover analysis with the envelope of hysteresis loops obtained from the physical test were the initial stiffness, the point of significant yielding, the inclination of the tension field, and the shear resistance at the drift where the peak capacity was reached during the test. For the cyclic loading case, in addition to the aforementioned characteristics, the hysteresis loops (mainly pinching and stiffness at different stages of the hysteresis loops), the amount of energy absorbed during cyclic loading, and the deformed configuration of shear wall at different stages of the response were used as a basis of comparison between the cyclic load analysis and the test results.

6.2 Finite element analysis of the three-storey steel plate shear wall

6.2.1 Pushover analysis

To determine how accurately the proposed finite element model is able to predict the stiffness and the capacity of the three-storey steel plate shear wall specimen, a pushover analysis was carried out using the finite element model of the specimen described in Chapter 5. As explained in section 4.5, because of presence of the tension field in the west direction in the first panel before starting the test, the behaviour was not symmetrical in the elastic range. Since the plastic deformation history from the prior test on the four-storey steel plate shear wall was not considered in the finite element analysis, for simplicity, the pushover analysis was obtained by loading the model towards the west direction only. A gravity load of 540 kN was applied to the top of each column in the first load step. This magnitude is equal to the target gravity load used in the physical test and was kept constant for the remainder of the analysis.

The loading frame designed for displacement control of three-storey steel plate shear wall (see Figure 5.12) was used to apply increments of displacement at node B7. This displacement was increased monotonically until the displacement at the first level (node S1 in Figure 5.12) reached a value well beyond the displacement at which the specimen reached its ultimate capacity during the test. Monotonically increasing the displacement of node B7 is equivalent to monotonically applying equal horizontal in-plane forces at each floor level of the test specimen. Since this is a displacement control procedure, the response of the shear wall can be controlled well past the ultimate strength.

A frequency analysis of the test specimen indicated that the period of the first mode is 3.51 seconds. The associated mode shape, shown in Figure 6.1, corresponds to an out–of–plane plate movement with no drift of the overall frame. This mode is clearly similar to a buckling mode resulting from the application of gravity loads. The total time of the analysis was set at about 50 times the period of the first mode and the initial time increment of the model, which depends on mesh size and material properties (see equation 5.14), was obtained as 2.322×10^{-4} second.

The gravity load was applied to the shear wall over a loading period of 30 seconds. The time period of 30 seconds created a quasi-static loading condition. In the pushover analysis, in order to control the amount of kinetic energy of the specimen, velocity rather than displacement was imposed smoothly to node B7. Starting at 30 seconds, the velocity history shown in Figure 6.2 was applied horizontally to node B7 in order to load the shear wall laterally. The shear wall was pushed using a smooth amplitude function (see section 5.3.4), so that the velocity and acceleration at the beginning and end of the loading step are zero, thus reducing the influence of the inertia forces. Application of the velocity history shown in Figure 6.2 resulted in a horizontal displacement of 80 mm at node B7, which created enough drift at the first level to pass the limit point.

The history of different types of energy (see sections 5.3.6.1) developed in the whole system during the pushover analysis is shown in Figure 6.3. The internal and external energies are equal and the other forms of energy are negligible relative to internal energy. This indicates that the analysis has been carried out in a quasi-static condition. The artificial energy is also very small compared to the internal energy, which indicates that the hourglass mode has not affected the simulation (section 5.4.1). The kinetic energy versus time curve presented in Figure 6.4 shows that the kinetic energy varies smoothly over time except when the tension field is being developed. When the tension field develops the kinetic energy increases rapidly. This behaviour is characteristic of thin unstiffened steel plate shear walls and it was observed during the test when the development of the tension field was accompanied by loud reports and rapid out–of–plane deformations in the infill plates.

The horizontal velocity history of the top storey (all the nodes on the floor beams had almost the same velocity history) is depicted in Figure 6.5. The velocity response oscillates with small amplitude and intensifies when the tension field develops. In order to test the influence of this oscillation on the response of the specimen, the model was reanalyzed with the analysis time doubled. As shown in Figure 6.5, the velocity history of the top storey became smoother, but the global response was unchanged. Therefore, it was concluded that application of the velocity history shown in Figure 6.3 results in a reasonable quasi-static pushover analysis of three-storey steel plate shear wall.

Figures 6.6 to 6.8 show the predicted storey shear versus storey drift obtained from the pushover analysis and the envelope of the hysteresis curves obtained from the test results for storeys 1 to 3. The base shear versus horizontal displacement at the top storey is shown in Figure 6.9. Figures 6.6 to 6.9 all indicate that the finite element model predicts the stiffness of the shear wall very well in all storeys. The slightly higher predicted stiffness in the second and third panels is attributed to the fact that the applied loads were maintained horizontal in the finite element model, whereas the loads applied to the test specimens rotated slightly as the test specimen deformed. The resulting vertical component of the load, due to rotation of the hydraulic jacks, reduces the stiffness of the panel. Since this rotation increases along the height of the test specimen, the apparent reduction in wall stiffness is more visible for the top panels than for the lower panel. Another reason for the slight overestimation of the wall stiffness could be the effect of residual stresses, which are ignored in the finite element model. In addition to the response of the steel plate shear wall, the response of the bare frame is also shown in figures 6.6 to 6.9. It can be seen that the infill plate has significantly increased the stiffness and capacity of the frame.

The gradual post-ultimate strength degradation exhibited by the test specimen is not observed in the finite element model because the cracks and tearing of the shear wall were not included in the model. The strength of the shear wall after significant yielding is underestimated by the finite element model, especially in the first panel. Taking the capacity of the finite element model as the storey shear at the ultimate displacement observed in the test, the predicted capacity is lower than the observed capacity by as much as 12%.

Since the stiffness of the shear wall is predicted accurately with the finite element model, the lower predicted strength can reasonably be attributed to the difference in material properties between the finite element model and the three-storey steel plate shear wall test specimen. As stated before, the three-storey test specimen consisted of the top three storeys from the four-storey steel plate shear wall tested by Driver *et al.* (1997). The plastic deformations imposed to the second panel of that specimen during testing of the four-storey specimen may have changed the initial yield strength of the infill plate of the first storey of the three-storey specimen. This increase in yield strength is not uniform since the stress field in the infill plate is not uniform over a panel, which makes this factor very difficult to assess and incorporate into the finite element model. Since most plastic deformations from the previous tests are mainly concentrated in the first panel of the three-storey specimen, this is where the largest discrepancy between predicted and test capacities are found to lie.

A vector plot of the in-plane principal stresses at the mid-surface of the elements is shown in Figure 6.10 when the shear wall is loaded at its ultimate capacity. Except at the corners of the infill panels the orientation of the principal stresses is almost the same over the entire infill plate. The angle of inclination of the tension field, relative to the vertical, is measured from this vector plot as 51°, 38°, and 42° in the first, second and third panel, respectively. The angle of inclination of the tension field at ultimate load during the test was measured as 51° for the first panel and 45° for the second panel (see Chapter 4). There is an excellent agreement between the measured and the calculated tension field angle of inclination in the first panel. The orientation of the tension field in panel 2 obtained from the finite element analysis is 15% less than the angle measured during the test. The angle of inclination of the tension field predicted using Equation 2.2 is 42°, 42°, and 44° for the first, second, and third panels, respectively. This equation for the calculation of the tension field orientation is based on some simplifying assumptions, including elastic behaviour, whereas the measured values from the test and the finite element analysis are obtained at the limit points.

6.2.2 Cyclic analysis

A pushover analysis provides an estimate of the stiffness and capacity of a steel plate shear wall as it captures closely the envelope of cyclic response of a system. However, to evaluate the energy dissipation characteristics and the efficiency of a steel plate shear wall under cyclic loading, the finite element model should be able to simulate accurately the cyclic response of the system.

Any pattern of displacement history can be applied to the shear wall by controlling the displacement or velocity of node B7 (see Figure 5.12). For simplicity, drift of the first panel was taken as a control parameter to cycle the finite element model. In the first step the target gravity load of 540 kN was applied to the top of each column and was kept constant during the rest of analysis. Based on the relationship between horizontal displacement of node 7 and drift of the first panel (obtained from the pushover analysis of the shear wall discussed in section 6.2.1) the history of displacement at node B7 was set to create the desirable drift history for the first panel. In the following load steps the shear wall was cycled by increasing drift of the first panel as a multiple of the yield drift. At each displacement level the shear wall was cycled two times in order to develop a stable hysteresis curve.

In order to better control the kinetic energy of the system, node B7 was displaced following a velocity history equivalent to the desired displacement history. Figures 6.11 and 6.12 show velocity versus time and displacement versus time curves used at node B7, respectively. The velocity history of node B7 was generated using the SMOOTH STEP option (see section 5.3.4). The velocity was kept small in order to minimize the delivered kinetic energy to the steel plate shear wall and the time period was calculated in such a way that the area under the velocity curve results in the desired displacement at node 7. The resulting drift in the first panel as a function of time is presented in Figure 6.13. The variation with the time of the different energies for the whole model is shown in Figure 6.14. The internal and external energies are similar and the kinetic and artificial energies are negligible during the cyclic loading, which indicates that the load model simulated a quasi-static condition. The ripples seen in the internal and external energy curves are related to the loss of elastic energy of the system during the unloading portions of each loading cycle.

The hysteresis curves generated from the storey shear versus storey drift are shown in figures 6.15 to 6.17 for both finite element analysis and test results. Figure 6.18 presents a comparison of the hysteresis curves generated for the whole specimen and the finite element analysis. Using the response characteristics outlined in section 6.1 as a basis of comparison, it was concluded that very good agreement between the test and the finite element analysis exist. The pinching of the hysteresis curves, which is an important feature of unstiffened steel plate shear walls, is captured reasonably well by the finite element model. During the early reloading phase, a significant reduction of stiffness occurs after a load reversal. This reduction of stiffness remains until redevelopment of the tension field in the infill plate. Figure 6.19a shows the deformed configuration of the steel plate shear wall at full development of tension field during loading of the wall in the positive 1-direction. For comparison, the configuration of the first and the second panels of the specimen during the test is also depicted in Figure 6.19b. The deformed shape obtained from the finite element analysis is very similar to the one observed during the test. Both have the same configuration and number of buckle waves in the infill plates. The deformed configuration of the steel plate shear wall at an early stage of the redevelopment of the tension field and at full tension field development during loading of the shear wall in the negative 1-direction are shown in figures 6.20 and 6.21, respectively.

Although the finite element model successfully emulates the cyclic behaviour of the steel plate shear wall, there are a few differences between the test and the finite element model responses. Starting at load cycle 21, a number of tears and cracks developed in the shear wall because of localized plastic deformation. The size of these tears increased with each loading cycle. This phenomenon causes a gradual stiffness reduction after each cycle of loading, which can be observed in the experimental response but not in the finite element response.

The hysteresis curves generated by the analysis show slightly less pinching than the pinching observed in the test results. The test specimen showed a significant reduction in stiffness immediately after reloading in the opposite direction, whereas this stiffness reduction is somewhat delayed in the finite element model. One reason for this behaviour might be the effect of the fish plates, which were not incorporated in the finite element model. Referring to Figure 3.3, which shows the details of the connection of the infill plates to the boundary members, it can be seen that the tension field developed in the infill plates is transferred to the boundary members at an eccentricity equivalent to the average thickness of fishplate and infill plate. The eccentricity of the force on the boundary members may affect the response of the system. As a result, considering the fishplate in the finite element model may improve the pinching simulation.

6.2.3 Energy dissipation

The ability of a structural system to dissipate energy is one of the key parameters for evaluating the performance of a system in a severe earthquake. A common approach used to account for inelastic seismic performance of a structural system is to employ a seismic force reduction factor. This factor reduces the elastic spectral demands to a design level that would be encountered if a system possesses significant inelastic behaviour. Structural systems that can effectively dissipate energy are permitted a larger reduction. The National Building Code of Canada (NBCC, 1995) introduces a force modification factor, R, to account for inelasticity in the response of a system. Energy dissipation ability is a key parameter used to establish a value for this factor. The area enclosed by hysteresis loops generated during a specific load or displacement history is used as a measure of the energy dissipated by the system.

In order to compare the energy dissipation ability of the finite element model with that of the test specimen, hysteresis loops that have reached a stable behaviour will be used. Because the behaviour of the test specimen was not symmetrical, as discussed in Chapter 4, an unsymmetrical cycle is assumed to be equivalent to a symmetrical cycle with the drift level taken as the average drift from the two excursions.

The amount of energy dissipated during a stable cycle is obtained by measuring the area enclosed by the hysteresis curve using the trapezoidal rule. Figures 6.22 to 6.24 present the amount of energy dissipated by the first, second, and third panels from both the test and the finite element analysis plotted against the drift level. Figure 6.25 plots the dissipated energy for the system, which was calculated using the base shear versus displacement at the top of the steel plate shear wall. In general, there is good agreement between the test and the finite element analysis, although the finite element model overestimates the dissipated energy in all the panels. At a drift level of 1% the test-to-predicted energy dissipation in panels 1 and 2 is 0.75 and 0.85, respectively. The test-to-predicted energy dissipation at a drift level of 2% is 0.85 and 0.90 for panels 1 and 2, respectively.

6.3 Finite element analysis of the four-storey steel plate shear wall tested by Driver *et al.* (1997)

Although good agreement between the finite element analysis and the test results from the three-storey steel plate shear wall was observed in section 6.2 based on the observed characteristics of the steel plate shear wall outlined in section 6.1, some of the differences were attributed to the effect of the previous test by Driver *et al.* (1997). Since the history of plastic deformations was not considered in modelling the three-storey shear wall, a further test of the finite element model was carried out by modelling the four-storey steel plate shear wall tested by Driver *et al.* (1997).

The geometry of the four-storey steel plate shear wall is shown in Figure 2.5. Modelling of the boundary conditions, infill plate, and material properties in the first panel is similar to the first panel of the three-storey model discussed earlier, except that the first plate-buckling mode of the shear wall was used as initial imperfections instead of measured values. The peak amplitude of the imperfection was set at 10 mm in order to represent a reasonable maximum out–of–flatness of the infill plate.

As explained in Chapter 2, the test was conducted with a constant gravity load applied at the top of the columns and equal cyclic horizontal loads, which were applied at each floor level. In order to conduct a displacement control analysis, a loading frame was designed for the finite element model, similar to the one used for the three-storey analysis. Details of this loading frame are depicted in Figure 5.13. The loading frame is an assembly of rigid elements that form a statically determinate system. The horizontal force or displacement is applied only at node B14 on the loading frame. As with the three-storey shear wall analysis, a velocity history was applied at node B14, and this translated into a displacement history and associated boundary forces. The geometry and connections of the loading frame were selected so that the force at node B14 was distributed equally to all four levels.

6.3.1 Pushover analysis

The same procedure and controls used for the pushover analysis of the three-storey shear wall model were followed for conducting a monotonic pushover analysis of the four-storey shear wall model. A gravity load of 720 kN was first applied to the top of each column and was kept constant for the remainder of the analysis.

The displacement at node B14 of the load frame (see Figure 5.13) was increased smoothly and monotonically until the displacement at the first level, node S1, reached a value well beyond the drift at ultimate capacity of the specimen. The energy content of the model was investigated to assure a smooth quasi-static analysis.

The storey shears for all four panels are plotted against the storey drift and compared with the envelope of the hysteresis curves obtained from the test results in figures 6.26 to 6.29. The base shear is plotted against the displacement at the top of the wall in Figure 6.30. Figures 6.26 to 6.30 show an excellent agreement between the test and the finite element analysis. As was the case for the analysis of three-storey steel plate shear wall, the elastic stiffness is predicted well. The predicted elastic stiffness of all four panels is the same as observed during the test. Any slight variations can be attributed to the rotation of the hydraulic jacks during the experiment, which was not considered in the finite element model.

The post-yielding response of the test specimen is also predicted well by the finite element analysis. The capacity of the shear wall is under-predicted by only 7.8% on average at all panels compared to 12% under-prediction for the three-storey shear wall. Compared to the three-storey steel plate shear wall, the prediction of the response of the four-storey steel plate shear wall in the post-yielding region is closer to the observed test result. This improvement in the prediction of the test result was expected since the four-storey specimen had no prior history of plastic deformation.

Figure 6.31 shows a vector plot of the in-plane principal stresses at the ultimate load at mid-surface of the shell elements. The orientation of principal stresses is uniform for relatively large portions of the infill plate in each panel. From the plot of the principal stress vectors, the angle of inclination of the tension field is obtained as 45°, 43°, and 45° for panels 1, 2, and 3, respectively. The corresponding angles of inclination of the tension field are obtained by Equation 2.2 as 42° for all three panels. As was observed for the three-storey steel plate shear wall, the inclination of the tension field predicted using equation 2.2 is in very close agreement to the inclination observed in the finite element model.

6.3.2 Cyclic analysis

Cyclic analysis of the four-storey steel plate shear wall was conducted in the same way as for the three-storey steel plate shear wall. The gravity load was first applied to the top of each column and was kept constant for the rest of the analysis. Drift of the first panel was selected as the control parameter to establish a cyclic load history.

The drift at significant yielding and the relationship between the horizontal displacement of node B14 (on the loading frame) and node S1 (at level 1) were obtained from the pushover load analysis. Using this information, a proper velocity history was applied at node B14 in order to create the desired displacement history at the first panel. It should be noted that, despite the fact that the test specimen was not loaded symmetrically because of stroke limitation of the actuator at level 3, the finite element model was loaded symmetrically for simplicity.

Hysteresis loops obtained from the finite element analysis of the four-storey steel plate shear wall are compared with the hysteresis loops obtained from the test results in figures 6.32 to 6.36 for each panel and the displacement at the top of the shear wall. For simplicity, only the portion of the test results where the test specimen was loaded symmetrically in both directions is presented in the figures. In general, there is good agreement between the test and the finite element analysis. The capacity and stiffness of the shear wall are in excellent agreement with the test results but, as was the case for the three-storey steel plate shear wall, pinching of the hysteresis loops is not as pronounced as the test. A possible reason for this discrepancy was discussed in section 6.2.2.

6.3.3 Energy dissipation

Figures 6.37 to 6.40 show the energy dissipated by each panel of the steel plate shear wall as a function of drift level. The overall energy absorbed by the steel plate shear wall as a function of the displacement at the top of the wall is plotted in Figure 6.41. As expected, the finite element model overestimates the energy dissipation primarily because the pinching of the hysteresis loops is not simulated accurately. The limitation in the stroke of the third level actuator during the test is also another cause of the lower energy dissipation observed in the test specimen as compared to the finite element model.

A comparison of the predicted behaviour of a three-storey and a four-storey steel plate shear wall with test results has indicated that the finite element procedure developed in Chapter 5 is able to provide a reliable prediction of the stiffness, point of significant yielding, pinching of hysteresis loops, energy absorption, and strength of steel plate shear walls subjected to cyclic loading. The validated procedure will be used in Chapter 8 to conduct a parametric study.

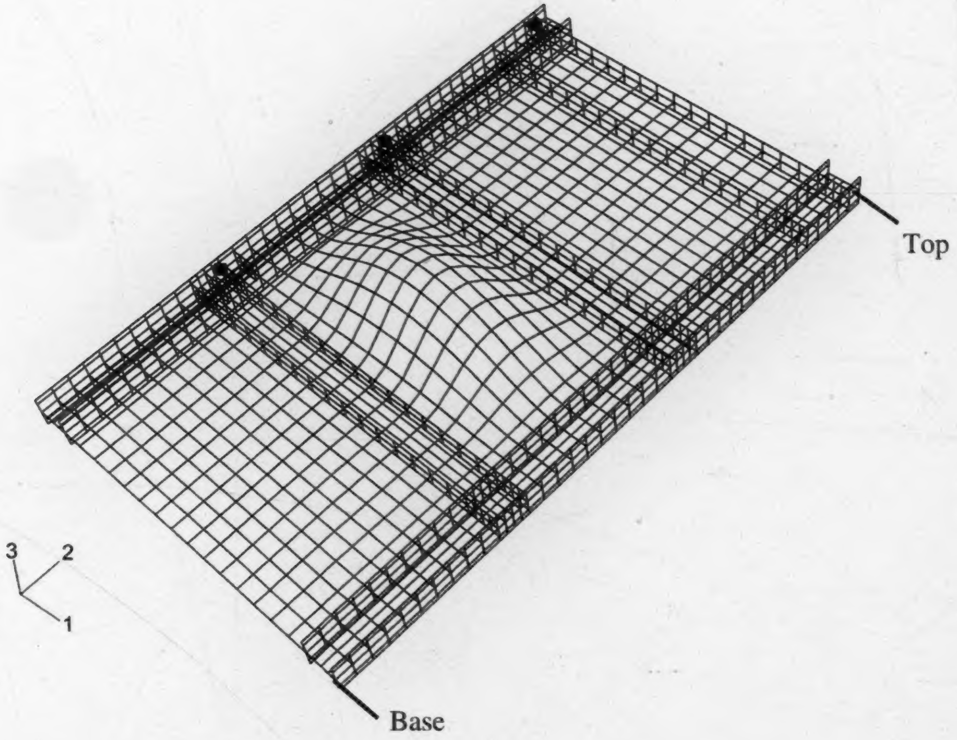
Top
Base
3
2
1

Figure 6.1: First vibration mode of the three-storey steel plate shear wall

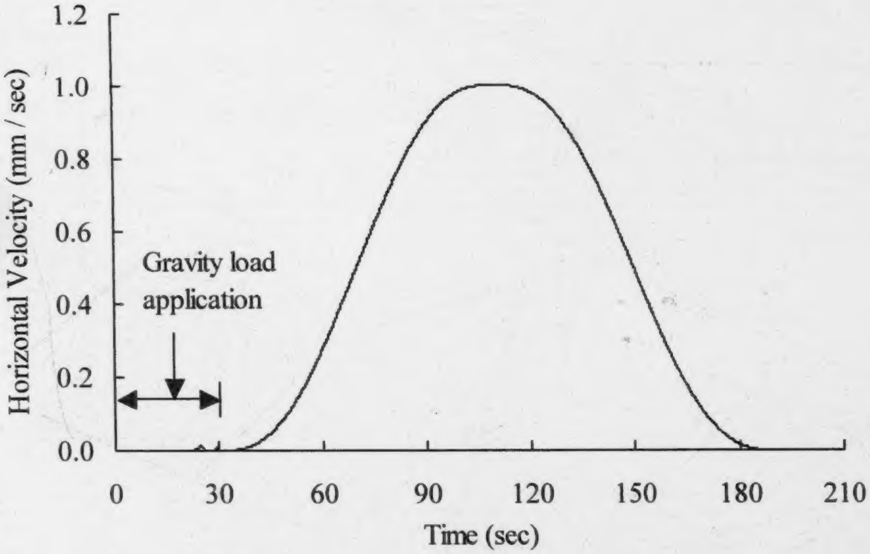

Figure 6.2: Velocity history for node B7 in the pushover analysis of the three-storey steel plate shear wall

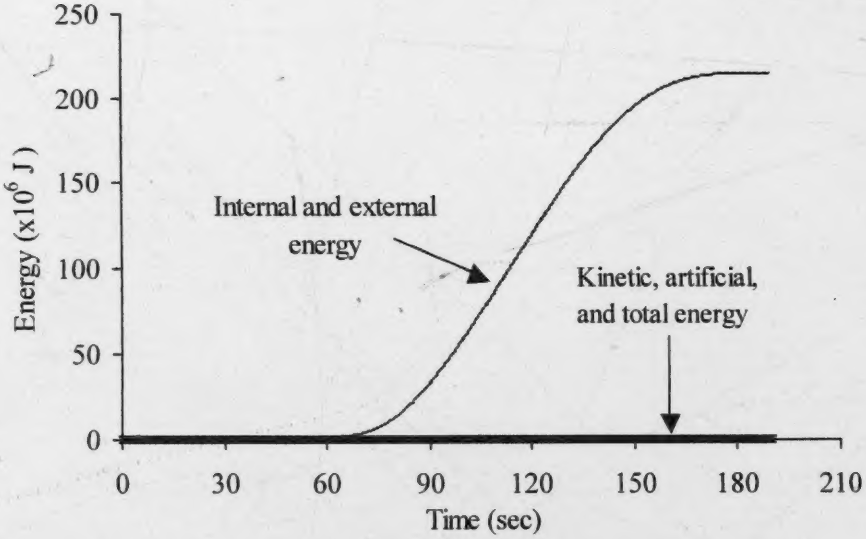

Figure 6.3: Energy history of the pushover analysis of the three-storey steel plate shear wall

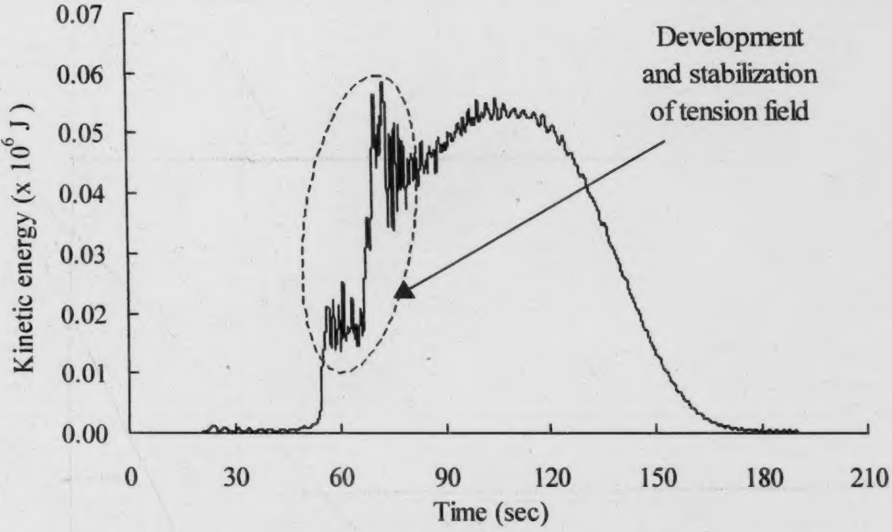

Figure 6.4: History of kinetic energy of the pushover analysis of the three-storey steel plate shear wall

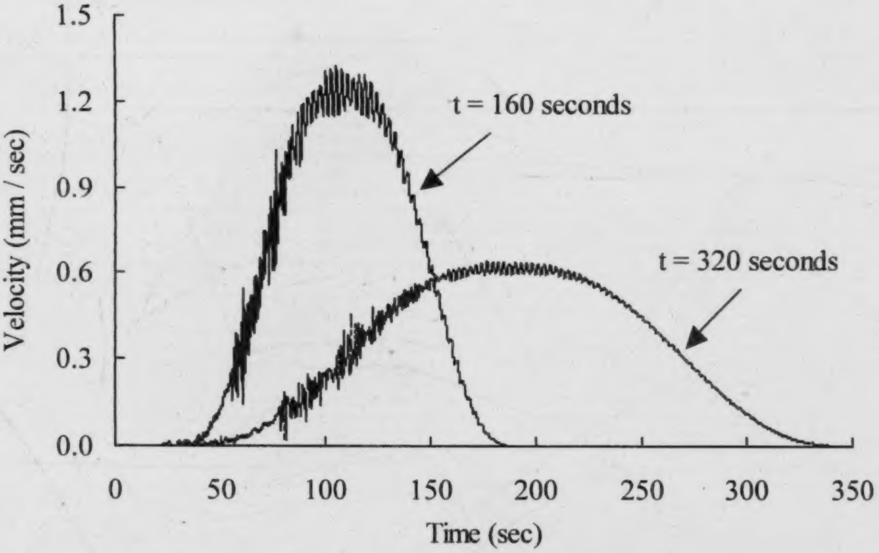

Figure 6.5: Top storey velocity history during a pushover analysis of the three-storey steel plate shear wall for two different time periods

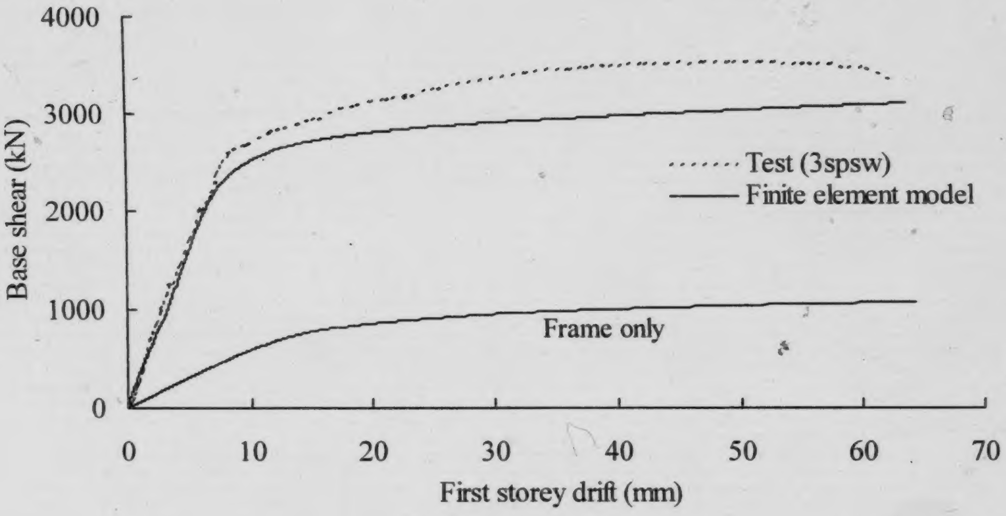

Figure 6.6: Monotonic finite element analysis compared with the envelope of the test cyclic response — Panel 1

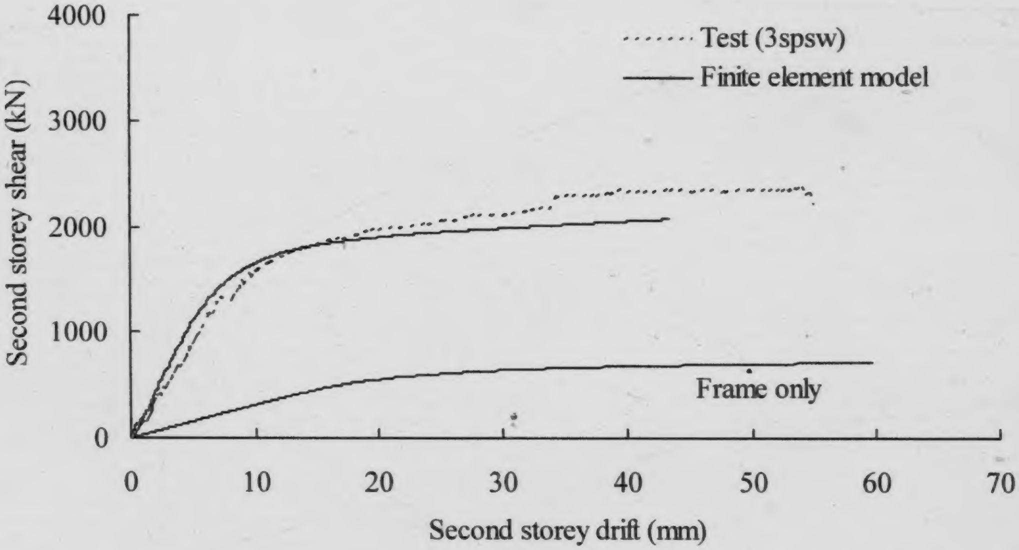

Figure 6.7: Monotonic finite element analysis compared with the envelope of the test cyclic response — Panel 2

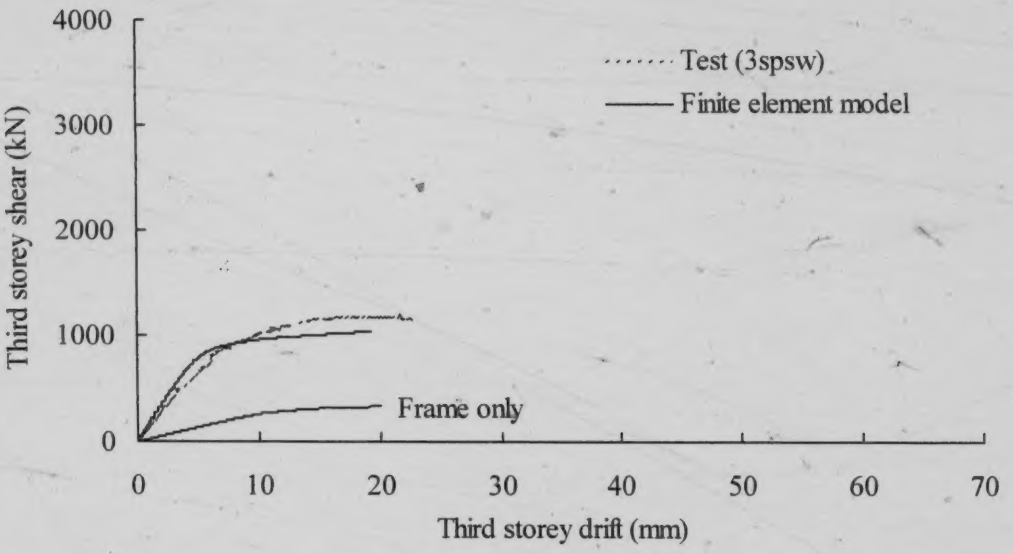

Figure 6.8: Monotonic finite element analysis compared with the envelope of the test cyclic response — Panel 3

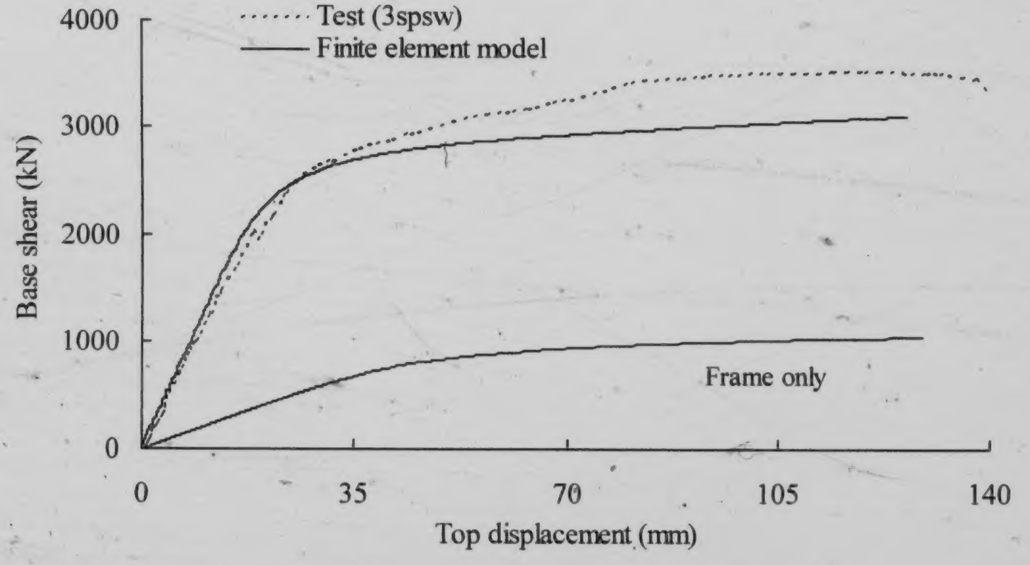

Figure 6.9: Monotonic finite element analysis compared with the envelope of the test cyclic response — Top displacement

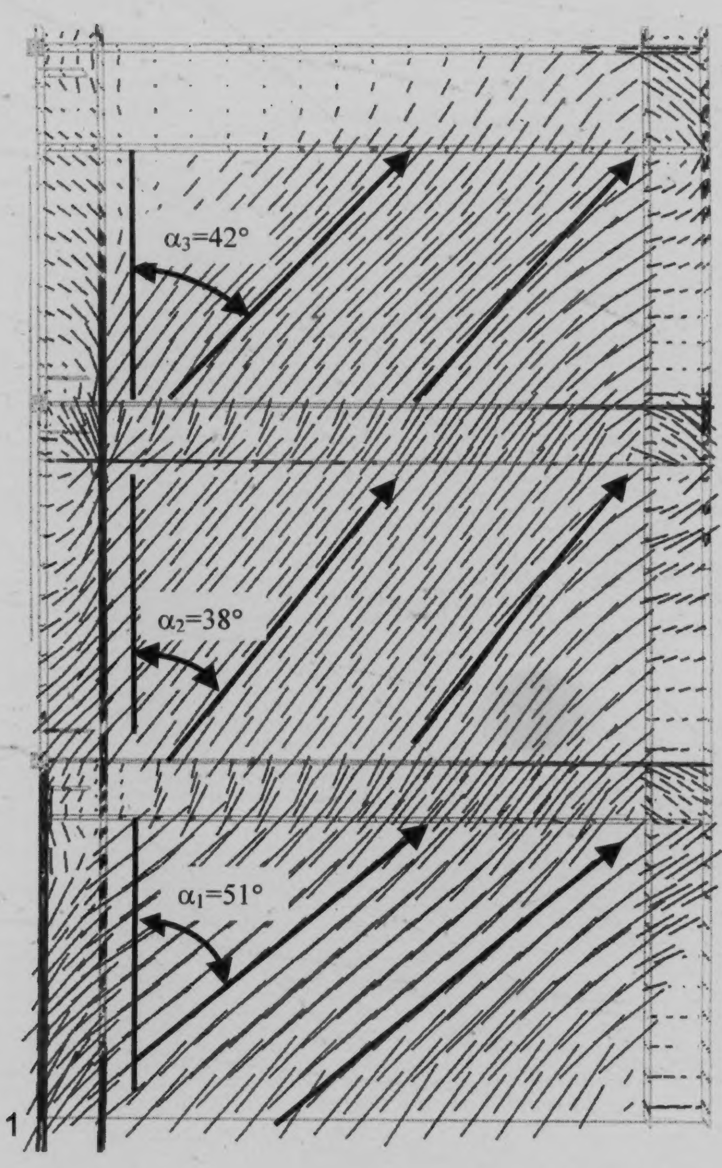
α_3=42°
α_2=38°
α_1=51°
1

Figure 6.10: Vector plot of maximum in-plane principal stress at ultimate load—Mid surface of shell elements

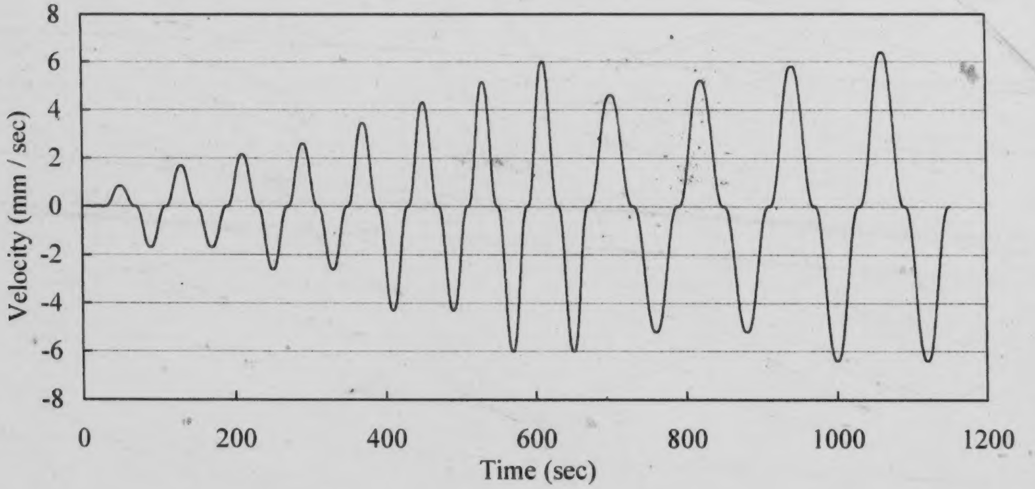

Figure 6. 11: History of horizontal velocity applied to node B7 on loading frame

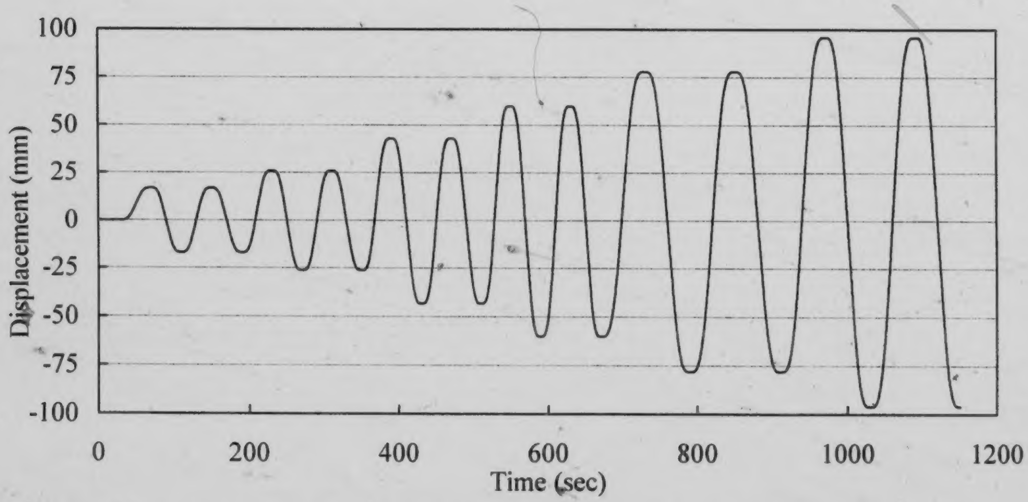

Figure 6.12: History of horizontal displacement at node B7 on loading frame

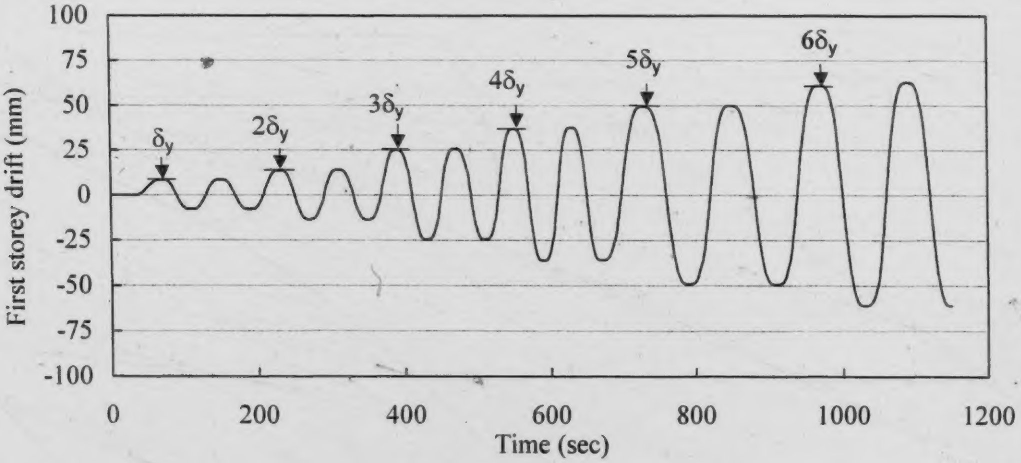

Figure 6.13: History of first storey drift

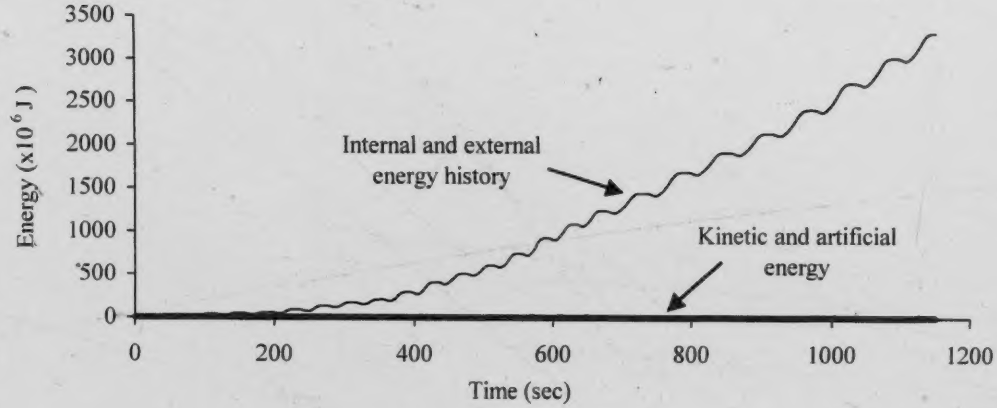

Figure 6.14: Energy history in cyclic analysis of the three-storey steel plate shear wall

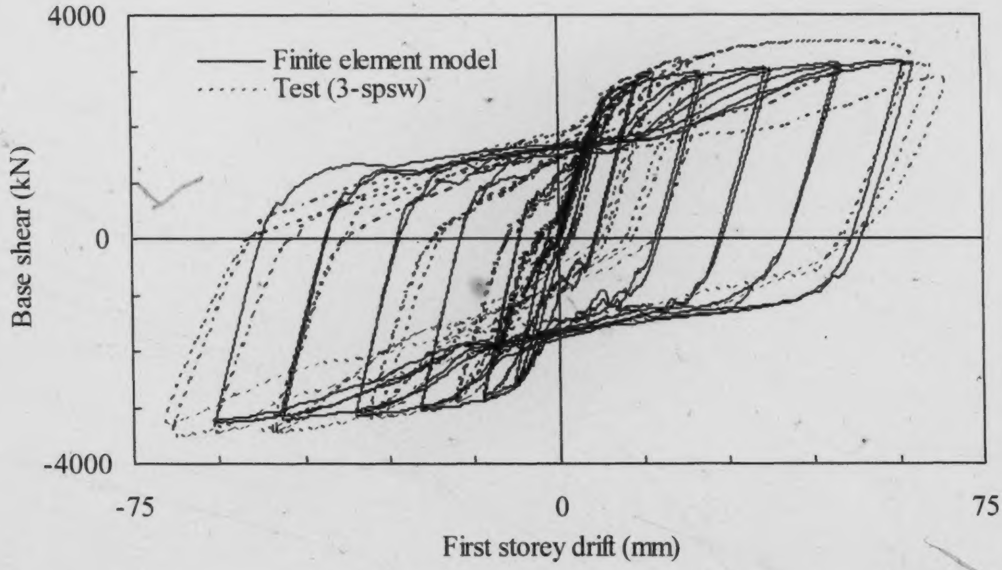

Figure 6.15: Comparison of finite element hysteresis analysis with test results—Panel 1

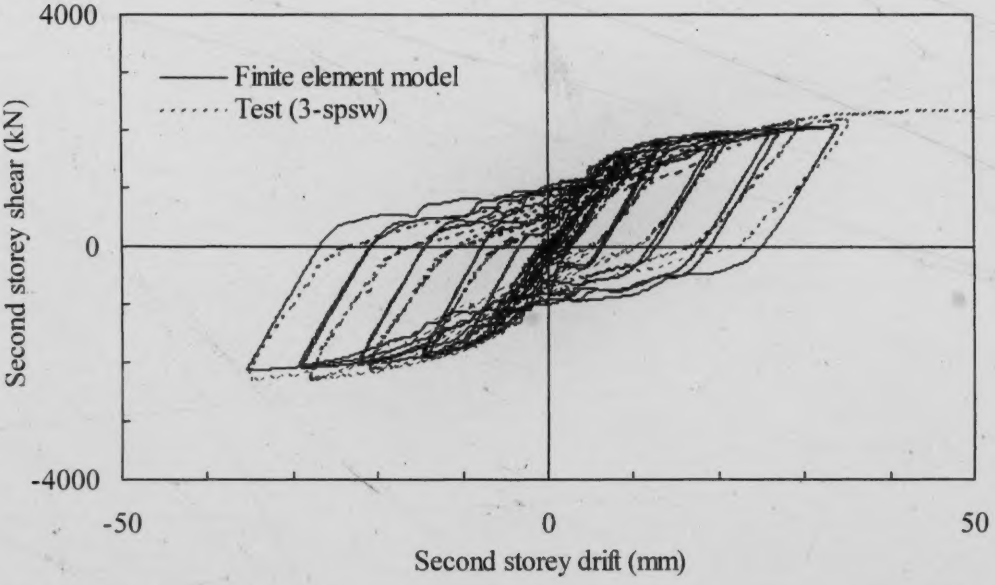

Figure 6.16: Comparison of finite element hysteresis analysis with test results—Panel 2

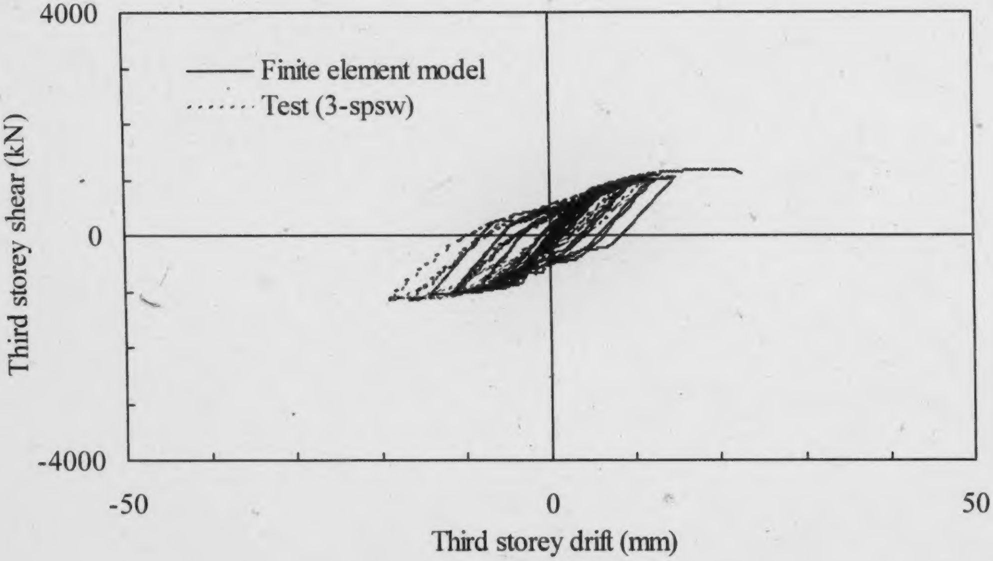

Figure 6.17: Comparison of finite element hysteresis analysis with test results—Panel 3

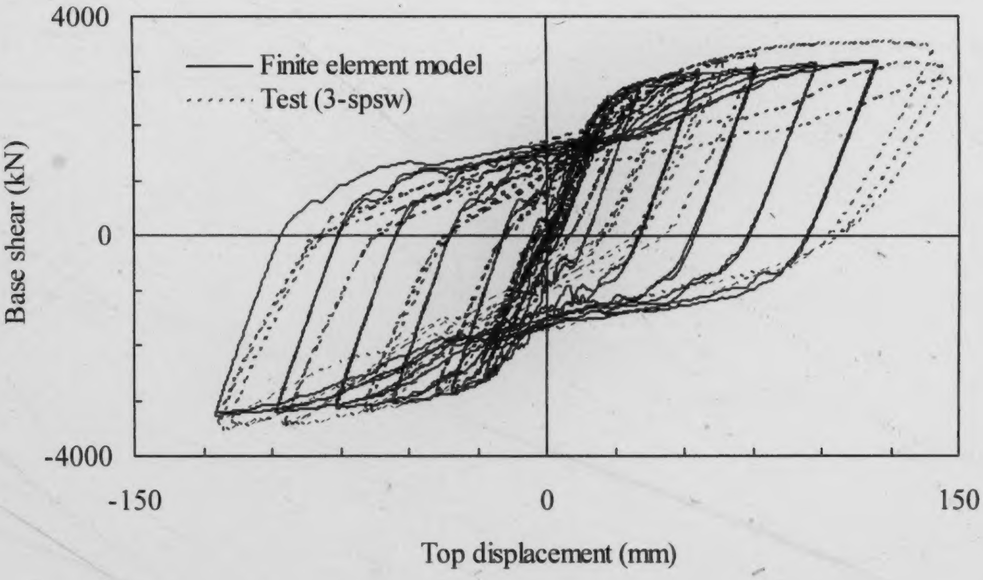

Figure 6.18: Comparison of finite element hysteresis analysis with test results—Top displacement

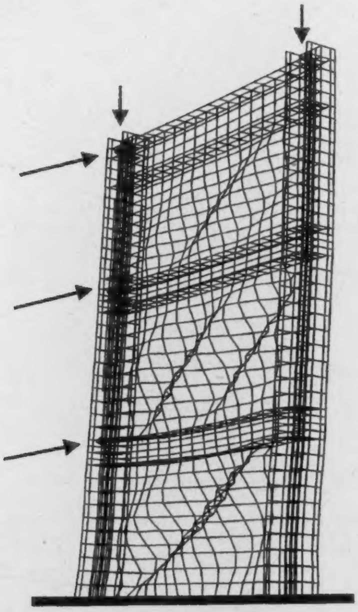

(a) Finite element model

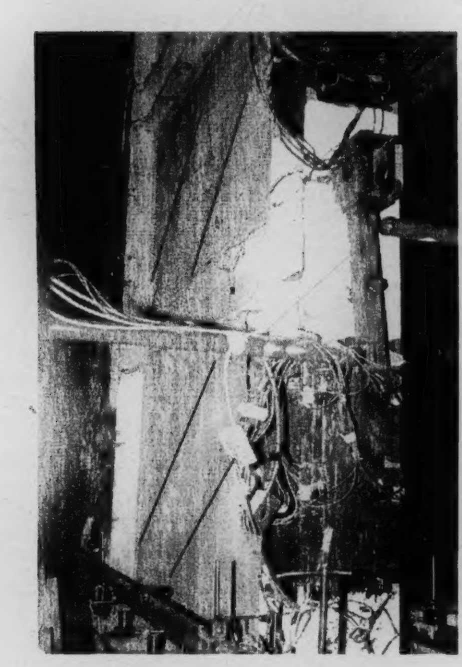

(b) First and second panels of test specimen

Figure 6.19: Deformed shape of steel plate shear wall loaded in positive 1-direction — Tension field fully developed

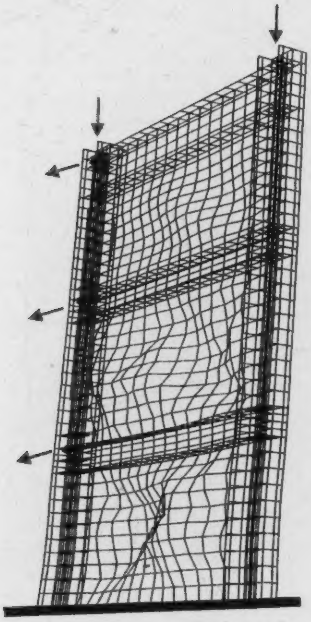

Figure 6.20: Deformed shape of steel plate shear wall loaded in negative 1-direction — Early stage of tension field redevelopment

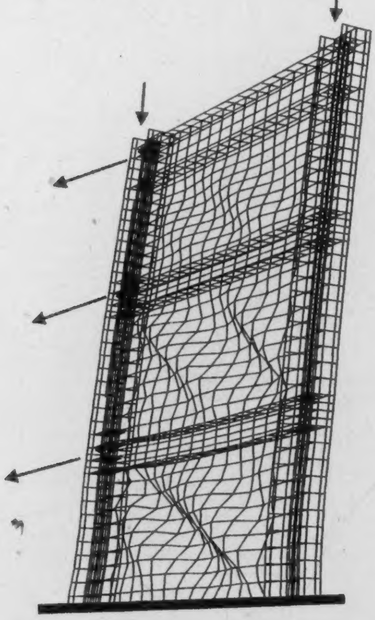

Figure 6.21: Deformed shape of steel plate shear wall loaded in negative 1-direction — Tension field fully redeveloped

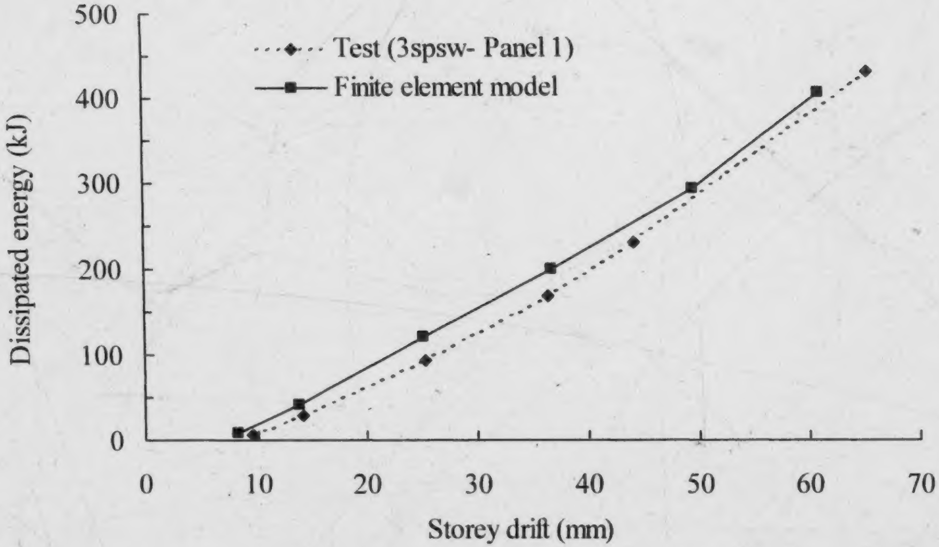

Figure 6.22: Energy dissipation as a function of drift level—Panel 1

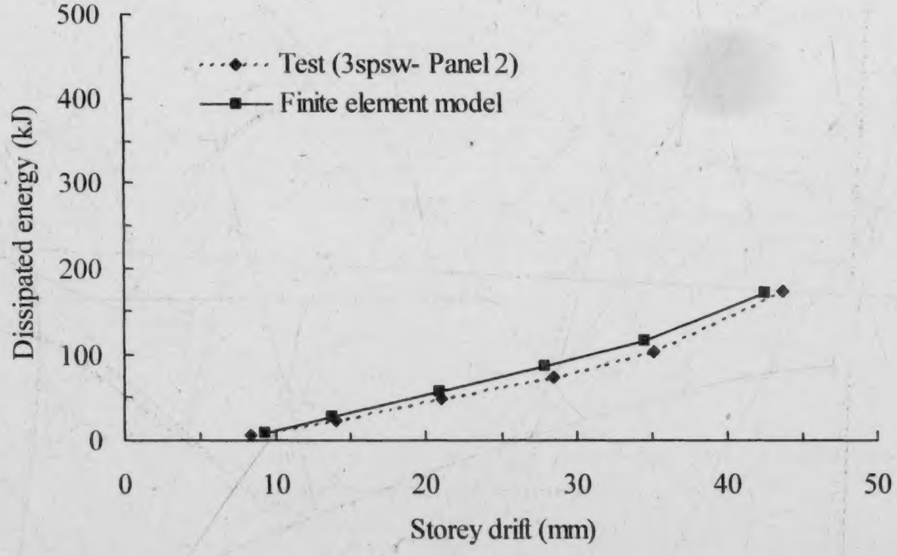

Figure 6.23: Energy dissipation as a function of drift level—Panel 2

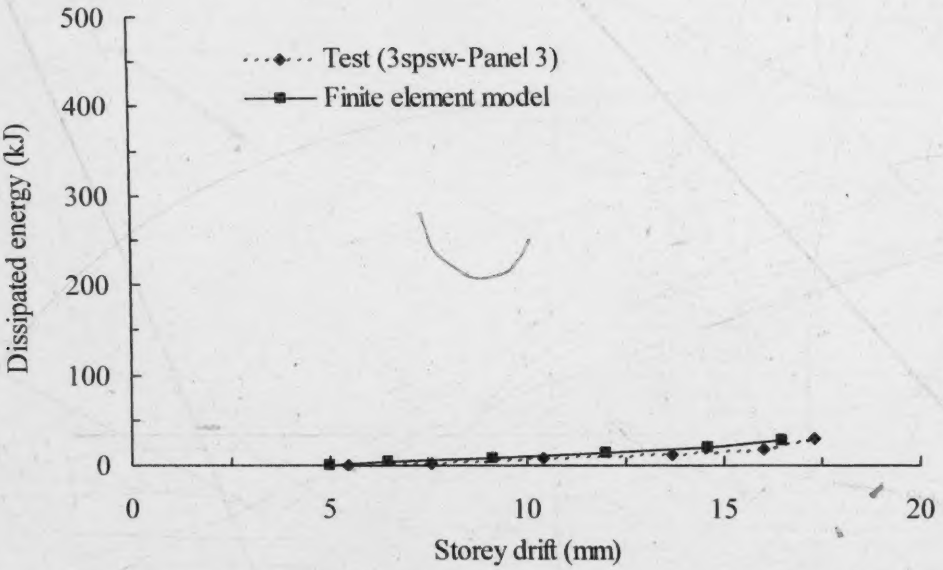

Figure 6.24: Energy dissipation as a function of drift level—Panel 3

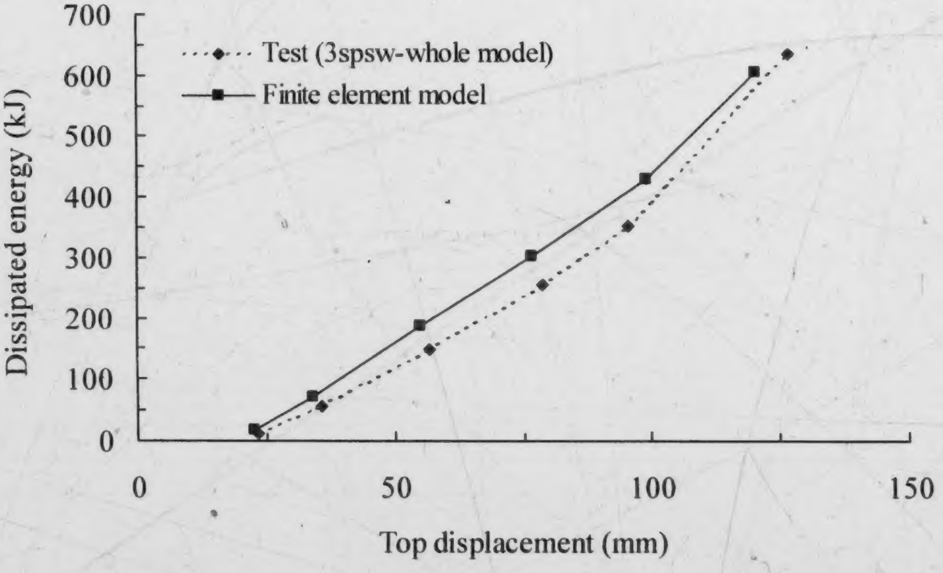

Figure 6.25: Energy dissipation as a function of displacement at the top

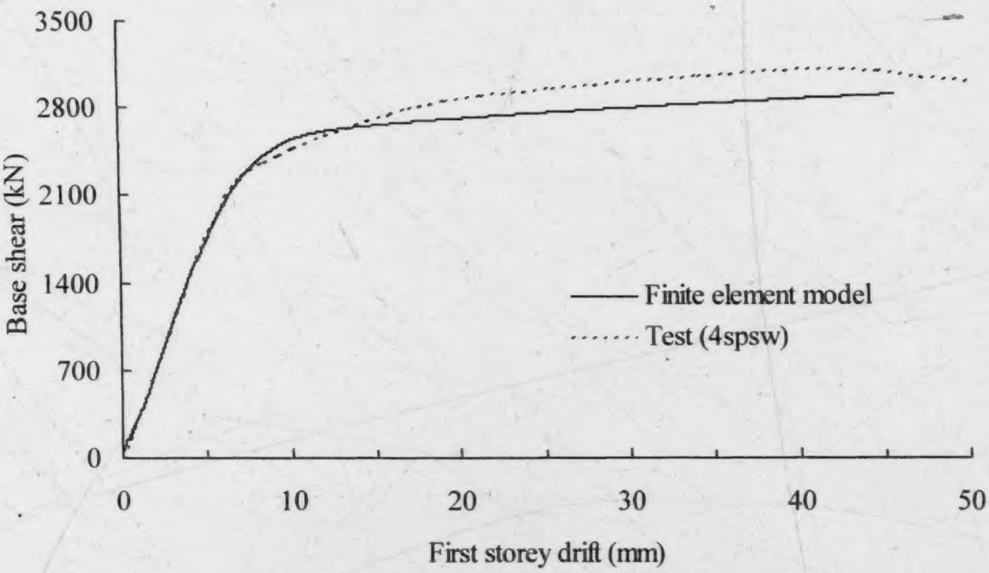

Figure 6.26: Monotonic finite element analysis compared with the envelope of the test cyclic response — Panel 1

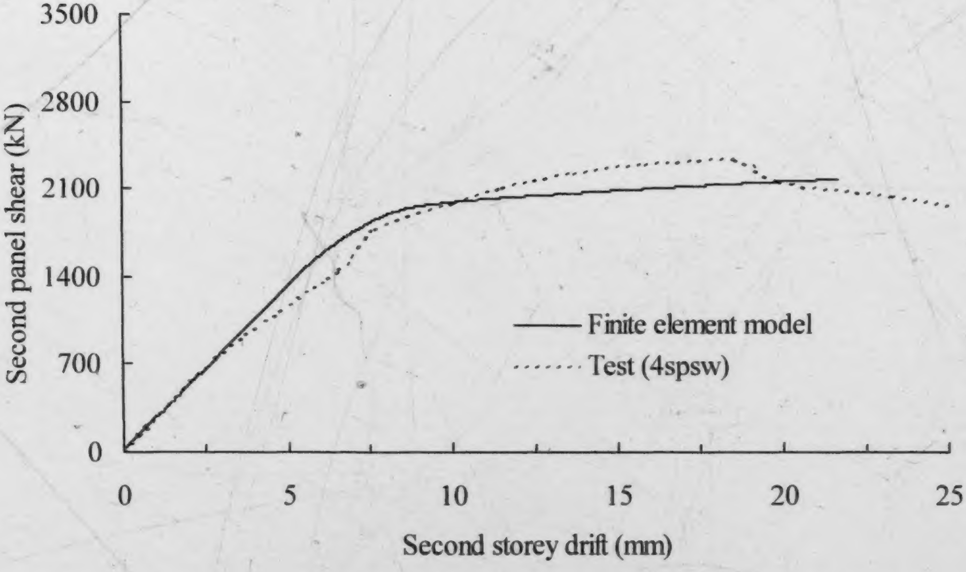

Figure 6.27: Monotonic finite element analysis compared with the envelope of the test cyclic response — Panel 2

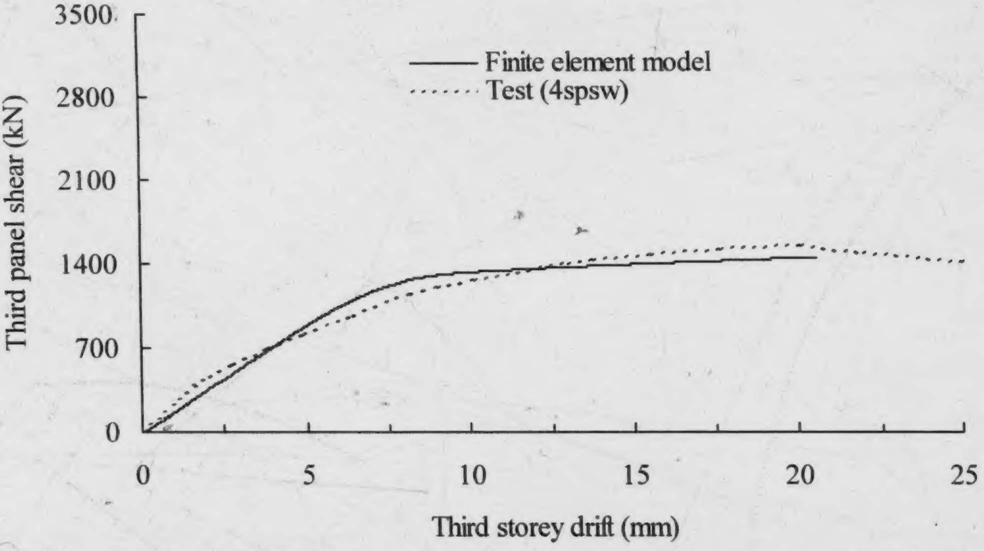

Figure 6.28: Monotonic finite element analysis compared with the envelope of the test cyclic response — Panel 3

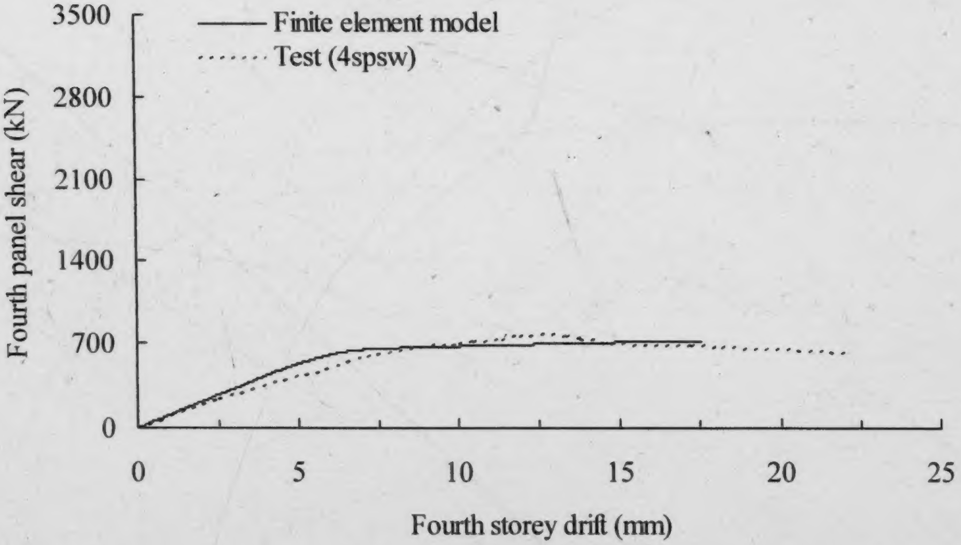

Figure 6.29: Monotonic finite element analysis compared with the envelope of the test cyclic response — Panel 4

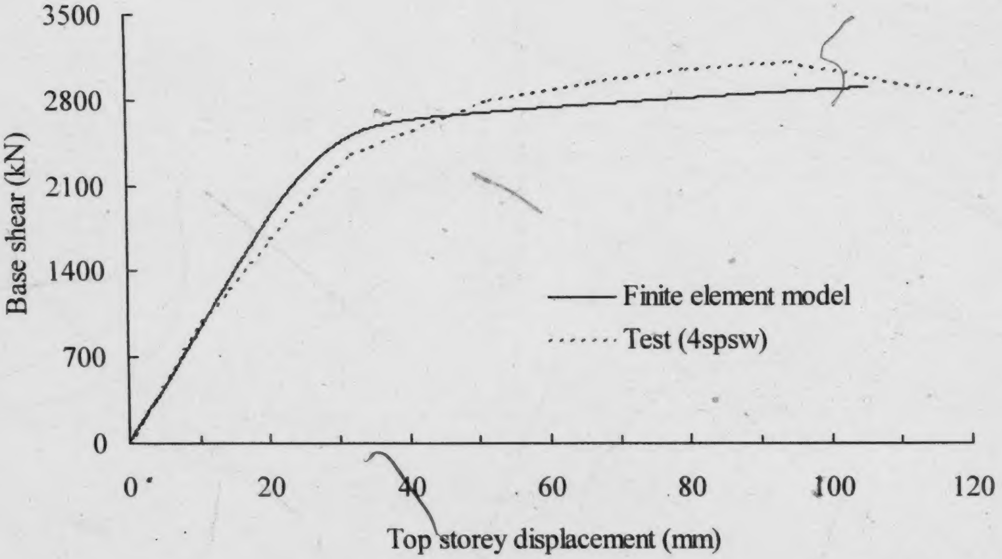

Figure 6.30: Monotonic finite element analysis compared with the envelope of the test cyclic response — Top displacement

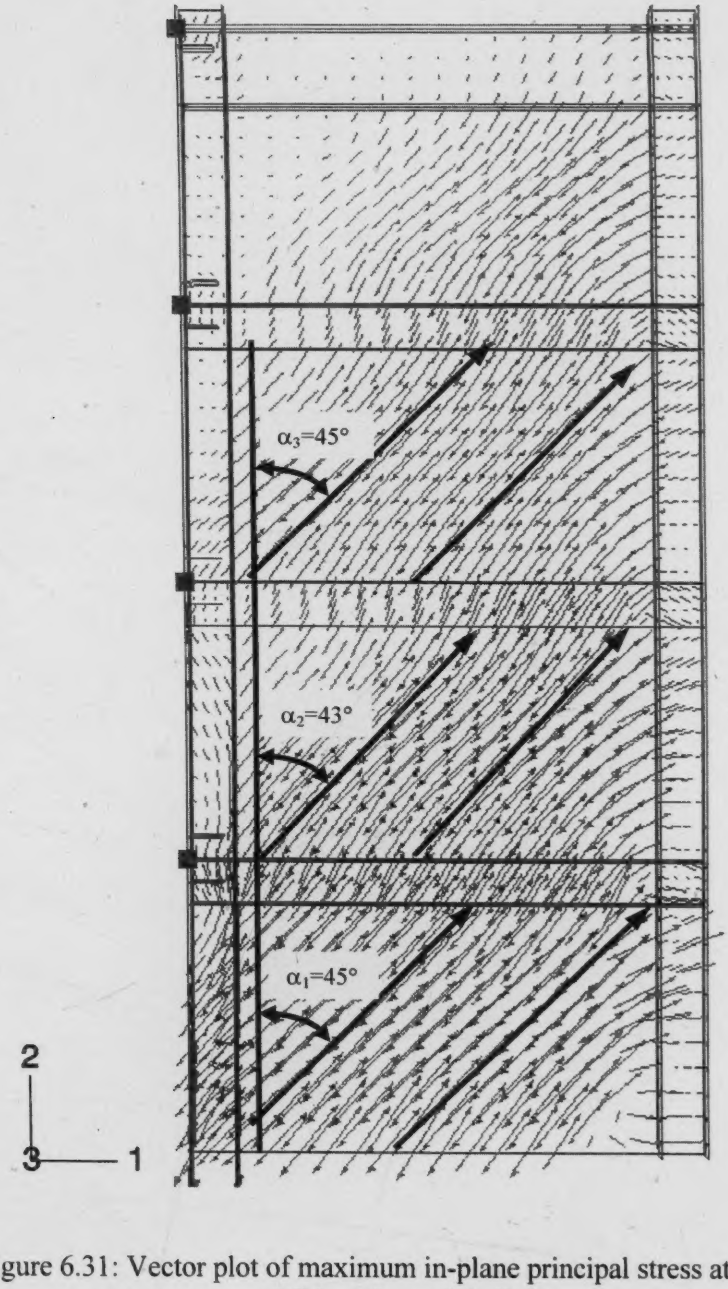

Figure 6.31: Vector plot of maximum in-plane principal stress at ultimate load—Mid-surface of shell elements

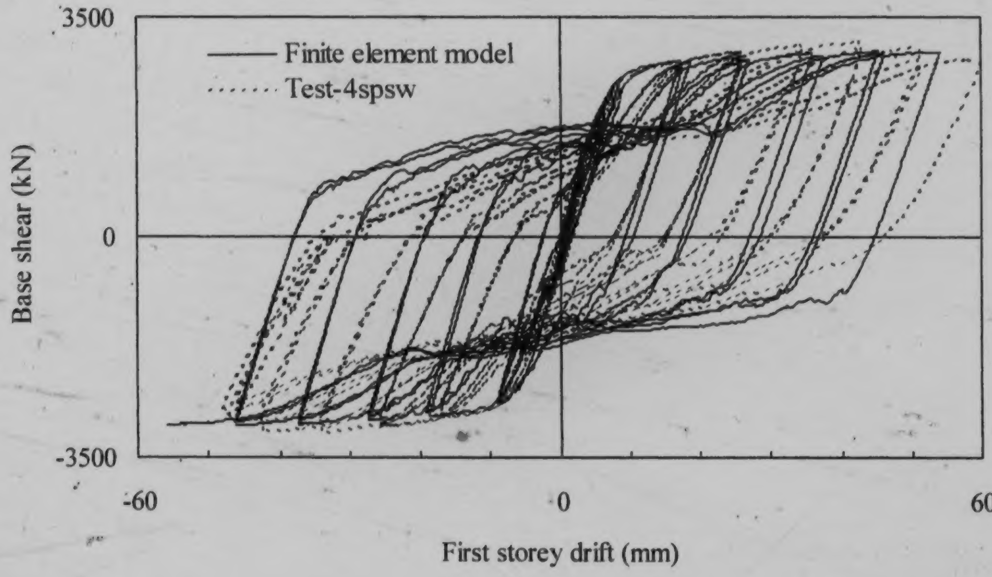

Figure 6.32: Comparison of finite element hysteresis analysis with test results—Panel 1

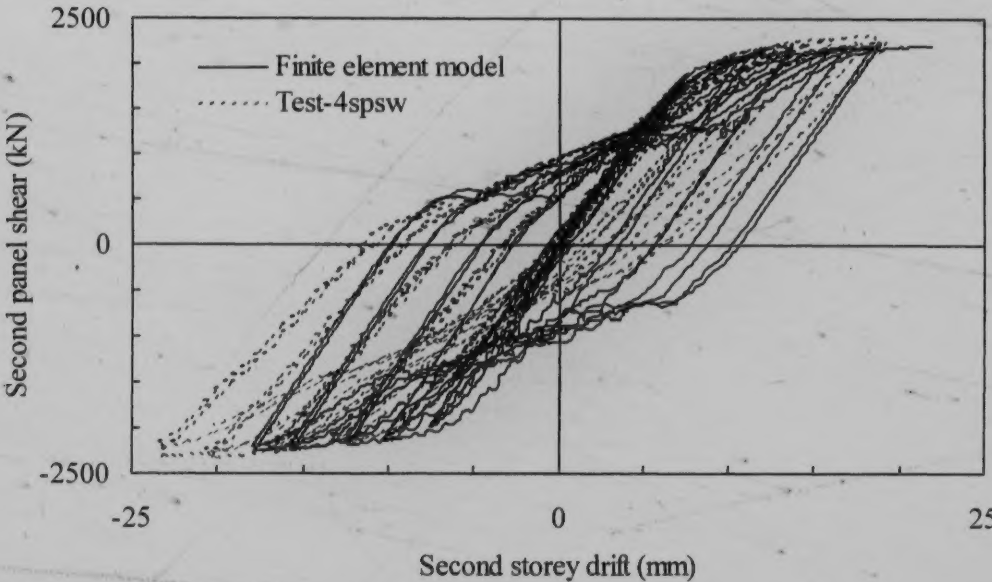

Figure 6.33: Comparison of finite element hysteresis analysis with test results—Panel 2

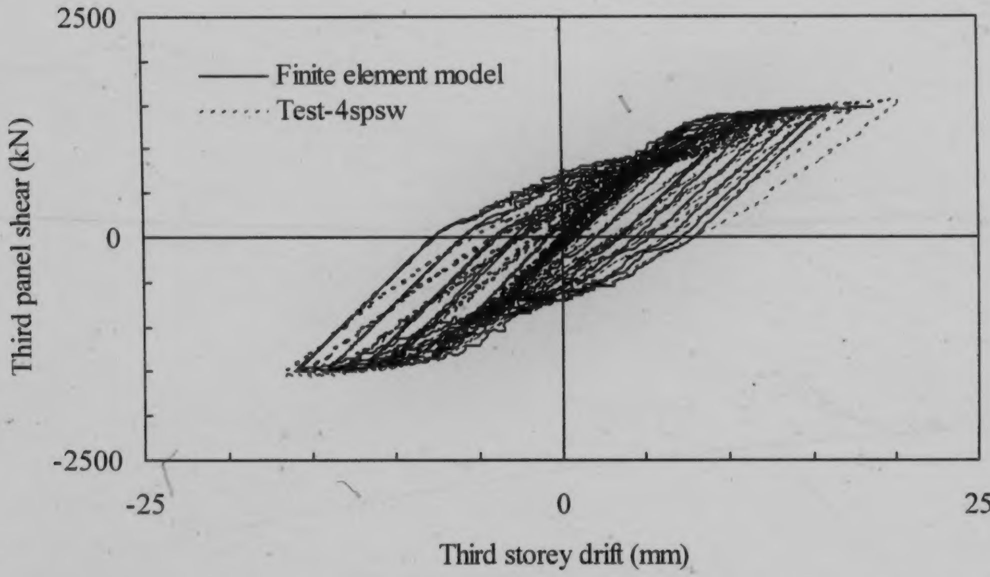

Figure 6.34: Comparison of finite element hysteresis analysis with test results—Panel 3

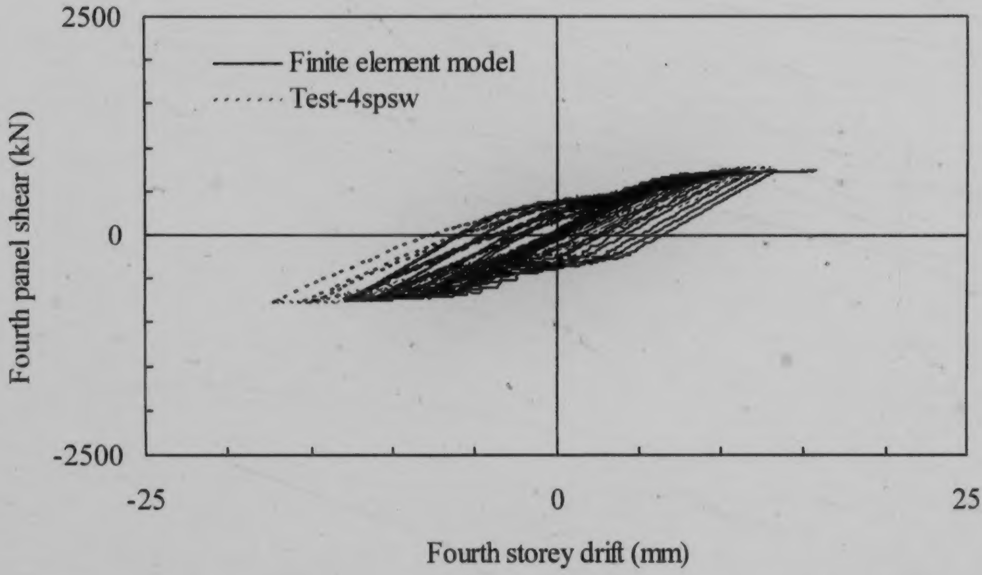

Figure 6.35: Comparison of finite element hysteresis analysis with test results—Panel 4

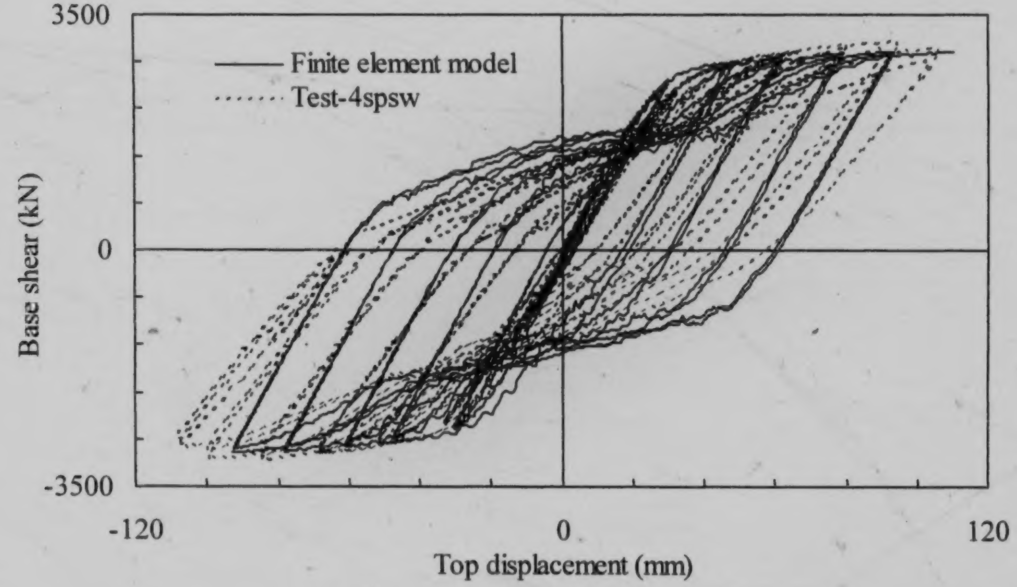

Figure 6.36: Comparison of finite element hysteresis analysis with test results—Displacement at the top

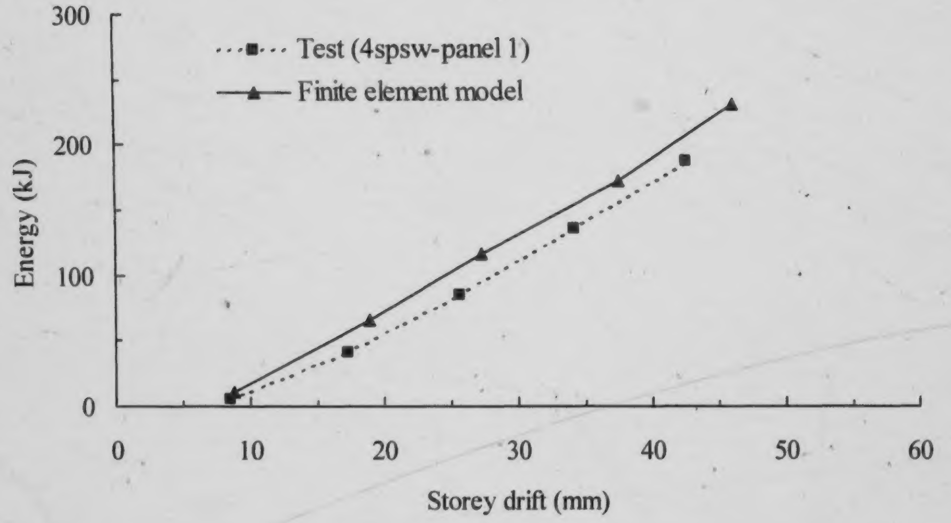

Figure 6.37: Energy dissipation as a function of drift level—Panel 1

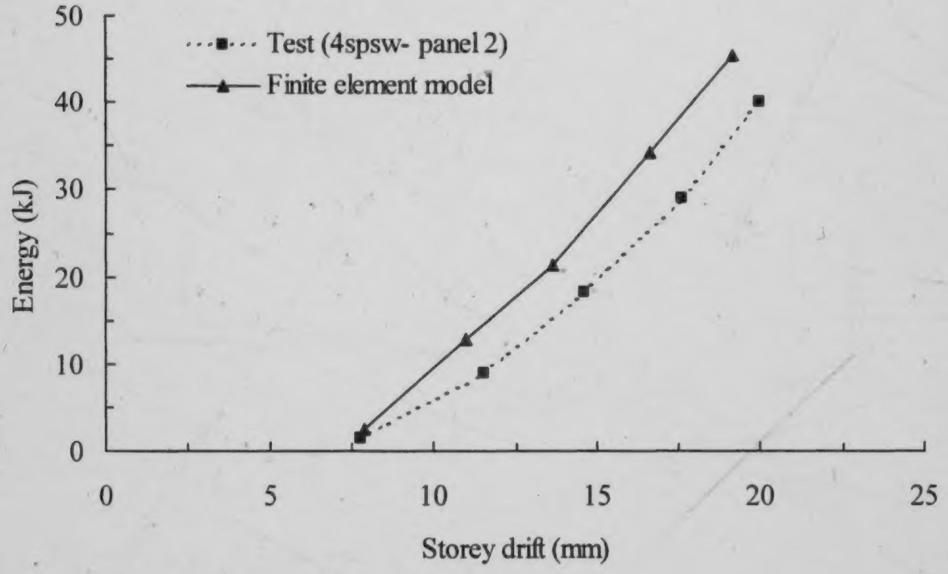

Figure 6.38: Energy dissipation as a function of drift level—Panel 2

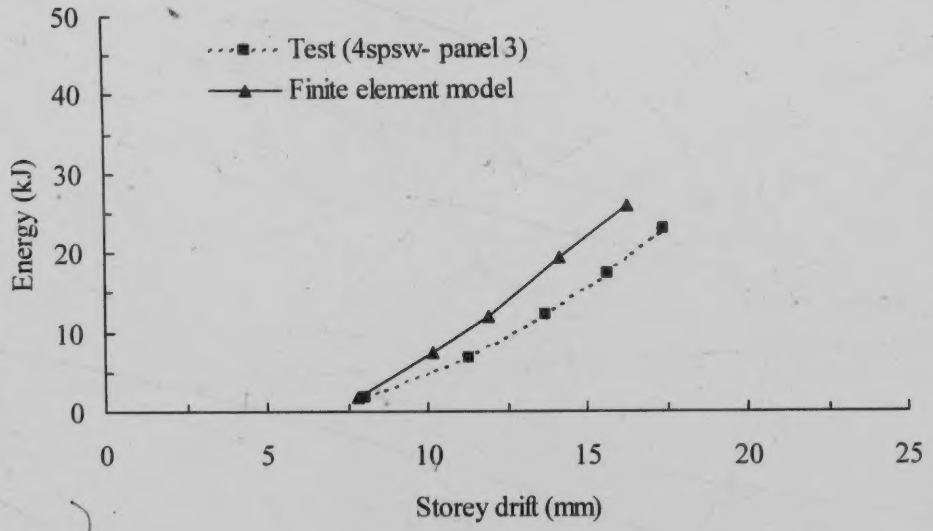

Figure 6.39: Energy dissipation as a function of drift level—Panel 3

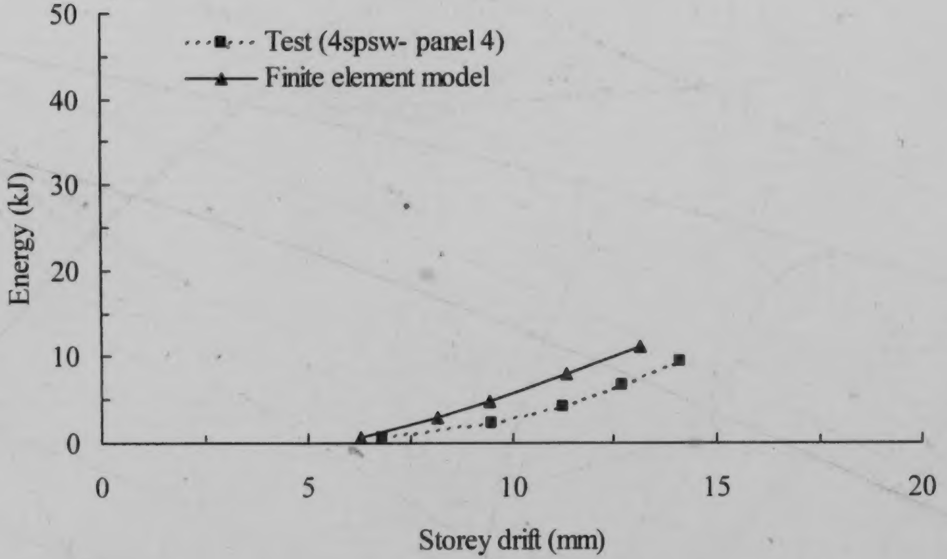

Figure 6.40: Energy dissipation as a function of drift level—Panel 4

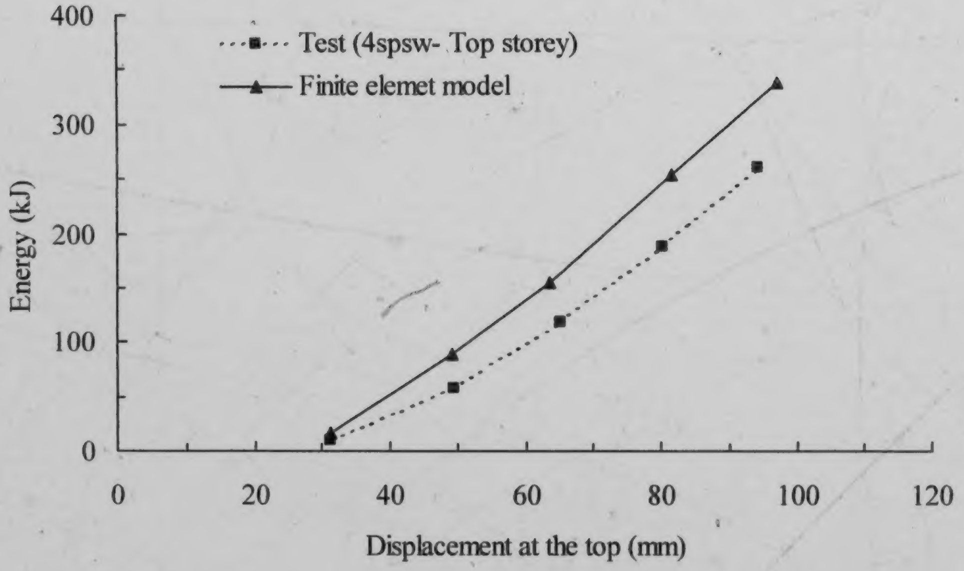

Figure 6.41: Energy dissipation as a function of displacement at the top

7 EVALUATION OF STRAIN DATA

7.1 Introduction

Testing of a three-storey steel plate shear wall was conducted as described in Chapter 3. The behaviour of boundary members was monitored using 91 strain gauges mounted at 20 different sections along the beams and columns. The objective was to compare the cyclic response to pushover finite element analysis results. If the shear capacity predicted by a pushover analysis is in good agreement with the test results, a pushover analysis can be used to carry out a parametric study. The location of these strain gauges was presented in Figure 3.9. Since the second panel of the test specimen is representative of a panel in a multi-storey building and was expected to be the critical panel, most of the strain gauges were mounted on the boundary members of this panel. A minimum of four strain gauges was mounted at each instrumented cross-section. For model validation purpose, boundary elements are more suitable than infill plates because the latter are more susceptible to local buckling.

The measured strain distributions across the depth of the cross-sections were used to calculate the axial force and bending moment at cycles 6, 12, 15 and 18 when the lateral loads were applied in the west direction (hydraulic actuators pushing against the test specimen). The strain data and calculated member forces are compared with the results of a pushover finite element analysis at the same load level as the test. In cycle 6 the shear wall behaved elastically. Cycles 12, 15 and 18 are the third cycle from the corresponding load blocks with the second panel drift at δ_y, $2\delta_y$ and $3\delta_y$, respectively.

7.2 Strain measurements in the flanges

In order to estimate the average strain of the flange at any cross-section two strain gauges were mounted longitudinally near the flange tips, as shown in Figure 3.9. To check the validity of the measured strains, readings from each pair of strain gauges mounted on a flange were plotted as a function of the applied load and the differences between the two gauges were investigated. Theoretically, the two strain readings should follow almost the same trend. However, for a localized effect such as local buckling, the strain readings will be significantly different and the average of two gauges cannot be taken as the average strain at the surface of the flange. A plot of strain versus base shear for gauges 8c and 8d, mounted on the west flange of section 8, during cycles 18 and 19 is presented in figures 7.1a and 7.1b. Figure 7.1a shows that the two strain gauges responded similarly during cycle 18 (this similarity in response was also observed in previous cycles). However, in cycle 19 and at a load level of approximately 3000 kN (see Figure 7.1b), the reading from strain gauge 8d diverged suddenly from the strain gauge reading at 8c, indicating onset of a local instability. At some instrumented sections a small discrepancy was observed between the two gauges on the flange, which could be caused by out–of–plane bending of the cross-section. Since the strains recorded in the flanges were averaged, the calculations based on the average flange strains did not include the effect of any out–of–plane bending.

7.3 Strain measurements in the web

The interaction between the infill plates and frame members and the presence of high shear forces resulting from the development of the tension field can affect the distribution of axial strain across the depth in the beams and columns. In order to investigate the distribution of axial strain along the depth, one more strain gauge was mounted longitudinally at the middle of the web on the north face of the wall. In wide flange sections the flanges carry most of the bending moment, whereas the web contributes approximately 10% of the moment carrying capacity in the elastic range. Therefore, any error in the strain measurements in the web should lead to only a small error in the bending moment calculation. On the other hand, axial forces create a uniform stress in the cross-section and the web contribution becomes more significant.

- Initial imperfections in the web and flanges of rolled wide flange sections, resulting from the manufacturing and fabrication processes create out–of–plane deformations because in-plane stresses are introduced in the cross-sections. This unavoidable out–of–plane bending of the web creates different magnitudes of strain on opposite faces of the web, but no net strain on the cross-section. As the applied load increases, the difference between the membrane strain and the measured strain on one face of the web increases. To obtain the membrane strain of the web during the test, the average strain on both faces of the web should be used, especially at high load levels. In this study, however, strains were measured only on the north face of the web, which was not enough to capture the membrane strain in the web in the presence of out–of–plane bending of the web.

The measured strain distribution at section 13 in the west column (see Figure 3.9) is shown in Figure 7.2. The strain distribution across the depth of the beam near the column (section 20) is presented in Figure 7.3. These two sections are highly strained sections in the column and the beam. At low load levels (up to about cycle 12) the strain distribution at both sections is linear, but at high load levels the strain distribution in the cross-section is no longer linear. As shown in these figures, the rate of change of strain at the surface of the web (mid-height of the cross-sections) is much higher than the strain rate in both flanges. One possible reason for this behaviour at high load levels, as discussed above, could be the out–of–plane deformation of the web. Because of this out–of–plane deformation, the strain reading on one side of the web cannot be considered as the membrane strain of the web, especially at high load levels. This nonlinear behaviour was not observed in the finite element analysis, which did not include out–of–plane member imperfection. In the remaining portion of this chapter a linear strain distribution was assumed across the sections.

7.4 Comparison of finite element analysis with test results

7.4.1 Strain distribution in boundary members

The strain distributions at various sections of the beams and columns were obtained using the finite element model presented in Chapter 5. In order to minimize the data storage requirement during the finite element analysis, the strains in the boundary members were obtained from a pushover analysis. The comparison between the finite element analysis and the test was performed for one elastic cycle, cycle 6, and three plastic cycles namely, cycles 12, 15 and 18, which are stabilized cycles in the blocks of cycles with drift of δ_y, $2\delta_y$, and $3\delta_y$, respectively. In Chapter 5 it was demonstrated that the pushover analysis successfully predicts the envelope of hysteresis loops. Therefore, in the finite element analysis the strains were obtained at the peak load level of these cycles.

A comparison between measured and predicted strains at sections 10, 11, 12, and 13 in the west column is presented in figures 7.4 to 7.7. Excellent agreement was obtained between the test results and the finite element analysis at all sections for low load levels. At sections 10 and 11 a good correlation between the measured strains and the strains predicted by the finite element analysis is observed even at high load level and after as many as 18 cycles. However, at sections 12 and 13 the accuracy of the analysis deteriorates as the load increases. The strain distributions predicted by the finite element analysis show approximately a linear distribution at all load levels across these cross–sections.

The strain distributions at sections 7, 8, 9, located in the west column of first storey, and in sections 17, 18, 19, and 20, located in the beam at level 2, are presented in figures 7.8, through 7.14. A comparison of the measured strains with the strains predicted by the finite element analysis indicates that at strain levels less than about 1600 με the finite element predictions are in excellent agreement with the test results. Although the difference between the measured and predicted strains increases with increasing load and number of cycles, the predicted and measured shape of the strain distributions are similar. The strain magnitudes at different sections of the beam are relatively small compared to the strains in the columns. This is caused by equal and opposing tension fields from the panels above and below the beam.

7.4.2 Bending moment and axial force diagrams in the boundary members

In this section comparisons of the strain data obtained from the test results and with the finite element analysis are made in the form of bending moments and axial forces for the beams and columns. In order to obtain the axial force and the bending moment at various sections from the strain data, a number of assumptions had to be made. It was assumed that the bending moment is uniaxial. Hence, the strain at the extreme fibres of the cross-section was taken as the average of the readings from the two gauges on each flange. A linear strain distribution was assumed over the depth of the cross-section. An elastic perfectly plastic material model with the mean measured value of the modulus of elasticity (obtained from ancillary tests by Driver *et al.* (1997)) was used to determine the associated stress values. It was also assumed that the boundary members in the previous four-storey test remained elastic and, as a consequence, the effect of previous cyclic loading on the moment versus curvature response of a section was considered negligible. The resultant axial force and bending moment at the instrumented sections were calculated from a numerical integration of the stress distribution on the cross-section.

The presence of residual stresses affects the calculation of bending moment and axial force from the measured strain data. Although residual stresses do not affect the ultimate strength of a member, it softens the moment versus curvature or axial force versus axial deformation responses by initiating yielding at an earlier loading stage. The effect of residual stresses remains negligible as long as the sum of the applied stress and the residual stress is less than the yield stress at every point on the cross-section. The axial load and bending moment calculations were carried out without considering the softening effect from residual stresses.

Welding of the fishplates to the boundary members introduces an unknown pattern of residual stresses in the cross-section of the boundary members. To assess the error that results from neglecting the residual stresses in calculating the bending moment from strain readings, a simplified residual stress pattern typical for a hot rolled section (shown in Figure 7.15) was assumed on a W310×118 section (which is the beam cross-section at levels 1 and 2) and used in a series of calculations. A modulus of elasticity of 200 000 MPa, yield stress of 300 MPa and elastic perfectly plastic material model was assumed in the residual stress investigation. Moment versus curvature relations was obtained for three conditions. One was free of residual stresses and the other two had maximum residual stresses of 30% and 100% of the yield strength, respectively. The moment versus curvature (**M**–Φ) responses for these three residual stress conditions are presented in Figure 7.15 and the error resulting from neglecting the residual stresses is presented in Figure 7.16. Figure 7.15 indicates that residual stresses soften the response but do not change the capacity. Neglecting the residual stresses in a W310×118 section can result in an overestimate of the bending moment by as much as 21% in bending moments under these assumptions (see Figure 7.16). The same observation can be made concerning the effect of neglecting the residual stresses when calculating the axial load response. This source of error should, therefore, be considered when interpreting the internal forces.

The axial force and bending moment diagrams in the west column of the first storey are shown in figures 7.17 and 7.18, respectively. The axial force along the column is predicted very well by the pushover analysis, even after significant yielding. On the other hand, the bending moment along the column is in good agreement with the test results only in the elastic range. In the plastic range, the discrepancy between the finite element predictions and the test values increases with increasing load level and number of cycles.

The effect of the tension field on the columns can be assessed by comparing the axial force and bending moment diagrams, shown in figures 7.17 and 7.18, with the axial force and bending moment diagrams expected for a frame without infill plates. In a rigid frame with no infill plate the axial force would be uniform along the column length. This is not the case, however, in a rigid frame with an infill plate. Because of the presence of the tension field, the axial force varies over the length of the column. The gradient of the axial force along the column represents the vertical component of tension field, which, in turn, depends on the inclination and the magnitude of the tension field at that location. As shown in Figure 7.17, the axial force gradient in cycles 12 and 15 is greater than the gradient in cycle 6, which indicates that the tension field in the infill plate has increased from cycle 6 to cycle 12. The gradient of the axial force in cycles 12 and 15 is unchanged, which indicates that the tension field has reached its maximum value corresponding to yielding in tension. The gradient of the axial force is maximum at the top of the column and minimum at the bottom of the column, although the gradient does not vary much along the column. This indicates that the vertical component of the tension field is slightly larger at the top corner of the panel.

The axial force and bending moment diagrams in the west and east columns at the second storey are shown in figures 7.19 to 7.22. The predicted axial force diagram for the east column (see Figure 7.21) is in excellent agreement with the test results even in cycle 15 and after a number of inelastic cycles, which is consistent with the results obtained for the west column at the first storey. The axial tension force in the east column increases from the top to the bottom of the column. Similarly, the axial compression force in the west column was observed to increase from the top to the bottom of the column. This is consistent with a tension field running diagonally across the steel plate shear wall panel.

The bending moment diagram obtained from the test for the west column in the second panel (Figure 7.20) is similar to the bending moment diagram in a portal frame without infill plate subjected to lateral load. The bending moment diagram predicted by the finite element analysis shows a nonlinear variation, which is the effect of tension field on the column. In the east column the bending moment diagram is somehow different from that the west column. In this column, which is shown in Figure 7.22, the inflection point in both the test and the finite element analysis is shifted towards the bottom of the column, and as a result a major portion of the column is subjected to a positive bending moment. The difference in the bending moment diagrams of the two columns is mainly attributed to the restraining effect of the infill plate at the lower corners of the panel. As the wall is pushed in the west direction the infill plate at the bottom west corner can effectively restrain the west column, but this is not the case at the bottom portion of the east column.

The axial force and bending moment diagrams in the beam at level 2 are shown in figures 7.23 and 7.24, respectively. As expected, the pushover analysis accurately predicts the internal force effects in the beam in the elastic range. Unlike the columns, the axial force was not predicted accurately in the plastic range. One probable reason could be the localized effects due to welding of fish plates to the boundary members, which is more pronounced in the beams than in the columns (fishplates were welded to the beams from both flanges and only to one flange of the columns). As shown in Figure 7.23, the slope of the axial force diagram in the beam is close to zero, which indicates that the tension field transferred to the beam from the top and bottom panel almost counteract each other, resulting in a very small variation of axial force along the beam. The bending moment diagrams shown in Figure 7.24 show a good agreement between the test and the finite element analysis in the inelastic range. The beam curvature and the inflection point are predicted accurately by the finite element model. The predicted bending moment diagram shows almost the same pattern as a bending moment for a beam in a frame without any infill plate; opposite curvatures at beam-ends and an inflection point near the midspan, except that because of the tension field the bending moment diagram is no longer linear and the inflection point is shifted towards the west column.

There are a number of factors that have not been considered in the finite element model, such as the difference between a pushover analysis and a cyclic loading response. Therefore, in the plastic range the history of plastic deformations and accumulation of effective plastic strains have not been considered in the finite element model. This causes the pushover finite element analysis to diverge from the test results as the number of cycles in the plastic range increases. Residual stresses, localized imperfections and plastic flow history from the previous test on the four-storey steel plate shear wall are all factors that were not included in the finite element model. Although discrepancies exist, the overall trends are in good agreement.

7.5 Summary

The strain data collected from strain gauges mounted at various sections along the beams and columns of the test specimen were used to determine the strain distribution in the beams and columns, from which the axial forces and in-plane bending moments were calculated. The pushover finite element analysis developed in Chapter 5, which successfully predicted the envelope of the hysteresis loops, was also used to predict the strains and internal forces of the instrumented cross-sections at the peaks of some of the hysteresis loops.

Up to cycle 12 (third block of cycle with displacement drift of δ_y), the strains and the corresponding forces and bending moments at most instrumented sections were predicted accurately by the finite element analysis. In the inelastic range, and even after several plastic cycles, the axial forces in the west column of storey 1 and the east column of storey 2 were in excellent agreement with the test results. In general, as the number of inelastic cycles increased, the pushover analysis prediction started to diverge from the test results. However, both followed the same trend. In this range the difference between the analysis and the test was reasonable and all the features of the behaviour (inflection points, slopes, and curvatures) were predicted accurately in all locations.

The good agreement of the pushover finite element predictions in the elastic range and in the plastic range with the test results once again demonstrates the effectiveness of the finite element model in simulating the cyclic behaviour of steel plate shear walls.

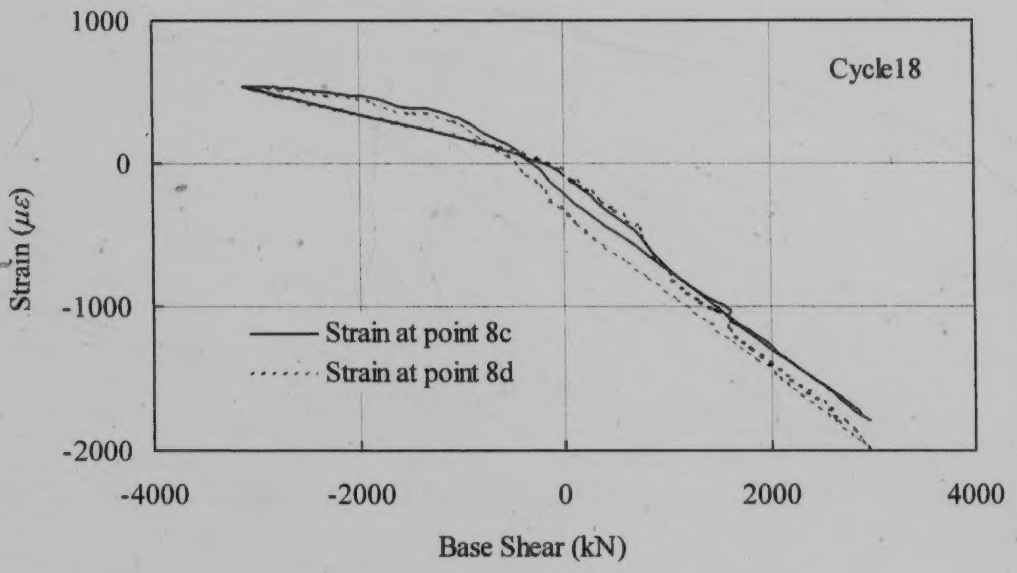

(a) Cycle 18

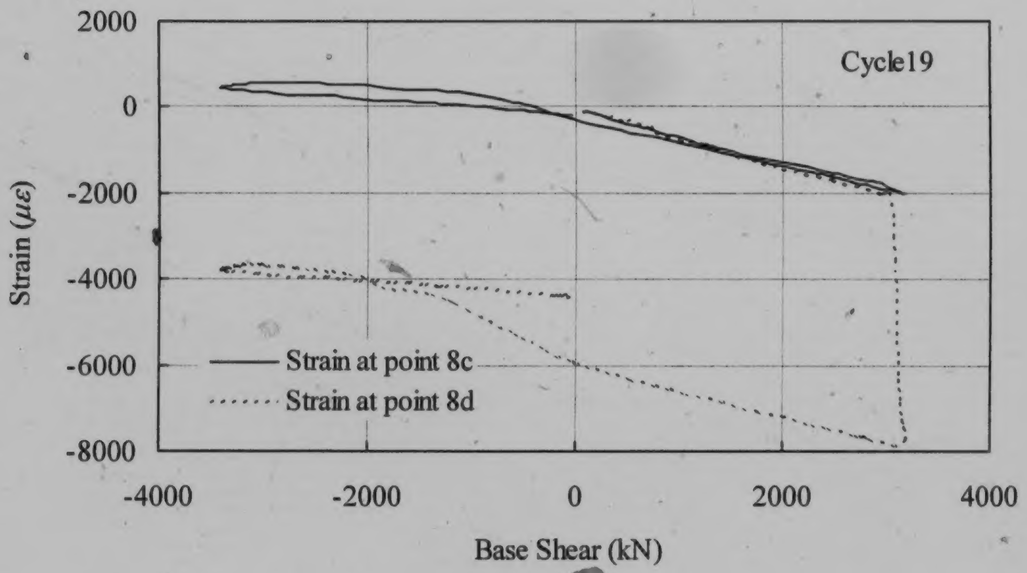

(b) Cycle 19

Figure 7.1: Strain versus base shear at points c and d of section 8

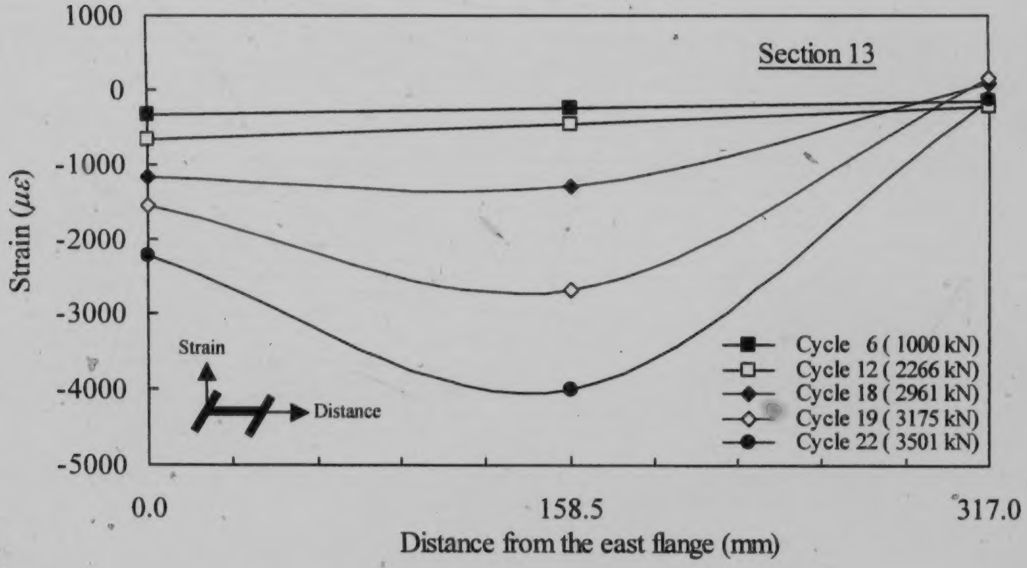

Figure 7.2: Strain distribution at section 13 in west column

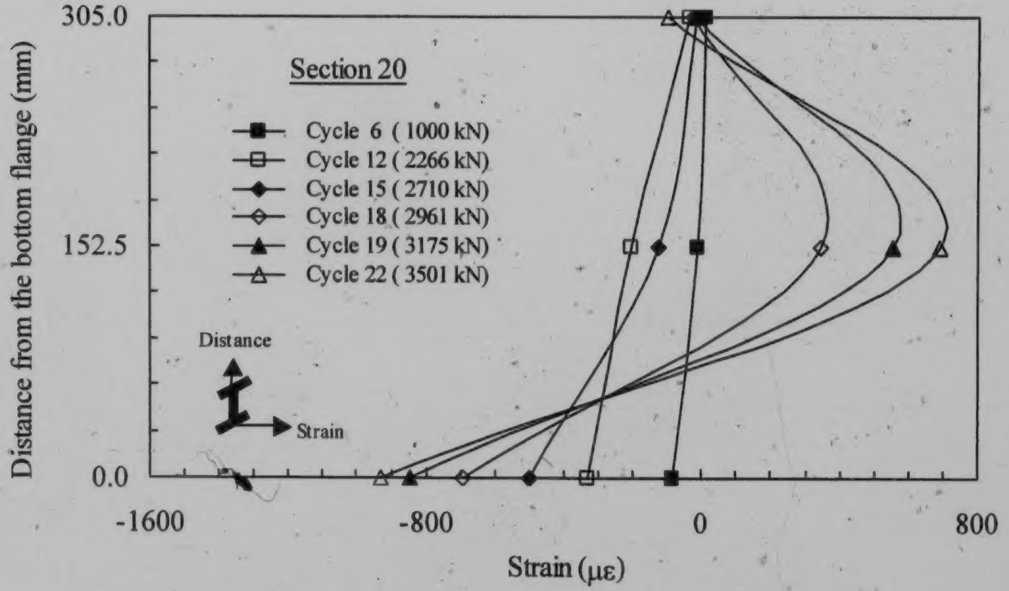

Figure 7.3: Strain distribution at section 20 in beam at level 2

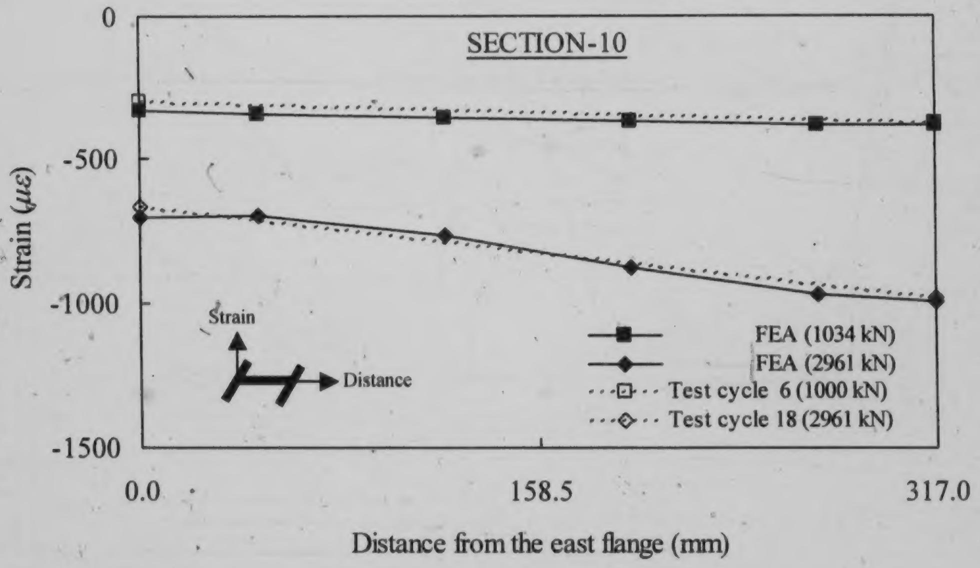

Figure 7.4: Strain distribution at section 10 in west column

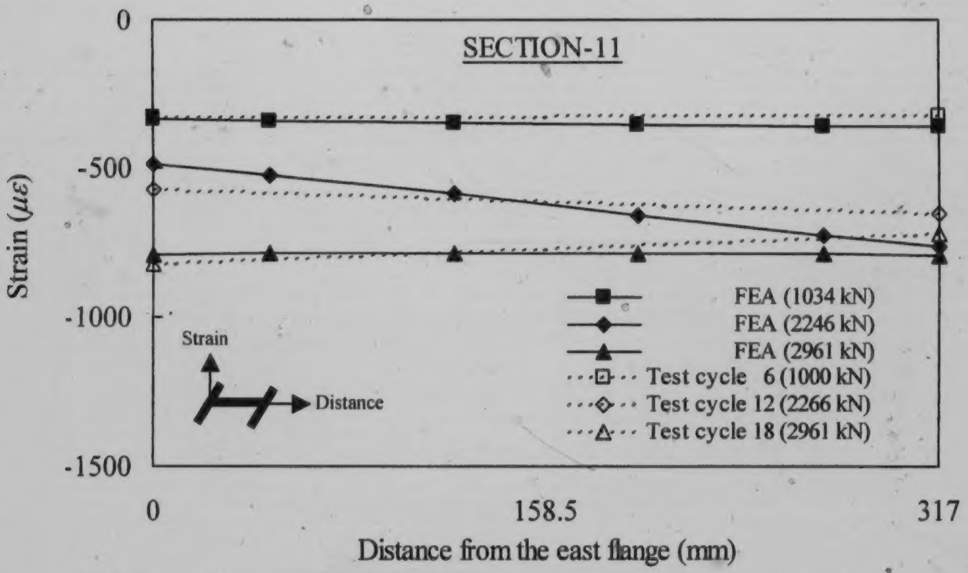

Figure 7.5: Strain distribution at section 11 in west column

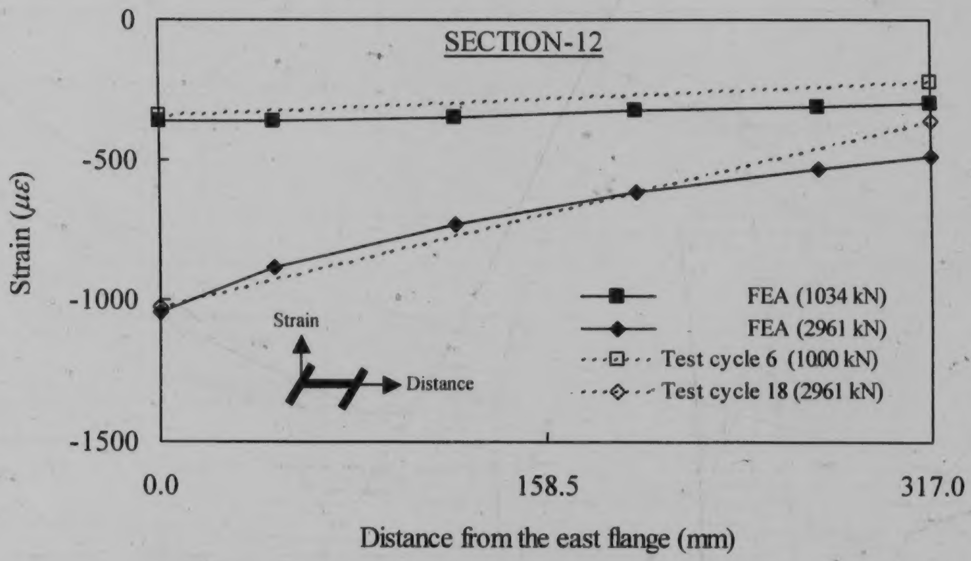

Figure 7.6: Strain distribution at section 12 in west column

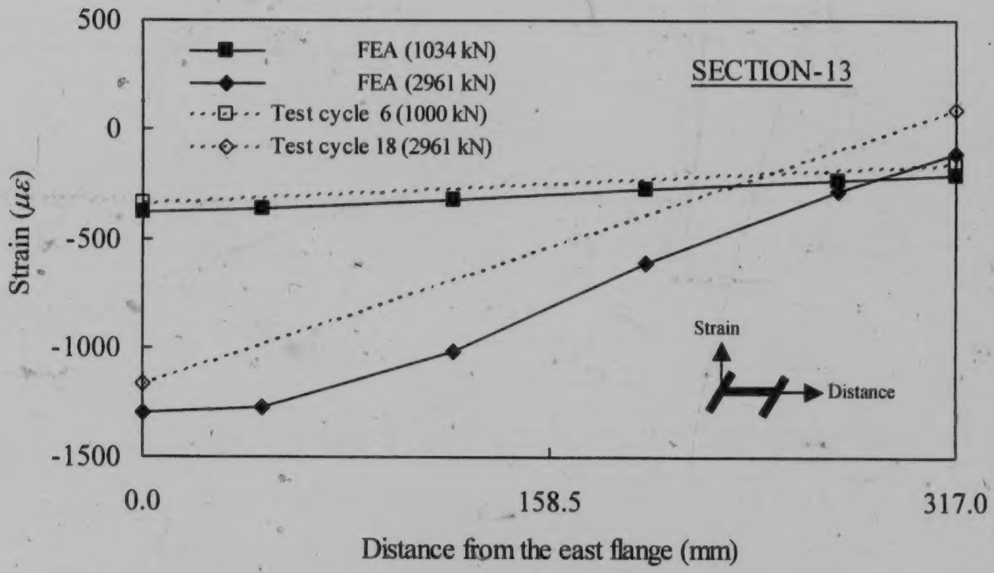

Figure 7.7: Strain distribution at section 13 in west column

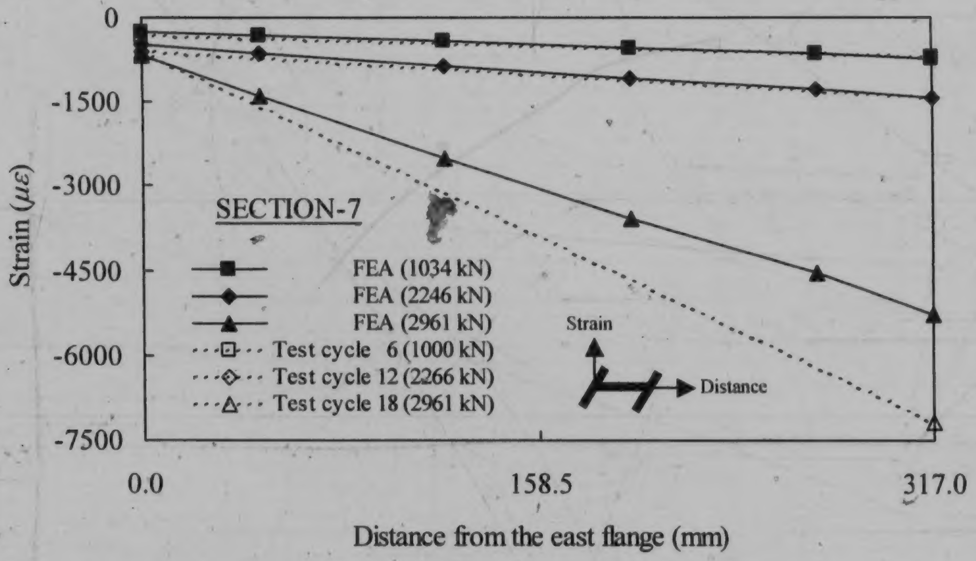

Figure 7.8: Strain distribution at section 7 in west column

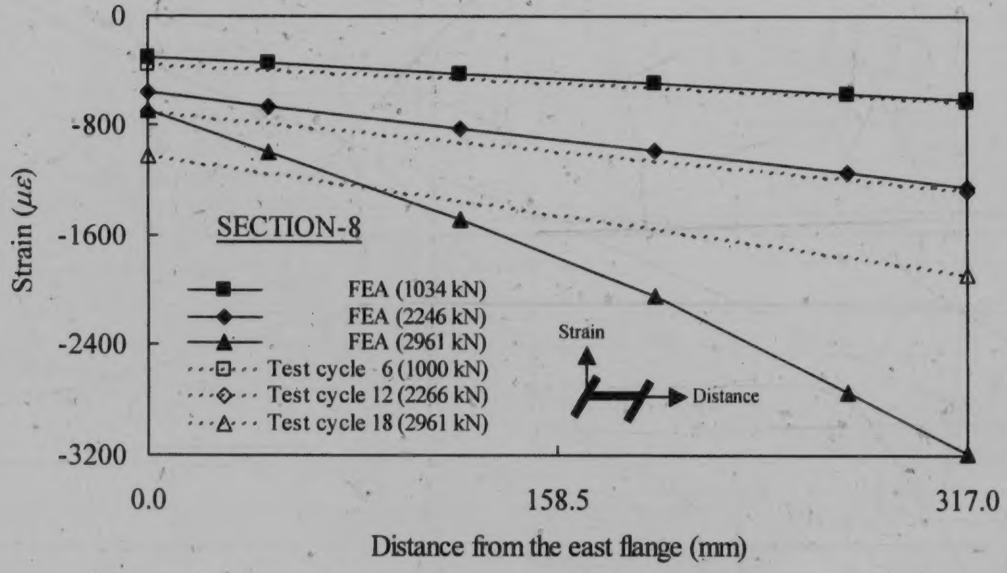

Figure 7.9: Strain distribution at section 8 in west column

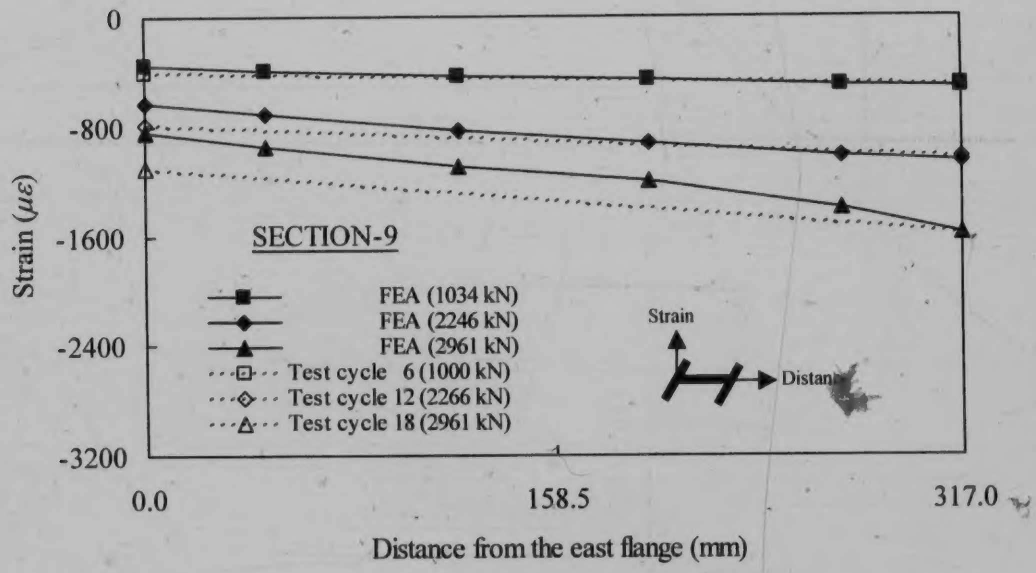

Figure 7.10: Strain distribution at section 9 in west column

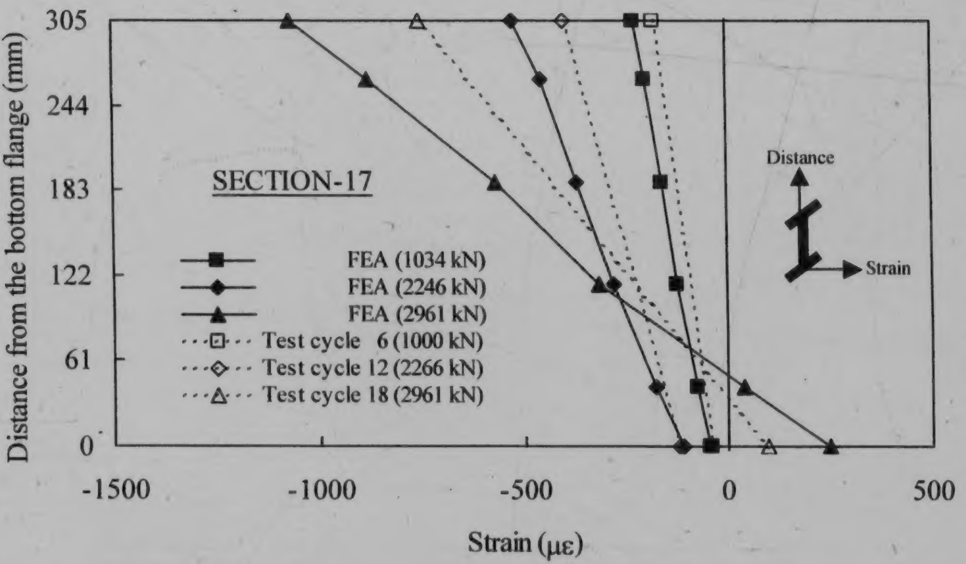

Figure 7.11: Strain distribution at section 17 in the beam at level 2

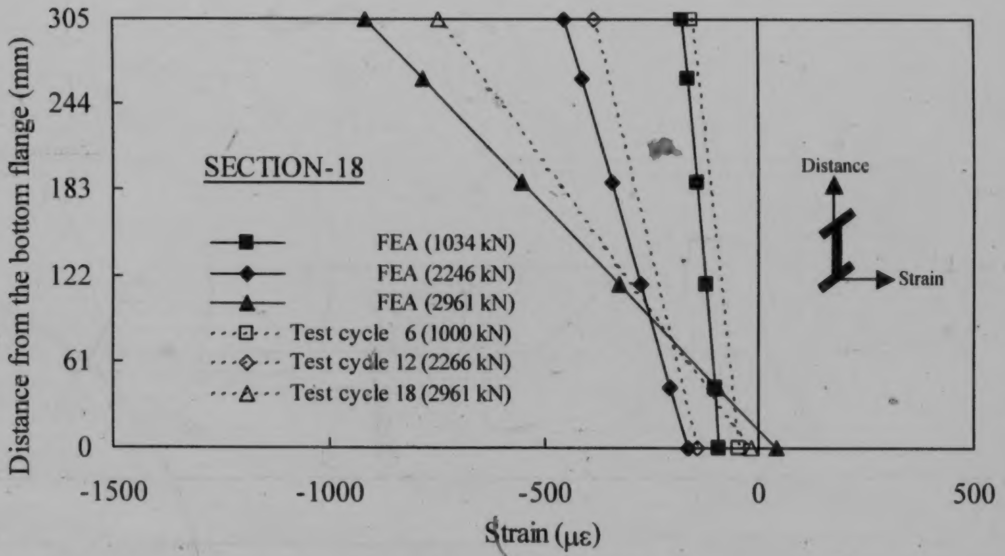

Figure 7.12: Strain distribution at section 18 in the beam at level 2

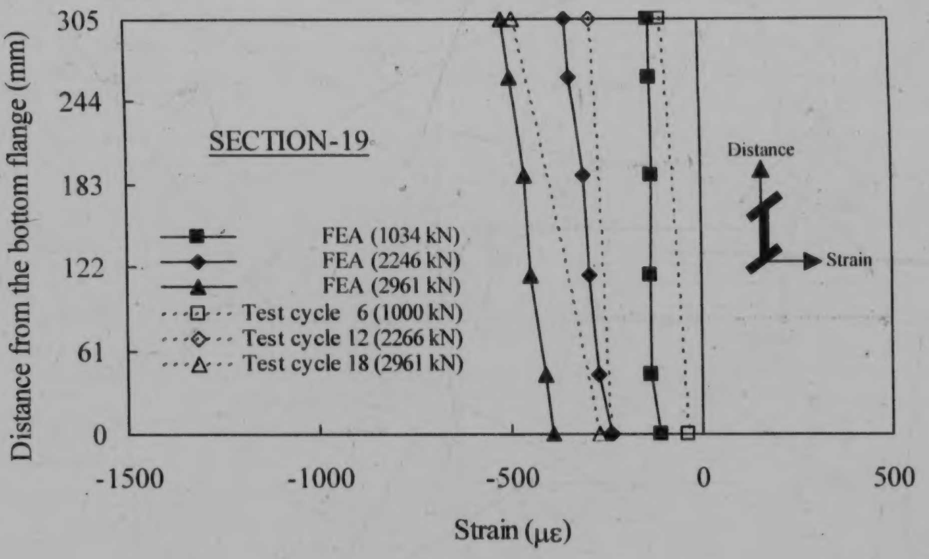

Figure 7.13: Strain distribution at section 19 in the beam at level 2

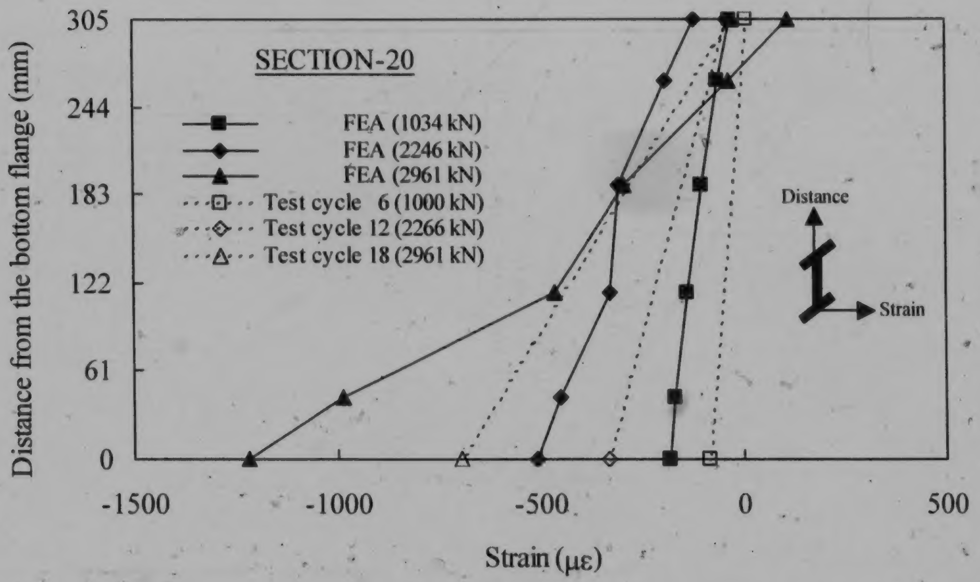

Figure 7.14: Strain distribution at section 20 in the beam at level 2

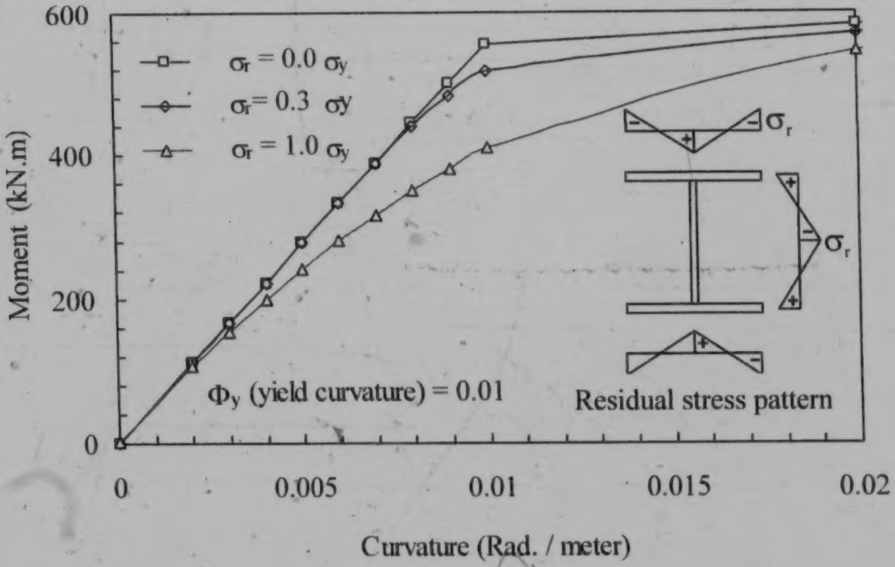

Figure 7.15: Effect of residual stresses on the moment versus curvature response for a W118×60

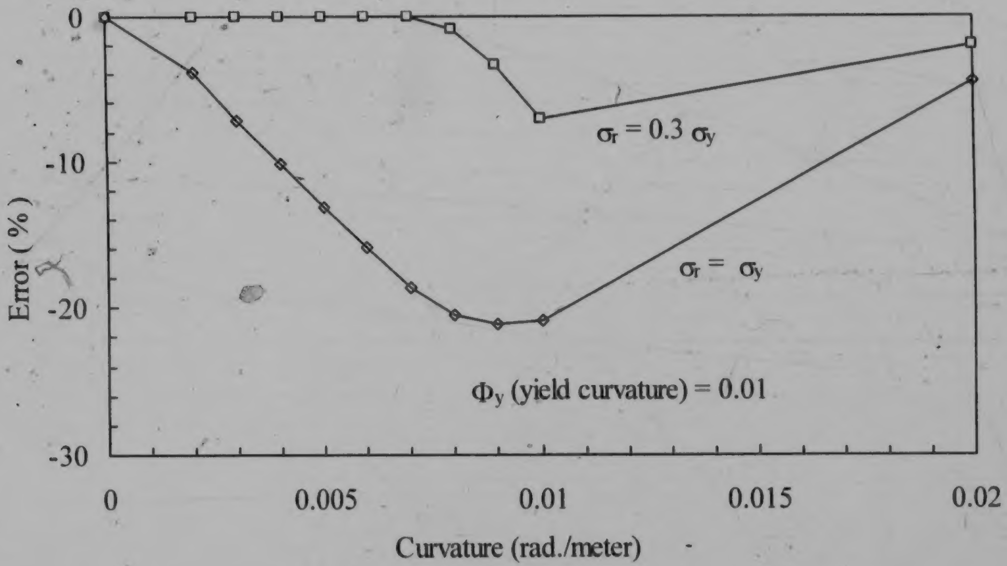

Figure 7.16: Error introduced when residual stresses are ignored in moment calculation

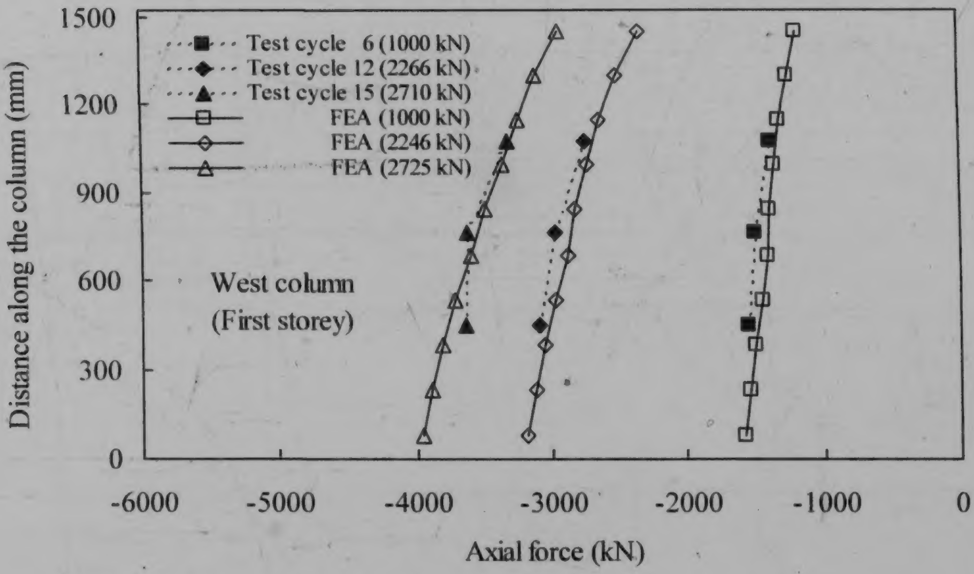

Figure 7.17: Axial force diagram of the west column in the first storey

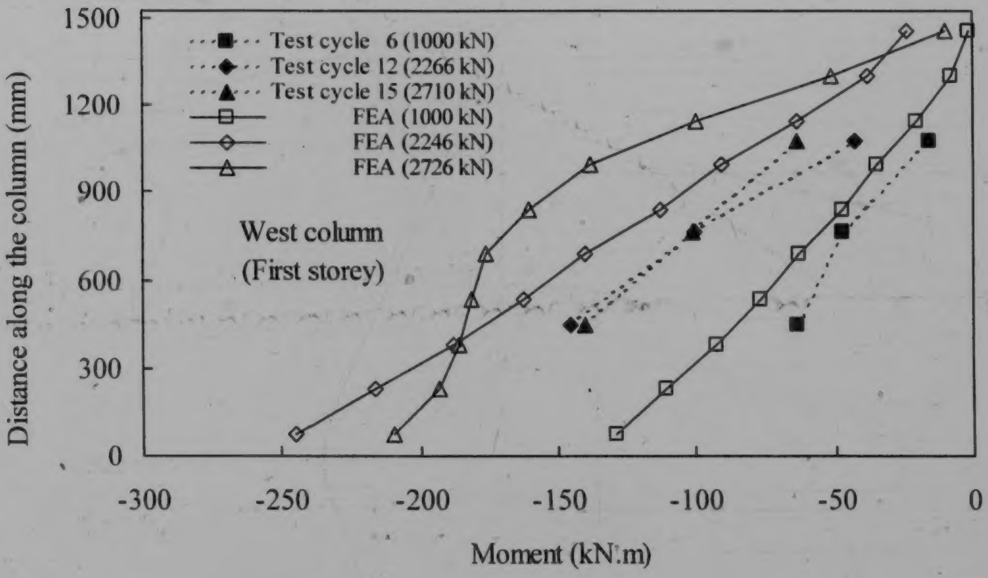

Figure 7.18: Bending moment diagram of the west column in the first storey

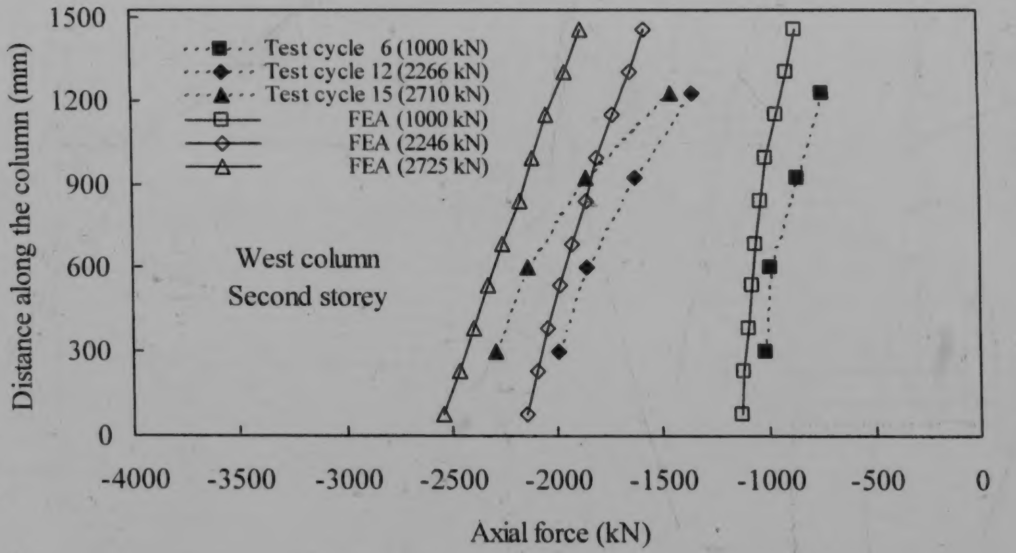

Figure 7.19: Axial force diagram of the west column in the second storey

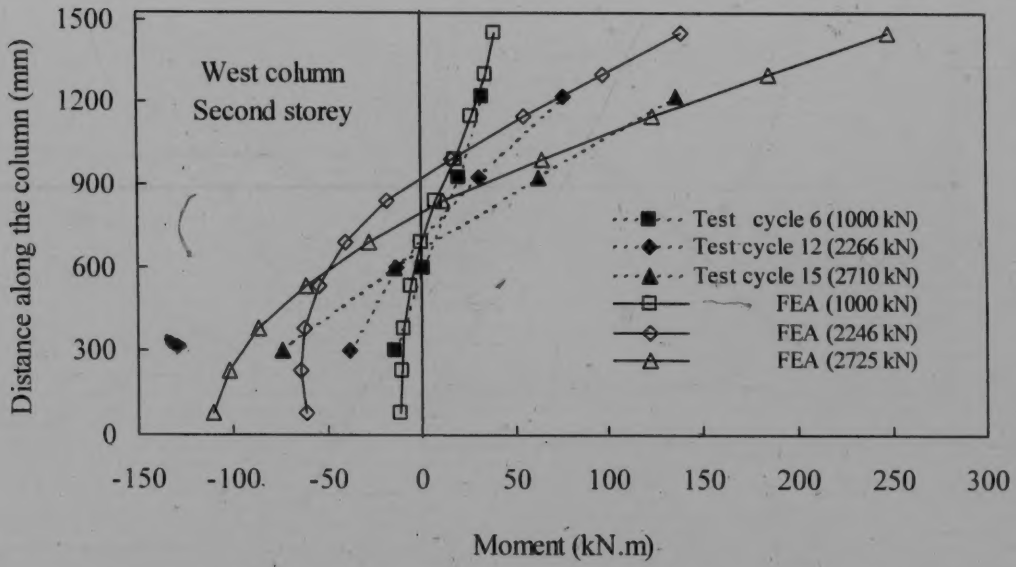

Figure 7.20: Bending moment diagram of the west column in the second storey

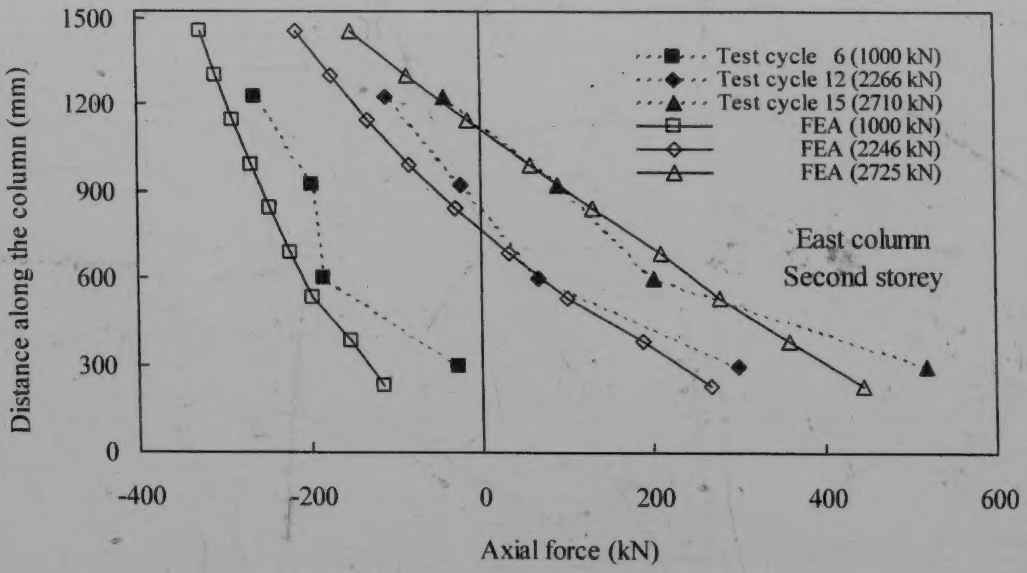

Figure 7.21: Axial force diagram of the east column in the second storey

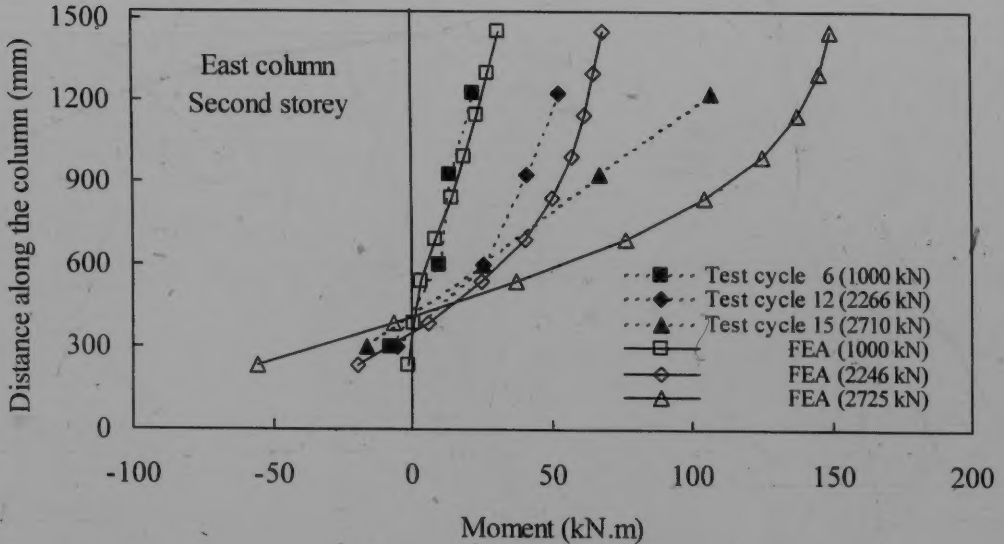

Figure 7.22: Bending moment diagram of the east column in the second storey

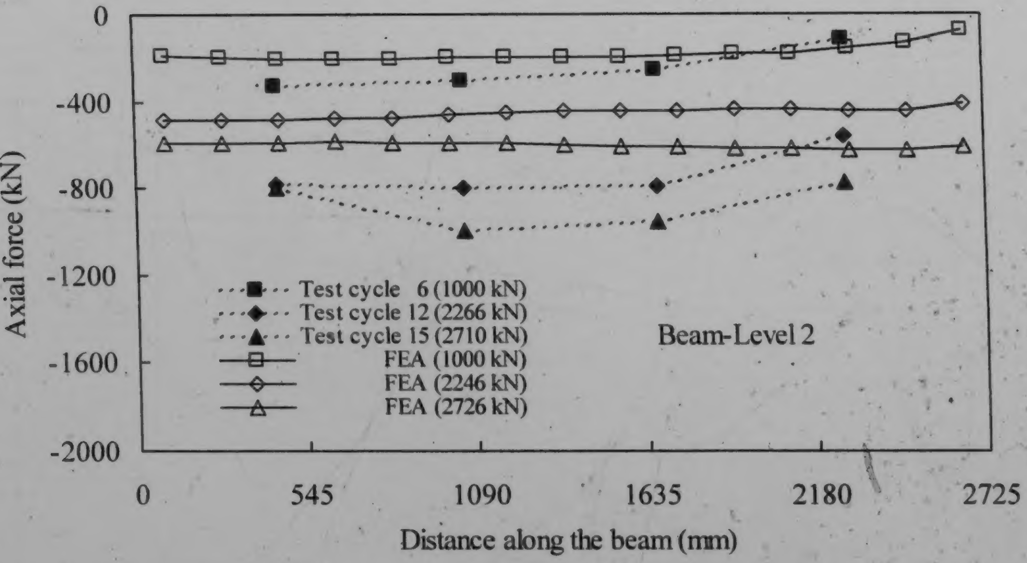

Figure 7.23: Axial force diagram in the beam at level 2

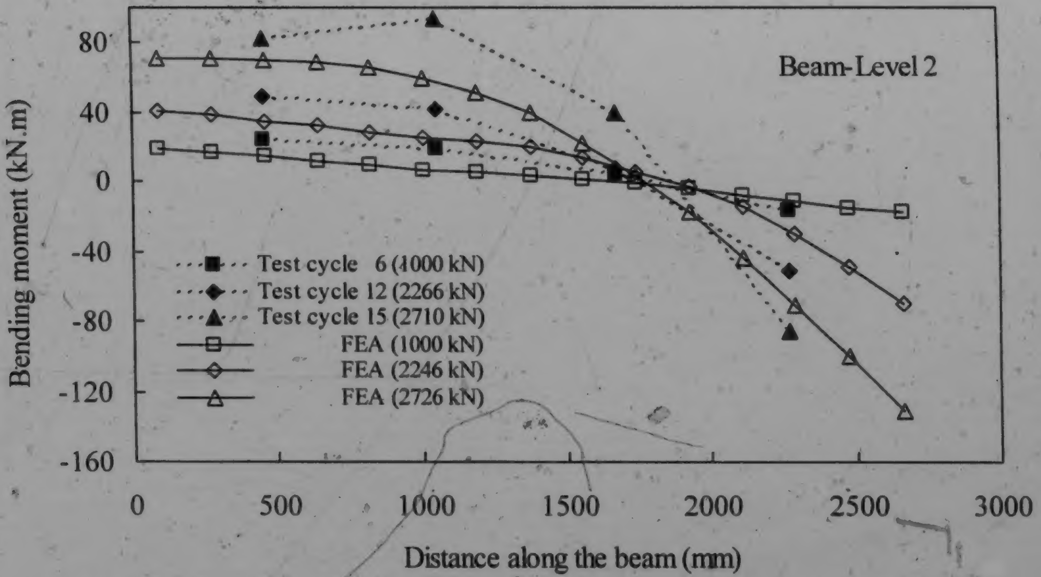

Figure 7.24: Bending moment diagram in the beam at level 2

8 PARAMETRIC STUDY

8.1 Introduction

A finite element model based on a nonlinear dynamic formulation was developed in Chapter 5 for the analysis of unstiffened steel plate shear walls. The model was validated by comparing the predicted behaviour of a three-storey and a four-storey steel plate shear wall against the test results presented in chapters 3 and 4 and the work of Driver *et al.* (1997). It was shown that the finite element model is able to predict accurately both the monotonic and cyclic behaviour of steel plate shear walls.

The main objective of this chapter is to identify the parameters that affect the behaviour of a steel plate shear wall system. The model selected for this investigation is a single steel plate shear wall panel with rigid floor beams subjected to shear force and constant gravity load. A set of non-dimensional parameters that define the behaviour of the model is identified from a dimensional analysis. The effects of the primary non-dimensional parameters are investigated and a method for considering the effect of the number of storeys in a multi-storey frame is proposed.

8.2 System selected for investigation

The steel plate shear wall model selected for the parametric study presented in section 8.3 is shown in Figure 8.1. The model consists of a single panel bounded by two rigid beams at the top and bottom. Neglecting the bending deformation of floor beams in a multi-storey unstiffened steel plate shear wall is a reasonable assumption, because equal and opposite tension fields applied to the interior beams tend to counteract the double curvatures expected in a beam in a drifting frame. The results of the test described in chapters 3 and 4 and the tests by other researchers (Driver *et al.*, 1997 and Rezai, 1999) showed that the strains developed in the top and bottom flanges of the storey beams were relatively small, indicating that the contribution of flexural and axial stiffness of the floor beams to the overall behaviour of the shear wall is relatively small and that the shear wall system behaves more as a cantilever wall than a frame. It is assumed that any gravity loads applied directly to the beams in the steel plate shear wall will be small.

Assuming cantilever behaviour, the rotational flexibility of the lower floor beam of an isolated panel in a multi-storey building can be neglected with the top floor beam allowed to rotate as a rigid body relative to the lower floor beam. This allows each panel of a multi-storey shear wall to be analysed separately ("panel-by-panel analysis") if the effect of over-turning moments from the top storeys is considered in the analysis. The analysis of a single storey model gives an accurate result for the first storey, assuming the shear wall is connected to a rigid foundation. By accounting for the rotation of the upper floor beams, this model can be extended to capture the behaviour of top panels as well. At first, only the shear force and gravity loads are considered in the panel. The effect of the number of storeys above the panel is discussed in sections 8.4 and 8.5.

8.2.1 Model parameters

In general, parameters affecting the behaviour and capacity of a system can be classified into four categories: geometric variables, loading variables, deformational variables, and material variables. The parameters that govern the behaviour and capacity of the selected model of steel plate shear wall with rigid floor beams are defined below.

Referring to Figure 8.1, the geometric variables are the width of the infill plate, L, the height of the panel, h, the thickness of infill plate, t_p, the moment of inertia of the columns, I_c, the cross-sectional area of the columns, A_c, and the magnitude of the maximum out–of–plane imperfection in the infill plate, Δ_{imp}. The loading variables are the applied gravity load in the columns, W, and the shear force, V, while the deformational variable is selected as the drift of the panel (δ). The material variables are the modulus of elasticity, E, the elastic shear modulus, G, Poisson's ratio, ν, the static yield strength of column material, σ_{yc}, and the static yield strength of the infill plate material, σ_{ypl}. Of these, the modulus of elasticity, the elastic shear modulus, and

Poisson's ratio are nearly constant for all grades of steel. The first two are also related through Poisson's ratio. Thus, only the modulus of elasticity needs to be considered an independent parameter.

8.2.2 Simplification of parametric study- Dimensional analysis

A total of 12 parameters are therefore believed to affect the behaviour and capacity of the selected model: L, h, t_p, A_c, I_c, Δ_{imp}, W, V, δ, σ_{yc}, σ_{ypl}, and E. Considering the number of parameters, along with the practical range for each parameter, a comprehensive study of this system requires an analysis of an unmanageable number of models. By implementing methods of dimensional analysis, the complexity of the study can be reduced. This can be achieved by selecting a representative set of parameters that are scale independent and dimensionless (Taylor, 1974).

Assuming that the behaviour of a physical problem can be obtained by a set of n variables, $A_1, A_2, \dots A_n$, the relationship between these variables can be expressed in terms of a homogeneous function (Taylor, 1974):

$$F(A_1, A_2, \dots A_n) = 0 \tag{8.1}$$

For practical reasons, it is useful to reduce the number of variables and identify a proper set of dimensionless parameters that can characterize the behaviour of the physical problem. This can be done by using the Buckingham Pi theorem (Langhaar, 1951), which is stated as follows:

If an equation is dimensionally homogeneous, it can be reduced to a relationship among a complete set of dimensionless products.

Langhaar (1951) showed that the number of independent dimensionless groups of variables needed to correlate the variables in a given process is equal to n-r. Here, r is the rank of the dimensional matrix of the variables $A_1, A_2, \dots A_n$. Rank of a matrix is the largest order of any square sub-matrix that has a non-zero determinant. As a result of using Buckingham theorem, the function (8.1) can be rewritten in terms of a smaller set of dimensionless parameters, β :

$$F(\beta_1, \beta_2, ...\beta_{n-r}) = 0 \tag{8.2}$$

Transformation of the primary variables into a set of dimensionless parameters is useful because the number of parameters that must be considered is reduced by r, and this represents a significant saving of computational effort. This transformation, however, may have scale effects, which must be ruled out in a successful parametric study.

8.2.3 Application of dimensional analysis to the selected model

Using the fundamental units of mass, M, length, L, and time, T, the dimensional matrix of the primary variables described above takes the form:

	L	h	t_p	I_c	A_c	Δ_{imp}	W	V	δ	σ_{yc}	σ_{ypl}	E
M	0	0	0	0	0	0	1	1	0	1	1	1
L	1	1	1	4	2	1	1	1	1	-1	-1	-1
T	0	0	0	0	0	0	-2	-2	0	-2	-2	-2

The rank of the above dimensional matrix is 2. Therefore, ten non-dimensional β -parameters must be formed in order to obtain a complete set of dimensionless products. For the one storey steel plate shear wall model the following trial set of parameters was chosen:

$\beta_1 = L / h$ (aspect ratio)

$\beta_2 = \dfrac{t_p L}{2A_c}$ (ratio of axial stiffness of infill plate to that of columns)

$\beta_3 = 0.7\sqrt[4]{\dfrac{h^4 t_p}{2LI_c}}$ (column flexibility parameter)

$\beta_4 = \dfrac{W}{W_y}$ (ratio of gravity load to axial yield load or normalized gravity load)

$\beta_5 = \dfrac{\delta}{h}$ (drift index)

$\beta_6 = \dfrac{V}{V_y}$ (ratio of shear load to the shear yield capacity or normalized base shear)

$\beta_7 = \dfrac{\sigma_{yc}}{E} = \varepsilon_{yc}$ (column yield strain)

$\beta_8 = \dfrac{\sigma_{ypl}}{E} = \varepsilon_{ypl}$ (plate yield strain)

$\beta_9 = \dfrac{\Delta_{imp}}{\sqrt{Lh}}$ (imperfection ratio)

$\beta_{10} = \dfrac{(A_c)^2}{I_c}$ (local buckling index)

in which W_y is the axial load that causes yielding of the whole cross section of the shear wall, V_y is the shear force that causes yielding of the whole cross section of the shear wall, ε_{yc} is the yield strain of the column material, and ε_{ypl} is the yield strain of the infill plate material. Using the von Mises yield criterion, W_y and V_y can be obtained as follows:

$$W_y = 2A_c\sigma_{yc} + Lt_p\sigma_{ypl} \tag{8.3}$$

$$V_y = 2dt_w(0.577\sigma_{yc}) + Lt_p(0.577\sigma_{ypl}) \tag{8.4}$$

Of the above parameters, the normalized gravity load, β_4, and the normalized base shear, β_6, are loading parameters, while the drift index, β_5, is obtained as an output. The remaining β-parameters define the finite element model. In terms of limit states design, the ultimate limit state is defined as the maximum value of β_6 and the serviceability limit state can be described in terms of β_5, the drift index.

The aspect ratio, β_1, is an important parameter since it is expected that it will strongly influence the inclination of the tension field and the resulting general behaviour of the steel plate shear wall. In a narrow and tall shear wall (small aspect ratio) the tension field is close to vertical, which makes the tension field contribution to shear resistance small and bending becomes the governing factor. In a wide and short shear wall (large aspect ratio) the tension field is more inclined, which results in shear deformations governing the behaviour of the shear wall. Changing the aspect ratio in a steel plate shear wall changes the relative stiffness of the columns to the infill plate, and this affects the stiffness and the capacity of the shear wall. The effect of the aspect ratio is investigated in section 8.3.1.

The ratio of the in-plane stiffness of the infill plate in the vertical direction to the axial stiffness of the columns, β_2, affects the compressive stress field in the infill plate, which depends, in an average sense, on the gravity load. The effect of this parameter on the behaviour of the selected model is investigated in section 8.3.2.

The non-dimensional parameter β_3 is proportional to the ratio of the in-plane bending flexibility of the column, $\left(h^3/EI_c\right)$, to the in-plane flexibility of the infill plate in the horizontal direction, $\left(L/Et_p h\right)$. This parameter was originally introduced by Wagner (1931) in order to study the effect of flexibility of the plate girder flange on the redistribution of the tension field in a plate girder web. By analogy with the plate girder, a relatively flexible column prevents a uniform and complete tension field from developing in the infill plate, thus reducing the stiffness and the capacity of the steel plate shear wall system. The parameter β_3 is similar to ω_h, which is designated in CSA–S16–01 as column flexibility. The effect of this parameter is investigated in section 8.3.3.

The normalized gravity load, β_4, is the ratio of applied gravity load to the gravity load that causes yielding of the horizontal cross-section of the shear wall. An increase in gravity loads causes an increase in the secondary bending moments, and this reduces both the stiffness and capacity of the shear wall. This may have contributed to the higher capacity observed in the three-storey steel plate shear wall compared to the four-storey steel plate shear wall. A gravity load of 1080 kN was applied to the three-storey steel plate shear wall whereas 1440 kN was applied to the four-storey steel plate shear wall. An investigation of the effect of this parameter on the behaviour of steel plate shear walls is presented in section 8.5.

The parameters β_7 and β_8 are the yield strains of the columns and infill plate, respectively. These parameters are important because they affect not only the capacity but also the failure mode of the shear wall. Ideally, most of the yielding and plastic deformation in a steel plate shear wall system would take place in the infill plates rather than in the columns so that the infill plates contribute most of the inelastic energy dissipation while the surrounding boundary elements just enhance the hysteresis loops during cyclic loading. Column yielding should not occur until an infill plate has gone through large plastic deformations. This can be achieved by proper selection of geometric parameters and also by using low-yield steel for the infill plate. However, because of time constraint, an investigation of β_7 and β_8 is beyond the scope of this parametric study.

The imperfection ratio, β_9, is a parameter that takes into account the effect of maximum infill plate imperfection relative to the size of the panel. The shape and the magnitude of the out–of–flatness identify an imperfection pattern for an infill plate. However, only the maximum out–of–flatness, Δ_{imp}, is considered as a parameter in this investigation. The first buckling mode of the infill plate is used as an imperfection shape for all analyses. The effect of this parameter on the behaviour of steel plate shear walls is presented in section 8.3.4.

The parameter β_{10} reflects the ability of the column section to undergo large plastic deformations without local web or flange buckling. CSA–S16–01 recommends a cross-section that satisfies Class 1 requirements for the columns in a steel plate shear wall In order for the cross-section to reach its plastic capacity with sufficient reserve plastic deformation capacity before local buckling of the web or flanges, the ratios of flange width to the thickness and web depth to the thickness must be less than the following limiting values (CSA-S16-01):

$$\frac{b_f}{2t_f} \le \frac{145}{\sqrt{\sigma_{yc}}} \tag{8.5}$$

$$\frac{d}{t_w} \le \frac{670}{\sqrt{\sigma_{yc}}} \tag{8.6}$$

Substituting equations (8.5) and (8.6) into the expressions for the cross-sectional area and the expression for the moment of inertia, the following equation for t_w can be obtained:

$$\left(\frac{670}{\sqrt{\sigma_{yc}}}\right)^3 \frac{t_w{}^4}{6} - \left(\frac{670}{\sqrt{\sigma_{yc}}}\right)^2 \frac{A_c t_w{}^2}{4} + I_c = 0 \tag{8.7}$$

In order to ensure that the web thickness will be greater than zero, the following condition must also be satisfied for a Class 1 section:

$$\beta_{10} = \frac{A_c{}^2}{I_c} \ge \frac{32\sqrt{\sigma_{yc}}}{2010} \tag{8.8}$$

8.2.4 Suitability of non-dimensional parameters

One of the requirements of the Buckingham Pi theorem is that all of the fundamental variables necessary to describe the mechanics of a problem must be included in the set of A_n quantities used in equation 8.1. For the selected steel plate shear wall model, the fundamental variables were identified earlier as L, h, t_p, I_c, A_c, δ, V, W, σ_{yc}, σ_{ypl}, E, and Δ_{imp}. To determine whether all of the essential variables that play a role in the behaviour of the system are represented in this set, a preliminary investigation was conducted on several steel plate shear walls having identical β-parameters but with different scales. If the set contains all of the essential quantities, then the results from these analyses should not be affected by changes in scale.

In order to check for potential scale effect, three models designated as A, C, and E were analysed. A description of these three models is presented in Tables 8.1 and 8.2. Model C has the same scale as the first panel of the four-storey steel plate shear wall tested by Driver *et al.* (1997). Except for material properties, all other variables in the selected models are different for each of the three models. However, the β-parameters, shown in Table 8.3, are the same for the three models.

The base shear versus drift for the three models are presented in Figure 8.2. The responses of the models are different since different scales have been used. However, a comparison of the models is presented in Figure 8.3 in terms of the normalized base shear, β_6, plotted against the drift index, β_5. Examination of the figure reveals that the change of scale did not have any effect on the non-dimensional response of the models. Therefore, it can be concluded that these parameters are the true representative parameters that are scale independent and that fully describe the behaviour of a steel plate shear wall panel. The β-parameters can therefore be used for an investigation of the selected model of steel plate shear wall.

8.3 Effect of the β –parameters on the behaviour steel plate shear wall panels

In this section only four parameters are investigated in depth in the context of the single storey model. These are the aspect ratio, β_1, the axial stiffness ratio, β_2, the column flexibility parameter, β_3, and the imperfection index, β_9. As in the previous section the material parameters β_7 and β_8 are kept constant at 0.00152 and 0.00166, respectively. The gravity load is kept at 10% of the yield capacity.

8.3.1 Effect of aspect ratio (β_1)

The effect of infill plate aspect ratio on the behaviour of steel plate shear wall was investigated using four models with aspect ratios of 0.7, 1.0, 1.5, and 2.0. The remaining non-dimensional parameters were kept constant for these models. An aspect ratio of 0.7 represents a narrow and high shear wall panel whereas an aspect ratio of 2.0 represents a wide and short shear wall. The other β –parameters were obtained in such a way that the combination of non-dimensional parameters result in practical and reasonable dimensions for each model. The various geometric and material properties used for each model are presented in Table 8.4, with the actual cross-sectional dimensions of the columns presented in Table 8.5. Table 8.6 presents the value of all the β –parameters used for all four models.

The normalized base shear, β_6, versus the normalized drift, β_5, for the four models, are plotted in Figure 8.4. The slope of the linear portion of the response represents a non-dimensional stiffness, $(V/\delta)(h/V_y)$. Figure 8.4 indicates that a decrease in aspect ratio results in an increase in the capacity and the non-dimensional stiffness of steel plate shear walls. This increase of capacity and stiffness, however, is negligible within the range of aspect ratio between 1.0 and 2.0. For aspect ratios less than 1.0, the increase in capacity and non-dimensional stiffness is noticeable. By decreasing the aspect ratio of the steel plate shear wall from 1.0 to 0.7 the non-dimensional stiffness is increased by 35% and the capacity is reached at a smaller drift. At a value of $\beta_5 = 0.007$

local buckling occurred at the top of the right column in the steel plate shear wall with aspect ratio of 0.7. This local buckling, which is depicted in Figure 8.5, is believed to have limited the capacity of the shear wall as the drift increased.

In order to investigate the effect of this local buckling, a new model for the steel plate shear wall with an aspect ratio of 0.7 was prepared. Local buckling was prevented in the new steel plate shear wall panel by providing a stiffener at that location. The response of the steel plate shear wall when local buckling of the columns is precluded is depicted in Figure 8.6. As expected, the portion of the curve before local buckling of the earlier model has not changed. However, the normalized capacity has increased by approximately 11%, which confirms the detrimental effect of column local buckling on the shear resistance.

8.3.2 Effect of axial stiffness ratio (β_2)

Three different values of β_2, namely, 0.31, 0.44, and 0.62, were selected for this investigation while the other non-dimensional parameters were kept unchanged in the models. The value of 0.44 is the same as for the lower storey of the three-storey steel plate shear wall tested in this program. The selected dimensions for the models and the value of the other dimensionless parameters are presented in Tables 8.7 to 8.9.

The normalized response is shown in Figure 8.7 for three different values of β_2. The base shear has reached 90% of V_y in all models. As the β_2–parameter increases, the slope of the non-dimensional response, which can be considered as a non-dimensional stiffness, increases. For instance, by increasing the β_2–parameter from 0.31 to 0.62 the non-dimensional stiffness increases from 250 to 310, which is a 24% increase. However, the axial stiffness ratio, β_2, does not affect the strength of the shear wall.

8.3.3 Effect of column flexibility parameter (β_3)

The stiffness and capacity of an unstiffened steel plate shear wall system mainly depends on the development of the tension field in the infill plate. In order to develop a uniform tension field, the boundary members should have enough flexural stiffness to anchor the tension field. In-plane transverse deformations of the boundary members release the tension field in the infill plate and reduce the effectiveness of the system. For interior beams or columns of a steel plate shear wall, the presence of equal and opposite tension fields usually keeps the flexural deformations small. At the top and bottom panels, however, enough rigidity should be provided to anchor the tension field. Similarly, in order to increase the effectiveness of a steel plate shear wall, enough flexural stiffness should be provided by the columns on the perimeter of the shear wall. The minimum stiffness of a column $\left(EI_c / h^3\right)$, however, depends on the magnitude of the tension forces that need to be transferred by the columns and this can be related to the in-plane stiffness of the infill plate in the direction of shear force $\left(Et_p h / L\right)$. As a consequence, β_3 should play an important role in a steel plate shear wall system. As β_3 increases in a steel plate shear wall panel the flexibility of the columns and corresponding in-plane deformation of the columns increase. This reduces the efficiency of the system.

In order to investigate the effect of β_3 on the behaviour of a steel plate shear wall, three models with column flexibility ratios of 1.5, 2.5, and 3.5 were analysed. The scales of the models were selected to keep the other non-dimensional parameters constant for this investigation. A column flexibility ratio of 2.5 is the maximum value allowed by CSA–S16–01, and β_3 of 1.5 is the column flexibility of the bottom panel of the three-storey steel plate shear wall tested in this project.

Figure 8.8 shows the normalized response of the three steel plate shear walls with varying β_3 values. As can be seen in the figure, β_3 has a major effect on both the stiffness and the capacity of the steel plate shear wall. As the column flexibility parameter decreases, the shear wall capacity approaches the yield capacity, V_y, resulting in a more economical system. For instance by reducing the column flexibility of the model from 3.5 to 1.5 the capacity of the steel plate shear wall is increased from 72% of V_y to more than 90% of V_y. As mentioned above, CSA–S16–01 has limited the column flexibility parameter to a value of 2.5. For the set of β–parameters selected for this study the shear wall capacity corresponding to this limit is $0.8V_y$.

The slope of the linear portion of the normalized response is 160, 180, and 278 for column flexibilities of 3.5, 2.5, and 1.5, respectively (see Figure 8.8). The relationship between the column flexibility parameter and the stiffness of the shear wall is therefore nonlinear. The wall stiffness is more sensitive to a change in β_3 at lower values of β_3. As a consequence the column flexibility parameter has a major effect on both stiffness and capacity and should be considered as a key parameter in the design of a steel plate shear wall systems.

8.3.4 Effect of the imperfection index (β_9)

In order to investigate the effect of the magnitude of initial imperfections on the behaviour of steel plate shear walls, five different values of β_9, namely, 0.0, 0.0045, 0.0113, 0.0227, and 0.0340 were used. The other β–parameters were kept constant for all the models. These steel plate shear walls have the same dimensions as case C in Table 8.1. The values of β_9 are equivalent to maximum imperfection sizes of $0t_p$, $2t_p$, $5t_p$, $10t_p$, and $15t_p$, where t_p is the thickness of the infill plate. All these models have the same imperfection shape, i.e., the first buckling mode of the infill plate.

Since the only difference between the models is the size of imperfection, instead of normalized responses the base shear versus the drift are plotted at different imperfection sizes. These plots, depicted in Figure 8.9, show that the initial imperfection magnitude does not have a major effect on the capacity but affects slightly the stiffness of the system. As long as the imperfection magnitude is less than 1% of $\sqrt{Lh}$ the effect is very small and can be neglected. For imperfection sizes larger than 1% of $\sqrt{Lh}$ the stiffness reduction is noticeable and should be accounted for in the design. For instance, by increasing the imperfection size from 1.1% to 3.4% of $\sqrt{Lh}$ the stiffness of the steel plate shear wall panel reduces by 18% (from 550 kN/mm to 450 kN/mm). From the above findings, it seems reasonable to limit the imperfection size, in a steel plate shear wall panel to 1% of $\sqrt{Lh}$. For the test specimen presented in Chapter 3, this limit corresponds to an imperfection magnitude of 20.5 mm. This is well within the normal fabrication tolerances.

8.4 Inclusion of overturning moment in the one-storey model

In the parametric study presented above the gravity load was kept constant at 10% of the axial yield load. To take into account the effect of the number of storeys above a certain panel in a multi-storey structure the overturning moment that is transferred from the structure above the panel of interest should be considered in the analysis. The overturning moment on the top of panel *j*, $(M_{ov})_j$, in a multi-storey shear wall (see Figure 8.10) can be calculated from the following equation of equilibrium:

$$(M_{ov})_j = \sum_{i=j+1}^{n} F_i(H_i - H_j) + \sum_{i=j+1}^{n} w_i(U_i - U_j) \tag{8.9}$$

where n is the total number of storeys, j is the panel under investigation, F_i is the horizontal force applied to the i^{th} floor, w_i is the gravity load applied to the i^{th} floor, H_i is the height of the i^{th} floor above the base, and U_i is the horizontal displacement of the i^{th} floor relative to the base of the shear wall. If the second order overturning moment resulting from gravity loads acting over the drift is neglected and a constant horizontal force, F, and equal storey height, h, are assumed for all panels, expression for the overturning moment is simplified to:

$$(M_{ov})_j = V_j\left[\left(\frac{n-j}{2}\right)h\right] \tag{8.10}$$

where V_j is the shear force applied in panel j and given as:

$$V_j = (n-j+1)F \tag{8.11}$$

The overturning moment can be converted to a couple composed of two equal and opposite forces applied at the centre of the columns by dividing the overturning moment obtained from equation 8.10 by the column spacing (L'). All loads required for the analysis of the panel are shown in Figure 8.11 where W_j is the total gravity load applied from the higher storeys on panel j and V_j is the shear force in this panel. By applying a fixed boundary condition to the bottom of the panel and then, considering the rigid body rotation of the lower floor beam separately, the total drift of the panel can be obtained from the following equation:

$$u_j = (u_j)_{fix} + h\theta_{j-1} \tag{8.12}$$

where u_j is the total drift of panel j, $(u_j)_{fix}$ is the drift of panel j assuming a fixed boundary condition at the base of the panel, and θ_{j-1} is the rotation of the base of the panel about an axis normal to the plane of the shear wall (see Figure 8.11). Using this two-step procedure, the total drift in a given panel can be obtained. If the rotation at the base of a multi-storey shear wall is assumed to be zero (assuming the wall to be anchored to a rigid foundation), the drift in the first panel can be obtained from the model shown in Figure 8.11(a). Using equation 8.12, the total drift of the second panel can be obtained by determining the rotation of floor 1 (θ_1), obtained from the analysis of single store model of first panel, and the analysis of single storey model of panel 2 from which the drift for rigid boundary condition, $(u_2)_{fix}$, can be obtained. This procedure can be continued to assemble a panel-by-panel analysis of the steel plate shear wall. The total rotation of a floor can be obtained as:

$$\theta_j = \theta_{j-1} + \theta_{j/j-1} \tag{8.13}$$

where, θ_{j-1} is the rotation at the base of the panel and $\theta_{j/j-1}$ is the rotation of floor j in the analysis of panel with fixed boundary condition.

To assess the accuracy of the proposed model depicted in Figure 8.11 for the analysis of an intermediate panel of a multi-storey steel plate shear wall, the panel-by-panel procedure is applied to the four-storey steel plate shear wall tested by Driver *et al.* (1997). Rigid floor beams were assumed at all the levels. Constant gravity loads of 360 kN were applied at each level. The shear wall was pushed monotonically by applying equal horizontal loads at each floor. The response of the first, second, and the third panels of the model was obtained from the panel-by-panel method and compared with the analysis of the whole model.

The drift and rotation at the first level of the shear wall were obtained by analysing a single storey model of the bottom panel. Figure 8.12 shows that the base shear versus storey drift obtained from the analysis of the whole model and the single storey model of first panel are the same. Figure 8.13 presents the base shear versus the rotation of the beam at the first level, θ_1, which was obtained from the analysis of the single storey model. A single storey model of the second panel was analysed to obtain $(u_2)_{fix}$ and $\theta_{2/1}$ (see Figure 8.11a). Knowing $(u_2)_{fix}$, which is presented in Figure 8.14, and θ_1, the total drift of the second panel, u_2, was obtained from equation 8.12 where the storey height, h, is 1830 mm. Figure 8.15 presents the shear versus storey drift response of the second storey obtained from the panel-by-panel procedure and from a four-storey steel plate shear wall model. Both models give identical predicted load response. Base shear versus total rotation of beam at second level, θ_2, is presented in Figure 8.16, where θ_2 was obtained by adding the rotation at the first level, θ_1, to the relative rotation of second floor to the first floor, $\theta_{2/1}$ (also shown in Figure 8.16). An analysis of the single storey model of the third panel and application of the procedure used for the second panel yields the total drift of third panel (see Figure 8.17). The results clearly demonstrate that the proposed panel-by-panel analysis is successful and the model shown in Figure 8.11 is valid for use in accounting for the effect of overturning moment and number of storeys above a panel.

8.5 Effect of gravity load and overturning moment

In order to investigate the effect of the gravity load and overturning moment on the behaviour of a steel plate shear wall panel, the response of the first panel of a four and an eight-storey steel plate shear wall are compared with the response of a one-storey steel plate shear wall at different gravity load levels. The effect of gravity load and overturning moment was investigated for only one panel geometry, namely, panel C described in Table 8.1. That panel geometry was repeated for each storey of the four and eight storey frames investigated. Equal horizontal loads are applied at each floor level and increased monotonically under constant gravity load. Four different gravity load levels are applied to the shear walls, namely, β_4 magnitudes of 0.0, 0.1, 0.3, and 0.5 for the bottom panel of each shear wall. The gravity load is assumed to be distributed equally between the floors. The four and eight storey steel plate shear walls are analysed using the model shown in Figure 8.11a.

As discussed in the previous section, the overturning moment applied at the top of a panel can be obtained from equation 8.10. If both sides of equation 8.10 are divided by $(V_j L')$, the following non-dimensional parameter is obtained for panel j:

$$\beta_{11} = \frac{(M_{ov})_j}{V_j L'} = \frac{(n-j)}{2(\beta_1 + d/h)} \qquad 8.14$$

where β_{11} is a normalized overturning moment in panel j, β_1 is the aspect ratio and the storey shear V_j is defined in equation 8.11. Although β_{11} is a non-dimensional parameter, its scale independence has not been verified.

As the non-dimensional overturning moment β_{11} increases, the behaviour should gradually be governed by flexural action rather than shear deformation. In this investigation, three values of β_{11} are investigated, namely, 0.0, 0.9, and 2.07 for the bottom panel of a single panel, a four panel, and an eight panel steel plate shear wall, respectively. Using four different values of β_4, namely, 0.0, 0.1, 0.3, and 0.5, for each value of β_{11}, a total of twelve different combinations are obtained for this investigation. The values of the remaining β-parameters selected for this investigation are tabulated in Table 8.1.

The elastic stiffness, taken as the slope of the base shear versus storey drift, of the bottom panel from one, four, and eight-storey steel plate shear walls versus the normalized gravity load (β_4) is shown in Figure 8.18. As expected, both the gravity load and the overturning moment reduce the elastic stiffness of the shear wall panel. The rate of reduction of the elastic stiffness is almost the same for the range of the normalized overturning moment parameters selected in this study (β_{11} from 0.0 to 2.07). An increase of the normalized gravity load parameter (β_4) from 0.0 to 0.5 results in a decrease of the stiffness of the first panel of about 20% in all shear walls. For a given gravity load level, an increase of the non-dimensional overturning moment from 0.0 (one-storey shear wall) to 0.9 (four-storey shear wall) results in a reduction of the elastic stiffness of the first panel of about 12% on average. This stiffness reduction is about 24% in the bottom panel of the eight-storey shear wall (β_{11}=2.07).

The normalized capacity of the panel (maximum base shear divided by the shear force that causes yielding of the whole cross section of the panel) is plotted against the normalized gravity load (β_4) for three values of the normalized overturning moment, β_{11}, in Figure 8.19. The figure shows that the gravity load and overturning moment have a significant effect on the capacity of the shear wall panel. The shear wall panel can reach up to 95% of V_y when both β_4 and β_{11} are zero. However, an increase of β_4 to 0.5 and

β_{11} to 2.07 (eight-storey shear wall) results in a reduction of the panel capacity down to only 22% of V_y. Figure 8.20 presents the same data as in Figure 8.19, except that in this figure the reduction in the shear capacity (from the case with no gravity load), has been normalized by dividing with the shear capacity obtained under no gravity load. The figure shows that the capacity of the panel reduces at a higher rate when the overturning moment is larger. For instance, at a β_4 of 0.5, the ratio of the capacity with gravity load to the capacity with no gravity load is reduced by 26% in the one-storey (β_{11}=0) shear wall, 53% in the four-storey (β_{11}=0.9) shear wall, and 63% in the eight storey (β_{11}=2.07) shear wall.

The gravity load and overturning moment also reduce the ductility of the shear wall panel. If ductility of a steel plate shear wall panel is defined as the drift at which the peak capacity is reached, the forgoing analysis indicates that the gravity load and overturning moment reduce the ductility of shear walls. This is illustrated in Figure 8.21 where the normalized base shear, β_6, is plotted against the drift index, β_5, for the bottom panel of the eight-storey shear wall at four different gravity load levels. The circles at the peak load indicate where the maximum capacity of the shear wall was reached. The figure clearly indicates that the maximum capacity is reached at a smaller drift when the normalized gravity load is increased. The normalized response of the panel at a constant normalized gravity load level of 0.5 is plotted in Figure 8.22 for different normalized overturning moments. The drift, at which the peak capacity is reached, indicated by the circles also decreases as the moment is increased.

Table 8.1: Parameters for investigation of potential scale effects

	Case A	Case C	Case E
L (mm)	2000.0	2751.8	4000.0
h (mm)	1183.5	1628.4	2367.0
t_p (mm)	3.49	4.80	6.98
I_c (mm^4)	7.67E+07	2.75E+08	1.23E+09
A_c (mm^2)	7923	15000	31694
σ_{yc} (MPa)	313	313	313
σ_{ypl} (MPa)	341.2	341.2	341.2
E (MPa)	2.06E+05	2.06E+05	2.06E+05
W (kN)	760.7	1440.0	3042.6
Δ_{imp} (mm)	6.98	9.6	13.96

Table 8.2: Cross-sectional dimensions of columns in the trial cases

	t_f(mm)	t_w (mm)	b_f(mm)	d (mm)	$b_f/2t_f$	d/t_w
Case A	14.4	5.46	236	206.9	8.2	37.87
Case C	19.8	7.52	324.7	284.7	8.2	37.87
Case E	28.8	10.9	472.1	412.8	8.2	37.87

Table 8.3: β –parameters for trial cases (A, C, and E)

β_1	β_2	β_3	β_4	β_7	β_8	β_9	β_{10}
1.69	0.44	1.52	0.1036	0.00152	0.00166	0.0045	0.81818

Table 8.4: Primary parameters for investigation of the effect of β_1

	β_1=0.7	β_1=1	β_1=1.5	β_1=2
L (mm)	1048	3001.6	6906.0	13098.0
h (mm)	1497.5	3001.6	4605.0	6548.0
t_p(mm)	8.0	5.5	2.5	1.5
I_c (mm^4)	1.179E+08	4.57E+08	5.00E+08	6.47E+08
A_c (mm^2)	7678.2	15117	15812	17991
σ_{yc} (MPa)	313	313	313	313
σ_{ypl} (MPa)	341.2	341.2	341.2	341.2
E (MPa)	2.06E+05	2.06E+05	2.06E+05	2.06E+05
W (kN)	766.8	1509.6	1578.9	1796.6
Δ_{imp}	2.71	6.48	12.19	20.0

Table 8.5: Cross-sectional dimensions of columns used to study the effect of β_1

	t_f(mm)	t_w (mm)	b_f(mm)	d (mm)	$b_f/2t_f$	d/t_w
β_1=0.7	13.21	7.18	216.7	272	8.2	37.87
β_1=1.0	18.55	10.07	304.0	381.36	8.2	37.87
β_1=1.5	18.96	10.31	310.9	390.3	8.2	37.87
β_1=2.0	20.22	10.99	331.66	416.32	8.2	37.87

Table 8.6: β –parameters in the study of the effect of β_1 (β_1=0.7, 1.0, 1.5, and 2.0)

β_2	β_3	β_4	β_7	β_8	β_9	β_{10}
0.546	2.5	0.1	0.00152	0.00166	0.0022	0.5

Table 8.7: Primary parameters for investigation of β_2

	β_2=0.31	β_2=0.44	β_2=0.62
L (mm)	2751.8	2751.8	2751.8
h (mm)	1628.4	1628.4	1628.4
t_p (mm)	2.4	4.8	9.6
I_c (mm^4)	1.38E+08	2.75E+08	5.50E+08
A_c (mm^2)	10606.6	15000.0	21213.2
σ_{yc} (MPa)	313	313	313
σ_{ypl} (MPa)	341.2	341.2	341.2
E (MPa)	2.06E+05	2.06E+05	2.06E+05
W (kN)	921	1440	2309
Δ_{imp}	9.6	9.6	9.6

Table 8.8: Cross-sectional dimensions of columns used to study the effect of β_2

	t_f(mm)	t_w (mm)	b_f(mm)	d (mm)	$b_f/2t_f$	d/t_w
β_2=0.31	16.65	6.325	273	239.5	8.2	37.87
β_2=0.44	19.81	7.517	324.7	284.7	8.2	37.87
β_2=0.62	23.55	8.94	386.2	338.6	8.2	37.87

Table 8.9: β –parameters in the study of the effect of β_2

(β_2=0.31, 0.44, and 0.62)

β_1	β_3	β_4	β_7	β_8	β_9	β_{10}
1.69	1.52	0.1036	0.00152	0.00166	0.0045	0.81818

Table 8.10: Primary parameters for investigation of β_3

	β_3=1.5	β_3=2.5	β_3=3.5
L (mm)	2751.8	6241.0	9071.0
h (mm)	1628.4	3693.0	5368.0
t_p(mm)	4.54	1.33	0.51
I_c (mm^4)	2.75E+08	1.22E+08	3.70E+07
A_c (mm^2)	15000.0	10000.0	5500.0
σ_{yc} (MPa)	313	313	313
σ_{ypl} (MPa)	341.2	341.2	341.2
E (MPa)	2.06E+05	2.06E+05	2.06E+05
W (kN)	1365.22	910.2	500.6
Δ_{imp}	4.57	10.37	15.07

Table 8.11: Cross-sectional dimensions of columns used to study the effect of β_3

	t_f(mm)	t_w (mm)	b_f(mm)	d (mm)	$b_f/2t_f$	d/t_w
β_3=1.5	19.8	7.517	324.7	284.7	8.2	37.87
β_3=2.5	16.17	6.14	265	232.5	8.2	37.87
β_3=3.5	12	4.55	196.6	172.4	8.2	37.87

Table 8.12: β –parameters in the study of the effect of β_3 (β_3=1.5, 2.5, and 3.5)

β_1	β_2	β_4	β_7	β_8	β_9	β_{10}
1.69	0.416	0.1	0.00152	0.00166	0.0022	0.81818

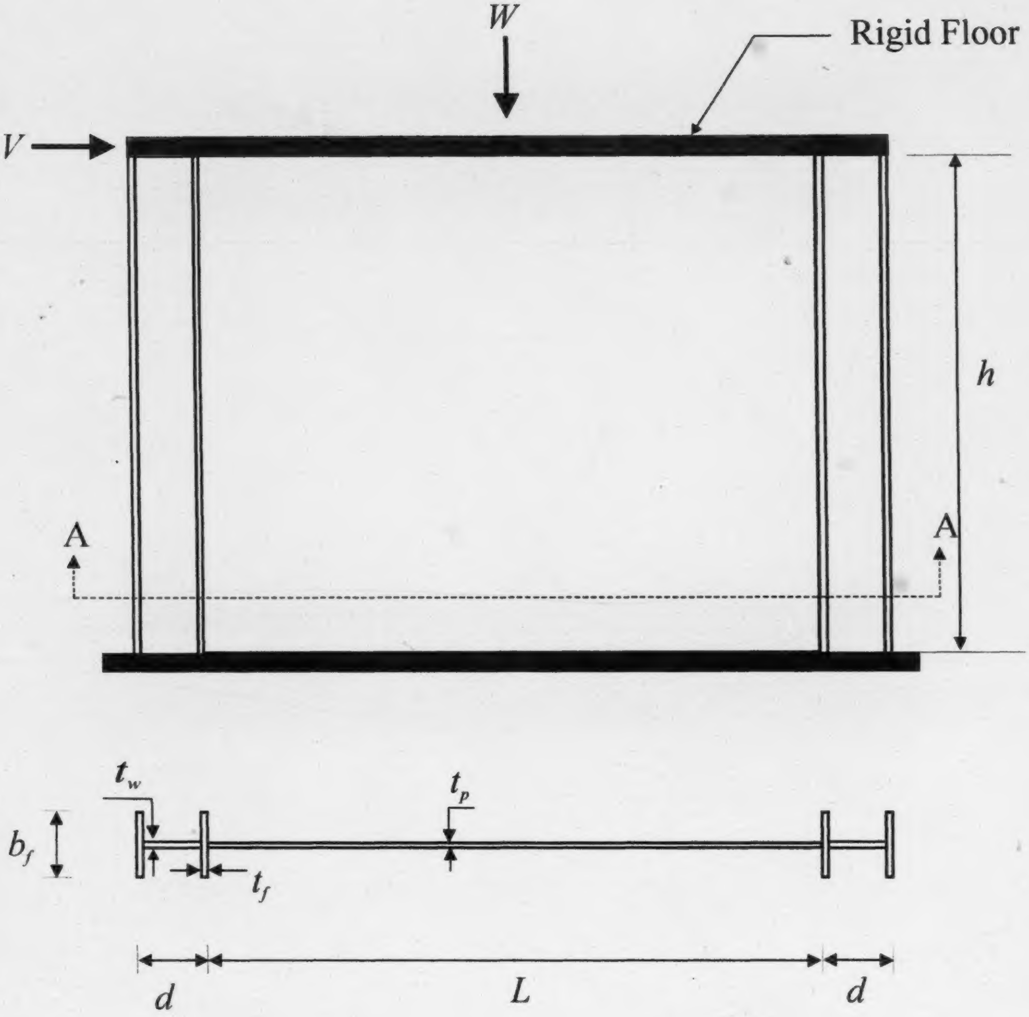
W
Rigid Floor
V
h
A
A
t_w
t_p
b_f
t_f
d
L
d

Figure 8.1: Selected model for parametric study of a panel

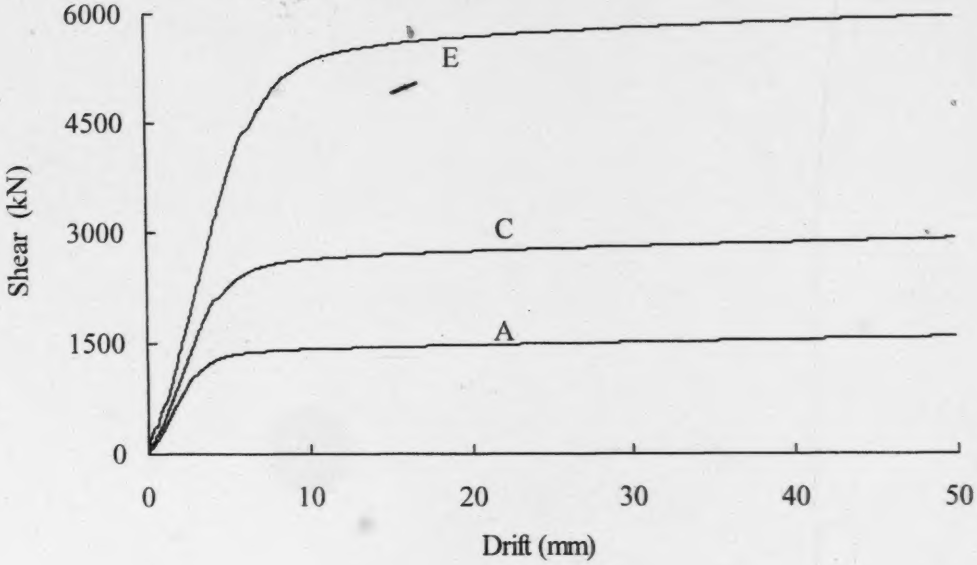

Figure 8.2: Base shear versus drift for three models with similar β -parameters

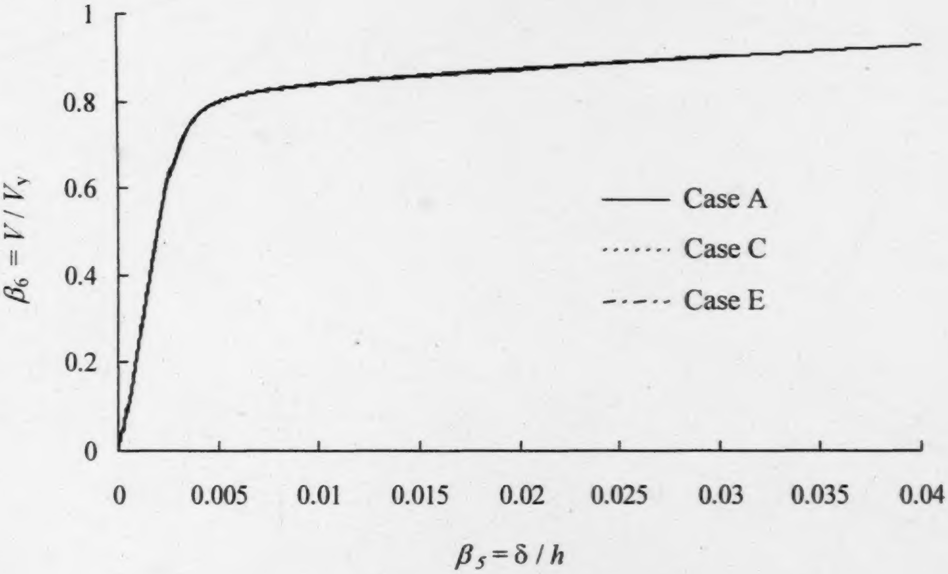

Figure 8.3: Normalized responses for three different models with similar β –parameters

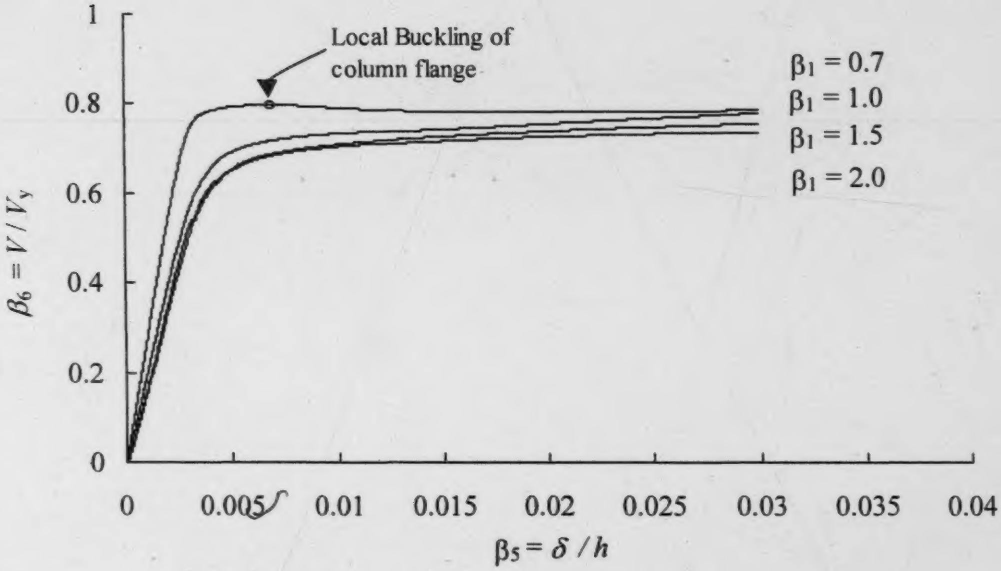

Figure 8.4: Effect of aspect ratio parameter, β_1, on behaviour of steel plate shear wall

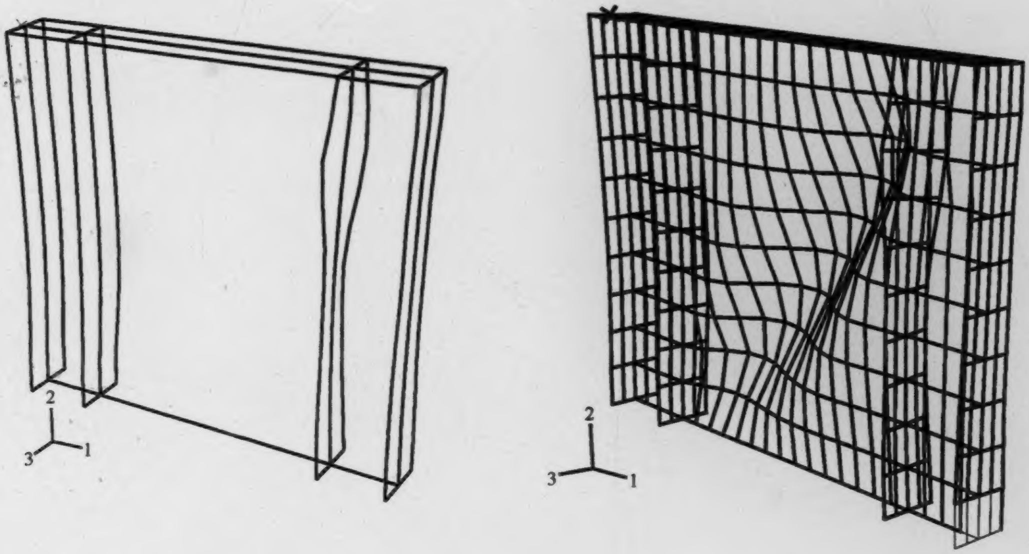

Figure 8.5: Column local buckling and deformation of model with β_1=0.7

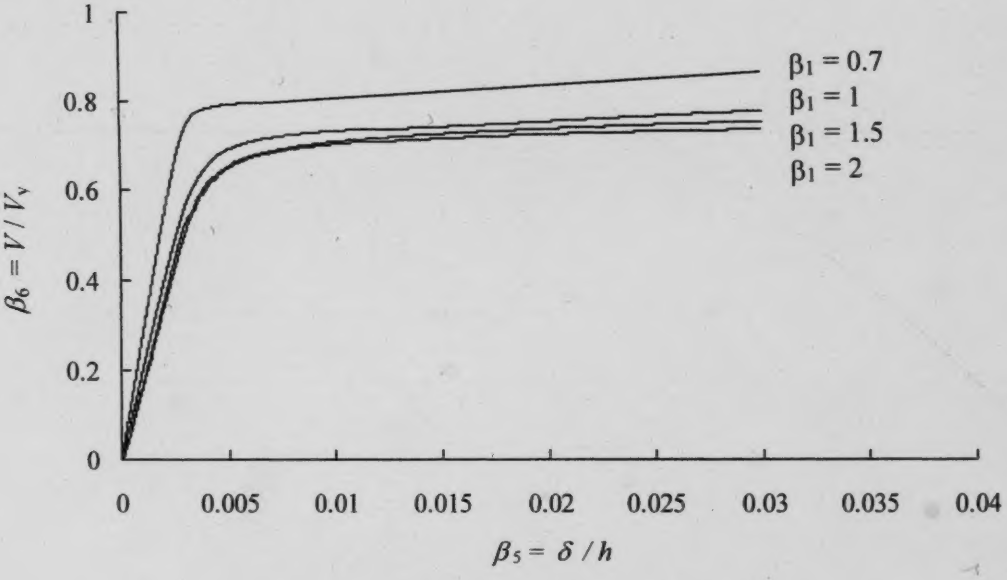

Figure 8.6: Normalized response for different aspect ratios
(if column local buckling prevented)

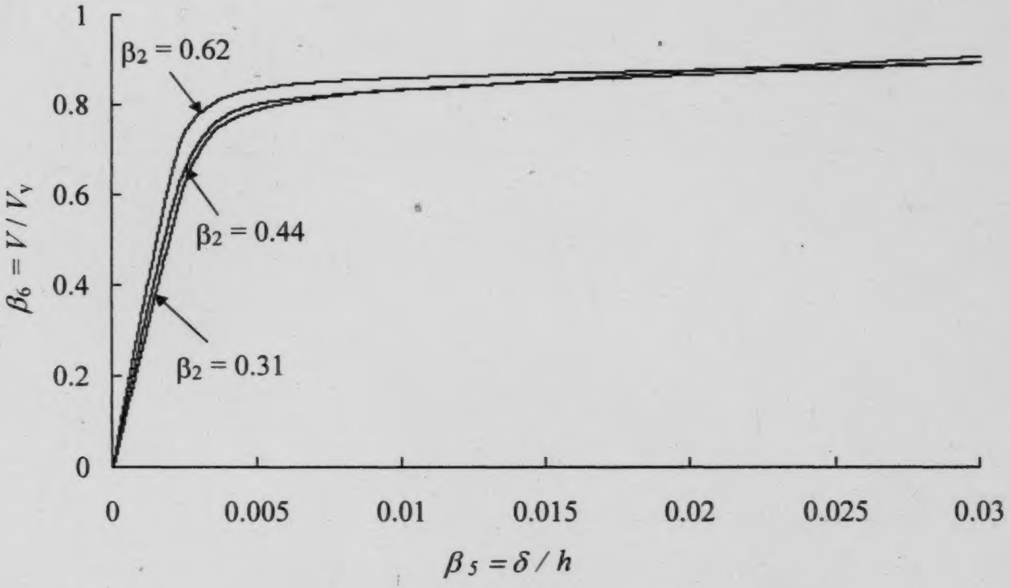

Figure 8.7: Effect of β_2 on steel plate shear wall response

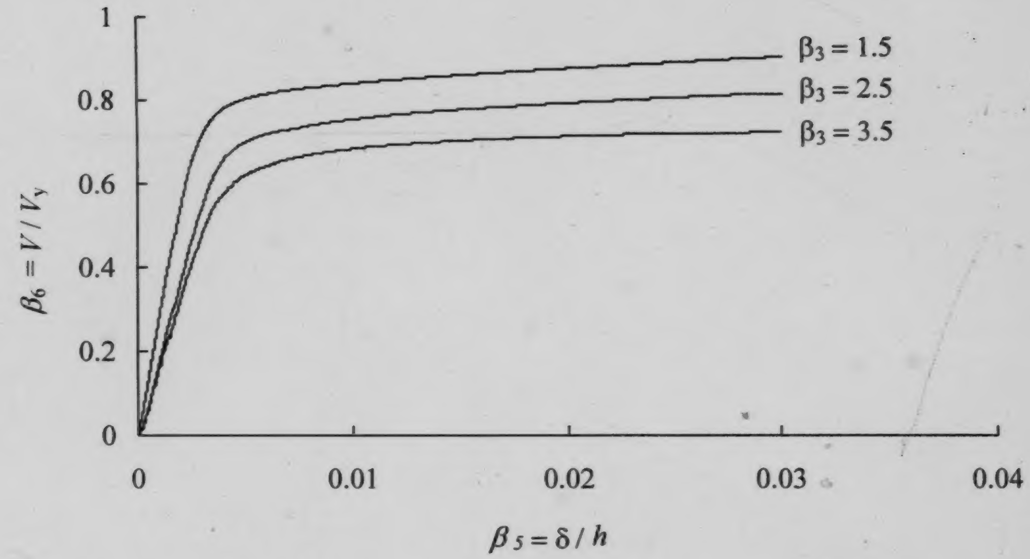

Figure 8.8: Effect of β_3 on the normalized response of steel plate shear wall

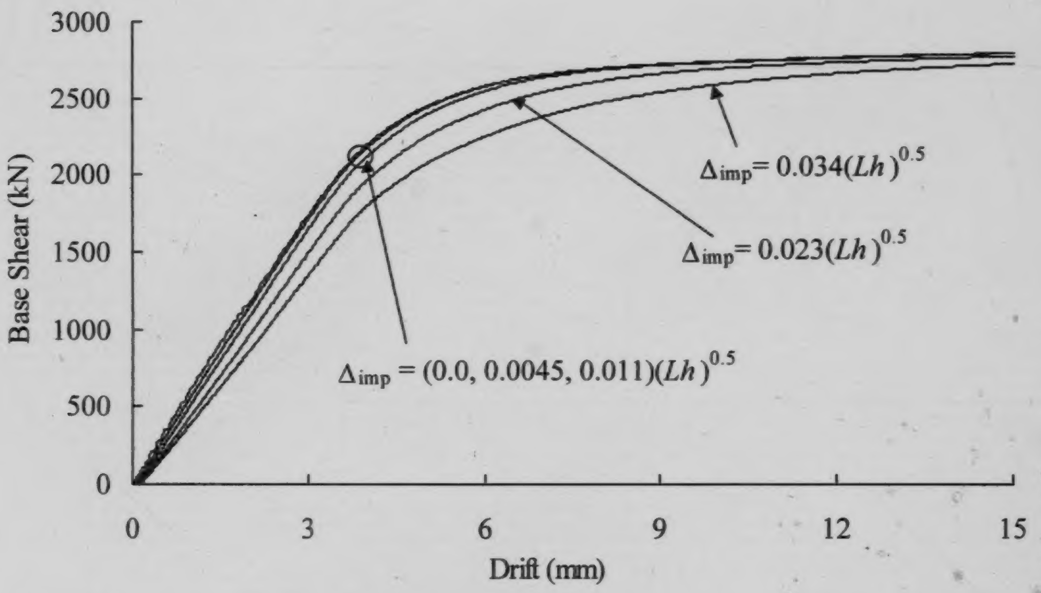

Figure 8.9: Effect of imperfection magnitude on the behaviour of a steel plate shear wall panel

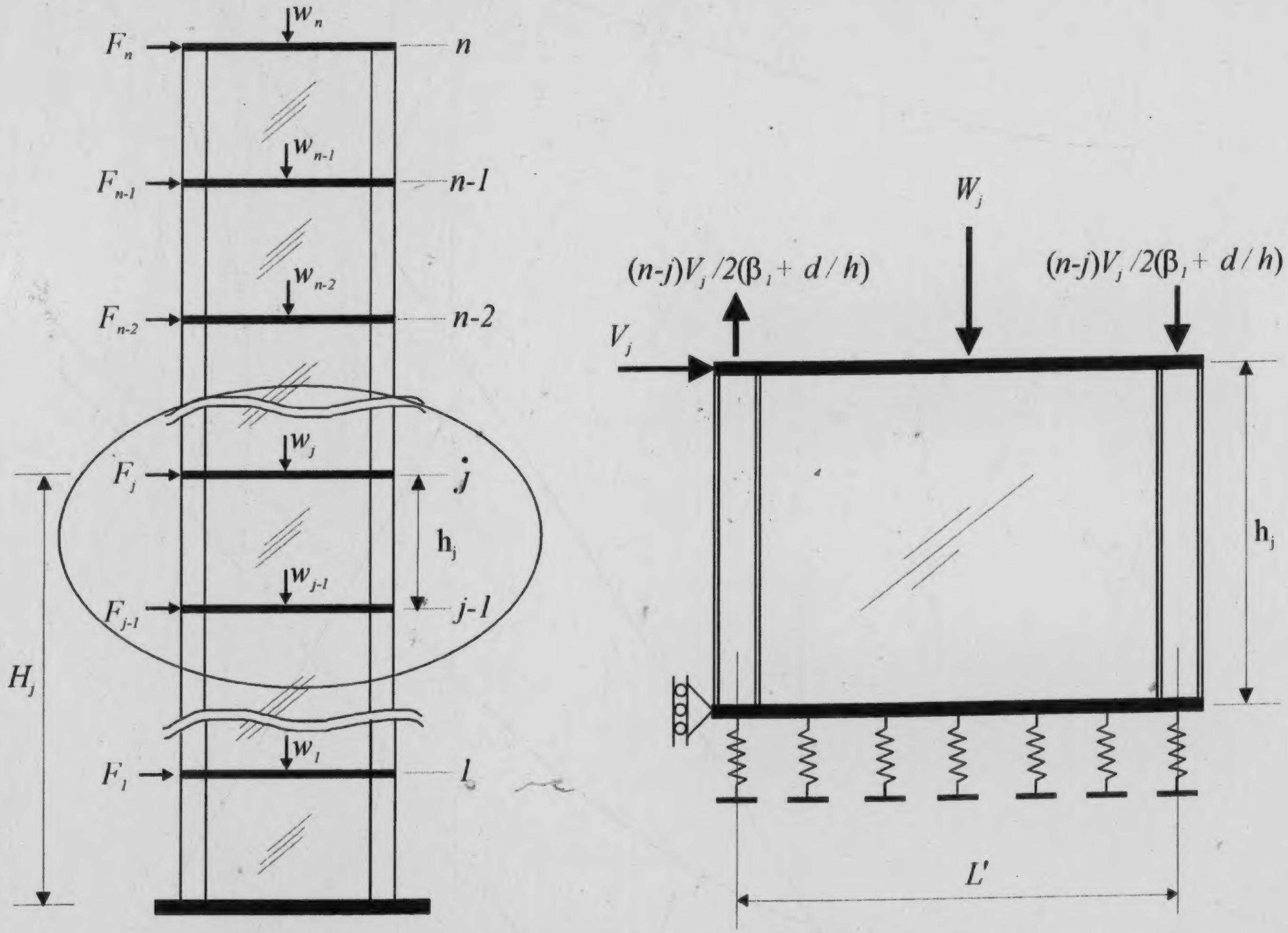
w_n
F_n
n
w_{n-1}
F_{n-1}
$n-1$
w_{n-2}
F_{n-2}
$n-2$
w_j
F_j
j
h_j
w_{j-1}
F_{j-1}
$j-1$
H_j
w_1
F_1
1
W_j
$(n-j)V_j/2(\beta_1+d/h)$
$(n-j)V_j/2(\beta_1+d/h)$
V_j
h_j
L'

Figure 8.10: Free body diagram of panel j from a multi-storey steel plate shear wall

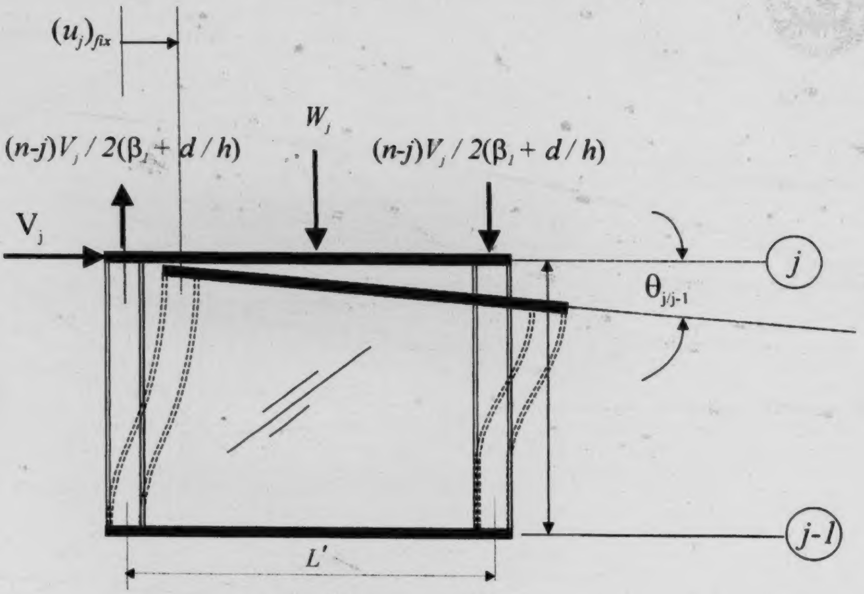
$(u_j)_{fix}$
W_j
$(n-j)V_j / 2(\beta_1 + d / h)$
$(n-j)V_j / 2(\beta_1 + d / h)$
V_j
j
$\theta_{j/j-1}$
$j-1$
L'

(a) Fixed boundary condition

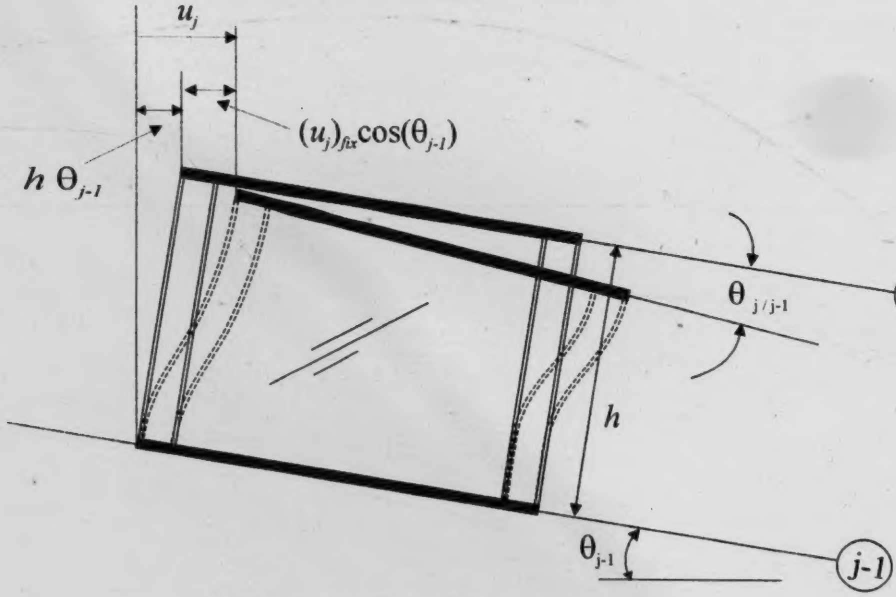
u_j
$(u_j)_{fix}\cos(\theta_{j-1})$
$h\,\theta_{j-1}$
$\theta_{j/j-1}$
j
h
θ_{j-1}
$j-1$

(b) Effect of rotation of lower floor beam

Figure 8.11: Panel *j* of a steel plate shear wall in deformed configuration

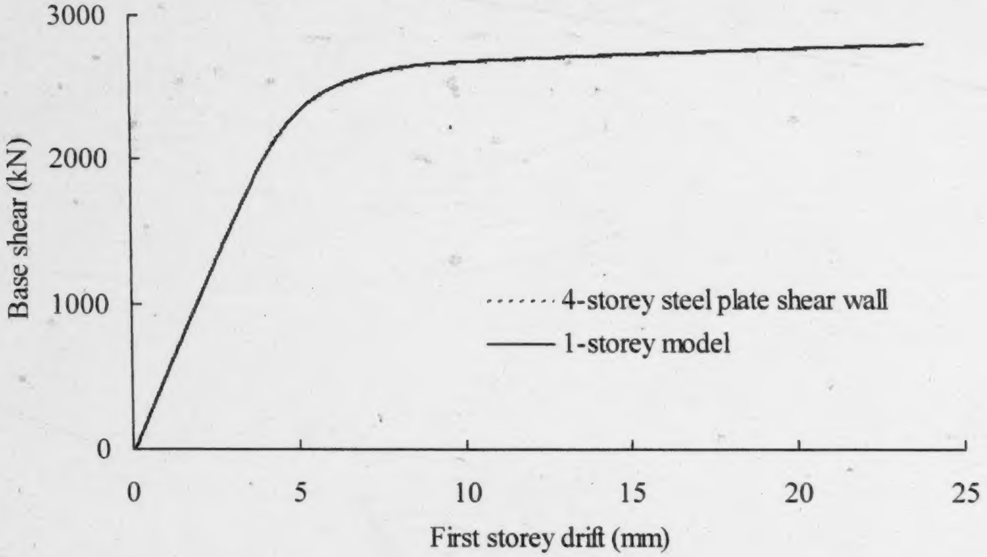

Figure 8.12: Base shear versus first storey drift obtained from the analysis of whole model and single storey model

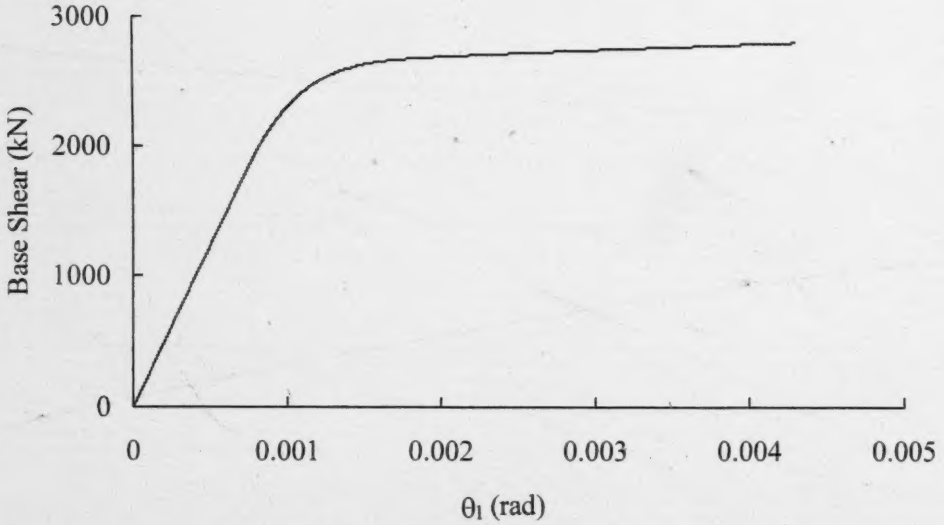

Figure 8.13: Rotation of the first floor obtained from the analysis of a single storey model of the first panel

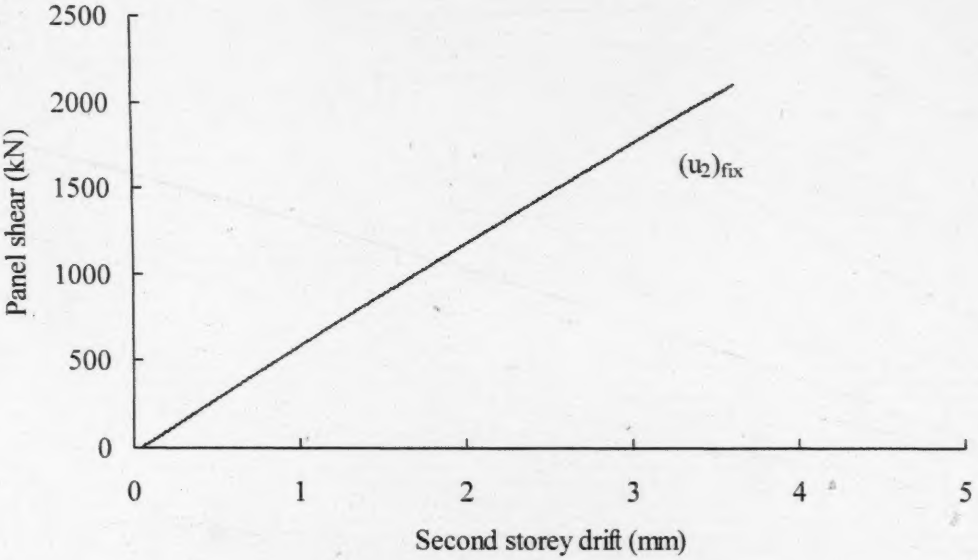

Figure 8.14: Panel shear versus storey drift obtained from single storey model of the second panel with fixed boundary condition

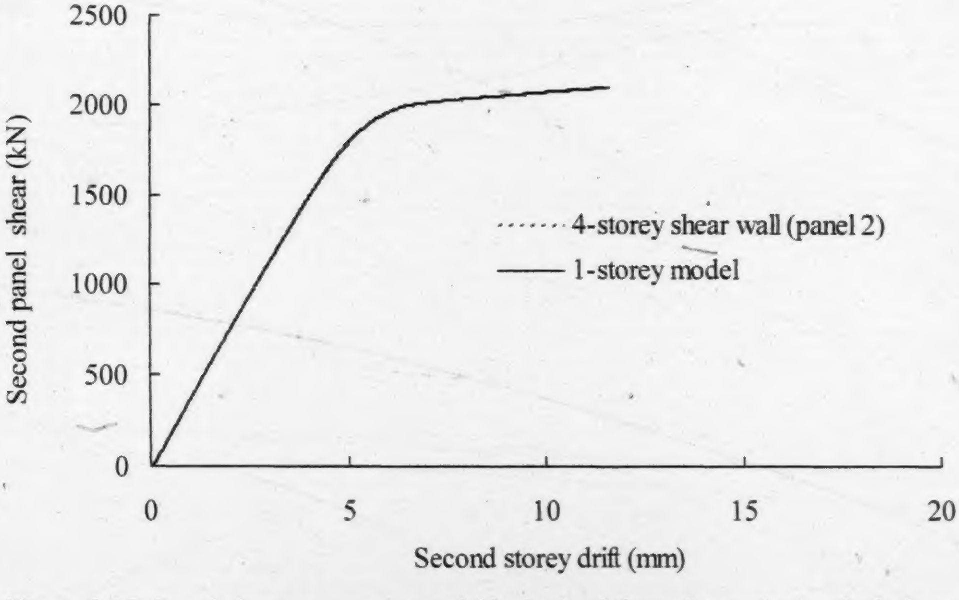

Figure 8.15: Panel shear versus storey drift obtained from the analysis of whole model and single storey model of the second panel

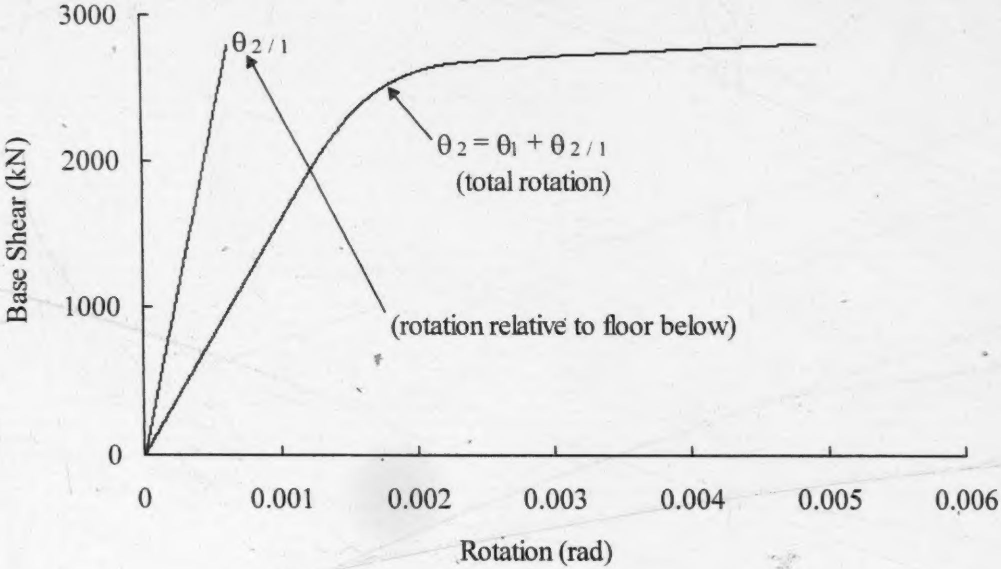

Figure 8.16: Rotation of the second floor

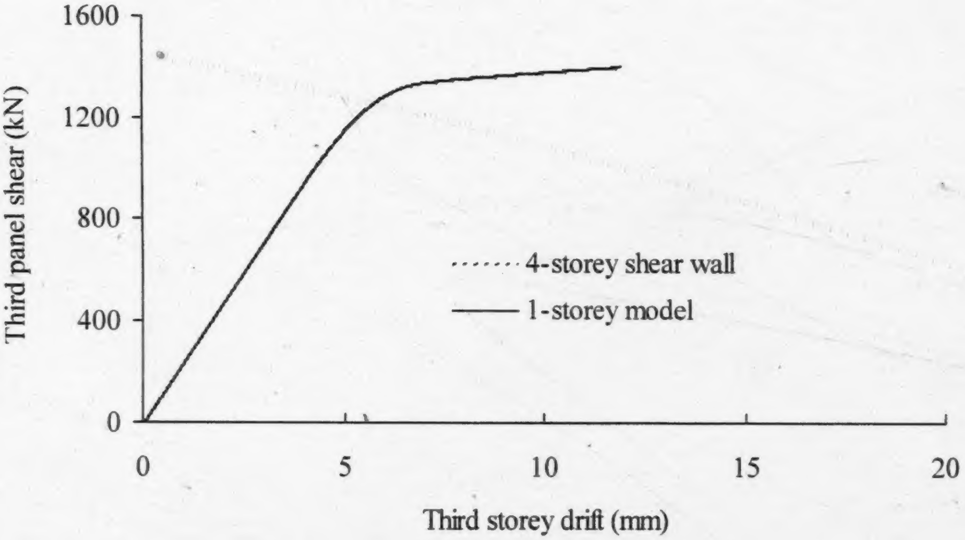

Figure 8.17: Third storey shear versus third storey drift obtained from the analysis of whole model and single storey model of the third panel

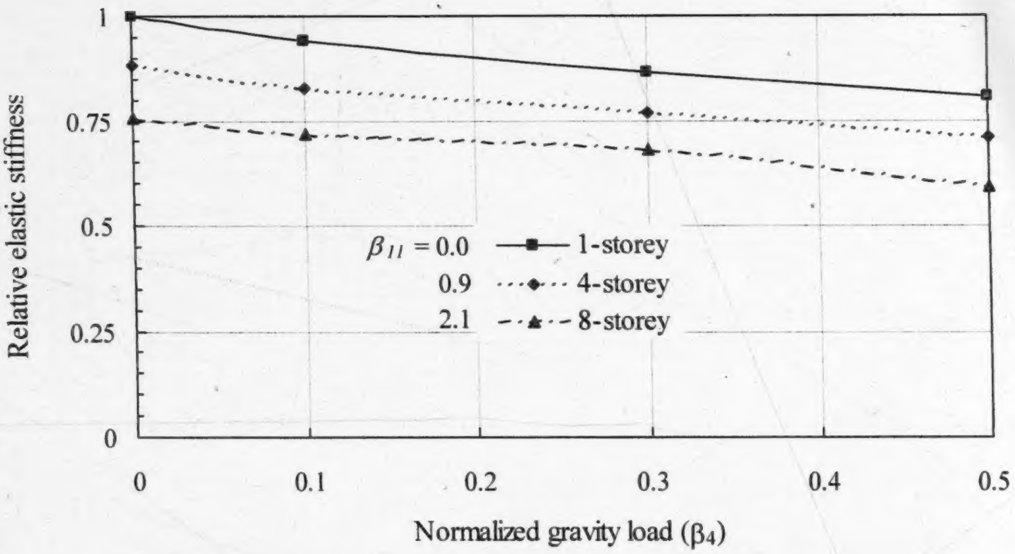

Figure 8.18: Elastic stiffness of the panel versus β_4 at different β_{11} parameters

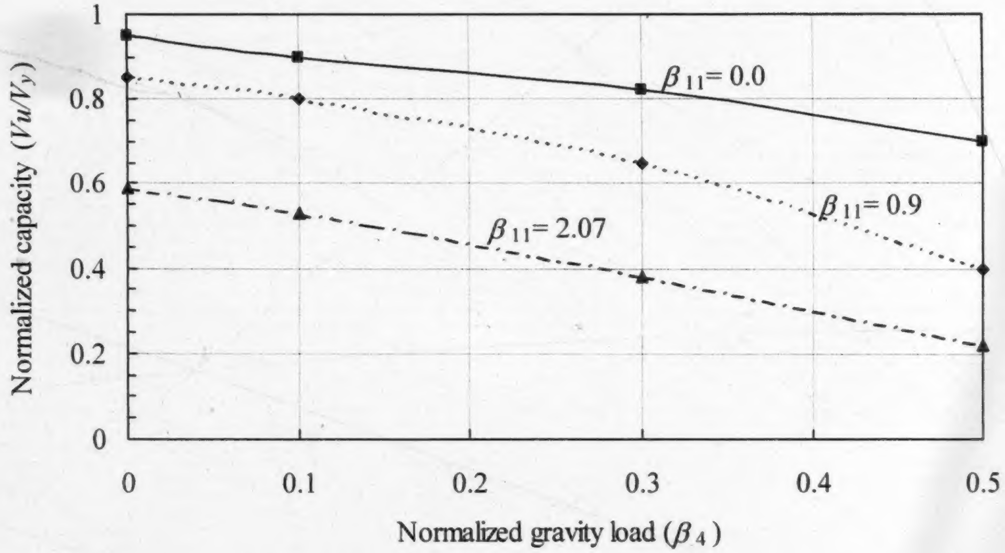

Figure 8.19: Effect of β_4 and β_{11} on shear wall panel capacity

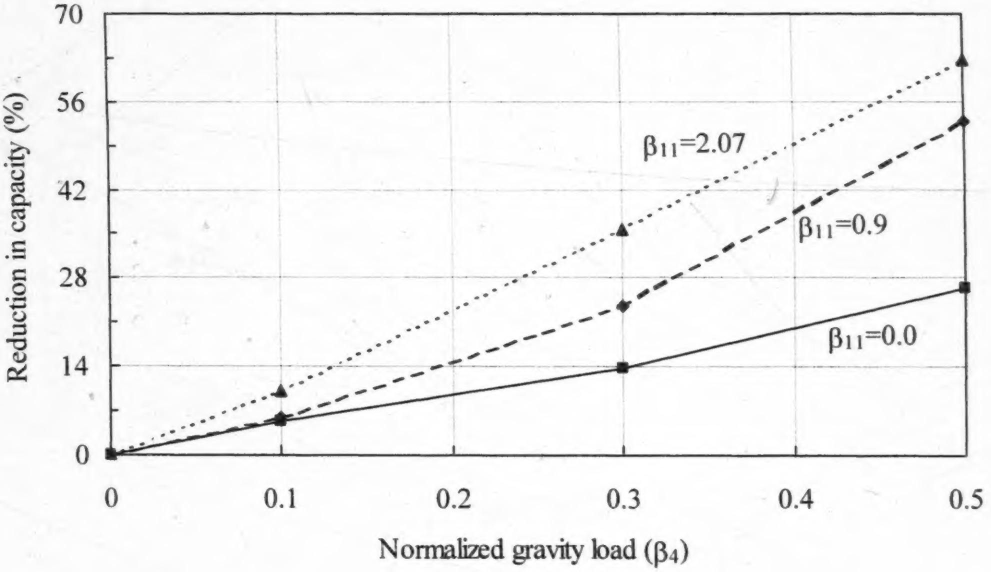

Figure 8.20: Effect of β_4 and β_{11} on reduction of shear wall panel capacity

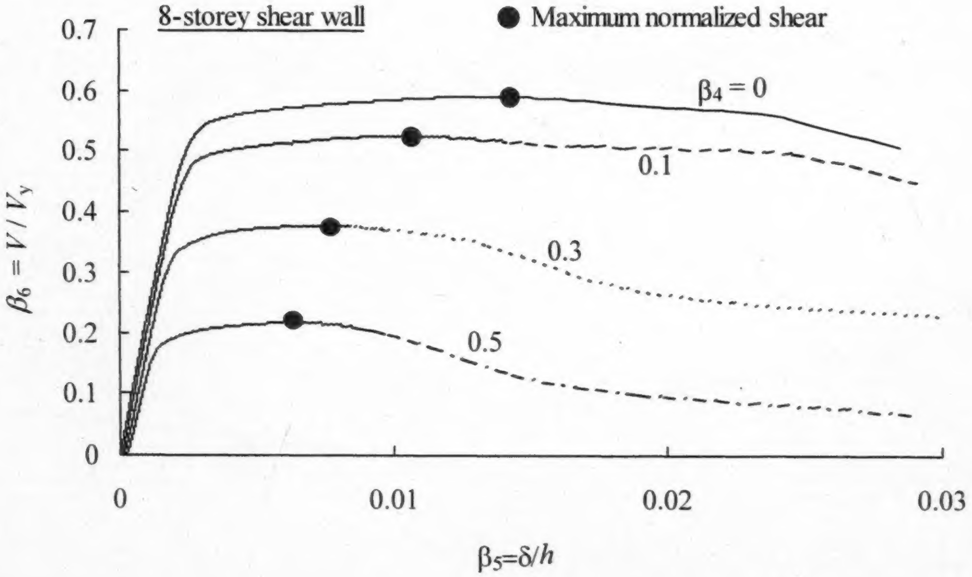

Figure 8.21: Normalized response of the first panel of an eight-storey shear wall at various β_4 parameter

δ

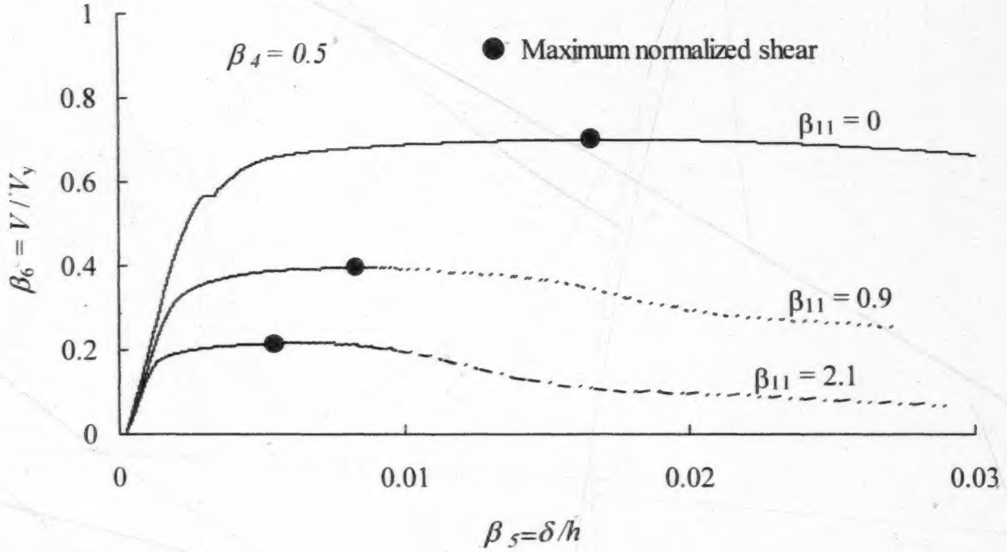

Figure 8.22: Normalized response at β_4 equal to 0.5 and various β_{11} parameter

9 SUMMARY, CONCLUSIONS, AND RECOMMENDATIONS

9.1 Summary

An experimental and numerical investigation of unstiffened steel plate shear walls was conducted in this research project. A three-storey unstiffened steel plate shear wall was tested under quasi-static cyclic condition. The test specimen consisted of the undamaged upper three storeys of a four-storey steel plate shear wall tested by Driver *et al.* (1997). It consisted of a single bay rigid frame with column-to-column spacing of 3050 mm and typical storey height of 1830 mm, representing a 50% model scale of a typical office building. The specimen was tested under a combination of constant gravity load and cyclic lateral loads. Equal lateral loads were applied at each beam level and were cycled according to the guideline ATC-24 (1992) in order to simulate a severe earthquake condition.

Twenty-four cycles of loading were applied to the test specimen, of which 14 cycles were in the inelastic range. Those cycles induced fully reversed large deformations in the shear wall, well beyond the point of significant yielding, which simulated a situation much worse than a severe earthquake. In the second excursion of cycle 21, one of the beam-to-column connections in the first level fractured at a drift of four times the drift corresponding to the point of first significant yielding. Fracture of the connection did not have any significant effect on the load carrying capacity of the shear wall because of the inherent load path redundancy and excellent load redistribution capability of the system. The load cycle at which fracture took place was completed at the target drift of five times the yield drift. Following the repair of the connection, the shear wall was loaded up to the stroke limit of the hydraulic jacks. The wall reached its maximum capacity at a ductility ratio of 7 at which point the shear capacity of the steel plate shear wall started to deteriorate gradually because of the formation of tears in the infill plate of the lower storey and yielding and local buckling of the columns and beam at level 1. The specimen showed high elastic stiffness, excellent ductility, high energy dissipation capability, and stable hysteresis loops.

A finite element model based on explicit dynamic formulation was developed for the analysis of steel plate shear walls. Material and geometric nonlinearity, and the initial imperfections of the infill plates were included in the model. A kinematic hardening material model subroutine was implemented in order to simulate the Bauschinger effect in the cyclic analysis of the shear wall.

The finite element model was used to simulate the monotonic and cyclic responses of the three-storey test specimen and the four-storey steel plate shear wall tested by Driver *et al.* (1997). Since the solution strategy in the explicit formulation does not involve iteration, the analysis was completed without any numerical difficulty. In general, excellent agreement was observed between the test results and the finite element predictions. The stiffness of the three-storey and the four-storey steel plate shear walls was predicted well with the finite element model, but the predicted capacity was 12% and 7.8% lower than the measured capacity for the three and four-storey specimens, respectively. Part of the discrepancies between the analysis and the measured three-storey specimen behaviour can be attributed to the effect of the earlier test on the material properties. In general, the hysteresis loops generated by the finite element model were in good agreement with those generated during the test. The pinching effect observed in the physical tests was also captured in the finite element analysis, although to a slightly lesser extent than observed in the physical tests. Strains and the derived internal forces obtained from the test on the three-storey shear wall were found to be in good agreement with the finite element model.

The parameters describing the behaviour of a single panel of steel plate shear wall with rigid floor beams subjected to shear and gravity loads were identified. A dimensional analysis using the validated finite element model was used to identify a set of ten non-dimensional and scale independent parameters that describe the behaviour of unstiffened steel plate shear walls. A parametric study was conducted to identify the effect of some of the main parameters on the stiffness and capacity of single panel steel plate shear wall. A method for extrapolating the findings of the parametric study on single panels to panels that form part of a multi-storey steel plate shear walls was proposed.

9.2 Conclusions

A test on a three-storey steel plate shear wall specimen demonstrated again the excellent behaviour of this system. The bottom storey of the three-storey test specimen was exposed to 34 inelastic loading cycles, including 20 cycles from a prior test. The specimen showed high initial stiffness, very ductile behaviour, and stable hysteresis loops. Despite the fact that a beam-to-column connection fractured during the test, the ability of the system to resist the applied shear force was not noticeably affected, which illustrates the high redundancy of steel plate shear walls. The dual system of steel plate shear wall and ductile moment-resisting frame provided excellent performance. Although plastic hinges developed at the top and bottom of the columns in the first panel, the infill plate limited the inelastic straining of the boundary members and prevented the creation of a soft storey during the experiment. The behaviour of the steel plate shear wall observed during testing demonstrates that the selected configuration is an excellent lateral load resisting system, both for wind and earthquake forces.

Gradual decrease in the capacity, caused by plate tearing and local buckling, started when the test specimen reached a drift of about 3% of the storey height in the first and the second panels. This deflection is greater than the limiting storey drift specified by design standards for all groups of buildings. Therefore, in a properly designed steel plate shear wall subjected to seismic loads, degradation of capacity is unlikely to occur.

A finite element model, developed by using a nonlinear dynamic explicit formulation, gave an excellent prediction of the monotonic and cyclic behaviour of three and four-storey unstiffened steel plate shear walls without any solution difficulty. The model showed much superior capability compared to earlier simplified models proposed by other researchers. The proposed model is able to capture all essential features of the behaviour of steel plate shear walls.

The non-dimensional parameters affecting the behaviour of a single steel plate shear wall panel with rigid floor beams subjected to shear and gravity loads were identified. A parametric study of some of the primary variables was conducted and the following conclusions can be drawn from this analysis:

- Changing the aspect ratio ($\beta_1 = L/h$) of the shear wall panels within the range of 1 to 2 has negligible effect on the behaviour of a shear wall panel. However, when the aspect ratio is less than 1.0, both the normalized stiffness, $\lfloor (V/\delta)/(h/V_y) \rfloor$, and the normalized shear capacity of the panel, β_6, increase.
- An increase in the ratio of the axial stiffness of infill plate to that of the columns ($\beta_2 = t_p L/2A_c$) leads to an increase in the stiffness of the shear wall panel, but has a negligible effect on the normalized capacity, β_6, of the system.
- As expected, the column flexibility parameter, β_3, has a significant effect on the behaviour of steel shear walls. An increase of β_3 results in increasing bending deformation in the columns. The inward displacement of the columns induced by the action of the tension field prevents the development of a uniform tension field. As a result, both stiffness and capacity of the system decreases.
- Initial imperfections in the infill plate can have a significant influence on the stiffness of steel plate shear walls, especially when subjected to low amplitude cyclic loading, but have little effect on the shear capacity. The parametric study showed that the effect of initial imperfections is negligible when the maximum imperfection size, Δ_{imp}, is less than 1% of $\sqrt{Lh}$, which corresponds to a value in excess of 20 mm for the specimen tested in this program.

9.3 Recommendations for future research

Although thin plates in the order of a few millimetres are sufficient to carry the applied shear forces and dissipate energy, in order to avoid fabrication problems related to the use of thin plates, thicker plates (6 to 8 mm) are often used. The impact of using infill plates thicker than that required for strength on the behaviour of steel plate shear walls should be investigated.

The column flexibility parameter is limited to a value of 2.5 by S16-01. An investigation of stress distribution along the boundary columns can lead to an optimum value for this parameter. The presence of high overturning moment in a panel and also ratio of yield strength of infill plate to that of the columns should be considered in establishing a limit for column flexibility parameter.

In the model selected for the parametric study the bending deformation of the floor beams was neglected. This was based on the assumption that equal and opposite tension fields would be present at interior beams. A finite element analysis of the four-storey specimen with rigid beams exhibited stiffer behaviour (but the same capacity) than the shear wall with actual beam bending stiffness. It is recommended that bending and axial stiffness of the floor beams be further investigated. Parameters equivalent to β_2 and β_3, introduced for columns, can be developed for considering axial and bending deformation of floor beams.

The ratio of overturning moment to the shear force has a significant effect on the behaviour of a steel plate shear wall panel. For a typical multi-storey shear wall subjected to equal horizontal load at each level and equal storey height a non-dimensional parameter, taken as $\beta_{11} = (M_{ov})_j / V_j L' = (n - j)/2(\beta_1 + d/h)$, was added to the set of governing parameters. The normalized moment factor was derived based on a number of simplifying assumptions such as equal lateral loads at each level. The study of this parameter should therefore be expanded to look at the effect of unequal lateral loads at each floor level.

A set of non-dimensional parameters affecting the behaviour of a single panel of steel plate shear wall was defined in this study. By extending the parametric study, an empirical formula suitable for preliminary design of this system can be derived. This empirical formula should consider the effect of overturning moment, in addition to shear and gravity loads. More research in this area is recommended.

Usually openings are required in order to allow mechanical and electrical services to pass through steel plate shear walls. The effect of these openings and their location on the behaviour of steel plate shear walls should be investigated.

LIST OF REFERENCES

AISC, 1999, "Load and Resistance Factor Design Specifications." American Institute of Steel Construction, Chicago.

Applied Technology Council, 1992, "Guidelines for Cyclic Seismic Testing of Components of Steel Structures." ATC-24, Redwood City, CA

ASTM, 1991, "Standard Specification for Steel, Carbon (0.15 Maximum Percent), Hot-Rolled Sheet and Strip Commercial Quality." A569/A569M–91a, American Society for Testing and Materials, Philadelphia, PA.

Astaneh-Asl, A., 2001, "Seismic Behaviour and Design of Steel Shear Walls." Steel TIPS Report, Structural Steel Educational Council, July, Moraga, CA.

Astaneh-Asl, A., Zhao, Q., 2002, "Cyclic Behaviour of Steel Shear Wall Systems." Proceedings, Annual Stability Conference, Structural Stability Research Council, April, Seattle.

Basler, K., 1961, "Strength of Plate Girders in Shear." Journal of Structural Division, ASCE, Vol. 87, No. ST7, October, pp. 151-180.

Bathe, K. J., 1996, "Finite Element Procedures." Prentice-Hall, Englewood Cliffs, NJ.

Belytschko, T., Lin, J. I., and Tsay, C. S., 1984a, "Explicit Algorithms for the Nonlinear Dynamics of Shells." Computer Methods in Applied Mechanics and Engineering, Vol. 42, pp. 225-251.

Belytschko, T., Liu, W.K., and Kennedy, J. M., 1984b, "Hourglass Control in Linear and Nonlinear Problems." Computer Methods in Applied Mechanics and Engineering, Vol. 43, pp. 251-276.

Benson, D. J., 1992, "Computational Methods in Lagrangian and Eulerian Hydrocodes." Computer Methods in Applied Mechanics and Engineering, Vol. 99, pp. 235-394.

Caccese, V., Elgaaly, M. and Chen, R., 1993, "Experimental Study of Thin Steel-Plate Shear Walls Under Cyclic Load." Journal of Structural Engineering, ASCE, Vol. 119, No. 2, February, pp. 573-587.

Celebi, M., 1997, "Response of Olive View hospital to Northridge and Whittier earthquakes." Journal of Structural Engineering, ASCE, Vol. 123,No.4, April, pp. 389-396

Canadian Standard Association, CAN/CSA-G40.21-92, 1992, "Structural Quality Steels." Toronto, Ontario.

Canadian Standard Association, CAN/CSA-S16.1-94, 1994, "Limit States Design of Steel Structures." Toronto, Ontario.

Canadian Standard Association, CSA-S16-01, 2001, "Limit States Design of Steel Structures." Toronto, Ontario.

Derecho, A.T., Iqbal, M., Fintel, M., Corley, W.G., 1980, "Loading History for Use in Quasi-Static Simulated Earthquake Loading Tests." ACI Publication SP63, Reinforced Concrete Structures Subjected to Wind and Earthquake Forces, American Concrete Institute, pp. 329-356.

Driver, R.G., Kulak, G.L., Kennedy, D.J.L., and Elwi, A.E., 1997, "Seismic Behaviour of Steel Plate Shear Walls." Structural Engineering Report No. 215, Department of Civil and Environmental Engineering, University of Alberta, Edmonton, Canada.

Driver, R.G., Kulak, G.L., Kennedy, D.J.L., and, Elwi, A.E., 1998a, "Cyclic Test of a Four-Story Steel Plate Shear Wall." Journal of Structural Engineering, ASCE Vol. 124, No. 2, February, pp. 112-120.

Driver, R.G., Kulak, G.L., Kennedy, D.J.L., and, Elwi, A.E., 1998b, "FE and Simplified Models of Steel Plate Shear Wall." Journal of Structural Engineering, ASCE Vol. 124, No. 2, February, pp. 121-130.

Elgaaly, M., Caccese, V., and Du, C., 1993, "Post-buckling Behaviour of Steel Plate Shear Walls Under Cyclic Loads." Journal of Structural Engineering, ASCE, Vol. 119, No. 2, February, pp. 588-605.

Elgaaly, M., and Liu, Y., 1997, "Analysis of Thin Steel Plate Shear Walls." Journal of Structural Engineering, ASCE, Vol. 123, No. 11, November, pp. 1487-1496.

Fujitani, H., Yamanouchi, H., Okawa, I., Sawai, N., Uchida, N., and Matsutani, T., 1996, "Damage and Performance of Tall Buildings in the 1995 Hyogoken Nanbu Earthquake." Proceedings, The 67th Regional Conference, Council on Tall Building and Urban Habitat, Chicago, pp. 103-125.

Hibbitt, Karlsson, & Sorenson, Inc., (HKS), 1998, "ABAQUS/Standard User's Manual." version 5.8, Hibbitt, Karlsson, & Sorenson Inc., Pawtucket, Rhode Island.

Hibbitt, Karlsson, & Sorenson, Inc., (HKS), 2001a, "ABAQUS/Explicit User's Manual." version 6.2, Hibbitt, Karlsson, & Sorenson Inc., Pawtucket, Rhode Island.

Hibbitt, Karlsson, & Sorenson, Inc. (HKS), 2001b, "ABAQUS/Standard Theory Manual." version 6.2, Hibbitt, Karlsson, & Sorenson Inc., Pawtucket, Rhode Island.

Kennedy, D.J.L., Kulak, G.L., and Driver, R.G., 1994, "Discussion of Postbuckling Behaviour of Steel Plate Shear Walls Under Cyclic Loads by Elgaaly, M., Caccese, V., and Du, C." Journal of Structural Engineering, ASCE, Vol. 120, No.7, pp. 2250-2251

Kuhn, P., Peterson, J.P., and Levin, L.R., 1952,"A Summary of Diagonal Tension, part I – Methods of Analysis." Technical Note 2661, National Advisory Committee for Aeronautics, Washington, DC.

Kulak, G.L., 1991, "Unstiffened Steel Plate Shear Walls." Structures Subjected to Repeated Loading—Stability and Strength, Narayanan, R., and Roberts, T.M., Editors, Elsevier Applied Science Publications, London, U.K., pp. 237-276.

Kulak, G.L., Kennedy, D.J.L., and Driver, R.G., 1994, "Discussion of Experimental Study of Thin Steel Plate Shear Walls Under Cyclic Load by Caccese, V., Elgaaly, M., and Chen, R." Journal of Structural Engineering, ASCE, Vol. 120, No. 10, pp. 3072-3073.

Kulak, G.L., Kennedy, D.J.L., Driver, R.G., and Medhekar, M., 1999, "Behaviour and Design of Steel Plate Shear Walls." Proceedings, North American Steel Construction Conference, Toronto, Canada, pp. 11–1-11–20.

Langhaar, H.L., 1951, "Dimensional Analysis and Theory of Models." John Wiley and Sons, N.Y.

Lee, S.W., Yoon, J.W., and Yang, D.Y., 1999, "Comparative Investigation into the Dynamic Explicit and the Static Implicit Method for Springback of Sheet Metal Stamping." Engineering Computations, Vol. 16, No. 3, pp. 347-373.

Lubell, A.S., 1997, "Performance of Unstiffened Steel Plate Shear Walls Under Cyclic Quasi-Static Loading." M.A.Sc. Thesis, Department of Civil Engineering, University of British Columbia, Vancouver, BC, Canada.

Lubell, A.S., Prion, H.G.L., Ventura, C.E., and Rezai, M., 2000, "Unstiffened Steel Plate Shear Wall Performance Under Cyclic Load." Journal of Structural Engineering, ASCE, Vol. 126, No. 4, April, pp. 453-460.

Lubliner, J., 1990, "Plasticity Theory." Macmillan Publishing Co., New York.

Mimura, H. and Akiyana, H., 1977, "Load-Deflection Relationship of Earthquake-Resistant Steel Shear Walls With a Developed Diagonal Tension Field." Transactions, Architectural Institute of Japan, 260, October, pp. 109-114 (in Japanese).

Montgomery, C.J., and Medhekar, M., 2001, "Discussion of Unstiffened Steel Plate Shear Wall Performance Under Cyclic Loading by Lubell, A.S., Prion, H.G.L., Ventura, C.E., and Rezai, M." Journal of Structural Engineering, ASCE, Vol. 127, No. 8, August, pp. 973

NBCC, 1995, "National Building Code of Canada." National Research Council of Canada, Ottawa, ON.

Ramm, E., 1981, " Strategies for Tracing the Nonlinear Response Near Limit Points." Nonlinear Finite Element Analysis in Structural Mechanics, Edited by E. Wunderlich, E. Stein, and K. J. Bathe, Springer-Verlag, Berlin, pp. 63-89.

Rezai, M., 1999, "Seismic Behaviour of Steel Plate Shear Walls by Shake Table Testing." PhD Dissertation, Department of Civil Engineering, University of British Columbia, Vancouver, Canada.

Rezai, M., Ventura, C.E., and Prion, H.G.L., 2000, "Numerical Investigation of Thin Unstiffened Steel Plate Shear Walls." Proceedings, 12th World Conference on Earthquake Engineering, Auckland, New Zealand.

Riks, E., 1979, "An Incremental Approach to the Solution of Snapping and Buckling Problems." International Journal of Solids and Structures, Vol. 15, No. 7, pp. 529-551.

Roberts, T.M. and Sabouri-Ghomi, S., 1991, "Hysteretic Characteristics of Unstiffened Plate Shear Panels." Thin-Walled Structures, Vol. 12, No. 2, pp. 145-162.

Sabouri-Ghomi, S. and Roberts, T.M., 1991, "Nonlinear Dynamic Analysis of Steel Plate Shear Walls." Computers and Structures, Vol. 39, No.1/2, pp. 121-127.

Sabouri-Ghomi, S., Roberts, T.M., 1992, "Nonlinear Dynamic Analysis of Steel Plate Shear Walls Including Shear and Bending Deformations." Engineering Structures, Vol. 14, No. 5, pp. 309-317.

SAE, 1994, "Chemical Compositions of SAE Carbon Steels – SAE J403." Society of Automotive Engineers, Inc, Warrendale, PA.

Takahashi, Y., Takemoto, Y., Takeda, T., and Takagi, M., 1973, "Experimental Study on Thin Steel Shear Walls and Particular Bracings Under Alternative Horizontal Load." Prelim. Rep., IABSE Symp. on Resistance and Ultimate Deformability of Structures Acted on by Well-defined Repeated Loads, Lisbon, Portugal, pp. 185-191.

Taylor, E.S., 1974, "Dimensional Analysis for Engineers." Oxford University Press, London, UK.

Thorburn, L.J., Kulak, G.L., and Montgomery, C.J., 1983, "Analysis of Steel Plate Shear Walls." Structural Engineering Report No. 107, Department of Civil Engineering, University of Alberta, Edmonton, Canada.

Timler, P.A., Kulak, G.L., 1983, "Experimental Study of Steel Plate Shear Walls." Structural Engineering Report No. 114, Department of Civil Engineering, University of Alberta, Edmonton, Canada.

Timler, P.A., Ventura, C.E., 1999, "Economical Design of Steel Plate Shear Walls From a Consulting Engineer's Perspective." Proceedings, North American Steel Construction Conference, Toronto, Canada, pp. 36–1-36–18.

Tromposch, E.W., Kulak, G.L., 1987, "Cyclic and Static Behaviour of Thin Panel Steel Plate Shear Walls." Structural Engineering Report No. 145, Department of Civil Engineering, University of Alberta, Edmonton, Canada.

Uniform Building Code (UBC), 1988, "Structural Engineering Design Provisions." International Conference of Building Officials, Whittier, California.

Wagner, H., 1931, "Flat Sheet Metal Girders With Very Thin Webs, Part I–General theories and assumptions." Technical Memo. No. 604, National Advisory Committee for Aeronautics, Washington, DC.

Xue, M., Lu, L.-W., 1994a "Interaction of Infilled Steel Shear Wall Panels With Surrounding Frame Members." Proceedings, Structural Stability Research Council Annual Technical Session, Bethlehem, PA, pp. 339-354.

Xue, M., Lu, L.-W., 1994b, " Monotonic and Cyclic Behaviour of Infilled Steel Shear Panels." Proceedings of the 17th Czech and Slovak International Conference on Steel Structures and Bridges, Bratislava, Slovakia.

APPENDIX A

Transverse shear stiffness for element S4R in ABAQUS/Explicit

Element S4R in ABAQUS is based on first-order transverse shear deformable theory in which the transverse shear strain is assumed to be constant through the thickness of the shell. This assumption requires the use of a shear correction factor. The transverse shear stresses, σ_{13} and σ_{23} (see Figure 5.7 for local directions) are estimated by matching the elastic strain energy associated with the shear deformation of the shell section (expressed in terms of section forces and strains at the centre of the element) with that based on quadratic variation of the transverse shear stress across the section, under the condition of bending about one axis. In calculating the transverse shear stiffness, it is assumed that the shell section directions are the principal bending directions (bending about one principal direction does not require restraining moment about the other direction). For a shell subjected to only bending moment and shear force in the plane normal to direction 1 (see Figure A.1), the membrane forces in the shell are zero and the shear stresses on the section have a parabolic distribution, which can be obtained from the equilibrium by the following equation:

$$\sigma_{13} = \frac{6V_{13}}{t^3}\left(\frac{t^2}{4} - z^2\right) \qquad \text{A.1}$$

where, σ_{13} is the transverse shear stress at a distance z from mid-surface, V_{13} is the shear force per unit width, and t is the shell thickness.

The associated shear strain energy can be obtained for a unit length of the shell as:

$$E_{tr} = \int_{-t/2}^{t/2} \frac{(\sigma_{13})^2}{2G_{13}} dz = \frac{3V_{13}{}^2}{5G_{13}t} \qquad \text{A.2}$$

where, G_{13} is the shear modulus of the material in plane (1-3).

By introducing transverse shear stiffness, K_{13}^{tr}, the shear strain energy of the shell section can also be calculated as:

$$E_{tr} = \frac{V_{13}^2}{2K_{11}^{tr}} \qquad \text{A.3}$$

By equating the expressions of A.2 and A.3, the transverse shear stiffness of the shell in the plane normal to direction 1 is obtained as:

$$K_{13}^{tr} = \frac{5}{6} G_{13} t \qquad \text{A.4}$$

For an isotropic shell element K_{13}^{tr} and K_{23}^{tr} are equal.

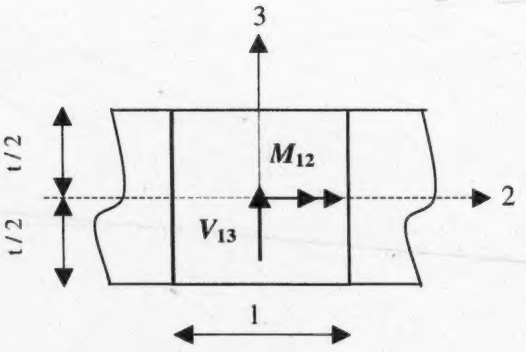

Figure A.1: Shell element subjected to bending and shear in the plane normal to direction 1.

APPENDIX B

Kinematic hardening subroutine for shell element in ABAQUS/Explicit

a) Options to define the material modelling:

*MATERIAL, NAME = name
*DENSITY
ρ
*DEPVAR
5,
*USER MATERIAL, CONST=4
E, ν, σ_y, H

b) Option to define transverse shear stiffness of a homogenous, isotropic shell element:

*TRANSVERSE SHEAR STIFFNESS
K_{13}^{tr}, K_{23}^{tr}

c) Subroutine:

```
C Read only (unmodifiable)variables -
   1 nblock, ndir, nshr, nstatev, nfieldv, nprops, lanneal,
   2 stepTime, totalTime, dt, cmname, coordMp, charLength,
   3 props, density, strainInc, relSpinInc,
   4 tempOld, stretchOld, defgradOld, fieldOld,
   5 stressOld, stateOld, enerInternOld, enerInelasOld,
   6 tempNew, stretchNew, defgradNew, fieldNew,
C Write only (modifiable) variables -
   7 stressNew, stateNew, enerInternNew, enerInelasNew )
C
    include 'vaba_param.inc'
C
    dimension props(nprops), density(nblock), coordMp(nblock,*),
   1 charLength(nblock), strainInc(nblock,ndir+nshr),
   2 relSpinInc(nblock,nshr), tempOld(nblock),
   3 stretchOld(nblock,ndir+nshr),
   4 defgradOld(nblock,ndir+nshr+nshr),
   5 fieldOld(nblock,nfieldv), stressOld(nblock,ndir+nshr),
   6 stateOld(nblock,nstatev), enerInternOld(nblock),
   7 enerInelasOld(nblock), tempNew(nblock),
   8 stretchNew(nblock,ndir+nshr),
     8  defgradNew(nblock,ndir+nshr+nshr),
     9  fieldNew(nblock,nfieldv),
     1  stressNew(nblock,ndir+nshr), stateNew(nblock,nstatev),
     2  enerInternNew(nblock), enerInelasNew(nblock)
C
      character*80 cmname
C
      parameter( zero = 0.d0, one = 1.d0, two = 2.d0, three = 3.d0,
     1   third = 1.d0/3.d0, half = .5d0, two_thirds = 2.d0/3.d0,
     2   three_halfs = 1.5d0 )
c
c j2 mises plasticity with kinematic hardening for plane strain case.
c the state variables are stored as:
c
c        state(*, 1) = back stress component 11
c        state(*, 2) = back stress component 22
c        state(*, 3) = back stress component 33
c        state(*, 4) = back stress component 12
c        state(*, 5) = equivalent plastic strain
c
      e     = props(1)
      xnu   = props(2)
      yield = props(3)
      hard  = props(4)
c
c   elastic constants
c
      twomu  = e / ( one + xnu )
      thremu = three_halfs * twomu
      sixmu  = three * twomu
      alamda = twomu * ( e - twomu ) / ( sixmu - two * e )
      term   = one / ( twomu * ( one + hard/thremu ) )
      con1   = sqrt( two_thirds )
      terma= -xnu / (one - xnu )
c
c
c
c if steptime equals to zero, assume the material pure elastic and use
c initial elastic modulus
c
      if( steptime .eq. zero ) then
c
      do i = 1,nblock
c
c  trial stress
         strainZ= terma * (straininc (i, 1)+ straininc (i, 2))
```

```
        trace = straininc (i, 1) + straininc (i, 2) + strainZ
        stressnew(i, 1)=stressold(i, 1) + alamda*trace
     1  +           twomu*straininc(i,1)
        stressnew(i, 2)=stressold(i, 2) + alamda*trace
     1  +           twomu*straininc(i, 2)
        stressnew(i, 3)=stressold(i, 3) + alamda*trace
     1  +           twomu*strainZ
        stressnew(i, 4)=stressold(i, 4)
     1  +           twomu*straininc(i, 4)
      end do
c
      else
c
c     plasticity calculations in block form
c
      do i = 1, nblock
c  elastic predictor stress
        strainZ= terma * (straininc (i, 1)+ straininc (i, 2))
        trace = straininc(i, 1) + straininc(i, 2)+ strainZ
        sig1= stressold(i, 1) + alamda*trace + twomu*straininc(i, 1)
        sig2= stressold(i, 2) + alamda*trace + twomu*straininc(i, 2)
        sig3= stressold(i, 3) + alamda*trace + twomu*strainZ
        sig4= stressold(i, 4)                + twomu*straininc(i, 4)
c  elastic predictor stress measured from the back stress
        s1 = sig1 - stateold(i, 1)
        s2 = sig2 - stateold(i, 2)
        s3 = sig3 - stateold(i, 3)
        s4 = sig4 - stateold(i, 4)
c  deviatoric part of predictor stress measured from the back stress
        smean = third * ( s1 + s2 + s3 )
        ds1 = s1 - smean
        ds2 = s2 - smean
        ds3 = s3 - smean
c  magnitude of the deviatoric predictor stress difference
        dsmag = sqrt( ds1**2 + ds2**2 + ds3**2 + two*s4**2 )
c
c  check for yield by determining the factor for plasticity, zero for
c  elastic, one for yield
        radius = con1 * yield
        facyld = zero
        if( dsmag - radius .ge. zero ) facyld = one
c  add a protective addition factor to prevent a divide by zero when dsmag
c  is zero. if dsmag is zero, we will not have exceeded the yield stress
c  and facyld will be zero.
        dsmag  = dsmag + ( one - facyld )
c  calculated increment in gamma ( this explicitly includes the time step)
```

```
        diff   = dsmag - radius
        dgamma = facyld * term * diff
c  update equivalent plastic strain
        deqps  = con1 * dgamma
        statenew(i, 5) = stateold(i, 5) + deqps
c  divide dgamma by dsmag so that the deviatoric stresses are explicitly
c  converted to tensors of unit magnitude in the following calculations
        dgamma = dgamma / dsmag
c  update back stress
        factor  = hard * dgamma * two_thirds
        statenew(i, 1) = stateold(i, 1) + factor * ds1
        statenew(i, 2) = stateold(i, 2) + factor * ds2
        statenew(i, 3) = stateold(i, 3) + factor * ds3
        statenew(i, 4) = stateold(i, 4) + factor * s4
c  update stress
        factor   = twomu * dgamma
        stressnew(i, 1) = sig1 - factor * ds1
        stressnew(i, 2) = sig2 - factor * ds2
        stressnew(i, 3) = sig3 - factor * ds3
        stressnew(i, 4) = sig4 - factor *  s4
c  update the specific internal energy -
        stress_power = half * (
     1       ( stressold(i, 1)+stressnew(i, 1) )*straininc(i, 1)
     2  +    ( stressold(i, 2)+stressnew(i, 2) )*straininc(i, 2)
     3  +    ( stressold(i, 3)+stressnew(i, 3) )*strainZ
     4  + two*( stressold(i, 4)+stressnew(i, 4) )*straininc(i, 4) )
        enerinternnew(i) = enerinternold(i)
     1  +                  stress_power/density(i)
c  update the dissipated inelastic specific energy -
        smeana = stressnew(i, 1) + stressnew(i, 2) + stressnew(i, 3)
        smean = third * smeana
        equiv_stress = sqrt( one
     1  *             ( (stressnew(i, 1)-smean)**2
     2  +               (stressnew(i, 2)-smean)**2
     3  +               (stressnew(i, 3)-smean)**2
     4  +           two * stressnew(i, 4)**2 ) )
c

        plastic_work_inc = equiv_stress * deqps
        enerinelasnew(i) = enerinelasold(i)
     1  +                  plastic_work_inc / density(i)
c
      end do
c
      end if
c
```

```
return
end
```